Early application of mechanistic PKPD modelling to guide the preclinical development of a therapeutic mAb targeting complement receptor 2 (CR2/CD21) as a novel target for the treatment of autoimmune disease

A thesis submitted for a degree of Doctor of Philosophy

Edward Hooper-Greenhill

University of Strathclyde and GlaxoSmithKline

2021

Declaration of Authenticity and Authors Rights

This thesis is the result of the author's original research. It has been composed by the author and has not been previously submitted for examination which has led to the award of a degree.

Signed:  **Date: 25 February 2021**

Abstract

Mechanistic PKPD modelling has become the state of the art for the integration of preclinical data to improve early projection of the clinical efficacy of small molecule drug candidates. However, its application to the development of monoclonal antibody (mAb) based drug candidates has been relatively restricted to date. Typically, a key limiting factor is the necessity for a surrogate molecule to explore target pharmacology in well-established preclinical animal models. A need driven by the limited cross-species reactivity often seen with the fully human mAbs preferred for clinical development. Consequently, pharmacology is rarely established beyond target engagement during preclinical development, limiting the early projection of clinical efficacy.

The present work sought to explore the application of mechanistic PKPD modelling, early in the preclinical drug discovery environment, using a surrogate mAb as a tool with which to explore the pharmacology of the novel drug target complement receptor 2 (CD21). CD21 is thought to play a key role in the regulation of humoral immunity. As such, CD21 is receiving interest as a novel mechanism by which to treat autoimmune conditions characterised by the aberrant production of destructive autoantibodies, such as systemic lupus erythematosus.

Characterisation of three potential surrogate mAbs targeting murine CD21 identified non-dose-linear pharmacokinetics related to on target binding, characteristic of target mediated drug disposition (TMDD). To describe this behaviour, a minimal physiologically based pharmacokinetic (mPBPK) model was developed, incorporating target abundance, kinetics and binding affinity. This model highlighted critical gaps in the understanding of CD21 kinetics, particularly regarding the origin and impact of the soluble form of the protein (sCD21). Further experiments identified that the plasma concentration of sCD21(/35) in mice remained unchanged (12.8 nM) following treatment with an anti-CD21 mAb, despite near complete loss of B cell expressed CD21. This challenged the theory that sCD21 results from ectodomain shedding of membrane receptor, implicating secretion as a predominant source of the soluble protein in mice.

To explore the pharmacology of CD21 neutralisation, T-dependent immunisation was selected as a well-established acute mechanistic model of humoral immunity. To align with target biology and the clinical strategy, the protocol was optimised to comprise of a single IV immunisation with the T-dependent antigen keyhole limpet haemocyanin (KLH) at 1.2 mg/kg to C57BL/6 mice. The *in vivo* model was qualified using the clinically validated S1P receptor modulator Fingolimod. A relationship was established between Fingolimod blood exposure

and its pharmacodynamic effect on the T-dependent antibody (IgG) response (TDAR), using an integrated PKPD model. This resulted in an estimated EC_{50} of 4.59 nM (SE 3.09), showing remarkable similarity to reported EC_{50} estimates across species (versus peripheral lymphocyte reduction). The potential to translate this model system to project clinical efficacy was also demonstrated, providing an excellent prediction of the reported efficacy of Fingolimod on KLH induced TDAR (IgG) in the clinic.

Furthermore, CD21 pharmacology was explored in the mouse TDAR model using the widely published mAb 7G6 as a surrogate. A relationship was established between 7G6 plasma exposure and its pharmacodynamic effect on the KLH induced TDAR (IgM) using an integrated PKPD model, with an estimated EC_{50} of 0.13 nM (SE 0.02). Comparison with the measured receptor occupancy on peripheral B cells indicates this corresponds with approximately 60% target occupancy. Collectively, these data support the rationale that maintenance of mAb exposure to achieve >95% CD21 receptor occupancy at trough is an appropriate clinical benchmark. However, it also highlights that critical knowledge gaps remain with regard to CD21 and its pharmacology that would require further investigation.

Acknowledgements

The completion of this thesis has seen me develop a real passion for quantitative pharmacology that has taken my career on a journey from small molecule bioanalysis, through biopharm analysis, translational biology and now into a new role as a translational PKPD modeller. An eclectic mix that is mirrored in the content of this thesis. Clearly, I couldn't have achieved all of this if it wasn't for the help and support of a great number of talented scientists, both within GSK and at the University of Strathclyde, and for that I wholeheartedly thank each and every one of them.

I would like to thank more specifically my academic supervisors at the University of Strathclyde, Robin Plevin and Gavin Halbert, for making me feel so welcome and giving me the support and guidance to successfully complete this thesis. Equally, I would like to thank my industrial supervisor Cesar Ramirez Molina, for the many hours of scientific discussion and his unwavering support and encouragement to reach the end. I would also like to thank GSK for allowing me to complete the PhD program, Harry Kelly for overseeing all aspects of this collaborative program and the former DMPK council, particularly Martin Bayliss, for sponsoring me.

A huge number of incredible colleagues at GSK have gone above and beyond to help me in this project, certainly too many to list in its entirety, but I would particularly like to mention the following people. Tom Slocombe and Laura Tomlinson for their amazing help with many parts of the laboratory work, including performing the flow cytometry in this project. Stella Chime, David Lugo and Scott McCleary for acting as the study directors for the in life phases of the studies and all of the members of the Stevenage site *in vivo* study delivery (IVSD) team for completing these studies. Isobel Harada and Rob Willis for their advice and support with many aspects, particularly PK and modelling. My former managers Cesar Ramirez Molina and Andrea Haynes and my present manager Aarti Patel, for their support and encouragement. Bob Biddlecombe and Sarah Childs for teaching me to operate and letting me use their Gyrolab instruments, and for eventually donating one to me! Everyone in the CD21 project team, particularly Semra Kitchen, Christian Ellson and Eli Lekova.

Finally, and most importantly, I would like to thank my wife Chloe for all her support and for having forgone many evenings and weekends of my time over the past 5 years. And our son Jack, who joined this journey late on and has inspired me to reach its conclusion.

Table of Contents

Abbreviations List

ADA	-	Anti-drug antibody
ADME	-	Absorption, distribution, metabolism, elimination
AIC	-	Akaike information criteria
AUC	-	Area under the curve
AUEC	-	Area under the effect curve
BCR	-	B cell receptor
BIC	-	Bayesian information criteria
BLQ	-	Below limit of quantification
C_{av}	-	Average concentration
CDR	-	Complementarity-determining region
Cl ($_{p/b}$)	-	Clearance (plasma / blood)
C_{max}	-	Maximum concentration
CR2/CD21	-	Complement receptor 2 / Cluster of differentiation 21
CV	-	Coefficient of variation
DMPK	-	Drug metabolism and pharmacokinetics
EC_{50}	-	Half maximal effective concentration
ECL	-	Electrochemiluminescence
EDTA	-	Ethylenediaminetetraacetic acid
ELISA	-	Enzyme linked immunosorbent assay
E_{max}	-	Maximum efficacy
FcRn	-	Neonatal Fc receptor
FDC	-	Follicular dendritic cell
FTIH	-	First time in human
GC	-	Germinal centre B cell
GI	-	Gastrointestinal
HRP	-	Horseradish peroxidase
IgG	-	Immunoglobulin G
IgM	-	Immunoglobulin M
IM	-	Intramuscular
IP	-	Intraperitoneal
ISF	-	Interstitial fluid
IV	-	Intravenous
KLH	-	Keyhole limpet haemocyanin

LC-MS/MS	-	Liquid chromatography tandem mass spectrometry
LLQ	-	Lowest limit of quantification
mAb	-	Monoclonal antibody
MABEL	-	Minimum anticipated biological effect level
MFI	-	Mean fluorescence intensity
MHC	-	Major histocompatibility complex
mPBPK	-	Minimal physiologically based pharmacokinetic
MRD	-	Minimum required dilution
MSD	-	Mesoscale discovery
NCA	-	Non-compartmental analysis
NHS	-	N-hydroxy succinimide
PBPK	-	Physiologically based pharmacokinetic
PBS	-	Phosphate buffered saline
PD	-	Pharmacodynamics
PK	-	Pharmacokinetics
PKPD	-	Pharmacokinetic pharmacodynamic
PO	-	Per os (oral)
QD	-	Once daily
Q4D	-	Once every four days
RA	-	Rheumatoid arthritis
SE	-	Standard error
SD	-	Standard deviation
SC	-	Subcutaneous
SCR	-	Short consensus repeat
SIL	-	Stable isotope label
SLE	-	Systemic lupus erythematosus
SRBC	-	Sheep red blood cell
$T_{1/2}$	-	Half-life
TD	-	T-cell dependent
TDAR	-	T-cell dependent antibody response
T_{max}	-	Time of maximum concentration
TMB	-	3,3’,5,5’-Tetramethylbenzidine
TMDD	-	Target mediated drug disposition
TNP	-	2, 4, 6, trinitrophenyl

Chapter 1: Introduction

1.1. Introduction

In recent years the pharmaceutical industry has experienced an explosion of growth in the monoclonal antibody (mAb) market. Record numbers of antibody therapeutics are now progressing into early stage clinical studies, soaring from approximately 30 per year in the mid 2000's, to approximately 100 per year between 2015 and 2017 (Kaplon and Reichert, 2019). Collectively, pharma companies have over 570 unique mAbs in clinical development, of which approximately 90% are currently progressing through phase 1 and 2 (Kaplon and Reichert, 2019). In 2018 alone, 12 new mAbs were approved in either the US or EU, taking the present number of unique mAbs with marketing approval to over 80 (Kaplon *et al.*, 2020). This charge is being driven by the proven ability of mAbs and mAb like products to provide innovative therapeutic solutions to unlock the huge potential offered by modern molecular level understanding of disease. An understanding that has rapidly expanded thanks to the technological advances of the 'omics' era of molecular and systems biology. When compared with classical small molecule drugs, mAb based therapies offer a quicker and lower risk path to the clinic. With biologics boasting a likelihood of approval in their primary indication of approximately 1 in every 4 that enter clinical evaluation, compared with 1 in 8 for small molecules (Hay *et al.*, 2014). This has ensured that mAbs remain a popular modality for intervention of novel drug targets or pathways, enhancing the prospect of 'first to market' advantage for the inventor (Ecker *et al.*, 2015). Indeed, following an era of patent expiries and pipeline stagnation within big pharma, it is unsurprising that the industry has packed drug development pipelines with mAb based products. After all, with a 2017 market valuation in excess of $98 billion and growth predictions stretching this to between $137 and 200 billion by 2022 (Grilo and Mantalaris, 2019), a slice of the monoclonal antibody market is undeniably appealing.

Despite having a likelihood of approval of almost double that of classical small molecules (Hay *et al.*, 2014), failure still represents the most likely outcome (3/4) for a novel antibody drug candidate as it progresses into clinical investigation. This low probability of success has led the industry to perform retrospective analysis of clinical failures, to understand trends and seek opportunities for future improvement. One trend that similarly blights the development of small and large molecules alike, is a failure to demonstrate efficacy in early stage clinical studies. This issue accounted for 59% of all phase two clinical trial failures, both small and large molecule, in the period between 2011 to 2012 (Arrowsmith and Miller, 2013). Analysis of individual phase success rates by Kaplon and Reichert (2019), for mAbs entering clinical study in the period 2005 to 2014 (n=569), identified the phase 1 to 2, phase 2 to 3, phase 3 to

regulatory review and regulatory review to approval transition rates as 69%, 45%, 77% and 94%, respectively, with an overall success rate of 22%. This confirmed a similar analysis by Hay *et al.* (2014) over the period 2003 to 2011, highlighting that the rate of attrition in phase two is almost double that of any other phase. Phase two is typically the first time a drug is tested in patients with the target disease, representing the first opportunity to confirm clinical efficacy.

Whilst an inherent risk of the business is that a drug candidate may ultimately prove ineffective in the clinic, it does pose an incredibly costly gamble. It was estimated in 2010 that in the region of $65 million is spent to develop a drug through to phase II (Paul *et al.*, 2010). Whilst more recent analysis by DiMasi *et al.* (2016) indicates that it takes 4.2 years on average to progress from first time in human (FTIH) to the conclusion of phase II and the mean out of pocket cost of this clinical phase alone is now $83.9 million. Should a drug candidate ultimately prove ineffective in this clinical phase, it is essential that the research company can walk away knowing that they had at least thoroughly investigated the drugs mechanism of action (Morgan *et al.*, 2012). It is consequently of significant concern that when a retrospective analysis of clinical phase drug failure was performed by Pfizer in 2012, drug mechanism of action was cited as being insufficiently investigated in 43% of projects terminated due to a negative efficacy outcome in phase II (Morgan *et al.*, 2012). Inadequate testing of drug mechanism may be unavoidable, due to factors such as unexpected toxicology, which can often lead to dosage restrictions for safety reasons. But in many cases, it is likely due to a combination of poor clinical trial design and inadequate prediction of the relationship between drug dose and resulting efficacy. Clearly this represents the worst case scenario for the research company, who have invested considerable time and resource on an inconclusive outcome. However more crucially, this represents an unacceptable outcome for patients, who have not only been exposed to unnecessary risk but have been denied potentially life altering treatment.

Considering the identification of drug efficacy as the primary cause of drug failure in phase two clinical trials, the industry has undergone a period of reflection. A growing consensus is that the problem is rooted in early drug discovery, with a clear need to establish better tools to improve early prediction of concentration effect relationships for novel drugs (Morgan *et al.*, 2012, Morgan *et al.*, 2018, Cook *et al.*, 2014). Mechanistic pharmacokinetic pharmacodynamic (PKPD) modelling is one such tool which has become popular in early drug discovery. Here, mathematical functions quantitatively interrelate a drugs concentration with its effect on a biological system (Wong *et al.*, 2017). Mechanism based PKPD models take this a stage further, incorporating known factors into the model such as physiology, target

biology and drug potency, to allow translation of preclinical data where known differences occur (Wong *et al.*, 2017). Thus, translational mechanistic PKPD models can be harnessed to integrate all available preclinical data for the projection of an efficacious dose in humans (Bueters *et al.*, 2015). This integrated approach has been coined systems or quantitative pharmacology and has been implicated as a valuable tool in the early development of both small and large molecule drugs (van der Graaf and Benson, 2011, Tabrizi *et al.*, 2010b).

The application of translational mechanistic PKPD modelling to the early discovery of therapeutic mAbs has been relatively restricted to date. This is in spite of the fact that the majority of basic scientific research for target identification and validation is conducted in rodents. This slower uptake of translational mechanistic PKPD modelling, when compared with small molecule drug discovery that has actively engaged the field, is surprising given that modelling and simulation is a key priority in other areas of mAb development. For example, modelling and simulation has been widely adopted as an *in silico* method for target tractability assessment. Modelling is also now a critical part of selecting a safe first in human dose for many therapeutic mAbs in the wake of the TeGenero TGN1412 clinical trial incident (Lowe *et al.*, 2010). The review of the incident, led by Sir Gordon Duff and published in 2006, recommended the addition of the minimum anticipated biological effect level (MABEL) parameter for selection of a safe starting dose for high risk therapeutics, requiring some integrative modelling. One limiting factor that may be to blame for the slow uptake of translational PKPD modelling, is the often restricted cross reactivity to the analogous protein in lower species by the fully human mAbs favoured for clinical development. This often results in the requirement for a surrogate mAb to be raised against the analogous protein in the species of choice, prior to preclinical investigation in well established *in vivo* mechanistic and disease models (Luu *et al.*, 2013). Whilst PKPD modelling can then commence as normal, to date, limited attention has been applied by the industry as to how this surrogate data can be translated to predict clinical efficacy with the clinical candidate.

This research project focuses on the application of mechanistic PKPD modelling, early in the preclinical drug discovery environment, using a surrogate mAb as a tool with which to explore the pharmacology of the novel drug target complement receptor 2 (CD21). This is an immune target that is receiving interest both internally within GSK and across the wider scientific community. CD21 is a membrane bound complement regulatory protein expressed primarily on B cells and follicular dendritic cells (FDC), where it functions to promote B cell activation and regulate the generation of specific humoral immune responses. This mechanism, which is beneficial in host defence against foreign antigen, can also amplify the hosts autoimmune

response against self-antigen. It is hence thought that therapeutic blockade of CD21 may have benefit as a therapy for autoimmune conditions characterised by the production of destructive autoantibodies, such as systemic lupus erythematosus (SLE) and rheumatoid arthritis (RA) (Holers, 2014). In contrast to current therapeutic strategies for these diseases such as Rituximab (anti-CD20) and Belimumab (anti-BLyS), this would be without the need for depletion of B cells.

To date, targeting CD21 represents a novel, first in class therapeutic opportunity, with no presently disclosed clinical candidates in development against this mechanism. Consequently, target validation data is limited to knowledge gained from *in vitro* investigation combined with preclinical rodent studies. Information relating to target pharmacology is very limited, largely restricted to the effects of a single saturating dose of a neutralising mAb (7G6) in mouse models of autoimmune disease. At present, no pharmacokinetic data has been published for any mAb targeting CD21 and no mechanistic PKPD modelling has been conducted.

1.2. Project aim

This project aimed to explore the application of mechanistic PKPD modelling, early in the preclinical drug discovery environment, through leveraging a surrogate mAb to explore the pharmacology of mAbs targeting the novel, first in class drug target complement receptor 2 (CD21) in well-established murine models of inflammation. The overarching objective was to enhance preclinical understanding of this drug target and develop a translational framework with which to ultimately predict clinical efficacy. Despite differences in the genetic origin and expression of CD21 between mouse and man, contextualised quantitative evidence of *in vivo* pharmacology is invaluable to guide the projection of clinical efficacy.

1.3. Objectives

- ***Identify and characterise the PK of a suitable surrogate mAb to use as an investigative tool.***
  - Identify potential surrogate mAbs and generate pharmacokinetic data in mouse.
  - Define an appropriate mathematical PK model to describe the observed pharmacokinetics.
  - Confirm efficacy and primary pharmacology of the potential surrogate mAbs in a well characterised mouse model of humoral immunity.

- ***Design, test and qualify a suitable experimental mouse model of humoral immunity, aligned to both target biology and future clinical strategy.***
  - Select a suitable experimental model of humoral immunity and identify key translational biomarkers.
  - Optimise the *in vivo* study design to facilitate collection of PK and PD data suitable for PKPD modelling, through serial micro sampling and biomarker assay miniaturisation.
  - Qualify the experimental model with clinically validated 'gold standard' molecules.

- ***Investigate the concentration effect relationship of the surrogate mAb in the qualified mouse model and develop a translational mechanistic PKPD model to integrate the data.***
  - Test the surrogate mAb in the qualified mouse model across an appropriate concentration range to generate a data set suitable for mathematical modelling.
  - Build a mechanistic PD model that describes the response of key biomarkers.
  - Integrate the PK and PD models to describe the concentration effect relationship of the surrogate mAb on the response of key biomarkers.

This thesis discloses the preclinical results and mathematical modelling completed against each project objective, with the results subdivided into individual chapters around four central themes; PK characterisation (chapter 3), PK model development (chapter 4), PKPD characterisation (chapter 5) and integrated PKPD modelling (chapter 6). Each results chapter is comprised of a brief introduction, description and discussion of the results and a short conclusion. Detailed explanation of all the experimental methodology followed in this project are located in chapter 2, including the *in vivo* study designs, bioanalytical methodology and data analysis approaches. Finally, chapter 7 comprises an overall conclusion, drawing together the results of each chapter into a translational PKPD framework and identifying the knowledge gaps and future perspectives.

1.4. Scientific background

This thesis describes the application of mechanistic PKPD modelling, early in the preclinical drug discovery environment, to explore the pharmacology of a therapeutic mAb targeting complement receptor 2 (CD21). The following sections describe the background to this therapeutic drug target and its importance in mediating the interaction of the complement component of innate immunity with cells of adaptive immunity, playing a critical role in both host defence and autoimmunity. In addition, this section details the therapeutic potential of CD21 neutralisation and how this pharmacology can be explored preclinically within the context of acute mechanistic PKPD. Exploring concepts such as the pharmacokinetic considerations for therapeutic mAbs, its implication for modelling mAb PK and approaches to integrate PK and PD into mechanistic PKPD models.

1.4.1. The immune system

The immune system is an interconnected network of cells and molecules, each with a specialised role in defence of the host from infection by invading pathogens. The integrity of this immune system, combined with the pathogenicity of the invading organism, ultimately determines whether infection leads to disease. Conversely, overactivity of the immune system may also potentially spell trouble for the host, causing allergic or autoimmune disease in the individual. Consequently, the immune system represents a critical component in the health and wellbeing of the host and is thus a key target for potential medicines to combat disease in patients.

The immune system can be generalised as two fundamentally different responses; the innate response which occurs to the same extent on each occasion a particular pathogen is encountered and the adaptive response which improves on repeat exposure (Delves and Roitt, 2000). The innate response is comprised of a cellular component involving phagocytic cells (i.e. neutrophils, monocytes, macrophages) and cells that primarily release inflammatory mediators (i.e. basophils, mast cells, eosinophils), along with a molecular component involving complement, acute phase proteins and cytokines (Delves and Roitt, 2000). Adaptive immunity meanwhile involves the selection and proliferation of antigen specific T and B cells through interaction with antigen presenting cells (dendritic cells, etc.) to form a specific immune response, characterised by the release of high affinity antibodies. Unlike innate immunity, adaptive immunity has a memory and can mount a superior immune response upon subsequent exposure to the same antigen. The innate and adaptive response however do not

work in isolation, integrating into a complex interconnected immune system, forming a united host defence.

1.4.2. The role of complement in immunity

It was first recognised over 40 years ago that complement played an important role in linking innate and adaptive immunity, by acting to regulate the adaptive humoral immune response (Pepys, 1974). It is now generally accepted that this regulation is reliant on the interaction between complement receptor 2 (CR2 / CD21), found primarily on B cells and follicular dendritic cells (FDC), and antigen that has been opsonised with activated fragments of complement C3 (Carroll and Isenman, 2012). Thus, providing a bridge between the non-specific complement component of innate immunity and the generation of a specific adaptive immune response against an antigen driven by B cells and FDCs. But before delving further into the involvement of CD21 in the activation of B cells or retention and transfer of antigen, it is first necessary to consider the complement system, how it results in opsonisation of antigens and the identity of the regulatory protein CD21.

1.4.3. The complement system

The complement system is a series of plasma proteins and receptors that make up a fundamental component of the innate immune system (Carroll, 1998). These plasma proteins are predominantly synthesised in the liver as precursors and circulate in the plasma at very high concentrations, forming part of the acute phase response that reacts rapidly to antigens. Following activation, these proteins form a coordinated sequential enzymatic cascade that ultimately results in clearance of pathogens by recognition, opsonisation and finally lysis. Additionally, it can enhance other functions of the immune system such as cell recruitment, phagocytosis and humoral immunity. The complement system can be activated directly via the alternative pathway on contact with certain pathogen surfaces, or via the classical and lectin pathways following binding of a specific recognition molecule (Carroll, 1998). In the case of the classical pathway, this could be through antigen recognition by a natural repertoire IgM antibody or binding of acute phase proteins such as C reactive protein (Carroll and Isenman, 2012). Each of the three complement activation pathways converge at the formation of a C3 convertase, which can in turn cleave many additional molecules of C3, providing signal amplification.

A key outcome of complement activation is the covalent attachment of activated fragments of C3 to the antigen surface. Following proteolytic cleavage of C3 to remove C3a by the C3 convertase, a large conformational change occurs in the remaining C3b fragment. This exposes a reactive thioester carbonyl which can then react with exposed hydroxyl groups on the surface of the antigen to create a covalent ester linkage (Carroll and Isenman, 2012). Subsequent degradation of antigen bound C3b to iC3b and then C3dg occurs through factor I mediated cleavage in the presence of cofactors such as CR1, prior to further proteolytic degradation to C3d (Carroll and Isenman, 2012). These degradation fragments remain covalently attached to the antigen which is then termed as complement opsonised. Antigen bound C3 proteolytic fragments can then be recognised by high affinity complement receptors to direct other parts of the immune system, resulting in downstream effector functions.

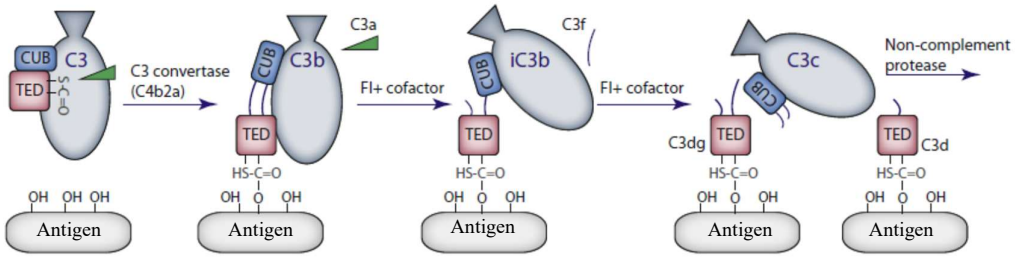

Figure 1.1. Depiction of the processes involved in the covalent attachment of C3b to antigen and its subsequent cleavage products. Adapted from Carroll and Isenman (2012) with permission.

1.4.4. Complement receptors

There are five identified high affinity complement receptors that can bind C3 proteolytic fragments. Of these five, the two best understood are complement receptor 1 (CR1 / CD35) and complement receptor 2 (CR2 / CD21), with CD21 representing the therapeutic target that underlies this thesis. CD21 is a 145 kDa transmembrane protein expressed on B cells, epithelial cells, follicular dendritic cells, thymocytes and a subset of peripheral T cells (Holers, 2014). This protein is formed of an extracellular domain composed of 15-16 repeated structural motifs termed short consensus repeats (SCR) or alternatively sushi domains. These are a characteristic structural motif found in many complement regulatory proteins and forms the structure of all the complement receptor proteins. CD21 has been demonstrated to interact specifically with the C3 proteolytic fragments iC3b, C3dg and C3d through the SCR 1-2

region, which represents the proximal N-terminal region of the protein (Molina *et al.*, 1995). This observation was confirmed through site mutation experiments by Clemenza and Isenman (2000) in the SCR1-2 region, whilst also demonstrating that CD21 binding of iC3b and C3dg was equipotent through competitive binding assays. CD21 is also known to be the receptor for the Epstein-Barr virus (EBV) envelope protein gp350/220 in human but not mouse (Tanner *et al.*, 1987, Carel *et al.*, 1990). In addition to the extracellular complement binding region, CD21 also contains a 24 amino acid transmembrane domain and a 34 amino acid cytoplasmic tail region that was identified by Tessier *et al.* (2007) to be essential for antigen internalisation. The closely related complement receptor 1 (CR1 / CD35) ranges in size between 190 and 300 kDa in human and acts as a cofactor to facilitate Factor I mediated cleavage of C3b and C4b (Jacobson and Weis, 2008). CD35 is more widely expressed than CD21, found on erythrocytes, polymorphonuclear leukocytes, mononuclear phagocytes, B cells, some T cells and mesangial phagocytes (Holers, 2014). In addition, CD35 acts as a phagocytic receptor on macrophages and neutrophils for complement opsonised immune complexes, whilst expression on erythrocytes facilitates adherence and transport of these opsonised complexes to the liver and spleen for phagocytosis (Jacobson and Weis, 2008).

In human, CD21 and CD35 are encoded by distinct but closely linked loci on chromosome 1, whereas in mouse they represent alternative splice products of a single gene Cr2 found on chromosome 1 (Ahearn *et al.*, 1996). The alternative splice variant that results in murine CD35 contains an additional 6 N-terminal SCR domains, giving rise to a 190 kDa protein that has the added ability to bind C3b and C4b. Because of the shared genetic origin in mouse, CD35 is constrained to co-express with CD21 primarily on B cells and FDCs and to a lesser extent T cells, in contrast to its wider expression in human. This causes some of the functions of CD35 demonstrated in human to be absent in mouse, such as its role as an adherence receptor for immune complexes on erythrocytes. At some stage in primate evolution the Cr2 gene lost its ability to encode the longer CD35 protein. However to recapitulate its critical function, another gene encoding a separate regulatory protein Crry in lower species was sacrificed to give rise to the human Cr1 gene (Jacobson and Weis, 2008). Crry is a complement regulatory protein bearing a similar SCR motif based structure, that has been shown to protect normal cells from inadvertent destruction by complement (Kim *et al.*, 1995). The activity of this protein is reminiscent of two alternative human proteins, decay accelerating factor (DAF) and membrane cofactor protein (MCP) (Kim *et al.*, 1995). These proteins are widely expressed and act cooperatively to inhibit complement activation, DAF by blocking convertase assembly and MCP through its requirement as a cofactor for Factor I mediated cleavage of C3b and C4b

(Kim *et al.*, 1995). It is therefore clear that tight regulation of complement is crucial for viability of a species during evolution.

1.4.5. Complement receptor 2 (CR2 / CD21)

The complement receptor CD21 plays an important role in the regulation of humoral immunity through its interaction on B cells and follicular dendritic cells (FDC) with C3d opsonised antigen (Carroll and Isenman, 2012). The best characterised mechanism is through the involvement of CD21 in the B cell coreceptor complex, which through coligation with the B cell receptor (BCR) lowers the threshold of activation for B cells. In the presence of a high antigen dose, there is sufficient crosslinking of the BCR so that the signal can directly induce activation of the antigen specific B cell (Carroll and Isenman, 2012). However, in the presence of limited amounts of antigen, the signal generated is insufficient to trigger B cell activation unless coligation with the B cell coreceptor complex occurs. This coreceptor complex is formed of CD21, CD19 and CD81 and triggers positive signalling pathways through the cytoplasmic tail of CD19, which is brought into the proximity of BCR associated kinases and rapidly phosphorylated (Fearon and Carroll, 2000). Coligation of BCR and the coreceptor complex leads to signal enhancement, lowering the threshold for activation by up to 1000-fold compared with BCR signalling alone (Dempsey *et al.*, 1996, Lyubchenko *et al.*, 2005, Luxembourg and Cooper, 1994).

In addition to its role in the coreceptor complex, CD21 expressed on FDC within secondary lymphoid tissues can act by presenting C3d opsonised antigen to naive or previously antigen engaged B cells during the process of affinity maturation, class switching and the generation of effector and memory B cells (Fang *et al.*, 1998). In this case CD21 is acting as a molecular adjuvant, lowering the antigen requirement to generate an antibody response (Carroll and Isenman, 2012). Meanwhile, Whipple *et al.* (2004) identified that CD21 on marginal zone B cells was important in the capture, relocation and transfer of immune complexes to FDCs. Whilst CD21 is also reported to be important in the transfer of immune complexes from macrophages to follicular B cells for delivery to germinal centres (Phan *et al.*, 2009).

There is some evidence to suggest that CD21 activation can directly result in intracellular signalling via a PI3 kinase related pathway, independent of CD19 (Bouillie *et al.*, 1999), implicating a signalling role of the short cytoplasmic domain. Indeed, the cytoplasmic domain is also critical for the internalisation of cross linked C3dg and for the internalisation and infection of cells by EBV (Carel *et al.*, 1990). Tessier *et al.* (2007) confirmed this observation

using human CD21 cytoplasmic tail mutants, whilst also demonstrating that internalisation of CD21 following binding of non-crosslinking anti-CD21 antibody or C3dg follows a clathrin-mediated internalisation mechanism that differs to that followed when engaged by a strongly cross-linking ligand. This implies that the intracellular signalling and trafficking outcomes differ depending on the nature of the ligand (Tessier *et al.*, 2007). Although internalisation following binding of anti-CD21 mAbs to murine CD21 has not been reported specifically, down modulation of surface expressed CD21 has been observed (Kulik *et al.*, 2015).

1.4.6. Soluble CD21

In addition to CD21 as membrane bound receptor, a shorter (126 kDa) soluble form of CD21 (sCD21) exists that is widely considered to result from the proteolytic cleavage of cell surface receptor in a process known as ectodomain shedding, retaining its capacity to bind its natural ligands (Larcher *et al.*, 1995, Masilamani *et al.*, 2003a, Hoefer *et al.*, 2008). Although the biological function of sCD21 has not been fully described, it has been reported that purified sCD21 can regulate human monocyte activation and differentiation through its binding of CD23 (Frémeaux-Bacchi *et al.*, 1998). Whilst recombinant sCD21 has been reported to suppress the antibody response to T-dependent antigen (Hebell *et al.*, 1991), suggesting a potential role for sCD21 in immune regulation. Reduced levels of sCD21 have been widely reported in patients with autoimmune disease when compared with healthy individuals, including systemic lupus erythematosus (SLE), Sjögren's syndrome (Masilamani *et al.*, 2004), rheumatoid arthritis (Masilamani *et al.*, 2003b) and systemic sclerosis (Tomita *et al.*, 2012). In contrast, sCD21 levels are reported as increasing in sera from patients with B cell chronic lymphocytic leukaemia (Lowe *et al.*, 1989).

CD21 ectodomain shedding is thought to result from cleavage close to the plasma membrane within the SCR16 region by an as yet unidentified protease (Aichem *et al.*, 2006). Although CD21 is constitutively shed, the shedding rate has been demonstrated to be enhanced following direct B cell activation *in vitro* using the mitogen PMA + ionomycin (Masilamani *et al.*, 2003a), by stimulation of the BCR with anti-IgM + anti-CD40 (Masilamani *et al.*, 2003a) or with the oxidant pervanadate (PV) (Aichem *et al.*, 2006). This was demonstrated by Aichem *et al.* (2006) to be redox-regulated process, inducible by oxidation via a tyrosine kinase mediated signalling pathway or alternatively through reducing agents that directly activate metalloproteases. Hoefer *et al.* (2008) confirmed the same stimuli induced shedding of murine CD21, whilst additionally identifying the cytoplasmic domain to be an important modulator.

This lead Hoefer *et al.* (2008) to suggest CD21 shedding may be a mechanism to fine tune B cell activation. Although binding by therapeutic antibodies has been reported in some cases to result in ectodomain shedding of the target receptor, such as CD30 and CD44 (Hayashida *et al.*, 2010), this has not been specifically reported for CD21.

1.4.7. Therapeutic potential of targeting CD21

While humoral immunity provides a critical barrier to infection by pathogens, its dysfunction is thought to underlie many autoimmune disorders. Autoreactive B cells are thought to follow the same mechanism as conventional B cells to become isotype switched memory and effector cells, thus would have similar requirement for CD21 during antigen presentation, activation and differentiation. Therapeutic blockade of CD21 may therefore present an opportunity as a therapy for autoimmune conditions that are characterised by the formation of germinal centre and ectopic lymphoid structures, ultimately resulting in production of destructive autoantibodies (Carroll and Isenman, 2012). This includes diseases such as rheumatoid arthritis (RA) and systemic lupus erythematosus (SLE) (Holers, 2014). Current clinical strategies for these diseases often result in decreased immunocompetence, such as Rituximab in RA or Belimumab in SLE, which are effective via the depletion of either the total B cell population or a subset of this population. In contrast, it is thought that an anti-CD21 mAb could specifically modulate the B cell response to self-antigen to subdue the humoral immune response, whilst leaving the naive immune system relatively intact.

An extremely rare clinical case of complete CD21 deficiency reported by Thiel *et al.* (2012), provides some insight as to the therapeutic outcome of CD21 blockade. This patient presented with recurrent infections, reduced class-switched memory B cells and hypogammaglobulinemia with a clinical phenotype similar to common variable immunodeficiency (CVID) (Thiel *et al.*, 2012). This supports the hypothesis that CD21 blockade would impact memory B cell function and reduce antibody response. However, despite these reported deficiencies, the patient displayed a normal immune response to vaccination with protein antigens in adjuvant (Thiel *et al.*, 2012), consistent with an ability for high antigen load to overcome the CD21 requirement. This suggests an encouraging safety profile, preserving the normal immune response to infection whilst selectively targeting low affinity antigen often characteristic of autoantigens.

1.4.8. Preclinical investigation of pharmacology using acute mechanistic PKPD

Acute, mechanistic pharmacodynamic models are a popular experimental approach for characterising the primary pharmacology of novel investigational drugs during preclinical development, in a relatively simple, short duration *in vivo* animal study. Mechanistic *in vivo* models take advantage of molecular level understanding of drug and target interactions, narrowing investigation to a specific biological pathway, without mimicking an overall disease phenotype. Through the assessment of biomarkers close to the mechanism of drug action, this type of study provides a quantitative and potentially translational bridge between *in vitro* experimentation and the disease setting. This translation can be achieved through establishment of a PKPD relationship, incorporating drug exposure, target engagement and the downstream biological effect into an integrated mathematical model. Where knowledge of the biological differences between species exists, such a PKPD relationship developed in preclinical species can potentially be scaled to make clinical projections. This strategy is popular in early drug discovery of small molecule therapeutics, providing a translational framework for predicting therapeutic dose. However, its application to the discovery of large molecule protein therapeutics is more limited.

Selection of an appropriate *in vivo* mechanistic model is the initial and critical step in this strategy, requiring alignment to the biology of the target, the primary pharmacology of the drug and the desired clinical pathway. Clinical line of sight is an important strategic consideration, even during early drug discovery, to extract maximum translational value from preclinical data. With the therapeutic potential for CD21 neutralisation in autoantibody driven disease, SLE was identified as one of the primary indications for clinical development. SLE is a multisystem autoimmune disease of unknown cause, with diverse clinical manifestations (Sullivan *et al.*, 2016). The aberrant production of autoantibodies against nuclear (ANA), cytoplasmic and cellular membrane antigens are a serological hallmark of SLE and a widely used diagnostic marker of disease activity (Cozzani *et al.*, 2014). Thus implicating immune dysregulation as a driving force behind disease pathogenesis (Sullivan *et al.*, 2016). The early clinical development of several recent experimental drugs that target the T-cell contribution to immune dysregulation in autoimmune disease, have incorporated primary immunisation in the FTIH study design. Quantification of the primary antibody response to antigen immunisation is a sensitive and widely used approach for assessment of immunocompetence, both preclinically and clinically (Swaminathan *et al.*, 2014). Through incorporation of this immunocompetence assessment into the FTIH exposure and tolerability study, it provides an early proof of mechanism readout and elaborates the relationship between PK, target

engagement and efficacy on a key disease biomarker. This clinical strategy was identified early as the desired progression route for an anti-CD21 mAb. Thus, enabling alignment of a similar mechanistic approach to build the preclinical PKPD package in rodents, utilising primary immunisation to investigate the relationship between PK, target engagement and efficacy.

1.4.9. T-dependent antibody response (TDAR)

There are two pathways through which primary immunisation with an antigen can stimulate B cell maturation to plasma cells capable of antigen specific antibody production. The first is when B cells that have engaged antigen are induced to grow, with or without help from CD4+ T cells, as plasmablasts in extrafollicular foci in the spleen or lymph node. This extrafollicular antibody response is the first wave of the primary humoral immune response. The second pathway occurs when B cells that have bound antigen make cognate interactions with antigen primed CD4+ T cells in a follicular response that results in germinal centre B cells. These B cells undergo a somatic hypermutation mechanism that introduces mutation into the rearranged immunoglobulin variable region genes. Through a periodic process of antigen and CD4+ T cell mediated selection, this germinal centre reaction propagates B cells containing high affinity sequences for the antigen, which can differentiate into long lived plasma cells and memory B cells. This results in the second high affinity wave of the primary immune response and provision of the strong recall (secondary) immune response that is characteristic of adaptive immunity.

Different antigen types vary in their ability to stimulate these two pathways. Protein antigens typically require help to stimulate B cells, through co-stimulatory signals from antigen primed Th cells, with this type of antigen denoted a thymus or T cell dependent (TD) antigen. However, not all antigens require Th cell help to activate B cells, with these denoted T cell independent (TI). TI antigens typically contain highly repetitive epitopes or contain ligands that can directly activate toll like receptors (TLR), with the group sub-divided into TI-1 antigens (e.g. LPS, peptidoglycan, etc.) and TI-2 antigens (e.g. polysaccharides, nucleic acids, etc.). These TI antigens provide strong B cell receptor (BCR) signalling, or a combination of BCR and TLR signalling, which can bypass the requirement for Th cell help in stimulating B cell proliferation. It is currently considered that TD antigens alone result in the formation of stable germinal centre structures, due to the requirement for cognate interaction with CD4+ T cells during the periodic B cell selection mechanism. With the appearance of high affinity self-antibodies and germinal centre structures the hallmark of many autoimmune diseases,

including SLE, it is TD antigens that represent mechanistic alignment and are thus the focus of investigation.

The primary immune response to immunisation with a TD antigen is typically referred to as the T-dependent antibody response (TDAR), providing assessment of the complex immune processes involved, including; antigen presentation, priming, collaboration of T and B lymphocytes, antibody production and class switching (Swaminathan *et al.*, 2014). The TDAR to antigens such as sheep red blood cells (SRBC) has been extensively evaluated in nonclinical studies for elaboration of the biology and characterisation of chemical and pharmaceutical immunotoxicity. Consequently, a lot is known about the sequence of events that follow immunisation with antigen and the kinetics of this response.

1.4.10. Phases of the T-dependent antibody response (TDAR)

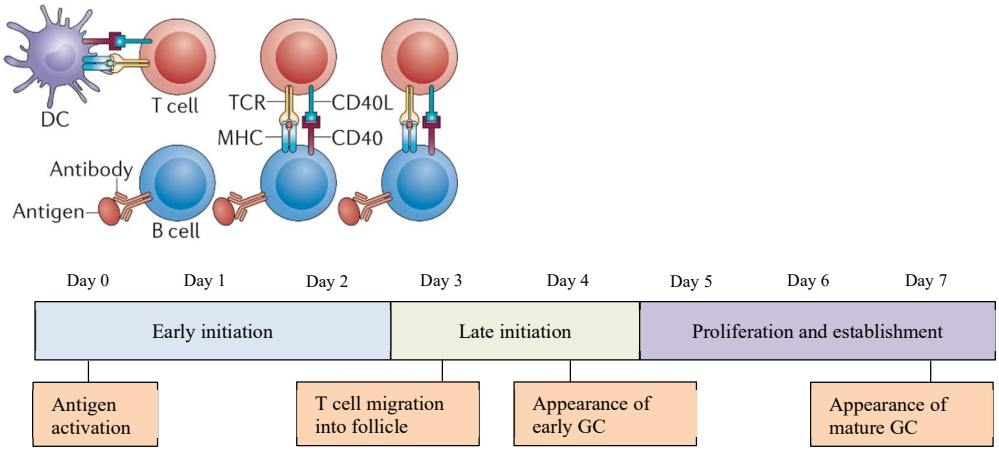

Figure 1.2. The three phases of the early T-dependent response to antigen. An early initiation phase characterised by the activation of B and T cells by their cognate antigen and their interaction via antigen bound MHC on the B cell surface. A late initiation phase characterised by the migration of T and then B cells out of the interfollicular region and early appearance of GC. Finally, a proliferation and establishment phase in which the GC grows and matures. Adapted by permission from Springer Nature, De Silva and Klein (2015).

As reviewed by De Silva and Klein (2015) and illustrated in figure 1.2, the TDAR is considered to occur in three distinct phases over the course of the first seven days following antigen exposure. The early initiation phase (1) between day 0 and 2 encompasses the activation of B and T cells by antigen and the long lived cognate interaction of these antigen

primed cells within the interfollicular region of secondary lymphoid tissue. The response starts when B cells bind antigen through cognate binding to antigen specific surface immunoglobulin, known as the B cell receptor (BCR) (reviewed in MacLennan *et al.*, 2003). Binding of the BCR has two outcomes, intracellular signalling to activate the B cell and internalisation of antigen for degradation and return to the cell surface as peptides bound to MHC class two molecules. To maximise the probability of this rare binding event occurring, the secondary lymphoid organs are specially adapted to facilitate efficient presentation of antigen to lymphocytes (Batista and Harwood, 2009). Blood borne antigen is efficiently sampled by the spleen, with antigen encountered in blood by recirculating B cells, or in the highly perfused splenic marginal zone by nonrecirculating B cells, inducing rapid translocation of the B cells to the splenic T zone. Lymph nodes are also positioned throughout the lymphatic system to enable antigen sampling of afferent lymph, with antigen binding inducing B cells to translocate and interact with T cells within the same node.

During the early initiation phase, naïve T cells also encounter antigen. Tissue resident antigen presenting cells (APCs), such as dendritic cells, recognise pathogen via pattern recognition receptors and become activated, migrating to the secondary lymphoid organs. These activated APCs internalise and process antigen for presentation on the cell surface via MHC class I and II molecules. Antigen bound MHC class II complex can be recognised by the T cell receptor and CD4 coreceptor of antigen specific naïve T cells. The activated T cell receptor associates with CD3 to trigger a network of downstream signalling pathways, leading to CD4+ T cell proliferation and differentiation into specific effector cells (Tfh, Th1, Th2, etc.), dependent on the cytokine milieu, antigen, type of APC and other costimulatory molecules (Luckheeram *et al.*, 2012). These CD4+ T cells are now antigen primed and available to form long lived cognate interactions with antigen specific B cells through antigen bound MHC class II molecules displayed on their surface. T follicular helper cells (Tfh), a specialised subset of CD4+ T cells provide additional signals to activate and direct the B cell response, such as CD40L which binds to CD40 on the B cell, and various secreted effectors molecules such as IL4. Consequently, within the first 24 h following antigen exposure, specific B cells have bound antigen through BCR, processed and presented it on their surface and migrated to interact with antigen primed CD4+ T cells in the T cell rich zones of secondary lymphoid tissues (De Silva and Klein, 2015).

The late initiation phase (2) between day 3 and 4, is characterised by migration of T cells into the follicle, followed by B cells one day later (De Silva and Klein, 2015). At this stage, activated B cells can adopt one of two paths, through; (1) movement into the extrafollicular

areas and subsequent proliferation and terminal differentiation into short lived plasma cells, or (2) movement into the B cell follicle followed by proliferation and GC establishment, resulting in long lived plasma cells and memory B cells (Allen *et al.*, 2007). The specific signals that instruct this fate decision remain poorly understood, although various studies suggest that this may be driven by BCR affinity, the amount of antigen or costimulatory signals from T cells (Allen *et al.*, 2007). B cells recruited to the extrafollicular response enter into proliferation and terminal differentiation to antibody secreting cells that survive for only a few days, producing the early antibody response of predominately IgM isotype (MacLennan *et al.*, 2003).

The proliferation and establishment phase (3) occurs between day 5 and 7, in which the germinal centre grows and matures within the follicle into the characteristic dark and light zone pattern. Within the dark zone, activated B cells undergo a process of rapid proliferation and somatic hypermutation of their antibody variable region genes. Periodically, these cells travel to the light zone for competitive selection based on antigen binding and presentation to Th cells. Those expressing high affinity antigen specific BCR are positively selected, promoting survival or terminal differentiation. Surviving GC B cells may recycle to the dark zone for iterative rounds of mutation and selection or exit the GC and terminally differentiate into long lived antibody secreting plasma cells or memory B cells (Allen *et al.*, 2007). This efficient affinity maturation process results in the production of high affinity antigen specific antibodies that become apparent seven days post antigen exposure.

A key feature of the late phase of the TDAR is a change from an IgM to an IgG isotype dominated response. This change is modulated by a combination of cytokine and co-stimulatory signals received from Th cells which trigger activated B cells to undergo a DNA level mechanism referred to as class switch recombination. A process in which switch regions within the immunoglobulin gene are cleaved and re-joined to a different heavy chain constant region (IgG, IgA or IgE). The change results in cells that can secrete antibody with changed effector function, whilst retaining specificity. There are four subclasses of IgG (IgG1, IgG2a, IgG2b and IgG3) in both mouse and human, with the proportion of the different subclasses varying according to the prevailing cytokine environment (Collins, 2016).

1.4.11. Keyhole limpet haemocyanin (KLH)

There are numerous reported TD antigens, however selection of the ideal TD antigen for TDAR evaluation is dependent on factors such as manufacturing quality, immunogenicity and translational value. Whilst historically, sheep red blood cells (SRBC) represent the

predominantly reported TD antigen for nonclinical immunotoxicity investigation, obtaining a reliable and consistent source can be difficult, particularly in the pharmaceutical industry. Other widely reported TD antigens include; keyhole limpet hemocyanin (KLH), tetanus toxoid (TT), hepatitis B surface antigen (HbsAg) and bacteriophage ΦX174 (phi X174) (Lebrec *et al.*, 2014b). Although TT and HbsAg are potentially advantageous due to their clinical relevance, the human population is widely immunised against both antigens and thus cannot be used clinically to evaluate the primary neo-antigen response, restricting translational value. Meanwhile, despite the extensive publication with phi X174 in patient populations, it is not commercially available and is rarely used preclinically. In contrast, KLH has been widely adopted in pharmaceutical research, with commercial sources of high purity material available (including clinical grade) demonstrating robust immunogenicity and offering clinical options for primary neo-antigen and secondary recall studies.

KLH is a multimeric, oxygen carrying metalloprotein, extracted from the haemolymph of the giant keyhole limpet, Megathura crenulata. Modern aquaculture techniques mean that KLH can now be sustainably and responsibly sourced at relatively low cost, following depletion of the population of this uncommon species of mollusc. The KLH protein itself is a large, cylindrical, copper containing molecule comprising a variable number of the sub-units KLH1 (390 kDa) and KLH2 (350 kDa), resulting in an approximately 8000 kDa protein (Swaminathan *et al.*, 2014). The use of KLH as a TD antigen is widely reported, both preclinically and clinically in several formats, both with and without the use of an adjuvant. Whilst the KLH protein itself is highly immunogenic, adjuvants are often added to result in a stronger and more robust humoral immune response. KLH is frequently described as being co-administered with the mineral adjuvant Alum, a term covering several aluminium salt preparations. Whilst the biological mechanism by which adjuvants potentiate the immune response are not well characterised, Alum has been shown to result in increased local cytokine and chemokine release at the injection site, recruitment of immune cells and enhanced antigen presentation on antigen presenting cells (Awate *et al.*, 2013).

1.4.12. Clinical application of KLH TDAR

KLH immunisation has been widely used in the clinic to assess the impact of various physiological and disease states, along with novel therapeutics, on the humoral immune response in human, with an excellent clinical safety profile (Swaminathan *et al.*, 2014). In recent years, the use of the KLH TDAR test in first in human (FTIH) clinical trials has become popular as an early proof of mechanism read for novel immunosuppressants. This was the

approach adopted by Sullivan *et al.* (2016) in a FTIH study with the experimental ICOSL specific mAb AMG 557, which demonstrated efficacy against KLH specific IgG following primary and secondary immunisation. Similar approaches were used in the FTIH studies with two experimental CD28 antagonists, the domain antibody (dAb) Lulizumab pegol (Shi *et al.*, 2017) and the pegylated antibody fragment (fAb) FR104 (Poirier *et al.*, 2016), both demonstrating efficacy against antigen specific IgG. KLH immunisation was again used in an FTIH study with the experimental anti-CD40 mAb CFZ533 (Slade *et al.*, 2016), with efficacy again demonstrated against the IgG response. The drug target of each of these examples is the T cell component of the TD response, providing strong evidence of the TD nature of the humoral response to KLH immunisation.

The preclinical development path was reported in two of the examples described previously, with a KLH TDAR study implemented within the preclinical package, not only for proof of mechanism confirmation, but also as an opportunity to integrate the PK and PD aspects for selection of a safe and effective clinical dose. The experimental anti-CD40 mAb, CFZ533, was shown to inhibit the KLH recall TDAR in cynomolgus monkey following saturation of the target (Ristov *et al.*, 2018), which translated to the clinical efficacy observed (Slade *et al.*, 2016). However, the integrated preclinical PKPD strategy described by Yang *et al.* (2015) for progression of Lulizumab (BMS-931699), took this translational piece further. Due to the concern regarding CD28 as a drug target, following the well-publicised clinical trial disaster with the CD28 agonist TGN1412, a thorough preclinical PKPD safety and efficacy package was produced. This package describes the integrated approach taken to determine the minimal anticipated biological effect level (MABEL), using a mathematical PKPD model describing the relationship between PK, receptor occupancy and PD (KLH specific IgG) in mouse and cynomolgus monkey (Yang *et al.*, 2015). Indeed an *in vivo* EC_{50} of 7.6 nM was derived from the cynomolgus monkey PKPD modelling, which was subsequently proven to be in excellent agreement with the *in vivo* EC_{50} of 4.8 nM obtained from the human phase 1 clinical study (Yang *et al.*, 2015).

1.4.13. Evidence for the immunomodulatory effect of CD21 on TDAR

Therapeutic neutralisation of CD21 is a novel mechanism for the treatment of autoimmune disease, with no prior clinical trials and a paucity of preclinical data describing its pharmacology. However, the biological function of CD21 and the closely related receptor CD35 have been investigated in mice in some detail, with growing literature evidence that describes the immunomodulatory effect of CD21 inhibition. Indeed, a number of genetic

knockout studies in mice have demonstrated a severe deficiency in the humoral immune response to T-dependent antigens. Molina *et al.* (1996) showed that targeted disruption of the Cr2 gene in mice resulted in an impaired humoral immune response to the TD antigen SRBC. Meanwhile, Ahearn *et al.* (1996) described a similar outcome in Cr2-/- mice following immunisation with the bacteriophage phi X174, characterised by a reduction in serum antibody titre and the number and size of germinal centres in the spleen. Further, more elaborate, genetic studies in mice investigating affinity maturation specifically (Wu *et al.*, 2000), the separate roles of CD21 and CD35 (Donius *et al.*, 2013) or human CD21 transgenics (Kulik *et al.*, 2011), have all provided further evidence for the key role of CD21 in the humoral immune response to TD antigens. Similarly, therapeutic intervention of CD21 with murine specific antibodies (Heyman *et al.*, 1990, Kulik *et al.*, 2015) has been shown to impair the humoral response to T-dependent stimuli, as discussed in the following section.

1.4.14. Murine CD21 specific antibodies

The availability of good quality tool molecules underpins the relevance of pursuing preclinical pharmacology studies, dictating the translational value of the data generated. This is of particular importance when considering therapeutic targets which exhibit restricted homology across species. In mice, CD21 and CD35 are the product of a single gene, whilst in humans they are encoded by distinct genes. Consequently they share only 67% homology at the amino acid level (Kurtz *et al.*, 1989). This limits the potential cross reactivity of high affinity mAbs, adding the requirement for surrogate mAbs that are specifically raised against the protein in the species of interest. To be of translational value these surrogate mAbs must display identical binding specificity with similar affinity, along with the same downstream functionality.

The mouse was selected as the preclinical species of choice for PKPD investigation in this project for two reasons. The first is the availability of prior of knowledge of CD21 in the mouse and data pertaining to the therapeutic potential of CD21 neutralisation in well characterised murine models of disease. The second is the availability of a limited pool of blocking antibodies which neutralise the binding capacity of CD21 for its natural ligands (C3d/C3dg) in mouse. A handful of antibodies of rat origin have been published against mouse CD21, with the most widely described of these denoted 7G6. This mAb was first reported by Kinoshita *et al.* (1988) and was raised against purified full length murine CR1 (CD35), which contains the identical protein sequence to CD21 with the addition of 6 further SCRs that inherit CD35 its differentiated binding ability. Subsequent investigation identified 7G6 as neutralising the function of CD21, with pharmacological activity demonstrated *in vivo* through the inhibition

of the antibody response to T-dependent antigen stimuli such as sheep red blood cells (SRBC) and keyhole limpet haemocyanin (KLH) (Heyman *et al.*, 1990). Later characterisation of this mAb highlighted that its binding epitope is in the SCR1/2 region of CD21 and that binding results in blocking the binding of CD21s natural ligands iC3b, C3d and C3dg (Molina *et al.*, 1995, Martin *et al.*, 1991). Murine CD21 is additionally able to bind human C3dg, with Martin *et al.* (1991) demonstrating that this interaction can be blocked by mAb 7G6 but not the human specific neutralising mAb OKB7. However, species specific binding of mAbs 7G6 and OKB7 can be manipulated through substitutions among residues 8-15 (SCR1), demonstrating this site is a critical determinant of binding the natural ligands of both human and murine CD21 (Martin *et al.*, 1991). During identification of mAb 7G6, two additional antibodies were identified with differential binding. 7E9, that binds CD21 but is non-competitive with 7G6 and non-functional with regards to the downstream effects of complement binding (Heyman *et al.*, 1990, Kinoshita *et al.*, 1988). 8C12, that binds to CD35 alone and downregulates its expression on B cells, impacting EC3b rosette formation but not the T-dependent antibody response (Heyman *et al.*, 1990, Kinoshita *et al.*, 1988).

Recently, due to the limitation of the rat backbone of mAb 7G6, a neutralising mAb of mouse origin against murine CD21 was described by Kulik *et al.* (2015), denoted 4B2. This mAb was raised against a recombinant shortened form of murine CD21, consisting of the SCR1-4 (amino acid 1-257) region and raised in a *Cr2* knockout mouse strain (Kulik *et al.*, 2015). Activity of this mAb was characterised *in vitro*, through demonstration of competition for binding with 7G6 by ELISA and blockade of biotinylated human C3dg binding to recombinant CD21 (Kulik *et al.*, 2015). Activity was also demonstrated *in vivo*, through the ability of 4B2 to down regulate CD21 expression following dosing and through efficacy in a T-dependent SRBC model and in a mouse collagen induced arthritis model (Kulik *et al.*, 2015).

GSK also embarked on a campaign to raise a mouse species matched antibody, using a recombinant protein consisting of the extracellular region containing SCR 1-16 (amino acid 21 – 970) but excluding the cytoplasmic tail region. Specific antibodies were raised through inoculation of SJL/J mice with recombinant CD21 prior to clonal selection, fusion and production. A single clone denoted 9E10 was selected, based upon its ability to compete with 7G6 for binding to the recombinant CD21 protein and its ability to bind native CD21 on B cells measured by flow cytometry (Appendix IV).

1.4.15. Pharmacokinetic considerations for therapeutic antibodies

Pharmacokinetics broadly describes the fate of molecules once they enter the body, until the point that no trace remains. In general, the pharmacokinetic properties of therapeutic drugs are governed by the principles of absorption, distribution, metabolism and excretion (ADME). This remains true whether that therapeutic drug is a classic small molecule or a large molecule biotherapeutic, such as a mAb. However, in large part owing to the high molecular weight exhibited by mAbs, the specific pharmacokinetic behaviour may be significantly different. Whilst the underlying principles and mechanisms affecting the PK of small molecules are relatively well understood, significant gaps exist in mechanistic understanding of those underlying mAb ADME (Ezan, 2013, Vugmeyster *et al.*, 2012). Additionally, the PK of a mAb therapeutic may be significantly perturbed by its biology, both through its specific interaction with its protein target and through its interactions with the normal physiological processes affecting natural antibodies. The fundamental concepts underpinning mAb PK and driving the study design used to characterise the PK of the surrogate CD21 mAbs is reviewed here against current scientific knowledge.

1.4.15.1. Absorption

In pharmacokinetics, absorption describes the process of the drug reaching the systemic blood circulation from its site of administration. In the main, clinically approved mAb therapies are administered parenterally via intravenous (IV) infusion and as such bypass absorption. However, clinical limitations associated with IV infusions, such as the requirement for hospitalisation or the risk of infusion related reactions, has led to increased interest in subcutaneous (SC) and intramuscular (IM) routes of administration for mAb therapy. Except that to date, the number of mAbs approved for SC or IM administration is small, primarily as a result of physiological constraints which limit injection volume (Deng *et al.*, 2012). Typically this restricts use to highly potent mAbs or necessitates repeated administration (Deng *et al.*, 2012). Intraperitoneal (IP) administration, which is routinely employed during preclinical investigation of surrogate mAbs, is an administration route of little relevance to the clinic. This administration route is often used as a result of the physical and technical challenges associated with IV or SC administration in small rodents. The mechanisms that are involved in the absorption of mAbs from the interstitial space following SC, IM or IP administration are not well understood and the impact of these mechanisms on PK is the subject of some debate (Zhao *et al.*, 2013). It is generally thought that the primary route of systemic absorption for mAbs from the interstitial space is convective transport via the

lymphatic system. This is based on work by Supersaxo *et al.* (1990), who investigated the impact of molecular weight on lymphatic absorption in a cannulated sheep model. The study concluded that a linear relationship existed between molecular weight and the percentage of the dose absorbed into the lymph, with the majority of absorption for proteins greater than 16 to 20 kDa via the lymphatic system (Supersaxo *et al.*, 1990). Conversely, in a cannulated rat model reported by Kagan *et al.* (2007), where lymph was collected via a cannulated thoracic lymph duct, less than 3% of the SC administered dose was detected in the lymph for three therapeutic proteins. Neither group has thoroughly investigated the fate of IgG in their studies, leaving the exact mechanism of absorption for mAbs undefined.

The kinetics of mAb absorption following SC, IM or IP administration is relatively slow, with the time to reach maximal systemic concentration (T_{max}) typically reported in human to be in the region of 1-8 days. Adalimumab for example, has a T_{max} of 5.5 days (Zhao *et al.*, 2013). It is thought that lymphatic flow rate is the primary determinant of T_{max} (Zhao *et al.*, 2013). However other factors such as the site of injection, localised blood flow or external factors such as exercise or massage may also influence rate of absorption. Kagan *et al.* (2012) investigated the role of dose, injection site and injection volume in rats with the anti-CD20 antibody Rituximab. The study showed that bioavailability was inversely proportional to dose, whilst the anatomical site of SC injection influenced both the rate and extent of Rituximab absorption. The extent of bioavailability of proteins after SC administration is often demonstrated to be incomplete and highly variable (Porter and Charman, 2000). Catabolism at the injection site is primarily thought to be responsible (Wang *et al.*, 2008). Oral administration has limited applicability to mAbs, in part owing to their large molecular weight and high polarity leading to minimal diffusion through the gastrointestinal (GI) epithelium (Lobo *et al.*, 2004), but primarily due to denaturation of the protein structure by the acidic pH of the stomach combined with proteolytic degradation within the GI tract (Reilly *et al.*, 1997).

1.4.15.2. Distribution

Distribution describes the reversible dispersion of a drug from the systemic circulation out into the tissues of the body and is characteristically very different for mAbs compared with small molecule drugs. In general, small molecule drugs, as a consequence of their ability to readily diffuse across endothelial cells, are able to widely distribute into tissues along a concentration gradient and rapidly reach equilibrium. Large polar macromolecules like mAbs are conversely only able to diffuse very slowly across cells, largely restricting transcellular diffusion. Whilst it has been proposed that extravasation is primarily reliant on paracellular convective transport,

recent evidence has shown transcellular endocytosis may also play a role in the tissue distribution of mAbs (Garg and Balthasar, 2007). The pharmacokinetic impact of the slow distribution of mAbs is that the typical reported values of volume of distribution at steady state (Vd_{ss}) are low and approximately equal to the plasma volume (Keizer *et al.*, 2010). Commentators in the literature have highlighted shortcomings in the classic method for calculating Vd_{ss} using standard non compartmental analysis of plasma data (Wang *et al.*, 2008). Whilst this method is widely applied to small molecule PK, where in general drug in the plasma is in rapid equilibrium with both the elimination compartment, typically the liver or kidney, as well as the tissue compartment. For mAbs, which typically exhibit elimination from tissues sites that are not in rapid equilibrium with the plasma, standard non compartmental analysis of plasma concentration data will often lead to an underestimation of Vd_{ss} (Wang *et al.*, 2008).

It is generally considered that extravasation of mAbs into tissue interstitial fluid is dependent on paracellular transport. Paracellular transport proceeds by convection, a mechanism by which a macromolecule moves with fluid flow from the blood into the interstitial space of the tissue, along an osmotic pressure gradient through pores in the capillary wall (Tabrizi *et al.*, 2010a). Capillary physiology is therefore a determinant of the accessibility of a therapeutic mAb to various tissue types (Lobo *et al.*, 2004). In the majority of tissues, blood capillaries exhibit continuous endothelia where adjacent cells form a continuous lining separated only by tight junctions. This represents a significant barrier to macromolecules such as mAbs, with minimal pore size and increased tortuosity of the paracellular path leading to limited fluid flow and increased resistance to macromolecular movement (Lobo *et al.*, 2004). However in 'leaky' tissues such as the GI tract and kidney glomerulus, the endothelium contains fenestrae, small pores of 30 to 80 nm diameter that allow increased fluid flow into these tissues (Weinstein and van Osdol, 1992). Sinusoidal capillaries found in specialised tissues such as the liver, spleen and bone marrow have a discontinuous endothelium containing clefts approximately 100 nm in diameter, that bestow antibodies with free passage. The rate of extravasation is ergo determined by the product of lymph flow rate and a 'sieving' efficiency term $(1-\sigma)$ where σ is a reflection coefficient likely to be dependent on vascular endothelial porosity (Lobo *et al.*, 2004). In complete contrast the blood brain barrier has an extremely dense structure, where the intracellular junctions are held very close by a belt of tight junctions (Weinstein and van Osdol, 1992). Consequently, very little distribution of mAbs is possible to the brain.

It has been suggested that transcellular endocytosis mechanisms may also play a role in mAb extravasation and tissue distribution. IgG may be taken into the vascular endothelial cells via

non-specific fluid phase endocytosis, where it will encounter the acidic environment of the cellular endosome and become bound to the neonatal Fc receptor (FcRn), providing a mechanism by which to traverse the cell (Lobo *et al.*, 2004). It has been demonstrated that FcRn is expressed in vascular endothelial cells and that it may play a role in IgG homeostasis (Garg and Balthasar, 2007). But crucially it has also been demonstrated that FcRn can facilitate bidirectional transport across epithelial cells, suggesting that it may also play a role in the distribution of IgG (Dickinson *et al.*, 1999). This has been investigated in FcRn knockout mice by Garg and Balthasar (2007) who demonstrated lower tissue exposures of a mouse anti-platelet IgG1 antibody in FcRn knockout mice compared with wild type.

Following extravasation, mAbs are subject to slow distribution within the tissue driven by diffusion and convection (Wang *et al.*, 2008). This distribution may be impacted by high affinity binding of the antibody to its specific target or alternatively through non-specific binding mechanisms. This is commonly referred to as target mediated drug disposition (TMDD), a term first introduced by Levy (1994) to describe drugs whose PK is influenced by specific high affinity binding. This is not a concept unique to mAbs, with interest in this phenomenon first stimulated during clinical development of small molecule angiotensin-converting enzyme (ACE) inhibitors in the 1980's (Levy, 1994). Here they reported prolonged terminal phases that converged at the same plasma concentration regardless of the dose administered, which was attributed to binding of a fixed pool of target (Levy, 1994). In most cases, the extent of target available is small relative to the concentration of a small molecule drug, saturating any impact on the PK, with impact on the terminal phase likely to occur at concentrations far below those of clinical relevance and analytical performance. The phenomenon is in contrast commonly observed with mAbs, particularly those targeting cell membrane expressed targets with high target density or rapid turnover (Deng *et al.*, 2012). The increased observation of TMDD with mAbs is partly due to the high binding affinity, but also as a consequence of the typically low molar excess of drug in relation to target. The influence of target kinetics on the pharmacokinetics of a drug has been described in a mathematical TMDD model developed by Mager and Jusko (2001a). This model has been widely applied to mAb drugs, with increasingly complex modifications emerging, accounting for variables such as tissue localisation of target, shedding of receptors, FcRn recycling and much more (Li *et al.*, 2014, Dua *et al.*, 2015).

1.4.15.3. Clearance mechanisms

The removal, or elimination of a drug from the body typically occurs via three major mechanisms; excretion, secretion or biotransformation. Whilst excretion, primarily via filtration in the kidney and subsequent elimination in the urine, tends to be a major mechanism for small molecule drugs it plays a less important role for mAbs. Once again this is primarily due to the large molecular size, preventing efficient filtration in the glomerulus (Wang *et al.*, 2008). Similarly, secretion which for small molecule drugs occurs most commonly into the bile via the liver, tends to be an unimportant route of elimination for mAb drugs. This leaves biotransformation, a route of elimination one typically associates with the liver, involving enzyme catalysed detoxification reactions leading to increased polarity. Whilst this forms a fundamental cornerstone of classical DMPK for small molecules, allowing the understanding of *in vitro* metabolism to drive prediction of human PK characteristics, the biotransformation of mAb drugs does not comply with this paradigm. Instead, any cell of the body may act to process the mAb drug equivalently to any other protein, trafficking it to the lysosome for proteolysis to its constituent amino acids. Whilst this may appear ultimately conclusive for a mAb drug, the body places extremely high value on its endogenous IgG and has evolved the highly specialised FcRn driven salvage pathway to prolong its existence (described in 3.1.2.4). This salvage pathway not only results in the archetypal long half-life of mAbs, but also provides an essence of predictability about their PK, which some have suggested has ultimately led to its scientific neglect (Prueksaritanont and Tang, 2012, Xu and Vugmeyster, 2012).

It is generally regarded that the majority of IgG elimination occurs as a result of intracellular proteolysis following fluid phase or receptor mediated endocytosis (Wang *et al.*, 2008). Whilst every cell may indeed possess the potential to act as a route of clearance, the very nature which limits mAb absorption similarly limits intracellular accessibility. Thus it is thought that the endothelial cells of the vasculature and those surrounding the site of administration act as the primary clearance organ (Lobo *et al.*, 2004). Despite occurring widely across the body the actual kinetics of proteolysis are poorly characterised, particularly in the case of mAbs (Vugmeyster *et al.*, 2012). In some cases, specific binding of an mAb to its cell surface target can trigger endocytosis of the receptor-mAb complex, resulting in degradation of the mAb. This receptor mediated clearance pathway is a form of target mediated drug disposition, where binding of the target can lead to alteration of the mAbs PK. This by definition is a capacity limited pathway, dependant on the extent of target expression, target turnover kinetics and the rate of internalisation (Wang *et al.*, 2008). Often clearance by this route is non-linear, with a

shorter half-life and higher clearance seen at low mAb dose compared with that seen at a high dose where the specific clearance route is saturated (Deng *et al.*, 2012). Target mediated clearance may similarly impact the PK of mAbs which have soluble targets, where multivalent binding of the soluble target leads to antibody-target aggregation and triggers phagocytosis by immune cells such as macrophages.

An alternative form of receptor mediated clearance is elicited by the Fcγ receptor family, which are expressed on a variety of immune cell types (Nimmerjahn and Ravetch, 2008). The normal function of the FcγR family is to bind the Fc region of IgG molecules, resulting in activation of downstream immune effector functions. It is thought that binding of a therapeutic mAb to FcγR expressed on cells of the reticuloendothelial system, such as monocytes or macrophages, may trigger endocytosis of the FcγR-drug complex and result in degradation of the mAb by the lysosome (Vugmeyster *et al.*, 2012). This FcγR binding could be as downstream consequence of the mAb binding soluble antigens or cells, marking them out for destruction by phagocytic cells that express FcγR. The actual influence of this FcγR mediated clearance pathway on the pharmacokinetics of mAbs continues to remain a topic for debate (Wang *et al.*, 2008).

The hosts immune system itself may present an alternative and most unwanted clearance route for therapeutic mAbs. Here the host immune system can directly recognise the mAb as foreign, particularly in cases where the mAb is of non-self species origin, looking to remove it either through an anti-drug antibody (ADA) response or through aggregation of the antibody leading to clearance by phagocytotic mechanisms. Clearance of mAbs by the host immune system plagued early clinical efforts with therapeutic mAbs of rodent origin, leading to a very high failure rate in the clinic. Consequently, there was a drive in the field to move toward fully human mAbs as a means to reduce the 'foreignness' of the antibody backbone. Such humanised or fully human mAbs make up the vast majority of therapeutic mAbs which are in clinical development today.

1.4.15.4. Importance of the neonatal Fc receptor (FcRn)

The neonatal Fc receptor (FcRn) plays a critical role in the distribution and clearance of IgG, bestowing IgG its characteristically prolonged half-life when compared with other macromolecules. This prolonged half-life is conferred through the unique salvage pathway facilitated by the intriguing pH dependent binding properties of FcRn. The existence of this pathway was first postulated by Brambell *et al.* (1964) to explain the long IgG half-life when

compared with other plasma proteins, raising the idea of an IgG protection receptor. Identification of this protection receptor as FcRn was not until 30 years later, through experimentation with β2-microglobulin knockout mice by Junghans and Anderson (1996). FcRn is a heterodimer consisting of two subunits, a membrane integral major histocompatibility complex (MHC) class I like heavy chain and a β2-microglobulin light chain (Junghans and Anderson, 1996). Demonstrating the importance of this recycling pathway, IgG clearance increased 7 to 10-fold in β2-microglobulin knockout mice compared with the wild type (Junghans and Anderson, 1996, Ghetie *et al.*, 1996). The binding of FcRn to the Fc region on IgG is pH dependant with limited binding at physiological pH 7.4, but nanomolar affinity at the acidic pH 6 – 6.5 found in the endosome (Roopenian and Akilesh, 2007). This pH dependence is thought to be due to titration of histidine residues in the hinge region of IgG and their subsequent interaction with acidic residues on FcRn (Roopenian and Akilesh, 2007). The mechanism of IgG salvage is proposed to proceed following endocytosis of IgG, where it encounters the acidic environment of the endosome and preferentially binds FcRn. This rescues the bound IgG during sorting of the endosome, recycling it back to the membrane as opposed to trafficking it to the lysosome for destruction. More recently it has been demonstrated that albumin also exhibits this pH dependant binding to FcRn and is similarly salvaged, leading to an extended serum half-life (Chaudhury *et al.*, 2003). The salvage mechanism for IgG and albumin is illustrated in figure 1.3, highlighting the pH dependency of binding to FcRn. Modulation of the IgG-FcRn binding interaction has been successfully explored as a strategy for alteration of the half-life of therapeutic antibodies and derived products, with the potential to provide significant benefit to patients through reduced dosing frequency, as excellently reviewed by Kuo and Aveson (2011).

There are pronounced differences in the binding affinity of IgG to FcRn across species, complicating the use of rodents to predict the clinical half-life of therapeutic mAbs (Ober, 2001). Mouse and rat FcRn is relatively promiscuous in its binding, able to bind IgG of mouse, rat, cynomolgus monkey and human origin (Ober, 2001, Neuber *et al.*, 2014). In contrast, human FcRn is more stringent and unable to bind IgG of mouse or rat origin but is able to bind IgG of cynomolgus monkey origin (Ober, 2001, Neuber *et al.*, 2014). This provides an explanation as to why early mAb therapies using mouse IgG demonstrated short half lives in the clinic, limiting their efficacy. It is hence important that binding differences are considered when studying mAbs originating from a different species to the one its being tested in, to ensure the translational value of the information generated.

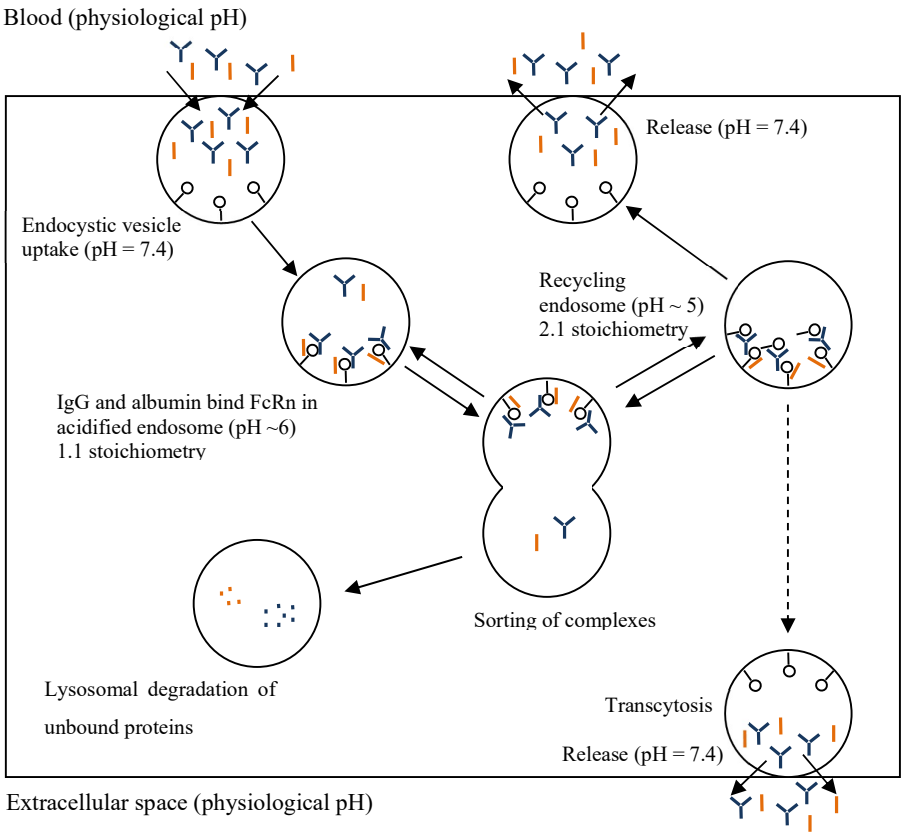

Figure 1.3. Illustration of the IgG and albumin protection mechanism by the neonatal Fc receptor (FcRn) via a pH dependent salvage pathway. Image adapted from Dostalek *et al.* (2013) with permission from Springer Nature.

1.4.16. Modelling therapeutic antibody PK

Extrapolation and prediction of drug exposure and pharmacokinetics across dosing strategies requires mathematical modelling of plasma concentration data. Therapeutic antibodies, because of their large size and poor membrane permeability, exhibit several unique PK properties when compared with small molecules (Wang *et al.*, 2008, Dostalek *et al.*, 2013). Classic compartmental mammillary PK modelling approaches, that are typically used to describe small molecule PK, are commonly adopted to assess mAb PK (Dostalek *et al.*, 2013). The two compartment model being the most commonly used to asses clinical mAb PK in man (Dostalek *et al.*, 2013). These mammillary models however fail to describe key properties of mAb disposition and clearance (Cao *et al.*, 2013). The major limitation when applied to mAbs is that the models assume rapid equilibrium between plasma and tissue compartments,

allowing the assumption that clearance is restricted to the central compartment. This has two drawbacks, firstly mAb clearance can often be attributed to peripheral tissues and is frequently found to be nonlinear. To overcome this, a saturable elimination route can be included in the model in addition to the basic linear clearance route, or alternatively a mechanistic TMDD model can be applied (Dostalek *et al.*, 2013). The second drawback is that two compartmental models often underestimate the true extent of mAb distribution (V_{ss}) (Dostalek *et al.*, 2013). This occurs because distribution between compartments is assumed to occur by rapid diffusion and be equivalent in both directions. However, mAbs typically distribute via convection and as a consequence of differing reflection coefficients on the vascular and lymphatic sides, do not equilibrate between plasma and tissue (Cao *et al.*, 2013).

1.4.16.1. Incorporating TMDD

The term target mediated drug disposition (TMDD) was first introduced to describe nonlinearity through high affinity peripheral binding of a drug to its biological target in tissue. However, the concept gains most prominence through its application to describe the additional saturable clearance pathway elicited through high affinity binding of a mAb to its biological target and its subsequent clearance. Mager and Jusko (2001a) proposed the initial general TMDD model (figure 1.4), which has subsequently been simplified or extended by other authors to fit a multitude of situations (Dua *et al.*, 2015). Within the basic TMDD model, binding of drug to target produces a complex through a reversible reaction described by a second order binding reaction and a first order dissociation reaction, which are represented by the rate constants k_{on} and k_{off} (Dua *et al.*, 2015). Elimination of each species is then modelled by the first order rate constants k_{el}, k_{deg} and k_m respectively, whilst synthesis of the target k_{syn} is also included (Dua *et al.*, 2015). In its simplest form, these reactions can be assumed to occur within a single compartment, however extension to a two-compartment model is typically applied to mAb PK interpretation.

The advantage of using the TMDD model to describe mAb nonlinearity, over simply adding a saturable clearance route into the PK model, is that it can provide insight into the antibody target interaction. This approach also allows prediction to be made regarding the potential impact of TMDD on a novel antibody, using *in vitro* target affinity measurements combined with knowledge of target kinetics (Dostalek *et al.*, 2013). Scaling nonlinear clearance across species also becomes an achievable objective, if differences in the biological target and binding kinetics are understood.

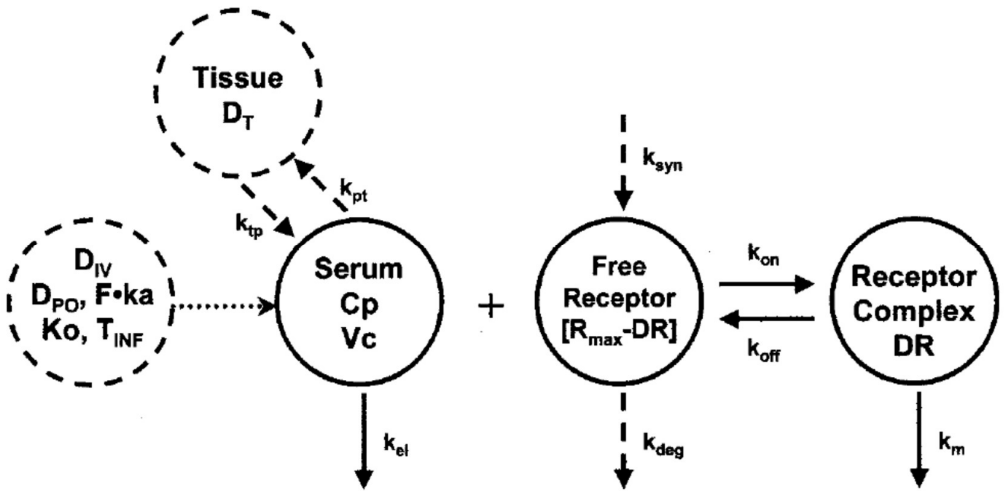

Figure 1.4. The general TMDD model as described by Mager and Jusko (2001a), modelling the specific kinetics of drug (D), receptor (R) and complex (DR) in relation to the drug binding affinity. Reprinted with permission from Springer Nature.

1.4.16.2. Incorporating physiology

Whilst two compartmental models incorporating TMDD provide a well validated approach to describe and project mAb pharmacokinetics when target mediated nonlinear clearance is identified, the individual compartments have no physiological relevance and thus provide no indication of drug exposure at peripheral tissue sites. Following the Pfizer 'three pillar' analysis of drug failures in the clinic, understanding the exposure and activity of drug at the site of action has become a major focus in early drug discovery (Morgan *et al.*, 2012). Typically, this site of action resides in a tissue or the extravascular space, thus methodology that allows prediction of exposure in tissues has significant added value. Consequently, physiologically based pharmacokinetic (PBPK) models have gained traction in recent years as a mechanistic and more realistic modelling approach compared with classic mammillary models (Shah and Betts, 2012). These models are hugely complex, combining drug specific parameters within a drug independent model structure, comprising anatomical compartments such as organs or tissues, connected via physiological processes such as the blood and lymph (Shah and Betts, 2012). This enables PBPK models to provide detailed prediction of both the plasma and tissue deposition of a mAb, whilst allowing a method by which to scale the model across species by altering physiological parameters (Shah and Betts, 2012). The downside however is that employment and validation of PBPK models requires a vast amount of information to parameterise the many physiological processes involved (Cao *et al.*, 2013).

Whilst Shah and Betts (2012) reported a 'platform PBPK model' for mAbs that described a set of typical physiological parameters for preclinical species with which to populate the basic PBPK model structure, there still remains a large number of mAb and target specific parameters to estimate. In addition, measurement of drug or target concentration in tissue to validate the model can be technically challenging. To tackle this issue, Cao *et al.* (2013) proposed a minimal PBPK model (mPBPK) that, whilst maintaining key physiological attributes of the full PBPK model, can lump tissue compartments and processes together to substantially reduce complexity but still provide parameters with more practical value than classic mammillary models (Cao *et al.*, 2013). The mPBPK model also retains the flexibility to employ different clearance sites and mechanisms, along with physiologically relevant distribution processes (Cao *et al.*, 2013). A simplified model structure with reduced need for input data fits nicely into the remit of preclinical PKPD investigation, where knowledge of drug and target kinetics is often minimal. The mPBPK model structure was therefore explored for its applicability to the anti-CD21 mAbs described within this report.

1.4.16.3. Incorporating complex target kinetics

In reality, target dynamics can often be more complex than accounted for by the single turnover model described within the basic TMDD model. It has been suggested that the majority of membrane bound proteins can shed their ectodomains to result in a membrane and a soluble form of the protein (Zhang and Pastan, 2008). Well characterised mAb targets that are examples of this include; CD20 targeted by Rituximab, epidermal growth factor receptor (EGFR) targeted by Panitumumab and human epidermal growth factor receptor 2 (HER2) targeted by Trastuzumab (Li *et al.*, 2014). The drug target CD21 being investigated in this thesis has been similarly shown to exhibit ectodomain shedding, resulting in soluble forms of the receptor which retain the ability to bind the surrogate mAbs, but are of undefined biological function (Larcher *et al.*, 1995, Masilamani *et al.*, 2003a, Hoefer *et al.*, 2008). Clearly the presence of shed antigen provides a certain additional layer of complexity to the modelling of mAbs targeting membrane bound proteins. To describe these additional factors an extension to the basic TMDD model was reported by Li *et al.* (2014), that incorporates target shedding within a mPBPK framework.

1.4.17. Integrative PKPD modelling

The dose of a drug needed to achieve a specific effect over a set time period is governed by the combination of its pharmacokinetic (PK) and pharmacodynamic (PD) properties. Pharmacokinetic pharmacodynamic (PKPD) modelling looks to integrate simplified mathematical descriptions of these properties into a relationship that describes the resulting effect-time course following drug administration. Thus, PKPD models are formed of a PK component that describes the time course of the drug in a body fluid (typically plasma due to its accessibility) and a PD component that relates the concentration of drug in this body fluid to a biological effect, with this integrated relationship conceptualised in figure 1.5 (Derendorf and Meibohm, 1999). By definition, PKPD models represent a simplified construct of the true biological process and therefore, whilst providing adequate description of the known, their true value lies in extrapolation beyond the existing data (Meibohm and Derendorf, 1997). This allows prediction of subsequent system responses under new test conditions, such as alternative dosing regimens, competing drug molecules, or importantly in early drug discovery, translation across species.

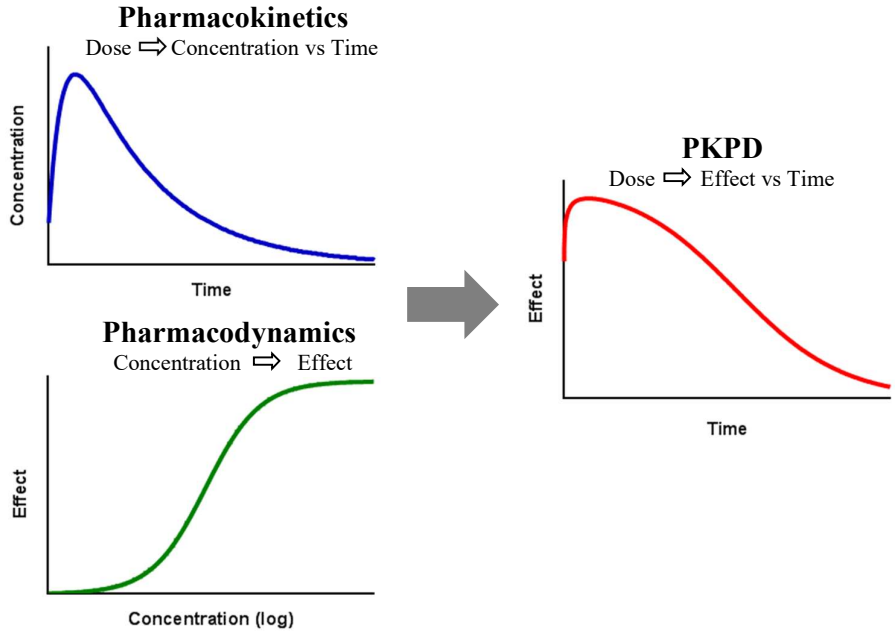

Figure 1.5. Conceptualisation of the integration of pharmacokinetics and pharmacodynamics within PKPD modelling to describe the effect-time course resulting from administration of a specific dose. Adapted by permission from Springer Nature, Derendorf and Meibohm (1999).

In the context of translational research in early drug discovery, the application of PKPD modelling looks to provide quantitative prediction of the PKPD properties of drugs in human, by using prior knowledge from preclinical *in vitro* and *in vivo* studies (Danhof *et al.*, 2008). To achieve this, PKPD modelling has developed from a descriptive into a mechanistic science, incorporating mechanistic elements that quantitatively characterise processes on the causal path between plasma concentration and effect, such as effect site distribution, drug target binding and activation, and transduction mechanisms (Danhof *et al.*, 2008). This concentration effect relationship is dependent on the properties of both the drug (target affinity (K_d), intrinsic efficacy, etc.) and the biological system (receptor expression, kinetics, transduction, etc.) with distinction crucial for translation across species (Danhof *et al.*, 2008). Whereby, whilst drug specific properties can often be estimated through *in vitro* experimentation or can remain unchanged directly from preclinical *in vivo* studies, biological system specific parameters may vary across species, disease state or even under differing experimental conditions. Thus, system specific parameters require more complex investigation and/or scaling to estimate.

1.4.17.1. Components of PKPD models

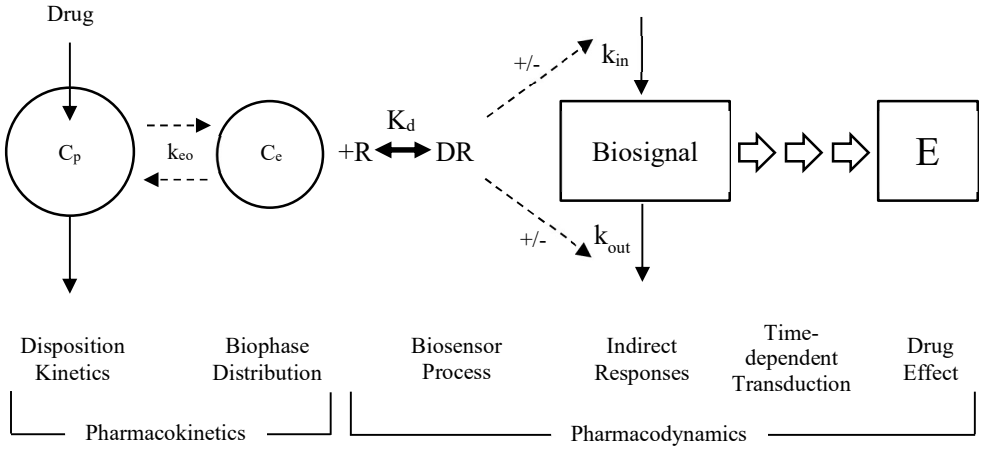

Figure 1.6. The principle components of PKPD models. Drug action is governed by its pharmacokinetics; defining the plasma concentration (Cp) and distribution (keo) to an effect site (Ce), and its pharmacodynamics; defining drug (D) binding to target (R) to form a complex (DR), inhibition or stimulation of the production (k_{in}) or loss (k_{out}) of a mediator biosignal and the transduction of this into an observable effect (E). Conceptualisation adapted by permission from Springer Nature, Jusko *et al.* (1995).

The connectivity of the typical mechanistic elements of PKPD models are illustrated in figure 1.6, adapted from Jusko *et al.* (1995). This schematic highlights that whilst the blanket term of pharmacokinetics governs the plasma concentration (C_p) of drug, critically it also governs drug distribution to the effect site (C_e), which can often be located outside of the plasma. This effect site distribution (k_{eo}) may in some cases represent a rate limiting step, characterised by a delay in the onset and duration of effect relative to drug concentration in plasma. A similar delay may equally be caused by more complex distributional kinetics or the presence of on or off target binding of the drug. Mechanistic models look to characterise the distributional relationship of the drug, either using physiologically based PK models or via more descriptive effect site driven elements.

The mechanism of action of a drug and its transduction into a measurable effect is captured by the umbrella term pharmacodynamics. This can be conceptualised (figure 1.6) as a biosensor process representing the mechanism of action of the drug, whereby receptor binding or endogenous mediator turnover may be altered by drug (Mager and Jusko, 2001b). Receptor (R) binding can often be modelled using equations that describe the reversible binding of agonist or antagonistic drugs (D) to form a complex (DR). However, many drug responses can be considered indirect in nature, whereby drug binding results in stimulation or inhibition of the production (k_{in}) or removal (k_{out}) of a mediator. This results in a delayed effect due to the time needed for the change in k_{in} or k_{out} to be realised in the measurable response, with this delay described by one of the four basic indirect response models reported by Dayneka *et al.* (1993). Furthermore, these 'biosensor' drug effects often activate additional downstream processes prior to the observable effect (E), that may be subject to further time dependent steps, a concept termed signal transduction (Jusko *et al.*, 1995).

1.4.17.2. Modelling downstream responses

Signal transduction in PKPD analysis can be complex to model because it is typically non-linear, may be subject to homeostatic feedback or compensatory mechanisms, and can exhibit large differences in the rate at which the processes involved occur (Danhof *et al.*, 2008). When the transduction process is fast (milliseconds to seconds) and free of compensatory feedback mechanisms, the time course of drug effect mirrors that of the effect site concentration. However, when the transduction process is slow (minutes to hours, or even days), it may be an additional determinant of the time course of drug effect (Danhof *et al.*, 2008). There are two popular approaches to account for time dependent transduction in PKPD modelling; turnover models that incorporate interlinked indirect response elements and transit

compartment models. Whilst cascading turnover models represent the more mechanistic approach to describe the intermediary processes between drug exposure and a downstream biological response, practical limitations often prevent molecular and cellular level understanding of the pharmacology at each intermediate step. In such circumstances, a transit compartment model may be used in its place, offering a more empirical description of time dependent signal transduction (Sun and Jusko, 1998).

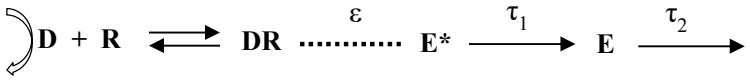

Figure 1.7. Illustration of the transit compartment model of time dependent transduction. Where D is drug, R is receptor, DR is drug receptor complex, ε is intrinsic efficacy, E* is biological effect signal, τ is transit time and E is effect. Adapted with permission from John Wiley & Sons, Mager and Jusko (2001b).

At its most simplistic, time dependent transduction of drug effect can be described in terms of receptor occupancy theory and the law of mass action by the transit compartment model, as illustrated in figure 1.7 (Mager and Jusko, 2001b). Here free drug (D) interacts with available receptor (R) to form a drug receptor complex (DR). Under the assumption of reversible binding, the relationship can be defined as;

Equation 1.1: $$DR = {Bmax \times D}/{(K_D + D)}$$

Where B_{max} is the total concentration of receptor and K_d is the equilibrium dissociation constant. Assuming receptor occupancy theory, the effect signal E* is directly proportional to the concentration of complex (DR), E* = ε x DR, where ε is drug intrinsic efficacy. Maximum induced signal (E_{max}) is assumed to occur when all receptors are occupied, thus E_{max} = ε x B_{max}. Therefore E* can be defined as;

Equation 1.2 $$E^* = {E_{max} \times C}/{(EC_{50} + C)}$$

where C is the free drug concentration and EC_{50}, the concentration of half maximal effect, is equivalent to the K_d. Production and loss of the observed effect (E) in this simple example are

dependent on the rate constants τ_1 and τ_2, with the rate of change of the observed effect defined as;

Equation 1.3 $$\frac{dE}{dt} = \frac{E^*}{\tau_1} - \frac{E}{\tau_2}$$

The transit compartment model is a flexible and versatile model, that can be extended to include additional system complexity where required. For example, alternative functions correlating drug concentration with the effect signal may be used, non-linearity may be included such as the Hill coefficient, feedback mechanisms may be added, specific rate limiting steps can be added with different values of τ, or a multitude of other additional elements. The number of transit compartments included can also be modulated, to alter the length of delay and the shape of the resulting response (Sun and Jusko, 1998).

Chapter 2: Experimental Methodology

2.1. Chapter introduction

The cornerstone of mechanistic PKPD investigation is the collection of high quality experimental data that accurately describes the pharmacokinetic and pharmacodynamic events over time. Collection of this rich data set represents a fundamental step to enable mathematical PKPD modelling. Hence, a critical component of this project became the development of bespoke experimental methodology to overcome the sample collection limitations and constricted reagent availability imposed by working in mouse. These two factors represent the major hurdles opposing application of PKPD modelling in the preclinical drug discovery space, often resulting in compromised data sets that inadequately describe PK and PD.

The present chapter describes the *in vivo* and analytical methodology conducted as part of this project, with a breakdown of the completed *in vivo* studies shown in table 2.1, along with the associated endpoints and analytical methods. The author developed all analytical methodology described in this project specifically for the task, performing all aspects of the work from sample preparation to data collection and final analysis. Flow cytometry was the only exception, with the methodology, instrument operation and data analysis completed by an expert user within GSK, with assistance provided by the author. The author designed the *in vivo* protocols described in this thesis, completing all of the pre-study administration and preparing for ethical review, under oversight by an approved study director. All hands-on laboratory animal husbandry and *in vivo* experimental steps were completed by expert technicians within the GSK animal facility in Stevenage, UK. The author also developed all of the mathematical models used to analyse and interpret the experimental data in this project, performing all aspects of the mathematical modelling.

2.1.1. Selection of mAb assay technology

Typical quantitative methodology, particularly for the measurement of protein biomarkers, have a relatively high sample volume requirement that is incompatible with the restricted blood draw volume in mice. In the past, this has often resulted in blood volume requirement becoming the driving force behind sampling decisions, often at the expense of concurrent sampling for PK and PD. Composite study designs are a common solution, allowing collection of full PK and PD response profiles by merging data collected across several animals sampled alternately. But whilst this provides a neat fix, it is limited regarding data quality and has considerable impact on the number of animals required. Therefore, to facilitate collection of a

rich data set for PKPD analysis by primary intent, selection of quantitative methodology in this project centred on minimising the required sample volume, with the concomitant adoption of in-life micro sampling techniques. In combination with modelling and simulation, these changes facilitated the enactment of some novel *in vivo* study designs using serial sampling for the simultaneous investigation of PK and PD.

The experimental design used to determine the pharmacokinetics of the three surrogate anti-CD21/35 antibodies investigated in this project lent itself to a serial sampling approach, collecting blood from a single animal across multiple time points. This approach is widely used for small molecule pharmacokinetic studies, facilitated through a combination of technological advances in mass spectrometry detection and improved blood sampling techniques that allow collection of small, precise volumes of blood in a technique known as micro sampling (Nilsson *et al.*, 2013). In contrast, preclinical investigation of mAb pharmacokinetics has historically required composite study designs (Joyce *et al.*, 2014), in large part owing to bioanalytical assay performance. Clearly a micro sampling based serial approach would have significant benefit in the reduction of animal use, drug material and ultimately cost. Therefore, focus was applied to improve mAb bioanalytical performance through assay miniaturisation, utilising the Gyrolab xP platform (Gyros AB, Uppsala).

Typical mAb bioanalytical strategies have employed immunoassay-based technologies to quantify drug concentration in biological matrices. The most commonly adopted of which is the sandwich ELISA format, relying on a pair of complementary antibodies to act as capture and detection reagents. In its simplest form the capture antibody is adsorbed onto a surface, where it can interact with its target in the biological sample prior to the addition of a second labelled antibody that binds the trapped analyte and elicits a signal. This signal often takes the form of a colorimetric endpoint, such as the conversion of 3,3',5,5'-tetramethylbenzidine (TMB) to a diimine by the enzyme horse radish peroxidise (HRP). Whilst ELISA is a gold standard analytical technique for protein quantification, it is typically limited by long and labour intensive assay times and high sample volume requirements. Development of immunoassay technology to combine automation with fluorescence assay endpoints have resulted in several novel solutions. Multiplexing systems such as those of the Meso Scale Discovery (MSD, Meso Scale Diagnostics LLC) and Luminex (Luminex Corporation) assay platforms allow the quantification of multiple analytes from a single sample. However, for analysis of a single analyte the Gyrolab platform (Gyros Protein Technologies AB) holds the greatest advantage. This platform applies an automated workflow to a microfluidic system to minimise sample and reagent volume requirement and significantly reduce assay time. Joyce

et al. (2014) have recently demonstrated the utility of this approach when applied to a serial sampling strategy, employing micro sampling for the assessment of mAb PK in mouse. In a direct head to head comparison with a classic composite study design, Joyce *et al.* (2014) not only demonstrated the validity of this approach, but also the reduction in variability it offered. Here they coined the phrase "one mouse one pharmacokinetic profile", which aptly describes the approach.

The Gyrolab assay platform has been strongly adopted for the bioanalysis of biological therapeutics within the discovery environment, particularly in support of pharmacokinetic and toxicokinetic studies, despite being a relatively new technology (Roman *et al.*, 2011, Liu *et al.*, 2013, Fraley *et al.*, 2013). The Gyrolab xP instrument is a fully automated system that requires minimal sample and reagent volume, limited hands on time and reduces assay duration to below 1.5 h. This is achieved using Gyros proprietary compact disc technology, that contains nanolitre scale microfluidic structures through which liquid flow is directed by centrifugal and capillary force under precise automated control (Andersson *et al.*, 2007). A 15 nL streptavidin coated bead column captures a biotinylated primary antibody or protein upon which the immunoassay is then formed. Detection occurs via laser induced fluorescence, typically through the application of a labelled secondary antibody. A key advantage of this platform in the early discovery setting is the ability to perform streamlined assay development and validation to rapidly create fit for purpose assays (Liu *et al.*, 2013). Liu *et al.* (2013) describe this as a four-step process, which can feasibly be completed for multiple assay formats simultaneously within a few days. This is achieved by taking advantage of the automated nature of the assay and short processing time to screen multiple reagent combinations, concentrations and sample matrices to optimise assay performance, sensitivity and repeatability (Liu *et al.*, 2013). The combined weight of the advantages described here for the miniaturisation of the bioassay and the resulting minimisation of sample usage, mean that the Gyrolab xP assay platform was adopted as the methodology of choice for the quantification of the mAbs investigated in this project.

2.1.2. Selection of biomarker assay technology

The sandwich ELISA, despite its drawbacks regarding long and labour intensive assay times and high sample volume requirement, remains the most widely implemented technique for quantification of protein biomarkers. This is partly as consequence of its low cost and accessibility. But also, because it remains a sensitive and selective way to detect protein

biomarkers when faced with poor quality reagents, such as low affinity antibodies. Paradoxically, as a direct result of the long incubation times required. Consequently, in this project the sandwich ELISA format was adopted for quantification of the antigen specific antibody response in plasma following T-dependent immunisation in mouse, where the antigen specific antibodies are likely of low affinity. A derivation of the ELISA assay format was also adopted for detection of the low affinity anti-drug antibodies raised against the surrogate CD21/35 mAbs. In addition, ELISA represented a useful technique to assay the soluble form of CD21/35, where only low quality reagents were available.

The soluble form of CD21 (sCD21) has the potential to impose significant impact upon the pharmacokinetics of CD21 neutralising antibodies, due to retention of the extracellular region of the protein and thus the antibody binding epitope. However, both the concentration and kinetics of sCD21 are unreported in mouse. Reliable quantitative assays for the determination of murine sCD21 are not commercially available, in large part owing to the lack of a high quality full length recombinant CD21 protein. To this end, a recombinant murine CD21 protein was synthesised within GSK for the generation of tool reagents and assays for preclinical investigation. Whilst a small amount of this protein was generated, its synthesis was not trivial, and the quality of the final protein product was not definitively proven. In addition, the single genetic origin of CD21 and CD35 in mouse results in an inability to distinguish the shorter CD21 protein from its longer relation. This complicates interpretation of the data. However, due to the retention of the CD21 binding epitopes on both proteins, the combined measurement is actually the critical value that impacts mAb PK. For this reason, considerable effort was expended to develop an assay to quantify the soluble forms of these proteins.

Unlike immunoassays, the quantification of soluble protein biomarkers by LC-MS/MS is not restricted to those with a supply of purified protein and high quality specific antibodies. This makes it an extremely attractive technique when reagent options are limited for immunoassay development. The general approach involves targeted enzymatic digestion of the protein sequence into short peptide sequences that are suitable for detection by LC-MS/MS. Therefore, essentially any protein of known amino acid sequence can be quantified by LC-MS/MS, so long as a representative and unique proteotypic peptide can be isolated from the sequence with amenable physicochemical properties. The major drawback with this technique is sensitivity, resulting in the requirement for laborious sample preparation and often large sample volumes. Modern mass spectrometry technology has improved the feasibility of the approach tremendously, with much improved selectivity, sensitivity and throughput. Which, coupled with the reduced cost burden for large scale sample preparation in recent years, has resulted in

LC-MS/MS becoming a more accessible technique for the quantification of biomarkers. For these reasons, LC-MS/MS was employed to provide a high confidence, confirmatory assay for the quantification of soluble CD21/35 in mouse plasma.

In combination with understanding the pharmacokinetics of the drug and its impact on downstream biomarkers, a critical aspect of mechanistic PKPD is integration of target engagement. For therapeutic mAbs this can often be measured directly, through assays for mAb-target complex where target is a soluble protein, or through monitoring receptor occupancy on the target cell by flow cytometry where target is membrane expressed. It can be harder to directly demonstrate target engagement with mAbs that lead to cellular depletion, where a downstream change in a cell population may be required as a surrogate. In this project, flow cytometry was adopted as the means to demonstrate and quantify the extent of target engagement achieved for each molecule.

Flow cytometry is a widely used technique for detecting and characterising different cell types in a heterogenous cell population, through analysis of cell size, volume and the expression of specific cell markers, providing simultaneous multi-parameter analysis of single cells. In simple terms, the flow cytometer flows individual cells past a laser and then detects the light scattered from the cell, along with any fluorescence emitted. Analysis of the forward and side scattered light, caused by the cells as they pass the laser intercept, can determine size and granularity. Almost simultaneously, the laser can excite fluorochromes associated with the cell to emit light at specific wavelengths. Harnessing their specificity for a target protein, antibodies can be conjugated with fluorochromes and used to stain the cells for simultaneous identification of multiple cell surface or internally expressed proteins. Whilst traditionally a qualitative technique for the identification or characterisation of different cell types and populations, standardisation approaches have become an accepted practice for the quantification of protein expression. One widely accepted standardisation approach is QuantiBRITE™ PE beads (BD biosciences), which has been reported for the quantification of multiple cell surface receptors, such as CD38 (Iyer *et al.*, 1998) and CD4 (Pannu *et al.*, 2001), amongst others.

2.2. Materials

2.2.1. Basic reagents and consumables

All basic chemical reagents used in this project were of laboratory grade and were purchased from ThermoFisher Scientific, Sigma Aldrich or similar life science provider, along with all basic laboratory consumable materials. The origin of critical chemicals or materials used in this project are detailed within the relevant methodology.

2.2.2. Antibodies and small molecule drugs

The CD21 specific rat IgG2b mAb 7G6 was purchased at 1 mg/mL in a no azide, low endotoxin (NA/LE) formulation suitable for *in vivo* use (BD Biosciences, New Jersey, #559831), with an additional custom batch purchased at 10 mg/mL to facilitate higher concentration administration. The CD20 specific rat IgG2b mAb SA271G2 was purchased at 1 mg/mL in a low endotoxin, azide free (LEAF) formulation suitable for *in vivo* use (Biolegend, San Diego, # 152104). Fingolimod (FTY720) was purchased from Sigma-Aldrich (SML0700) with a purity >98%. The CD21 specific murine IgG1 mAb 4B2 was synthesised in house at 10.7 mg/mL, under license from the University of Colorado, Denver, and is now commercially available from Abcam (#ab252778) in a formulation suitable for *in vivo* use. The in house raised murine IgG1 mAb 9E10 was likewise synthesised at GSK at 5.5 mg/mL. Isotype control antibodies of irrelevant binding specificity of the form rat IgG2b and mouse IgG1 were synthesised in house at concentrations of 2.4 and 30.5 mg/mL, respectively. All mAbs synthesised in house were formulated in phosphate buffered saline (PBS) and tested as having an endotoxin content <0.03 EU/mg, suitable for *in vivo* use.

Table 2.1. Summary table of the *in vivo* studies performed as part of this project, stating the objective, in life design, drug treatment and the primary study endpoints. The location of the associated in life study protocol, analytical methodology and results are listed for each study.

Protocol section	Study Title	Objective	In life design	Treatments	Endpoint	Method section	Results
2.3.1	Pharmacokinetic studies	Define the PK of the three tool mAb's; 7G6, 4B2 and 9E10	IV bolus admin at 3x doses, with mid dose IP leg	7G6/4B2: IV 0.2, 2 (IP) and 20 mg/kg. 9E10: IV 0.15, 1.5 (IP) and 15 mg/kg	• Drug concentration • PK interpretation	• 2.4.1 • 2.6	Chapter 3: 3.3.1 to 3.3.3
2.3.2	PKPD study 1: 7G6, 4B2, 9E10 head to head comparison	Compare relative efficacy of the three tool antibodies	IP administration at 100 µg/kg (TNP-KLH 1:1 Alum).	7G6/4B2/9E10/isotype: IP at 20 mg/kg day 0	• Drug concentration • TNP specific IgG/IgM • Splenic T/B cell	• 2.4.1 • 2.7.1 • 2.10	Chapter 5: 5.4.1
2.3.3	PKPD study 2: IV KLH TDAR pilot study	Explore feasibility of immunisation without adjuvant	IV immunisation at 10 µg/mouse (KLH)	n/a	• KLH specific IgG/IgM	• 2.7.2	Chapter 5: 5.4.2
2.3.4	PKPD study 3: IV KLH TDAR second pilot study	Explore feasibility of immunisation without adjuvant	IV immunisation at 10 or 30 µg/mouse (Imject mcKLH)	n/a	• KLH specific IgG/IgM • Splenic T/B cell	• 2.7.2 • 2.10	Chapter 5: 5.4.2
2.3.5	PKPD study 4: IV KLH TDAR follow up study	Extend challenge dose range, confirm reproducibility	IV immunisation at 30 or 100 µg/mouse (Imject mcKLH)	n/a	• KLH specific IgG/IgM • Splenic T/B cell	• 2.7.2 • 2.10	Chapter 5: 5.4.2
2.3.6	PKPD study 5: IV KLH TDAR qualification study	Qualify the experimental model with clinically validated therapies. Identify positive control	IV immunisation at 1.2 mg/kg (Imject mcKLH)	Fingolimod QD PO at 3 mg/kg SA271G2 IP at 10 mg/kg (day 0)	• Fingolimod drug concentration • SA271G2 drug concentration • KLH specific IgG/IgM • Splenic / blood T/B cell	• 2.5 • 2.4.2 • 2.7.2 • 2.10	Chapter 5: 5.4.3
2.3.7	PKPD study 6: Fingolimod concentration effect in IV KLH TDAR	Fingolimod dose response as training data for mathematical model development	IV immunisation at 1.2 mg/kg (Imject mcKLH)	Fingolimod QD PO at 0.003 to 10 mg/kg	• Fingolimod drug concentration • KLH specific IgG/IgM • Splenic T/B cell	• 2.5 • 2.7.2 • 2.10	Chapter 5: 5.4.4
2.3.8	PKPD study 7: Evaluation of mAb 7G6 concentration effect in IV KLH TDAR	mAb 7G6 dose response for mathematical PKPD modelling	IV immunisation at 1.2 mg/kg (Imject mcKLH)	7G6 IP every 96 h at 0.01 to 10 mg/kg Positive control: Fingolimod QD PO at 3 mg/kg	• 7G6 / Fingolimod drug concentration • KLH specific IgG/IgM • Splenic/blood T/B cell / CD21 quantification • Anti-drug antibody response • sCD21/35 concentration • KLH specific IgG isotypes	• 2.4.2 / 2.5 • 2.7.2 • 2.10 • 2.8 • 2.9.3 • 2.7.3	Chapter 5: 5.4.5

2.2.3. Animal husbandry

All animal studies were ethically reviewed and carried out in accordance with Animals (Scientific Procedures) Act 1986 and the GlaxoSmithKline (GSK) policy on the care, welfare and treatment of laboratory animals. In life study designs, protocols and pre-study administration were completed by the author, under oversight by an approved study director. All hands-on laboratory animal husbandry and *in vivo* experimental steps were completed by expert technicians within the GSK animal facility at Stevenage, UK. Pharmacokinetic studies were carried out under project licence numbers (PPL) 80/02573 and P5E0959B4, whilst PKPD studies were carried out under PPL 80/02380, 70/08657 and PC5B71730.

C57BL/6 male mice (supplied by Charles River UK Ltd.), between 8 and 12 weeks old were used in the generation of all data. Each mouse was individually housed in a plastic bottomed cage and the mice had free access to food (5LF2 EURodent Diet 14% supplied by PMI Labdiet, Richmond, Indiana, USA) and water at all times. It was considered that there were no known contaminants in the diet or water at concentrations that could interfere with the outcome of a study. Temperature and humidity were nominally maintained at 21 °C ± 2 °C and 55% ± 10%, respectively. Body weight was typically a criterion for entry onto a study to facilitate the sampling regimen within licence blood draw requirements.

2.3. In life study protocols

This section describes the in-life phase protocols for the *in vivo* studies performed to support this project (summarised in table 2.1), each designed specifically to generate key data to advance the science. This included the development and qualification of a novel T-dependent immunisation study design, suitable for PKPD interrogation, and its subsequent use in the exploration of a surrogate CD21 specific mAb. Through a process of continuous improvement, in life blood sampling methodology advanced as the project progressed to facilitate the ambitious data requirements. In addition, study designs advanced to increase the dose range tested without undue increase in animal use. Each study protocol is described here in detail, with associated analytical methodology described later in the chapter.

2.3.1. *In vivo* pharmacokinetic studies

Pharmacokinetic characterisation of the three surrogate CD21 neutralising mAbs was performed in the C57BL/6 strain of mouse, to attune with previous literature and the intended PKPD model. Intravenous (IV) bolus administration was selected as the dosing route to allow accurate pharmacokinetic characterisation. Each mAb was administered across a two log unit concentration range, intended to cover from partial to full saturation of CD21 over the duration of the study. This had the objective of highlighting potential non-linearity in the pharmacokinetics due to target protein kinetics. An intraperitoneal (IP) group was included to evaluate the T_{max} and bioavailability, contextualising historical data and providing a simpler dosing strategy for *in vivo* PKPD investigation. The studies were carried out over an extended period of two (7G6) or three (4B2/9E10) weeks following drug administration, to characterise the expected long terminal half-life. Investigation was limited to male mice to avoid potential sex differences and allow minimisation of group size to n=3. To enter the study, mice were required to have a minimum bodyweight of 25 g to enable the serial micro sampling regimen. The three mAbs were investigated individually over a period of 5 months.

In brief, the in-life protocol was as follows. The mAbs 7G6 and 4B2 were diluted in sterile PBS (pH 7.4) the day prior to the study, to achieve dose solution concentrations of 0.04, 0.4 and 4 mg/mL. Due to limited availability of drug material, 9E10 was diluted in sterile PBS (pH 7.4) to achieve dose solution concentrations of 0.03, 0.3 and 3 mg/mL. Each dose solution was filtered with a 0.22 μm gauge filter to remove particulates and refrigerated at 4ºC overnight. On the study day, groups of three mice were dosed via IV bolus administration using a weight adjusted dosing volume of 5 mL/kg, to target a final dose concentration of 0.2, 2 and 20 mg/kg (7G6, 4B2) or 0.15, 1.5 and 15 mg/kg (9E10). An additional group of three mice were dosed via IP administration using a weight adjusted dosing volume of 5 mL/kg, to target a final dose concentration of 2 mg/kg (7G6, 4B2) or 1.5 mg/kg (9E10). Dosing syringes were weighed before and after administration to determine the exact volume of dose administered. Residual dose solution was retained and stored at -80 ºC. Animals were observed throughout the course of the study to monitor wellbeing and identify adverse events.

Serial blood samples (25 μL) were collected via tail nick micro sampling from each mouse at (7G6) 0.17, 2, 8, 24, 48, 96, 144, 192 and 240 h following drug administration, or at (4B2/9E10) 0.17, 2, 8, 24, 72, 120, 168, 240 and 336 h following drug administration. A tenth, terminal blood sample was obtained via cardiac puncture under terminal O_2/isoflurane anaesthesia at (7G6) 336 h or at (4B2/9E10) 504 h. Blood samples were collected by positive

displacement pipette directly from the tail nick and transferred to micro-eppendorf tubes containing disodium EDTA (2 mg/mL blood), mixed and centrifuged at 2000x g for 10 minutes. A 10 µL aliquot of the resulting plasma was collected and stored at -80 ºC.

Plasma samples and residual dose solutions were assayed for the concentration of administered drug (mAb 7G6, 4B2 and 9E10) using a specific immunoassay as described in section 2.4.1. Pharmacokinetic interpretation of the resulting concentration time data was completed as described in section 2.6.

2.3.2. PKPD study 1: Mouse TDAR (IP TNP-KLH): 7G6, 4B2 and 9E10 head to head comparison

To characterise the relative efficacy of the surrogate CD21 neutralising antibodies, a head to head study was performed in a T-dependent antigen response (TDAR) *in vivo* efficacy model. The objective was to confirm literature target validation data describing the impact of CD21 neutralisation on the humoral immune response, whilst providing evidence of the best tool to take forward to further investigation. The study took advantage of a classic TDAR study design, involving administration of TNP-conjugated low molecular weight KLH in the presence of the adjuvant Alum. This drives the formation of antibodies directed against the hapten TNP after an appropriate period, typically 10 to 14 days, along with a concomitant germinal centre response in secondary lymphoid organs. The surrogate mAbs were administered at doses expected to result in saturation of the target, based on the observed PK profiles.

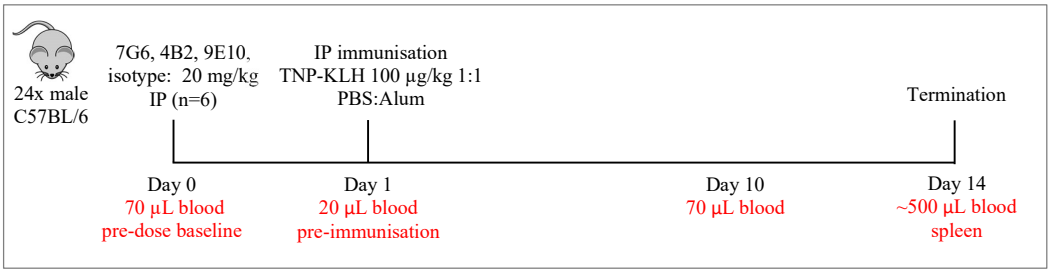

Figure 2.1. In-life protocol schematic for the TDAR mAb head to head comparison study (PKPD study 1), illustrating the timeline of in-life procedures and sampling occasions.

The in-life protocol proceeded as follows and is summarised in figure 2.1. On the day of the study, mAb 7G6, 4B2, 9E10 and a murine IgG1 isotype control were diluted in sterile PBS to achieve a dose solution concentration of 4 mg/mL. 24 C57BL/6 male mice were divided into four treatment groups (n=6) to receive either mAb 7G6, 4B2, 9E10 or isotype control. The mAbs were administered IP using a weight adjusted dosing volume of 5 mL/kg, to achieve a final dose of 20 mg/kg. On study day 1 (24 h after drug administration) each animal was immunised with TNP-KLH (2, 4, 6, trinitrophenyl hapten conjugated KLH) at 100 µg/kg, formulated at 20 µg/mL in 1:1 v/v PBS:Alum (Imject Alum, ThermoFisher Scientific, 77161) and administered IP using a weight adjusted dosing volume of 5 mL/kg. Animals were weighed every 2 days and observed throughout the course of the study to monitor wellbeing and identify adverse events.

Blood samples were collected by tail nick micro sampling from each mouse prior to drug administration on day 0 (70 µL), prior to immunisation at 24 h post dose (20 µL) and 240 h post dose (70 µL) for PK and PD endpoint determination. A final blood sample (~500 µL) was obtained via cardiac puncture under terminal O2/isoflurane anaesthesia at 336 h. Blood samples were collected into tubes containing disodium EDTA (2 mg/mL blood) mixed and centrifuged at 10000x g for 5 minutes. The resulting plasma was collected and stored at -80 ºC. All mice were terminated by cervical dislocation and the spleen excised post mortem and stored in RPMI 1640 media on wet ice for immediate analysis.

Plasma samples were assayed for the concentration of the administered drug (7G6, 4B2, 9E10) using a specific immunoassay as described in section 2.4.1. The antigen specificity of the murine isotype control antibody was unknown and thus cannot be differentiated from the natural IgG repertoire. The same plasma samples were also assayed for TNP specific IgG and IgM antibody concentration by ELISA as described in section 2.7.1. The B cell, germinal centre B cell and T follicular helper cell populations were analysed in the spleen tissue by flow cytometry as described in 2.10.

2.3.3. PKPD study 2: Pilot study - Development of an adjuvant free TDAR mouse model

To improve alignment with the underlying biology of the complement receptors and enhance translational value, the TDAR experimental model was redesigned. To simplify the immune response the challenge was administered IV, negating any complicating factors arising from a localised response. The challenge was also formulated in PBS alone, removing the use of adjuvants to drive the immune response. To initially generate confidence in the study design, a pilot study was performed at 10 µg /mouse based on prior literature.

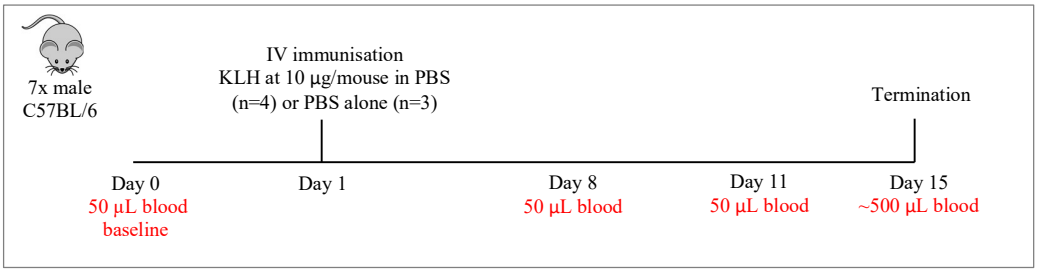

Figure 2.2. In-life protocol schematic for the adjuvant free TDAR pilot study (PKPD study 2), illustrating the timeline of in-life procedures and sampling occasions.

The in-life protocol is summarised in figure 2.2 and the detailed steps are as follows. On the day of the study, KLH (Sigma Aldrich, H7017) was prepared at 1 mg/mL, prior to further dilution in PBS to a final concentration of 0.1 mg/mL. Seven C57BL/6 male mice were divided into two treatment groups and challenged IV via the tail vein with 100 µL of either PBS alone (n=3) or 0.1 mg/mL KLH (n=4) to achieve a target challenge of 10 µg/mouse. Animals were weighed every 2 days and observed throughout the course of the study to monitor wellbeing and identify adverse events.

A baseline blood sample (50 µL) was collected by tail nick sampling from each mouse on day 0, 24 h prior to KLH immunisation. Further blood samples (50 µL) were collected on day 8 and 11, with a final sample obtained via cardiac puncture under terminal O2/isoflurane anaesthesia on study day 15. Blood samples were collected into tubes containing disodium EDTA (2 mg/mL blood), mixed and centrifuged at 12500x g for 2 minutes, with the resulting plasma stored at -80 °C. All mice were terminated by cervical dislocation following blood sampling on the final study day. Plasma samples were assayed for KLH specific IgG and IgM antibody concentration by ELISA as described in section 2.7.2.

2.3.4. PKPD study 3: Pilot study 2 - Development of an adjuvant free TDAR mouse model

The form of KLH was altered to a high molecular weight form with enhanced immunogenicity and administered IV formulated in PBS alone (Imject mcKLH, ThermoFisher Scientific, #77600). To generate confidence in the ability of the form and dose of KLH to elicit a measurable immune response, two KLH challenge doses were initially tested (10 and 30 µg/mouse), based upon prior literature.

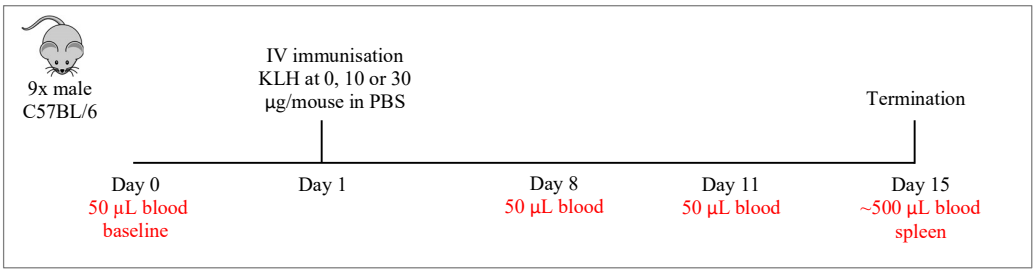

Figure 2.3. In-life protocol schematic for the adjuvant free TDAR second pilot study (PKPD study 3), illustrating the timeline of in-life procedures and sampling occasions.

The in-life protocol is summarised in figure 2.3 and the detailed steps are as follows. On the day of the study, lyophilised KLH (Imject mcKLH, ThermoFisher Scientific, #77600) was rehydrated to 4 mg/mL, prior to dilution with PBS to a final concentration of 0.1 and 0.3 mg/mL. Nine C57BL/6 male mice were divided into three treatment groups (n=3) and challenged IV via the tail vein with 100 µL of either PBS, 0.1 or 0.3 mg/mL KLH to achieve a target challenge of 0, 10 or 30 µg/mouse respectively. Animals were weighed every 2 days and observed throughout the course of the study to monitor wellbeing and identify adverse events.

A baseline blood sample (50 µL) was collected by tail nick sampling from each mouse on day 0, 24 h prior to KLH immunisation. Further blood samples (50 µL) were due to be collected on study day 8 and 11, with a final sample to be obtained via cardiac puncture under terminal O2/isoflurane anaesthesia on study day 15. However, in a deviation to the intended sampling days, blood samples were collected on study days 7, 10 and 14 (6, 9 and 13 days post IV KLH challenge), with mice terminated on study day 14. Blood samples were collected into tubes containing disodium EDTA (2 mg/mL of blood), mixed and centrifuged at 12500x g for 2 minutes, with the resulting plasma stored at -80 ºC. All mice were terminated by cervical

dislocation and the spleens excised post mortem and stored in RPMI 1640 media on wet ice for immediate analysis.

Plasma samples were assayed for KLH specific IgG and IgM antibody concentration by ELISA as described in section 2.7.2. The B cell, germinal centre B cell and T follicular helper cell populations were analysed in the spleen tissue by flow cytometry, as described in 2.10.

2.3.5. PKPD study 4: Protocol development follow up study - Development of an adjuvant free TDAR experimental mouse model

A follow up study was performed to confirm and extend the tested KLH challenge dose range. The primary objective was to provide confirmation of the repeatability of the IgG and IgM responses seen in pilot study 2 at the 30 µg/mouse challenge dose. Secondarily, the study sought to ascertain the strength of the KLH challenge, through exploration of the KLH concentration effect profile. To align with the biology of the target, a suboptimal challenge concentration was desired. However, identifying the correct challenge dose to use is a fine balance between a suboptimal response, yet one that is measurable, robust and with sufficient dynamic range to interrogate inhibition.

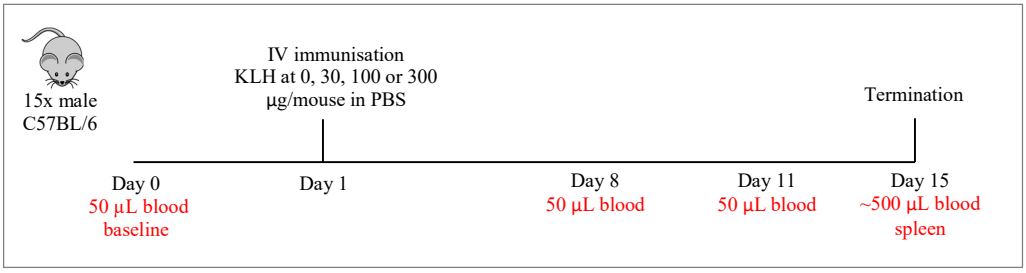

Figure 2.4. In-life protocol schematic for the adjuvant free TDAR development study (PKPD study 4), illustrating the timeline of in-life procedures and sampling occasions.

The in-life protocol steps are described here and summarised in figure 2.4. On the day of the study, lyophilised KLH (Imject mcKLH, ThermoFisher Scientific, #77600) was rehydrated to 3 mg/mL, prior to dilution with PBS to a final concentration of 0.3, 1 and 3 mg/mL. Fifteen C57BL/6 male mice were divided into four treatment groups and challenged IV via the tail vein with 100 µL of either PBS (n=3), 0.3, 1 or 3 mg/mL KLH (n=4) to achieve a target challenge of 0, 30, 100 or 300 µg/mouse respectively. Animals were weighed every 2 days

and observed throughout the course of the study to monitor wellbeing and identify adverse events.

A baseline blood sample (50 µL) was collected by tail nick sampling from each mouse on day 0, 24 h prior to KLH immunisation. Further blood samples (50 µL) were collected on days 8 and 11 post immunisation, with a final sample obtained via cardiac puncture under terminal O2/isoflurane anaesthesia on day 15. Blood samples were collected into tubes containing disodium EDTA (2 mg/mL of blood) mixed and centrifuged, yielding approximately 20 µL plasma which was stored at -80 ^{o}C. All mice were terminated by cervical dislocation, the spleens excised post mortem and stored in RPMI 1640 media on wet ice for immediate analysis.

Plasma samples were assayed by ELISA for KLH specific IgG and IgM antibody concentration as described in section 2.7.2. The B cell, germinal centre B cell and T follicular helper cell populations were analysed in the spleen tissue by flow cytometry, as described in 2.10.

2.3.6. PKPD study 5: Qualification of the IV KLH TDAR mouse experimental model

A small, statistically powered qualification study was carried out to confirm the performance of the IV KLH TDAR mouse experimental model. Qualification was performed using two clinically validated therapeutics, which have shown evidence of efficacy on the T-dependent response in experimental clinical studies. The first was Fingolimod, a small molecule S1P receptor modulator that impacts T cell trafficking. The second was a murine surrogate (SA271G2) of the anti-CD20 mAb Rituximab, which results in depletion of B cells. The objective of this study was to test the reproducibility and robustness of the IV KLH format TDAR experimental model, whilst confirming the feasibility of serial sampling for simultaneous PK and PD determination. A secondary objective was to identify if either Fingolimod or SA271G2 could be a suitable model positive control and if that molecule could additionally test the therapeutic responsiveness and translational value of the experimental model.

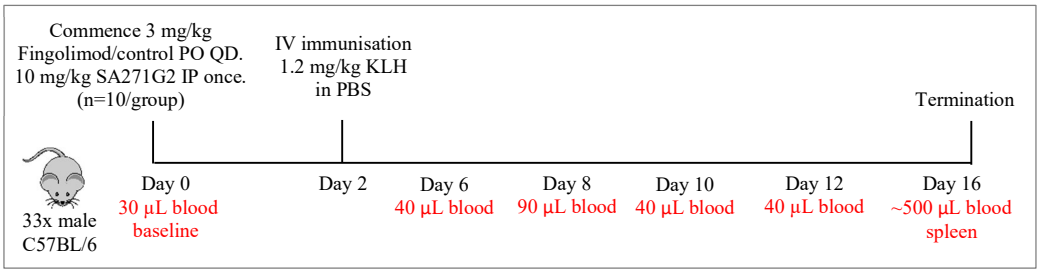

Figure 2.5. In-life protocol schematic for the IV KLH qualification study (PKPD study 5) investigating the effect of the clinically validated tools Fingolimod and a surrogate anti-CD20 mAb (SA271G2), illustrating the timeline of in-life procedures and sampling occasions.

The study design includes several modifications, compared to the IV KLH model development studies, to improve data collection and enhance suitability for mathematical modelling. The IV KLH challenge was altered to a weight normalised dose, to reduce variability. This was set at 1.2 mg/kg, assuming 30 µg KLH given to a standard 25 g C57BL/6 mouse. The number of sampling occasions was increased to assist mathematical modelling, through improvement in coverage of the KLH specific IgG and IgM response profiles. To facilitate the increased sampling frequency, the volume of blood drawn at each time point was reduced to 30 µL. This coincided with a change in the method used to collect and process the blood, with collection altered to using plasma separation capillary tubes (Drummond Scientific), a relatively new technique that has many advantages regarding sample wastage and ease of use. Group size was selected based on power analysis completed on the KLH specific IgG responses from the initial model development studies, incorporating the mean and coefficient of variance (CV). The sample size was selected to detect >60% inhibition of the 30 µg/mouse challenge, with the criteria of power >0.9 and statistical significance being a one sided two sample t-test, with a threshold value $\alpha = 0.05$. This analysis indicated a group size of 8 to 10 was required. To ensure maximum effect on the relevant cell populations, dosing of Fingolimod and SA271G2 commenced two days prior to the IV KLH challenge. To monitor this pharmacology, additional blood samples were collected for flow cytometry analysis on day 6 and 16 to monitor the T and B cell populations.

The in-life protocol is summarised in figure 2.5 and described as follows. On study day 0, thirty C57BL/6 male mice were divided into three treatment groups (n=10) to receive either Fingolimod, SA271G2 or control (1% methylcellulose 400). An additional n=3 mice were included as a naïve control, receiving no treatment. All mice were weighed daily, starting on day 0, to allow weight adjusted dosing and to monitor wellbeing throughout the study.

Fingolimod, formulated on the day of the study in 1% methylcellulose 400 (aq) at 0.6 mg/mL or 1% methylcellulose 400 (aq) alone was administered daily by oral gavage administration at 5 mL/kg, to achieve a weight adjusted target dose of 3 mg/kg. The mAb SA271G2, formulated on the day of the study in PBS at 1 mg/mL, was administered IP on day 0 only using a dosing volume of 10 mL/kg to achieve a target dose of 10 mg/kg. On study day 2, 1 h post oral Fingolimod or control administration, each mouse in all three treatment groups received a single IV administration via the tail vein of KLH (Imject mcKLH, ThermoFisher Scientific, #77600) formulated in PBS at 0.24 mg/mL, using a dose volume of 5 mL/kg to achieve a target challenge dose of 1.2 mg/kg. Lyophilised KLH was rehydrated on the day of the study to 2.4 mg/mL, prior to dilution with PBS to a final concentration of 0.24 mg/mL.

A baseline blood sample was collected prior to treatment on day 0 by tail nick sampling, with a 30 µL volume of blood taken using EDTA coated plasma separation capillary tubes (Drummond Scientific). The capillary tubes were centrifuged to isolate plasma, yielding approximately 10 µL, which was transferred to matrix tubes and stored frozen at -80 ºC. In study blood sampling commenced on day 6 by tail nick sampling, with blood samples collected every 2 days until study day 12. On each sampling occasion, two blood samples were drawn. A PD sample (30 µL) was collected by EDTA coated plasma separation capillary tubes and processed as described previously. A further PK blood sample (10 µL) was collected by pipette directly from the tail nick, added to a matrix tube and mixed with an equal volume of water. The pipette tip was precoated with EDTA, prior to sample collection, by drawing and expelling a volume of EDTA. Both samples were stored frozen at -80 ºC. On study day 8, an additional third sample of blood (50 µL) was collected by pipette for flow cytometry analysis and stored on wet ice for immediate analysis.

On study day 16, at 1 h post oral Fingolimod or control administration, all mice were anaesthetised using O_2/isoflurane and a terminal blood sample (ca 500 µL) was obtained via cardiac puncture. All mice were then euthanised via cervical dislocation with death confirmed by severing of a major thoracic arterial blood vessel. The terminal blood sample was split into three; a blood sample (100 µL) stored on ice for immediate analysis by flow cytometry, a PK sample (10 µL) diluted with an equal volume of water and stored frozen at -80 ºC and finally a PD sample (remaining blood) that was centrifuged to isolate plasma and stored frozen at minus 80 ºC. The spleen was collected from all mice, the tissue weight recorded and placed into RPMI 1640 media on wet ice for immediate analysis.

PD plasma samples were assayed by ELISA for KLH specific IgG and IgM antibody concentration as described in section 2.7.2, along with mAb SA271G2 concentration by a Gyrolab based immunoassay, as described in section 2.4.2. PK blood:water samples were assayed for Fingolimod and its phosphorylated metabolite by specific LC-MS/MS assay as described in 2.5. The B cell, germinal centre B cell, T cell and T follicular helper cell populations were analysed in the spleen tissue by flow cytometry, as described in 2.10. In addition, the B and T cell populations were monitored in blood collected on study days 8 and 16, as described in 2.10.

2.3.7. PKPD study 6: Evaluation of the concentration-effect relationship of Fingolimod in the mouse IV KLH TDAR model

To aid development of a simple mathematical PKPD model to describe therapeutic intervention of the primary humoral immune response to T-dependent KLH challenge, the clinically validated gold standard molecule Fingolimod was explored. To ensure collection of an ideal training data set for the PKPD model, a dose range was tested that would encompass both maximal and no drug effect extremes whilst providing sufficient coverage of the concentration effect relationship to enable mathematical modelling. The study was designed to generate data across a greater than 3000-fold dose concentration window, incorporating eight individual treatment levels. A maximum dose concentration of 10 mg/kg was selected, based on a combination of literature and in-house efficacy data. This dose would be expected to exceed the maximum effect level but results in no welfare concerns following repeated administration. Groups size was minimised to n=4, to ensure provision of a statistically relevant number of observations for covariance analysis (30) and sufficient coverage of the sigmoidal response curve, whilst keeping a firm grip on study size to ensure an ethical and efficient study design. A larger group size was selected for the control (n=8), due to the natural increase in variability at the extremes of the sigmoidal response and the necessity of generating a reliable baseline response for mathematical PKPD model definition.

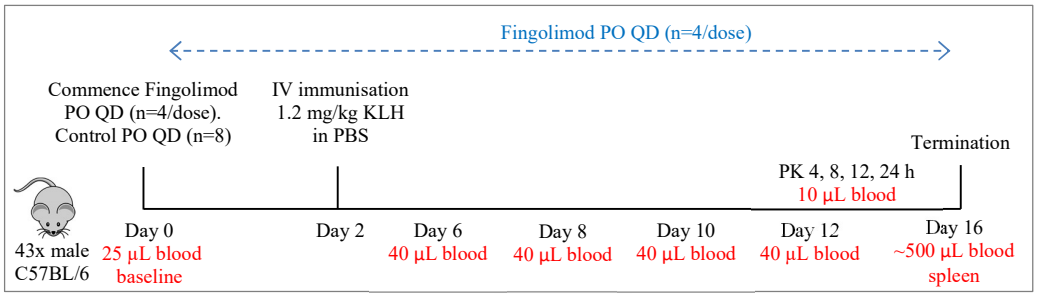

Figure 2.6. In-life protocol schematic for evaluation of the Fingolimod concentration-effect relationship in the IV KLH TDAR experimental model (PKPD study 6), illustrating the timeline of in-life procedures and sampling occasions.

The in-life study protocol is summarised in figure 2.6 and proceeded as follows. On study day 0, forty C57BL/6 male mice were divided into nine treatment groups to receive Fingolimod at eight individual dose concentrations (n=4) or receive control (n=8). An additional n=3 mice were included as a naïve control, receiving no treatment. All mice were weighed daily, starting on day 0, to allow weight adjusted dosing and monitor wellbeing throughout the study. Eight treatment groups (n=4) received Fingolimod suspended in a dosing vehicle of 1% methylcellulose 400 (aq) by daily oral gavage at half log unit descending dose concentrations from 2 mg/mL. The daily oral doses were administered at 5 mL/kg to achieve a weight adjusted target dose range of 10 mg/kg down to 0.003 mg/kg. A control group (n=8) received 1% methylcellulose 400 (aq) alone, by daily oral gavage at 5 mL/kg. On study day 2, 1 h post oral Fingolimod or control administration, each mouse in all treatment groups received a single IV administration via the tail vein of KLH (Imject mcKLH, ThermoFisher Scientific, #77600) formulated in PBS at 0.24 mg/mL, using a dose volume of 5 mL/kg to achieve a target challenge dose of 1.2 mg/kg.

A baseline blood sample was collected by tail nick micro sampling prior to treatment on day 0, with a 25 µL volume of blood taken using EDTA coated plasma separation capillary tubes (Drummond Scientific). Capillary tubes were centrifuged to isolate plasma, yielding approximately 10 µL, which was transferred to matrix tubes and stored frozen at -80 ºC. In study blood sampling commenced on day 6 by tail nick sampling, with blood samples collected every 2 days until study day 12. On each occasion, a PD sample was collected by EDTA coated plasma separation capillary tube (30 µL) and the plasma isolated as described previously. A further PK blood sample (10 µL) was collected by pipette directly from the tail nick, added to a matrix tube and mixed with an equal volume of water. The pipette tip was

precoated with EDTA prior to sample collection by drawing and expelling a volume of EDTA. Both samples were stored frozen at -80 ºC. On study day 12, additional blood samples were collected at 4, 8 12 and 24 h post drug administration to define the intraday pharmacokinetics of Fingolimod. A blood sample (10 µL) was collected by pipette directly from the tail nick as described previously, transferred to a matrix tube, diluted with an equal volume of water, mixed and frozen at -80 ºC.

On study day 16, at 1 h post oral Fingolimod or control administration, all mice were anaesthetised using O_2/isoflurane and a terminal blood sample (ca 500 µL) was obtained via cardiac puncture. All mice were then euthanised via cervical dislocation, with death confirmed by severing of a major thoracic artery. The terminal blood sample was split into a PK sample (10 µL) diluted with an equal volume of water and stored frozen at -80 ºC and a PD sample (remaining blood) that was centrifuged to isolate plasma and stored frozen at -80 ºC. The spleen was excised post mortem from all mice and placed into RPMI 1640 media on wet ice for immediate analysis.

PD plasma samples were assayed by ELISA for KLH specific IgG and IgM antibody concentration as described in section 2.7.2. PK blood:water samples were assayed for Fingolimod and its phosphorylated metabolite by a specific LC-MS/MS assay, as described in section 2.5. The B cell, germinal centre B cell, T cell and T follicular helper cell populations were analysed in the spleen tissue by flow cytometry, as described in section 2.10.

2.3.8. PKPD study 7: Evaluation of the concentration-effect relationship of the surrogate mouse CD21 specific mAb 7G6 in the IV KLH TDAR mouse experimental model

To generate the data required to mathematically model the extent of CD21 target engagement required to drive efficacy in the TDAR experimental mouse model, a study was performed using a similar protocol design to that used to investigate Fingolimod. The extensively published rat anti-mouse CD21 mAb 7G6 was selected for this study. This mAb has been widely characterised in the literature and was shown to be efficacious in this project in the head to head study (PKPD study 1, chapter 5, 5.4.1) performed in the adjuvant driven IP TNP-KLH TDAR experimental mouse model, demonstrating target engagement and strong inhibition of the germinal centre response when administered prophylactically IP at 8 mg/kg. There is no published data detailing the dose response of any antibody against CD21, with

data reported only at single saturating doses. Therefore, the objective of this study was to collect an ideal data set for PKPD modelling, encompassing both maximal and no drug effect extremes, whilst minimising study complexity to ensure an ethical and efficient study design.

The study was designed to generate data across a 1000-fold dose concentration window, incorporating seven individual treatment levels. A maximum dose concentration of 10 mg/kg was selected, based on earlier evidence that this dose would be expected to saturate the target. Repeated administration every 96 h (Q4D) was selected as an approach to maintain drug exposure across the study at the lower dose levels. This was selected based on a pre-study prediction of mAb 7G6 exposure, using the PK model described in chapter 4 (PK model v2), as illustrated in figure 2.7. Group size was again minimised to n=4, to ensure provision of a statistically relevant number of observations for covariance analysis and sufficient coverage of the sigmoidal response curve, whilst keeping a firm grip on study size to ensure an ethical and efficient study design. A larger group size was selected for the control (n=8) as previously, due to the natural increase in variability at the extremes of the sigmoidal response and the necessity of generating a reliable baseline response for mathematical PKPD model definition. An additional PBS only control was included as a negative control for any isotype effect, whilst Fingolimod was included as a study positive control to confirm experimental performance.

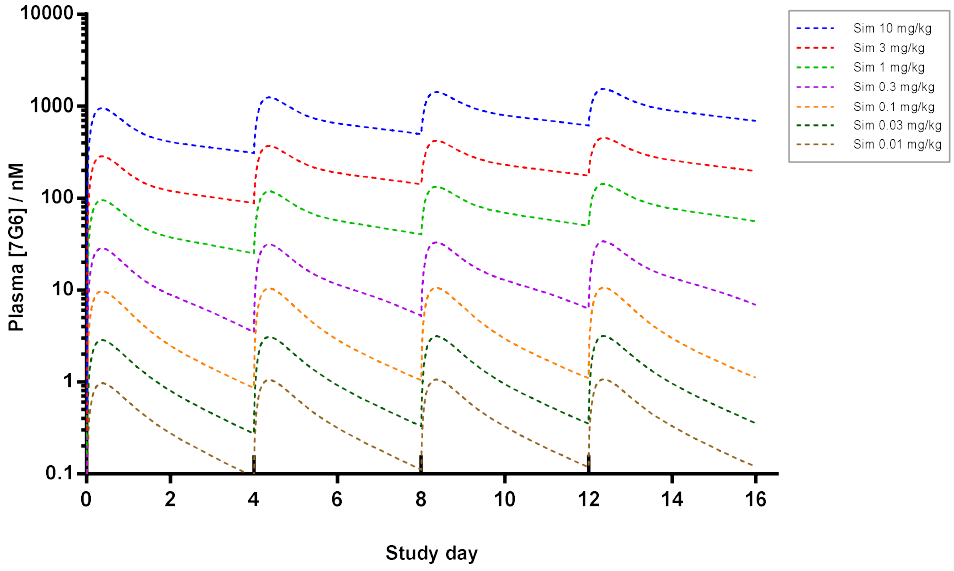

Figure 2.7. Pre-study prediction of mAb 7G6 plasma exposure at the seven proposed doses in PKPD study 7, completed with PK model v2 (described in chapter 4) using the Simbiology software package (v5.9). The proposed doses were at 0.01, 0.03, 0.1, 0.3, 1, 3 and 10 mg/kg, administered IP every 96 hours for a total of 4 doses.

The study design is summarised in figure 2.8 and described here as follows. On study day 0, the mice were weighed and divided into eleven treatment groups. Seven groups were administered mAb 7G6 in PBS (n=4) by IP injection every 96 h (day 0, 4, 8 and 12) at half log unit descending dose concentrations from 1 mg/mL. The IP dose was administered at 10 mL/kg to achieve a weight adjusted target dose range of 10 mg/kg down to 0.01 mg/kg. A control group received an isotype control mAb (rat IgG2b) in PBS (n=8) by IP injection every 96 h at 1 mg/mL, using a 10 mL/kg dosing volume to achieve a weight adjusted target dose of 10 mg/kg. An additional control group received PBS alone (n=4) by IP injection every 96 h using a 10 mL/kg dosing volume. A positive control group was also included, which was administered Fingolimod (n=4) suspended in a dosing vehicle of 1% methylcellulose 400 (aq) by daily oral gavage at 0.6 mg/mL, using a 5 mL/kg dosing volume to achieve a weight adjusted target dose of 3 mg/kg. A naive group (n=3) acted as a control for flow cytometry endpoints, receiving no treatment, challenge or sampling prior to the terminal day.

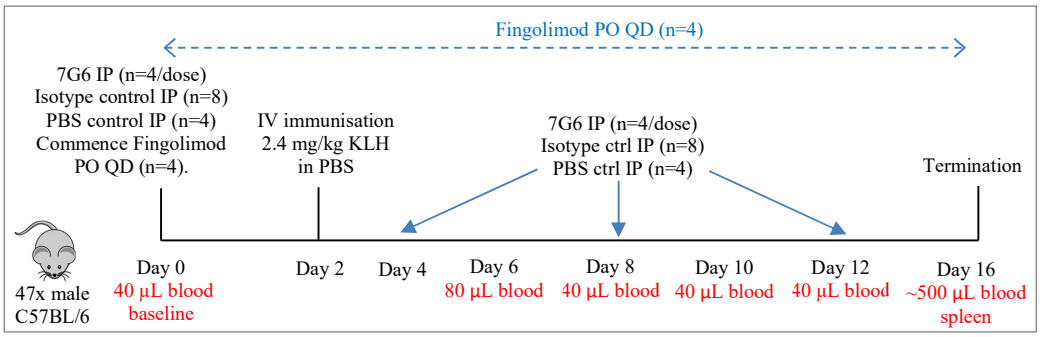

Figure 2.8. In-life protocol schematic for evaluation of the surrogate anti-CD21 mAb 7G6 in the IV KLH TDAR experimental mouse model (PKPD study 7), illustrating the timeline of in life procedures and sampling occasions.

Drug treatment commenced two days prior to IV KLH immunisation, to allow time for full distribution of the mAb to occur or to allow maximal biological impact of Fingolimod. On study day 2, at 1 h post Fingolimod administration to the positive control group, all mice received a single IV administration of KLH (Imject mcKLH, ThermoFisher Scientific, #77600) formulated in PBS at 0.24 mg/mL via the tail vein, using a dose volume of 10 mL/kg to achieve a challenge dose of 2.4 mg/kg. An error on the day of the study resulted in the dosing volume of 10 mL/kg and the higher challenge dose compared with previous studies.

A baseline blood sample (40 µL) was collected from all animals prior to initial drug administration by tail nick sampling using EDTA coated plasma separation capillary tubes

(Drummond Scientific). Capillary tubes were centrifuged to isolate plasma, yielding approximately 20 µL, which was transferred to matrix tubes and stored frozen at -80 ºC. In study blood sampling commenced on study day 6 by tail nick sampling, with blood samples collected every 2 days until study day 12. On each occasion, a blood sample (40 µL) was collected by EDTA coated plasma separation capillary tubes and plasma isolated as described previously. The plasma was transferred to matrix tubes and stored frozen at -80 ºC. On study day 6, an additional volume of blood (40 µL) was collected and stored on ice for immediate analysis by flow cytometry.

On study day 16, at 1 h post drug administration to group 10, all mice in each group (1 to 11) were anaesthetised using O_2/isoflurane and a terminal blood sample (ca 500 µL) was obtained via cardiac puncture. All mice were then euthanised via cervical dislocation with death confirmed by severing of a major thoracic artery. The terminal blood sample was divided so that 50 µL was retained on ice for immediate analysis by flow cytometry, whilst the remaining blood was centrifuged to isolate plasma and stored frozen at -80 ºC. The spleen was excised post mortem from all mice and stored in RPMI 1640 media on ice for immediate analysis by flow cytometry.

Plasma samples were sequentially assayed for several endpoints, performed in the following order. KLH specific IgG and IgM antibody concentration by ELISA, as described in section 2.7.2. Drug concentration, either by a Gyrolab based immunoassay for 7G6 or LC-MS/MS for Fingolimod, as described in sections 2.4.2 and 2.5 respectively. Terminal samples were additionally assayed for KLH specific IgG subtypes by ELISA, as described in section 2.7.3, and for soluble CD21 protein concentration by LC-MS/MS as described in section 2.9.3. Blood samples collected on day 6 and 16 were assayed for target engagement by flow cytometry, as described in section 2.10. The spleen tissue was assayed for B cell and germinal centre B cell populations, along with B cell target engagement by flow cytometry, as described in section 2.10.

2.4. Immunoassay quantification of mAbs 7G6, 4B2, 9E10 and SA271G2

2.4.1. Antigen capture immunoassay [7G6/4B2/9E10]

Specific antigen capture immunoassays were developed on the Gyrolab platform to determine the concentration of the three surrogate mAbs; 7G6, 4B2 and 9E10. The assay design involved an antigen capture - antibody detection format, utilising a recombinant mouse CD21 protein

(amino acid 21-970) generated in house as the capture antigen and an anti-species FC region specific antibody for detection. Prior to use in the assay, the recombinant mouse CD21 protein was conjugated with biotin to facilitate capture to the streptavidin coated column within the microfluidics well of the compact disc. The biotinylation procedure followed that provided with the EZ-link sulfo-NHS-LC-biotin kit (Thermofisher Scientific. #21327). In brief, the N-hydroxy succinimide (NHS) activated biotin reagent reacts with primary amino groups in the protein structure. The labelling reaction was conducted using a 20-fold molar excess of biotin at room temperature for 1 h. The labelled protein was purified using a 2 mL Zeba spin desalting column (Thermofisher Scientific. #89890) following the manufacturers guidelines.

A Gyrolab xP workstation instrument operating software version Gyrolab 5.2.0 was used to perform all assay development and sample analysis. Assay conditions were optimised for absolute sensitivity in advance utilising a bioaffy 1000 compact disc (Gyros AB, #P0004253). The selected final assay conditions used the biotinylated CD21 capture protein at 100 μg/mL, along with the AlexaFluor 647 AffiniPure goat anti-rat IgG Fcγ (Jackson ImmunoResearch. #112-605-071) or AlexaFluor 647 Dylight goat anti-mouse IgG Fc (Jackson ImmunoResearch. #115-495-071) detection reagents at 4 μg/mL. Standards were prepared in pooled male C57BL/6 control plasma (BioIVT) over the range 10 to 20000 ng/mL and assayed in duplicate. Quality control samples were included during analysis of PK study samples. These were prepared in pooled male C57BL/6 control plasma (BioIVT) as four individual replicates at a low, mid and high concentration across the calibration range. A set of 6 blank samples were also prepared in an identical manner in the absence of drug. All samples, standards, blanks and quality controls were further diluted 30-fold with Rexxip A buffer (Gyros AB, #P0004820) prior to addition to the assay plate. The assay was performed using an automated three step method, taking approximately 1.5 hours to complete. Where required, plasma samples and dose solutions were diluted into the range of the assay with pooled male C57BL/6 control plasma prior (BioIVT) to analysis.

Quantification of unknowns was conducted by exporting the response data into the GraphPad Prism 8.1.2 (GraphPad Software, Inc) software package and fitting the calibration standards with a $1/y^2$ weighted five-parameter logistic fit. The assay LLQ was set as the first standard that was statistically distinct from the group of blanks as determined by the Dixons Q test and within +/-20% of the nominal concentration. Any standards that were determined to be indistinct from the blanks by the Dixons Q test were included in the calibration line as anchor points to allow accurate fitting of the five-parameter logistic fit. Standards with a back calculated accuracy outside +/-20% of the nominal concentration were excluded from the final

calibration curve. A minimum of seven accepted standards were required to form the final calibration line, with at least 50% of the quality control samples within +/-20% of nominal concentration (where applicable) for confirmation of assay performance. Unknowns were then interpolated from this standard curve to give the drug concentration. Samples that fell outside of the range of the calibration curve were diluted and repeated where appropriate. Assay performance was maintained through strict adherence to these assay acceptance criteria, with analysis repeated when criteria were not met. Prior to implementation of the mAb plasma assay for sample analysis, it was assessed for reproducibility, freeze thaw stability, dilution linearity and matrix interference.

2.4.2. Generic capture immunoassay [7G6/SA271G2]

In a modification to the methodology used in earlier studies, a generic capture format immunoassay was employed to measure mAb 7G6. This differentiates the drug via its rat origin FC region, using a non-cross-reactive rat IgG2b specific capture antibody, as opposed to using its unique specificity for CD21. This change was made to overcome possible assay interference from soluble CD21, when measuring low drug concentrations in plasma. Due to a shared rat IgG2b origin, the anti-CD20 mAb SA271G2 was able to be assayed using the same methodology.

In brief, the assay utilised a biotinylated anti-rat IgG2b antibody at 5 µg/mL (Biolegend Inc, #MRG2b-85) as the capture, with an AlexaFluor 647 labelled goat anti-rat IgG antibody (Jackson ImmunoResearch, #112-605-071) at 4 µg/mL as the detection reagent, all performed on a bioaffy 200 compact disc (Gyros AB, #P0004180). Calibration standards and blanks were prepared in pooled male C57BL/6 control plasma (Envigo), over the range 10 to 20000 ng/mL, using either mAb 7G6 or SA271G2. All samples, standards and blanks were diluted 1:10 with Rexxip A buffer (Gyros AB, #P0004820) prior to analysis. The assay was performed on a Gyrolab xP workstation instrument operating software version Gyrolab 5.2.0, using an automated three step method, taking approximately 1.5 hours to complete. Where required, plasma samples were diluted into the range of the assay prior to analysis, using pooled male C57BL/6 control plasma. Quantification of unknowns was conducted as described in section 2.4.1, using the GraphPad Prism 8.1.2 (GraphPad Software, Inc) software package.

2.5. LC-MS/MS quantification of Fingolimod and Fingolimod phosphate

Fingolimod undergoes reversible phosphorylation to form its active moiety Fingolimod phosphate, in a dynamic process that can occur in blood and tissue, both *in vivo* and *ex vivo*. It is therefore important to quantify both compounds, ideally simultaneously, to monitor the concentration profile of each. Due to Fingolimod being highly distributed into the cellular component of blood, whole blood is the matrix of choice for this analysis. However, this results in the requirement for control of *ex vivo* interconversion between Fingolimod and Fingolimod phosphate post sampling, to preserve accurate portrayal of the systemic exposure for each compound. This sample stability problem was investigated by Nirogi *et al.* (2017), who concluded that dilution of whole blood at the point of collection to lyse the blood cells, followed by storage at -70ºC, resulted in stability of Fingolimod and Fingolimod Phosphate in the samples. This post collection procedure was therefore adopted for maximum stability when specifically investigating Fingolimod. In later studies, where Fingolimod was acting as a model positive control, 5 µL of plasma was collected and frozen at -70ºC to minimise the blood volume requirement on each sample occasion.

The simultaneous determination of Fingolimod and Fingolimod phosphate in blood or plasma was achieved using a specific LC-MS/MS based MRM assay, optimised for specificity, throughput and sample size minimisation. LC-MS/MS is widely reported for the detection of Fingolimod and Fingolimod phosphate in clinical studies, but typically these assays are performed separately. However, because absolute assay sensitivity was not a key objective in method development, a combined approach was adopted to minimise sample usage, similar to that recently described by Emotte *et al.* (2012). Again, because absolute assay sensitivity was not a key requirement, a complicated sample preparation process was not pursued. Instead, the relatively simple and inexpensive technique of protein precipitation was used to extract the two compounds from the biological matrix, providing sufficient assay sensitivity.

The final protocol is described in brief, as follows. Diluted blood samples (1:1 blood:water, v/v) or plasma samples were defrosted at room temperature prior to extraction via protein precipitation, using a 5-fold excess of acetonitrile containing an internal standard compound. The samples were thoroughly mixed, centrifuged at 4000x g and the resulting supernatant isolated for analysis by reverse phase LC-MS/MS. All analysis was undertaken with a Shimadzu Nexera integrated UPLC system, linked to an AB Sciex API4000 triple quadrupole mass spectrometer operating an ESI interface in positive ionisation mode. Nominal mass transitions were 308 to 255 Da and 388 to 255 Da for Fingolimod and Fingolimod phosphate

respectively. Chromatographic separation was achieved with a Phenomenex Kinetex C18 50 x 2.1 mm analytical column using a 3.15 minute gradient elution method, a 0.8 mL/min flow rate and a 0.1% formic acid (aq) (v/v) aqueous phase / acetonitrile + 0.1% formic acid (v/v) organic phase. Initial conditions were 10% organic, with a gradient transition to 100% organic achieved between 0.2 and 2.3 minutes. The conditions were held to 2.9 minutes, before a return gradient to 10% organic up to 3.0 minutes.

Unknowns were assayed against calibration standards prepared in either control diluted blood (1:1 blood:water, v/v) or plasma, across a 0.1 to 2000 ng/mL (Fingolimod) or 0.2 to 5000 ng/mL (Fingolimod phosphate) range and analysed in duplicate. A quadratic 1/x weighted regression analysis was used to fit the measured peak area ratio (analyte peak area / internal standard peak area) of the calibration standards, with this equation used to interpolate unknowns and derive the analyte concentration. Assay lower limits of quantification were typically 0.5 ng/mL for Fingolimod and 1 ng/mL for Fingolimod phosphate.

2.6. Pharmacokinetic interpretation

The plasma concentration time data was used to estimate PK parameters for each surrogate mAb using non-compartmental analysis (Phoenix Winnonlin, version 6.3. Pharsight). Pharmacokinetic parameters were calculated following IV administration for each animal prior to being summarised as a mean and standard deviation at each dose level. The AUC_t was calculated using the linear-up log-down trapezoidal rule up to the last quantifiable time point (C_{last}). Extrapolation to AUC_∞ was achieved using the C_{last} divided by the elimination rate constant, k, obtained by uniform weighted linear regression analysis of the terminal elimination phase containing at least three time points. AUC_∞ was only reported where the extrapolated area did not define greater than 20% of the total AUC_∞. The linear regression of the terminal phase was also used to estimate the terminal half-life ($t_{1/2}$) with the value reported where study duration continued for a minimum of three half lives. Total plasma clearance (Cl_p) was calculated using dose/AUC_∞ where the dose was defined by the weight of dose solution administered to the individual, except where otherwise stated. The apparent volume of distribution at steady state (V_{ss}) was calculated by dose*$AUCM_\infty$/ AUC_∞^2 where $AUCM_\infty$ is the area under the moment curve.

Pharmacokinetic parameters were also calculated following IP administration, with the AUC_t calculated using the linear trapezoidal rule up to the last quantifiable time point (C_{last}).

Extrapolation to AUC_{∞} was achieved using the C_{last} divided by the elimination rate constant, k, obtained by uniform weighted linear regression analysis of the terminal elimination phase containing at least three time points. The half-life was again estimated from the linear regression and the time to reach maximal plasma concentration T_{max} observed from the plasma concentration data. Bioavailability (F%) via the IP route was calculated by dividing the mean AUC_{∞} IP by the mean AUC_{∞} IV determined from the 2 mg/kg (7G6/4B2) or 1.5 mg/kg (9E10) dose group.

2.7. Antigen specific IgG / M quantification

A sandwich ELISA assay was selected as the most suitable approach for the measurement of the low affinity antigen specific antibodies generated in the T-dependent immunisation studies. Antigen, which here is the KLH immunogen, was used as the capture reagent, with detection through a labelled secondary antibody against murine IgG or IgM. Although high assay background is expected because of the low affinity basal antibodies present in control plasma, the antigen specific antibody response is expected to be strong. Therefore, the large minimum required dilution (MRD) should overcome the effect of the background response and provide a sufficiently sensitive assay.

2.7.1. TNP specific IgG / M ELISA

An antigen capture immunoassay was used to provide relative quantification of the TNP specific IgG and IgM antibody response in plasma. This was a sandwich format assay, utilising BSA conjugated TNP (TNP-BSA, LGC Biosearch Technologies, T-5050) at 10 µg/mL in PBS as the capture protein, adsorped overnight at 4 ºC to a Nunc MaxiSorp 96 well plate (ThermoFisher Scientific). Plates were washed between assay steps with PBS + 0.1% tween 20 to remove any unbound material. TNP specific antibody concentrations were determined with calibration standards prepared across the range 39 to 20000 pg/mL in buffer (1% BSA in PBS) and assayed in duplicate. The purified murine anti-TNP IgG antibody 107.3 (BD Biosciences, 554054) was used to standardise the IgG assay. In the absence of a suitable IgM standard, the biotin mouse anti-TNP IgG2b 49.2 was used to provide relative quantification. All samples were diluted into the range of the calibration standards with PBS + 1% BSA. 50 µL of diluted samples and standards were incubated in the plate for 2 h at room temperature with gentle shaking. Biotin conjugated secondary antibodies for IgG1 (Biotin rat anti-mouse

IgG1 A85-1, BD Biosciences, 553445) or IgM (Biotin rat anti-mouse IgM R6-60-2, BD Biosciences, 553406) were then added at 2 μg/mL for 1 h, prior to detection through streptavidin conjugated horseradish peroxidase (Thermo Fisher Scientific, 21126) at 0.1 μg/mL. The assay was read via colorimetric change, initiated by the substrate TMB (Sur Modics Biofx, TMBS-0100-01), quenched by a dilute acid stop reagent (Sur Modics Biofx, LSTP-0100-01) and quantified by spectrophotometry at a wavelength of 450 nm (Molecular Devices, Spectramax 250).

Quantification of unknowns was conducted by exporting the optical density (OD) values into the software package GraphPad Prism 8.1.2 (GraphPad Software, Inc) and fitting the calibration standard responses with a $1/y^2$ weighted 5 parameter logistic fit. The assay LLQ was set as the first standard that was statistically distinct from the group of blanks, as determined by a Dixons Q test, and within +/-20% of the nominal concentration. Any standards that were determined to be indistinct from the blanks by the Dixons Q test, were included in the calibration line as anchor points to allow accurate fitting of the 5-parameter logistic fit. Standards with a back calculated accuracy outside +/-20% of the nominal concentration were excluded from the final calibration curve. Unknowns were interpolated from the standard curve to give the concentration, before multiplication by the dilution factor to give the original sample concentration. Assay performance was maintained through strict adherence to assay acceptance criteria, with analysis repeated or results excluded when criteria were not met.

2.7.2. KLH specific IgG / M ELISA

The change to a high molecular weight KLH (Imject Mariculture (mc) KLH, ThermoFisher Scientific) challenge necessitated optimisation of a new assay for quantification of KLH specific IgG and IgM. A similar antigen capture immunoassay format was utilised, with Imject mcKLH (ThermoFisher Scientific) at 5 μg/mL adsorbed overnight at 4 ºC to Nunc MaxiSorp 96 well plates (ThermoFisher Scientific). Plates were washed between assay steps with PBS + 0.1% tween 20 to remove any unbound material. KLH specific antibody concentrations were determined using calibration standards prepared across the range 0.2 to 100 ng/mL (IgG) or 0.8 to 400 ng/mL (IgM) in buffer (1% BSA in PBS) and assayed in duplicate. KLH specific antibodies were identified to standardise the IgG and IgM assay through initial screening of several potential mAbs with reported KLH specificity, to find those that bound to the Imject mcKLH form. This identified the mouse anti-KLH IgG (Abcam, Ab34607) and mouse anti-KLH IgM (Ray Biotech, RB-14-006) antibodies to act as assay standards for quantification.

All samples were diluted into the range of the calibration standards with 1% BSA in PBS. 50 µL of diluted samples and standards were incubated in the plate for 2 h at room temperature with gentle shaking. Detection was achieved through HRP conjugated secondary antibodies against IgG (Goat anti-mouse IgG HRP conjugate, Biolegend, 405306) or IgM (Goat anti-mouse IgM HRP conjugate, Abcam PLC, Ab97230) added at 0.2 µg/mL for 1 h at room temperature. The assay was read via colorimetric change, initiated by the substrate TMB (Sur Modics Biofx, TMBS-0100-01), quenched by a dilute acid stop reagent (Sur Modics Biofx, LSTP-0100-01) and quantified by spectrophotometry at a wavelength of 450 nm (Molecular Devices, Spectramax 250). Quantification of unknowns was completed as described in 2.7.1.

2.7.3. KLH specific IgG isotype ELISA

To further unravel the observed antigen specific IgG response to the TD antigen KLH, an assay was developed to quantify the contributions of each IgG isoform to the overall response. There are four expressed isoforms of IgG in the mouse; IgG1, IgG2b, IgG3 and either IgG2a or IgG2c, dependent on the strain of mouse. Inbred mouse strains such as C57BL/6 express IgG2c (Collins, 2016). The format of the isotype specific assay is the same as the total KLH specific IgG assay previously described (2.7.2), a simple sandwich ELISA format utilising the antigen KLH as the capture reagent. The key difference is that an isotype specific secondary antibody, with minimal cross reactivity to the other isoforms, is used in place of the non-specific anti-IgG antibody. Therefore, a crucial step in method development was to confirm that each assay was indeed uniquely able to quantify the isoform of interest, with minimal detection of other isoforms. The specificity of the detection reagent also necessitated a change in the antibody used to standardise the assay to an isotype matched KLH specific antibody. The total KLH specific IgG assay (2.7.2) used an IgG1 antibody standard, so additional antibodies of the form IgG2b, IgG2c and IgG3 were sought. Several potential mAbs were purchased for testing, resulting in identification of the mouse anti-KLH IgG2b mAb MG2b-57 (Abcam, #ab18421) and the mouse anti-KLH IgG3 mAb MG3-35 (Abcam, #ab18394) as suitable standards. Disappointingly a suitable murine IgG2c antibody that recognised the form of KLH used in these studies (Imject mcKLH, Thermofisher Scientific) could not be identified, hence IgG2c was assayed via the alternative procedure described below. However, for IgG1, IgG2b and IgG3 the remaining assay steps followed that described for the total KLH specific IgG in section 2.7.2.

In the absence of an appropriate standard, an endpoint titre determination method was implemented for assessment of KLH specific antibodies of the IgG2c isotype. This approach follows the same basic sandwich assay principle as described for the other IgG isotypes. KLH was coated onto Nunc MaxiSorp plates (ThermoFisher Scientific) as the capture, with an isotype specific HRP conjugated antibody used for detection (goat anti-mouse IgG2c HRP conjugate, Abcam, #Ab97255). The remaining assay steps followed that described for the total KLH specific IgG in section 2.7.2. However, in place of a purified standard to create a calibration line, negative controls are used to define an absorbance cut off value with which to confirm a positive result. Each sample is then serially diluted to create a response curve in the assay, with the endpoint titre the reciprocal of the largest dilution required to result in an absorbance value equal to the cut off. Thus, providing a semi-quantitative measure for comparison of samples containing varying concentrations of analyte.

To provide an 8-point response curve, samples were serially diluted 1:1 across the range 1:100 to 1:25600. A curve was fitted to the response data for each sample, following the approach described by Zrein *et al.* (1986), to accurately determine the endpoint titre. A four-parameter logistic fit sigmoidal curve was fitted to the data for each sample using the software package GraphPad Prism v8.1.2 (GraphPad Software, Inc). An appropriate assay cut off was defined as the mean response measured in plasma from the naïve treatment group (n=3) plus three times standard deviation. This cut off was selected using the standard deviation multiplier methodology described by Frey *et al.* (1998) with a confidence level of 95%. The endpoint titre was then determined from each curve as the reciprocal of the dilution resulting in a response value equivalent to the cut off. Each plate contained a blank control sample to define the absolute assay background originating from the detection system.

2.8. Anti-drug antibody bridging ELISA

Due to the rat origin of the tool anti-CD21 mAb 7G6, it has a residual immunogenicity when administered to the mouse that can cause the rapid generation of anti-drug antibodies (ADA). Whilst loss of drug exposure is a tell-tale sign of the impact of an ADA response to the mAb, definitive evidence is required to ensure sensitive detection of ADAs and prevent them confounding results. Due to the rat IgG2b backbone of mAb 7G6, such an ADA response could be directed against multiple regions of the antibody and would thus be difficult to standardise. As such, a qualitative homogeneous bridging immunoassay was developed, utilising the MSD platform.

The homogeneous bridging format involves the simultaneous exposure of the sample to an excess of capture and detection antibodies, which here are biotin and SULFO-TAG labelled mAb 7G6 respectively. Biotin labelled mAb 7G6 was purchased (BD Biosciences, #562796), whilst SULFO-TAG labelled mAb 7G6 was prepared in house following the manufacturers guidelines (Gold SULFO-TAG NHS Ester conjugation kit, Meso Scale Diagnostics LLC, #R31AA). To overcome the high free drug concentration expected in the samples, an acid pre-treatment step was also included. Acid induced dissociation of drug-ADA complexes has been demonstrated to improve the drug tolerance of immunogenicity assays (Patton *et al.*, 2005). This pre-treatment step involves the exposure of the sample to low pH conditions, resulting in the reversible dissociation of antibody binding. Protocol development followed the basic approach recommended by Meso Scale Diagnostics, modified to accommodate the small volume of plasma available in the study. The final protocol was shown to provide a marked improvement in drug tolerance compared to a standard homogeneous assay, reducing the signal loss caused by 10 µg/mL 7G6 from 98% to 34%, when using the mouse anti-rat IgG2b antibody MRG2b-85 (Biolegend Inc, #408202) as an assay positive control.

The final homogeneous bridging assay protocol to detect 7G6 induced ADA in the mouse is described as follows. The acid pre-treatment was completed using a 1:10 dilution of the plasma samples with 300 mM acetic acid (v/v) and a 45 minute incubation at room temperature. During the incubation, a master mix was prepared of the biotin-7G6 (BD Biosciences, #562796) capture reagent and SULFO-TAG-7G6 (BD Biosciences, #559831, SULFO-TAG labelled in house) detection reagent at a final concentration of 2 µg/mL in PBS + 1% BSA. 60 µL of the master mix was added to each well of a 96 well plate along with 8 µL of 1.5 M Trizma base (pH 10). 33 µL of the acid pre-treated sample followed, the samples were mixed and incubated at room temperature for 2 h to enable binding of the capture and detection reagents to any ADA present. The samples were then transferred to a 96-well small spot Streptavidin Gold plate (Meso Scale Diagnostics LLC, #L45SA) that had been pre-blocked with PBS + 1% BSA and incubated for 1 h at room temperature to capture the bridged complex. The plates were washed and then read immediately with 150 µL of 2x Read Buffer T (Meso Scale Diagnostics LLC, #R92TC) on an MSD Sector S 600 plate reader (Meso Scale Diagnostics LLC). Positive control samples were prepared at 0.1, 1, 10 and 100 µg/mL with mouse anti-rat IgG2b MRG2b-85 (BioLegend Inc, #408202) and processed alongside samples to provide confirmation of assay performance. Plasma samples were identified as ADA positive where the electrochemiluminescence (ECL) signal was measured to be greater than double that of the mean baseline response prior to 7G6 treatment.

2.9. Soluble CD21/35 quantification

2.9.1. sCD21/35 MSD immunoassay

An immunoassay-based methodology was initially developed, utilising the small repertoire of murine CD21 specific antibodies and a recombinant murine CD21 protein. The approach had limitations, in that despite testing numerous commercially available murine CD21 specific antibodies during method development, only a single antibody 7E9 (Biolegend Inc, #123404) was determined by ELISA to bind the recombinant protein in a non-competitive manner with 7G6 and 4B2. A binding relationship previously published following the discovery of the antibodies 7G6 and 7E9 by Kinoshita *et al.* (1988). As a consequence of requiring at least one competitive antibody in the binding pair, the immunoassay approach was severely hampered by the presence of either 7G6 or 4B2 in the sample. Nevertheless, the assay was developed and used to define the baseline soluble CD21/35 concentration in pooled donor C57BL/6 male mouse plasma, revealing this to be 9975 ng/mL (0.0095 μM).

In brief, biotin conjugated 7G6 (BD Biosciences, #562796) was utilised as the capture reagent at 5 μg/mL, bound overnight at 4 ºC to pre-blocked (PBS + 1% BSA for 1 h) streptavidin gold 96 well plates (Meso Scale Diagnostics LLC, #L45SA). Plates were washed between each assay step with PBS + 0.1% tween 20 to remove any unbound material. Assay standardisation was completed using the in-house recombinant CD21 protein, diluted in buffer (PBS + 1% BSA) across the range 39 to 5000 ng/mL and assayed in duplicate. 25 μL of diluted samples and standards were incubated in the plate for 1 h at room temperature with gentle shaking. Detection was achieved via a SULFO-TAG labelled 7E9 (Biolegend Inc, #123404) secondary antibody, labelled in house following the manufacturers guidelines (Gold Sulfo tag NHS Ester conjugation kit, Meso Scale Diagnostics LLC, #R31AA), added at 0.5 μg/mL for 1 h at room temperature. Finally, the plates were read with 150 μL read buffer T x2 (Meso Scale Diagnostics LLC, #R92TC-1) using an MSD Sector Imager 6000 (Meso Scale Diagnostics LLC). Assay sensitivity was low, resulting in an assay LLQ of 78.1 ng/mL and plasma matrix interference was observed, resulting in a minimum recommended sample dilution of 1:10. Quantification of unknowns was conducted as previously described in section 2.7.1.

2.9.2. Alkaline degradation pre-treatment

To overcome the impact of competing drug (7G6/4B2) on the sCD21/35 MSD immunoassay, a sample pre-treatment approach was adopted, as described by Salimi-Moosavi *et al.* (2010).

This involves the use of high pH to dissociate and irreversibly denature protein bound antibody, whilst causing minimal degradation of the more pH stable protein. The alkaline treatment buffer was 1 M NaOH/0.5 M Glycine, 10% Casein (pH 13) prepared as described by Salimi-Moosavi *et al.* (2010). Plasma samples were diluted 1:1 with PBS + 1% BSA and added to a 96 well plate, prior to the addition of an equal volume of alkaline treatment buffer, mixed and incubated at 37 ºC with shaking. The alkaline pre-treatment period is protein dependent and was optimised to provide sufficient degradation of the interfering antibody, whilst retaining the target protein for detection via immunoassay. A 20 minute alkaline pre-treatment time was identified as optimal, providing assay tolerance to mAb 4B2 concentrations up to 50 µg/mL, returning sCD21/35 quantification to within 20% of the no drug control (figure 2.9). Following the pre-treatment period, the solution is neutralised via the addition of a 4-fold excess of 1 M potassium phosphate buffer (pH 6.0). The resulting sample is then ready for analysis using the MSD immunoassay procedure described in 2.9.1.

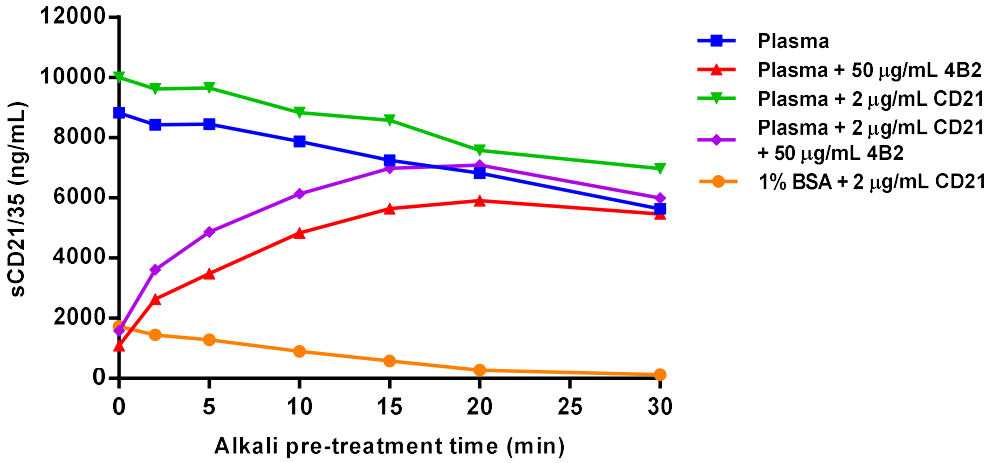

Figure 2.9. Comparison of the soluble CD21/35 concentration in male C57BL/6 mouse plasma alone or following the addition of either 50 µg/mL anti-CD21 mAb 4B2, 2 µg/mL recombinant CD21, or a combination of both, following pre-treatment under alkaline degradation conditions for a period of between 0 and 30 minutes. 1% BSA with the addition of 2 µg/mL recombinant CD21 served as an assay control and all samples were measured using an MSD based immunoassay (described in 2.9.1).

Whilst addition of the alkaline pre-treatment step to the immunoassay procedure successfully provided a method to quantify soluble CD21/35 with high drug tolerance, it additionally identified a difference in the behaviour of native and recombinant CD21/35. Under the same

alkaline pre-treatment conditions, 36% of the native CD21/35 concentration in plasma was degraded after 30 minutes, whereas a 3-fold higher loss (93%) of the recombinant CD21 protein was observed over the same period (figure 2.9). This was a concern, so LC-MS/MS was pursued as a confirmatory technique to provide confidence in the higher than expected sCD21/35 plasma concentration and to allay concern over the quality of the recombinant protein used to standardise the immunoassay.

2.9.3. sCD21/35 LC-MS/MS

2.9.3.1. Proteotypic peptide selection

Detection of proteins by standard LC-MS/MS technology requires the identification of a proteotypic peptide sequence, unique to the protein of interest and possessing amenable physiochemical properties, that can be enzymatically released from the protein. This exercise was completed *in silico*, utilising a combination of freely accessible online tools. The amino acid sequence for murine CD21 was retrieved (1025 amino acids) from the protein sequence database Universal Protein Resource Knowledgebase (UniProtKB) (UniProt, 2019), where it has the accession number P19070. An *in silico* enzymatic digestion was performed on the sequence with common proteases, utilising the PeptideCutter tool that forms part of the ExPASy bioinformatics software resources (Artimo *et al.*, 2012) operated by the Swiss Institute of Bioinformatics (SIB). This identified that trypsin, as the preferred protease due to its wide availability and low cost, resulted in 91 predicted cleavage sites of varying probability. Selection criteria were applied to identify peptides within this list that were potentially amenable to LC-MS, selecting peptides <2000 Da and with a 100% predicted trypsin cleavage probability. The predicted physicochemical properties of the identified peptide shortlist were then compared using the ExPASy ProtParam and Innovagen AB PepCalc online software tools. Successful peptides must be predicted to be; uncharged at pH 7, contain ionisable residues but unlikely to become multiply charged ($>M^{+2}$), have residual hydrophobic groups that may infer retention by reverse phase LC-MS, are stable, synthesisable, soluble and contain amino acid residues that can be isotopically labelled. Three candidate peptides were identified that passed these selection criteria, shown in table 2.2.

The three identified sequences were screened through the UniProtKB – Basic Local Alignment Search Tool (BLAST) tool to confirm sequence exclusivity to CD21, compared with the murine proteome. Peptide B is not unique to CD21, but also found within the protein Beclin-

1, thus was rejected from further consideration. The two remaining candidate peptides were unique and went forward to custom synthesis (Cambridge Research Biochemicals, UK) as both the parent and a stable isotopically labelled (SIL) form containing one $^{13}C_9$, ^{15}N-phenylalanine, to provide a +10 Da mass shift. The free cysteine in peptide A was blocked through a cysteine carbamidomethylation (CAM) modification to prevent instability due to oxidation, resulting in a monoisotopic mass increase of 57.02 Da. Later analysis concluded that peptide A provided superior selectivity in plasma for murine sCD21/35, with this peptide taken forward for quantitative analysis.

Table 2.2. Three candidate proteotypic peptide sequences identified from the CD21 protein sequence via an *in silico* scouting exercise. Key physicochemical properties are listed, demonstrating compatibility with LC-MS/MS analysis.

Peptide	AA Sequence	Location	Mwt	Theoretical pI	Hydrophobic group No.	Net charge at pH 7	Isotopic label (≥+8Da)	Unique
A	TISCSDPIVPGGFMNK	79 to 94	1665.94	pH 5.9	7	-0.1	F = +10	+
B	GVSFTLIGEK	304 to 313	1050.22	pH 6.8	5	0	F = +10 or L = +8	-
C	APYFYNDSVMFK	610 to 621	1481.69	pH 6.6	7	0	F = +10	+

2.9.3.2. LC-MS/MS conditions

A specific reverse phase LC-MS/MS analytical methodology was developed for the simultaneous detection of peptide A and its stable isotopically labelled internal standard, peptide A-SIL. This was completed using an AB Sciex Triple Quad 6500 mass spectrometer operating an ESI interface in positive ionisation mode, linked to a CTC autosampler and Jasco X-LC-3185PU modular HPLC system. Initial full scan analysis detected both peptides predominantly in the doubly charged state. Selection of MS/MS conditions for optimal sensitivity resulted in nominal MS/MS mass transitions for peptide A and peptide A-SIL of 861.8 to 750.2 and 866.7 to 760.1 Da respectively. Chromatographic separation was achieved with a Waters Xbridge BEH C18 (2.5 µM id, 2.1 x 100 mm) analytical column using a 10 minute gradient elution method, an 8 µL sample injection volume, a 0.3 mL/min flow rate and a 0.1% formic acid (aq) (v/v) aqueous phase / acetonitrile + 0.1% formic acid (v/v) organic phase. Initial conditions were 5% organic, with a gradient transition to 55% organic achieved between 0 and 7 minutes. A further gradient transition followed to 95% organic between 7 and

7.5 minutes, with conditions held until 8.5 minutes before a return gradient to 5% organic up to 9 minutes. A final 1 minute re-equilibration period was included between 9 and 10 minutes to ensure thorough column reconditioning in advance of the proceeding sample.

2.9.3.3. Enzymatic digestion

Excision of the proteotypic peptide from the parent protein requires a three step pre-treatment protocol in advance of enzymatic digestion. These steps denature the folded protein, reduce disulphide bonds and alkylate free reactive cysteines. The unfolded protein is then ready for in-solution digestion with purified trypsin. Rigorous sample clean-up is required post enzymatic digestion to prepare and concentrate the sample ready for LC-MS/MS analysis. The basic protocol steps were modified from Proc *et al.* (2010), with each step thoroughly optimised and tested for throughput, recovery and sample volume minimisation, without compromising sensitivity. The final protocol was shown to have a mean percentage recovery of 94% and 79% when recombinant CD21 was added to plasma at 5 and 20 µg/mL respectively, tested over five separate occasions (figure 2.10-B).

The final digestion protocol was optimised to require only 10 µL of plasma, added to a deep well 96 plate and denatured with 6 M guanidine HCl for 30 minutes at 60 ºC with shaking. Other denaturants were investigated, with deoxycholate the most suitable alternative, however guanidine HCl was shown to provide the best overall assay performance. Following denaturation, the samples were diluted 1:2 (v/v) with 15 mM TCEP (aq) and incubated for 30 minutes at 37 ºC for reduction of disulphide bridges. TCEP was preferable to common alternatives such as DTT, due to its compatibility with downstream processes negating the requirement to remove the reductant. To prevent reforming of disulphide bonds, the free thiol group of the cysteines was alkylated through a 1:3 (v/v) dilution with 40 mM iodoacetamide (aq) and incubated for 30 minutes at 37ºC in the dark. With the three-step pre-treatment complete, the samples were diluted with 25 mM ammonium bicarbonate to reduce the concentration of guanidine HCl below 1 M and provide conditions suitable for stable protease activity. 50 µg trypsin (Pierce trypsin protease, MS grade, ThermoFisher Scientific) was added and the samples were incubated overnight at room temperature in the dark with shaking. Other trypsin amounts were tested (figure 2.10-A), with 50 µg identified as the optimal ratio to the amount of protein present in the initial 10 µL of plasma. The following day, peptide A-SIL was added to the solution (25 ng) prior to quenching of the enzyme reaction with formic acid to result in a 2% acidified solution.

Excision of the proteotypic peptide is complete at this stage, but the sample digest also contains peptide fragments of the entire plasma proteome, along with the remaining unused reagents. To simplify this complex sample matrix, strong cation exchange solid phase extraction was used to clean up the samples but retain weakly basic peptides. The acidified sample digests were loaded into pre-conditioned (methanol / 2% formic acid (aq)) Phenomenex Strata-X-C 96 well SPE plates. The plates were washed with 2% formic acid (aq), followed by 0.1 M HCl in methanol, prior to elution into a 96 well collection plate with 5% NH4OH: 95% methanol. To concentrate the final sample, the eluent was evaporated to dryness under a stream of heated nitrogen (50 ^{o}C) and reconstituted in 95:5 0.1% formic acid (aq): acetonitrile, ready for analysis by LC-MS/MS.

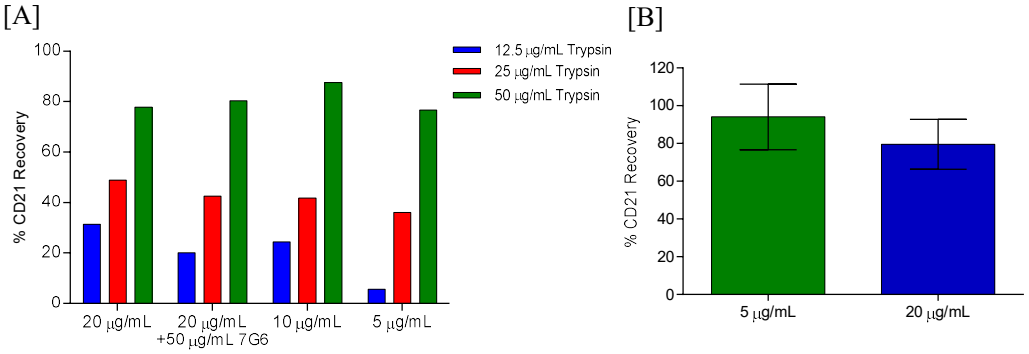

Figure 2.10. CD21 protein recovery results following tryptic digestion and LC-MS/MS analysis for optimisation of the experimental conditions and demonstration of assay performance and reproducibility. **[A]** Percentage recovery of recombinant CD21 when spiked into C57BL/6 mouse plasma at 5 to 20 µg/mL and at 20 µg/mL with 50 µg/mL mAb 7G6, testing digestion conditions of 12.5, 25 or 50 µg/mL trypsin. **[B]** Mean percentage recovery (+/-SD) of recombinant CD21 spiked into C57BL/6 mouse plasma at 5 or 20 µg/mL over five individual experiments and analysed using the final assay protocol described in 2.9.3.

2.9.3.4. Quantification

Quantification of peptide A in plasma samples was achieved using a technique known as isotope dilution quantification. This comprises a relative quantification approach through comparison to the known quantity of isotopically labelled peptide A (peptide A-SIL) added to the samples. The ratio of peptide A versus peptide A-SIL peak area was multiplied by the known molar concentration of peptide A-SIL, to provide the molar concentration of peptide A.

This can then be converted to the original protein concentration by accounting for the incurred sample dilution. The determined peptide A molar concentration is directly relatable to the original full length protein concentration because only a single peptide A molecule can be enzymatically released from each full length CD21/35 protein. The final values can be inter-converted to µg/mL using the molecular weight, with the full length recombinant protein mass of 104660 Da used for these calculations.

2.10. Flow cytometry

In each PKPD study (PKPD studies 1 to 7), the spleen was collected post mortem on the final study day for flow cytometry analysis of specific T and B cell populations. Terminal blood samples were also collected in PKPD studies 5 to 7, with an additional in life blood sample collected at an earlier time point in PKPD studies 5 and 7. The blood samples were used to confirm drug activity against the primary mechanism of action through analysis of either T or B cell populations. All flow cytometry analysis in this project was designed and performed by an expert user, with assistance in sample preparation provided by the author.

2.10.1. Sample preparation

Blood samples, along with spleen tissue samples collected into medium (RPMI 1640 containing 5% FCS, 1% Penicillin/Streptomycin, 1% L-Glutamine), were kept cool on wet ice prior to analysis on the day of collection. Each spleen sample was removed from the media and individually mashed with a syringe plunger through a 40 µm cell strainer in a 5 mL volume of medium. Gentle pipetting provided further disruption of remaining tissue clumps to form a homogeneous cell suspension, which was transferred to fresh falcon tubes and stored a 4 ^{o}C until further processing. The cells in blood are essentially already in a homogenous cell suspension, thus skip this first step. All samples (blood and spleen) were centrifuged at 400x g for 5 minutes at 4 ^{o}C, the supernatants were poured off and the pellets resuspended in an appropriate volume of red blood cell lysis buffer (eBioscience, #00-4300-54). After a 5 minute incubation at room temperature, samples were diluted 1:1 with medium and centrifuged at 400x g for 5 minutes at 4 ^{o}C. At this point the blood samples are ready to be plated for staining, so the pellet was resuspended in 200 µL FACS buffer (PBS + 2 µM EDTA + 2% BSA) and 100 µL was added to the appropriate well of a 96 well round bottom plate. However, the cell density of the spleen samples is too high for analysis at this point and must be diluted. The

spleen sample pellet was resuspended in 5 mL of medium and an aliquot of the cell suspension was taken and diluted 1:20 in trypan blue (Sigma Aldrich, #T8154) for cell counting on a haemocytometer. The total number of cells were calculated for each sample to allow dilution to 1E7 cells per mL, with a 100 µL aliquot (1E6 cells) of the resulting cell suspension plated onto a 96 well round bottom plate ready for staining.

2.10.2. Cell staining

Plated blood and spleen cell isolates were washed twice through the addition of 150 µL PBS, centrifugation at 400x g for 3 minutes at 4 ºC and aspiration of the supernatant. The cell pellet was then resuspended in 100 µL of a 1:500 dilution of live dead aqua (Invitrogen, #L34966) in PBS and incubated for 15 minutes at room temperature in the dark. Samples were diluted with 100 µL FACS buffer, centrifuged at 400x g for 3 minutes at 4 ºC and the supernatant aspirated. The pellet was resuspended with a cocktail of antibodies against the target proteins diluted in FACS buffer and incubated for 30 minutes at room temperature in the dark. The exact antibody cocktail panel used in each study varied according to the endpoints being measured, requiring different fluorescent tags to prevent overlap, with the final panels listed in 2.10.3. An equivalent staining panel was prepared for identification of background in each study using non-specific isotype and fluorochrome matched antibodies (not shown). The cells were washed a further three times with 150 µL of FACS buffer, centrifuged at 400x g at 4 ºC for 3 minutes and the supernatant aspirated, before a final resuspension in 200 µL of FACS buffer for acquisition on an Attune NxT (ThermoFisher Scientific) or FACSCANTO II (BD Biosciences) flow cytometer. All data analysis was completed using FlowJo™ version 10 software (Becton, Dickinson and Company).

2.10.3. Antibody panels

The exact panel of antibodies used to stain the cells varied between studies according to the endpoints being measured and following continuous improvement of the methodology. PKPD study 1 involved analysis of the B cell and germinal centre B cell populations in the spleen and an investigation of the target engagement of CD21/35 by three tool mAbs. As such the samples were analysed using two separate staining panels, one for the B cell and germinal centre B cell population (panel A, table 2.3) and one for the target engagement assay (panel B, table 2.4).

Table 2.3. Antibody panel A for flow cytometry analysis of the spleen samples in PKPD studies 1, identifying the antibody and fluorochrome, along with its source.

Antibody (anti-mouse)	Fluorochrome	Source	Catalogue No.
GL7 (clone GL7) rat IgM	AF488	Biolegend	144612
B220 (RA3-6B2) rat IgG2a	PerCP/Cy5.5	Biolegend	103236
IgD (11-26c.2a) rat IgG2a	Pacific Blue	Biolegend	405712
FcR block / CD16/32 (clone 2.4G2) IgG2b	n/a	BD Biosciences	553140

Table 2.4. Antibody panel B for flow cytometry analysis of the spleen samples in PKPD studies 1, identifying the antibody and fluorochrome, along with its source.

Antibody (anti-mouse)	Fluorochrome	Source	Catalogue No.
CD21/35 (clone 7G6) IgG2b	PE	BD Biosciences	552957
CD21/35 (clone 7E9) IgG2a	APC	Biolegend	123412
CD21/35 (clone 8C12) IgG2a	BV421	BD Biosciences	740029
B220 (RA3-6B2) rat IgG2a	PerCP/Cy5.5	Biolegend	103236
FcR block / CD16/32 (clone 2.4G2) IgG2b	n/a	BD Biosciences	553140

During development of the adjuvant free IV KLH TDAR experimental mouse model in PKPD studies 3 and 4, terminal spleen samples were analysed for B cell and germinal centre B cell populations alongside further transitional B cell subsets (follicular, marginal zone, T1 and T2 B cells). Thus, the more extensive antibody staining panel in table 2.5 was used.

Table 2.5. The antibody panel for flow cytometry analysis of the spleen samples in PKPD studies 3 and 4, identifying the antibody and fluorochrome, along with its source.

Antibody (anti-mouse)	Fluorochrome	Source	Catalogue No.
GL7 (clone GL7) rat IgM	PerCP/Cy5.5	Biolegend	144610
CD45 (clone 30-F11) rat IgG2b	PE/Cy7	Biolegend	103114
PNA (n/a)	FITC	Vector Laboratories	FL-1071
CD21/35 (clone 7G6) rat IgG2b	PE	BD Biosciences	552957
CD23 (B3B4) rat IgG2a	APC	Biolegend	101619
B220 (RA3-6B2) rat IgG2a	APC-Cy7	Biolegend	103224
IgD (11-26c.2a) rat IgG2a	Pacific Blue	Biolegend	405712
TruStain FcX / CD16/32 (clone 93)	n/a	Biolegend	101320

The IV KLH TDAR qualification studies (PKPD studies 5 and 6) again analysed the B cell and germinal centre B cell populations in the spleen, however also included additional cellular endpoints in the blood and spleen to monitor the effectiveness of Fingolimod and the anti-CD20 mAb SA271G2 on CD4+ and CD8+ T cells and B2 cells respectively. To facilitate this, different antibody staining panels were used for the blood (table 2.6) and spleen (table 2.7).

Table 2.6. The antibody panel for flow cytometry analysis of blood samples in PKPD study 5, identifying the antibody and fluorochrome, along with its source.

Antibody (anti-mouse)	Fluorochrome	Source	Catalogue No.
CD19 (clone 1D3) rat IgG2a	PE/Cy7	eBioscience	25-0193-82
CD5 (clone 53-7.3) rat IgG2a	PerCP/Cy5.5	Biolegend	100624
CD45 (clone 30-F11) rat IgG2b	APC/Cy7	Biolegend	103116
CD4 (clone GK1.5) rat IgG2b	BV711	Biolegend	100447
CD3ε (clone 145-2C11) A hamster IgG	AF647	Biolegend	100322
CD8a (clone 53-6.7) rat IgG2a	PE	Biolegend	100708
TruStain FcX / CD16/32 (clone 93)	n/a	Biolegend	101320

Table 2.7. The antibody panel for flow cytometry analysis of spleen samples in PKPD study 5 along with blood and spleen samples in PKPD study 6, identifying the antibody and fluorochrome, along with its source.

Antibody (anti-mouse)	Fluorochrome	Source	Catalogue No.
CD19 (clone 6D5) rat IgG2a	BV421	Biolegend	115538
GL7 (clone GL7) rat IgM	PerCP/Cy5.5	Biolegend	144610
CD95 (FAS) (clone SA367H8) mouse IgG1	PE	Biolegend	152608
CD4 (clone GK1.5) rat IgG2b	BV711	Biolegend	100447
CD3ε (clone 145-2C11) A hamster IgG	BV605	Biolegend	100351
CD279 (PD1) (clone 29F.1A12) rat IgG2a	APC-Cy7	Biolegend	135223
CD138 (clone 281-2) rat IgG2a	APC	Biolegend	142506
CD185 (CXCR5) (clone L138D7) rat IgG2b	PE-Cy7	Biolegend	145515
CD8a (clone 53-6.7) rat IgG2a	AF488	Biolegend	100723
TruStain FcX / CD16/32 (clone 93)	n/a	Biolegend	101320

PKPD study 7 required the analysis of target engagement by mAb 7G6 on CD21/35 expressed by B cells in both the blood and spleen, with the QuantiBRITE quantification approach described in 2.10.4 employed. This was completed in addition to the routine B cell and germinal centre B cell analysis, with the antibody staining panel listed in table 2.8.

Table 2.8. The antibody panel for flow cytometry analysis of blood and spleen samples in PKPD study 7, identifying the antibody and fluorochrome, along with its source.

Antibody (anti-mouse)	Fluorochrome	Source	Catalogue No.
CD19 (clone 6D5) rat IgG2a	BV421	Biolegend	115538
CD45 (clone 30-F11) rat IgG2b	APC/Cy7	Biolegend	103116
GL7 (clone GL7) rat IgM	PerCP/Cy5.5	Biolegend	144610
CD95 (FAS) (clone SA367H8) mouse IgG1	APC	Biolegend	152604
CD21/35 (clone 7E9) rat IgG2a	FITC	Biolegend	123408
CD21/35 (clone 7G6) rat IgG2b	PE (1.3:1)	Custom conjugate	n/a
TruStain FcX / CD16/32 (clone 93)	n/a	Biolegend	101320

2.10.4. QuantiBRITE™ PE florescence quantification

Typically, flow cytometry measurements are qualitative, so to quantify the number of CD21/35 receptors present on the cell surface to inform PKPD modelling, the QuantiBRITE™ phycoerythrin (PE) fluorescence quantification (BD Biosciences) approach was used. This technique involves standardisation of flow cytometry data through a set of four pre-calibrated PE bead solutions, with a known value of PE molecules per bead (BD Biosciences, #340495). These calibration standards are run using the same PMT voltage gains and compensation settings as the cellular samples. When used in conjunction with PE conjugated monoclonal antibodies with a 1:1 conjugate:mAb ratio, the PE response can be converted to the number of antibodies bound per cell. If the antibody binding stoichiometry is known, this can then be used to estimate the amount of antigen per cell. This analysis was performed on blood and spleen cell isolates from PKPD study 7 only.

PE molecules per bead for the QuantiBRITE™ PE beads (BD Biosciences, lot 23-3339-00) used in this assay were as follows; High 62336, Med-high 23843, Med-low 5359 and Low 474. The calculated geometric mean florescence intensity (MFI) of the four bead populations was plotted in GraphPad Prism v8.1.2 software (GraphPad Software, Inc) as log10 (MFI) against log10 (PE molecules per bead) and fitted with linear regression to create a calibration line. The 7G6-PE MFI on the B cell populations for each sample were calculated and the isotype stained control MFI was subtracted. The MFI value was then used to interpolate the PE molecules per cell from the calibration line. This was converted to the number of antibodies per cell using the average of 1.3 PE molecules per antibody (BD Biosciences, custom conjugation). In turn, 7G6 binding stoichiometry to CD21/35 is 1:1, thus the number of antibodies per cell is also the amount of target receptor per cell.

2.11. Mathematical modelling

The complex mathematical language and software involved in building bespoke PK models presents a significant challenge to the integration of modelling and simulation into early drug discovery, where specialist mathematicians may not be available to code models. Simbiology, an app within the MATLAB software environment (The MathWorks Inc), provides programmatic tools to model, simulate and analyse dynamic systems, with a focus on PKPD and systems biology applications. The software allows the user to build models using a block diagram based editor or alternatively via MATLAB programmatic language, catering for

scientific personnel and experienced programmers alike. The software has gained a well-deserved strong reputation within the area of PKPD and systems biology modelling, with several recent publications describing its use in this field (Sengers *et al.*, 2016, Saylor and Zhang, 2016).

Simbiology v5.9, an app within the Matlab R2019b software package (MathWorks) was used to complete all mathematical PK and PKPD model development, fitting and simulation in this thesis. The specific approach and all input parameters for the mAb PK models are detailed in chapter 4, with the full model code for the three PK model versions contained in appendix I, II and III. The specific approach and all input parameters for the Fingolimod and anti-CD21 mathematical PKPD models are detailed in chapter 6, including the model equations.

2.12. Statistical analysis

All graphical data representation and statistical analysis conducted in this thesis was completed using the software package GraphPad Prism v8.1.2 for Windows (GraphPad Software, San Diego, California USA), using standard approaches appropriate to the task.

Chapter 3: Pharmacokinetic characterisation of the surrogate murine CD21 specific mAbs

3.1. Chapter introduction

Initial investigation centred around pharmacokinetic characterisation of three surrogate murine CD21 specific mAbs in the C57BL/6 mouse. These three mAbs were; the rat anti-mouse CD21 mAb denoted 7G6 (Kinoshita *et al.*, 1988), the mouse anti-mouse CD21 mAb denoted 4B2 (Kulik *et al.*, 2015) and an in-house GSK raised mouse anti-mouse mAb 9E10 (appendix IV). Whilst historically, detailed pharmacokinetic investigation of preclinical antibodies has been neglected due to conceived irrelevance, here it represents a cornerstone of the integrated pharmacokinetic pharmacodynamic modelling approach. Literature data detailing the characteristics of the therapeutic target CD21 gives credence to the notion that the target may impact the pharmacokinetics of CD21 specific mAbs. With the underlying mechanism of the therapeutic strategy first in class, detailed pharmacology of the target is unavailable. Consequently, consideration of all these factors, combined with the unique PK characteristics that are typical of mAbs, form the basis for the experimental designs. This results chapter describes the pharmacokinetic data collected in mouse to elaborate the pharmacokinetic behaviour of the three potential surrogate CD21 neutralising mAbs. It also contains detailed interpretation of this data and how it can be used to inform progression of the PKPD approach.

3.2. Methodology

In-depth description of the experimental protocol for the *in vivo* pharmacokinetic studies is located in chapter 2. Chapter 2 also includes full description of the analytical methodology used to generate all experimental data and the methodology used to perform the pharmacokinetic analysis described herein.

3.3. Results

The pharmacokinetics of three surrogate mouse CD21 specific mAbs (7G6, 4B2 and 9E10) were investigated in the C57BL/6 male mouse following IV bolus administration at three doses across a 100-fold concentration range. In addition, the exposure and bioavailability following IP drug administration was also characterised for each mAb. The resulting plasma concentration profiles are shown in figures 3.2 to 3.4, over a period of two weeks following 7G6 administration and three weeks following 4B2 and 9E10 administration. Non-

compartmental analysis was performed on the individual plasma concentration time profiles for each drug, dose and route to define the pharmacokinetics, with the resulting parameters displayed in tables 3.1 to 3.3.

3.3.1. Pharmacokinetics of mAb 7G6

The pharmacokinetics of mAb 7G6 were investigated following IV administration at 0.2, 2 and 20 mg/kg and following IP administration at 2 mg/kg. Plasma samples collected over a two week period following drug administration were assayed for mAb 7G6 as outlined in chapter 2, with the resulting plasma concentration profiles displayed in figure 3.1. It is evident from these plasma concentration profiles that mAb 7G6 behaves differently when administered across this dose range, with the terminal phase of the three IV profiles demonstrating different rates of decline in observed plasma concentration.

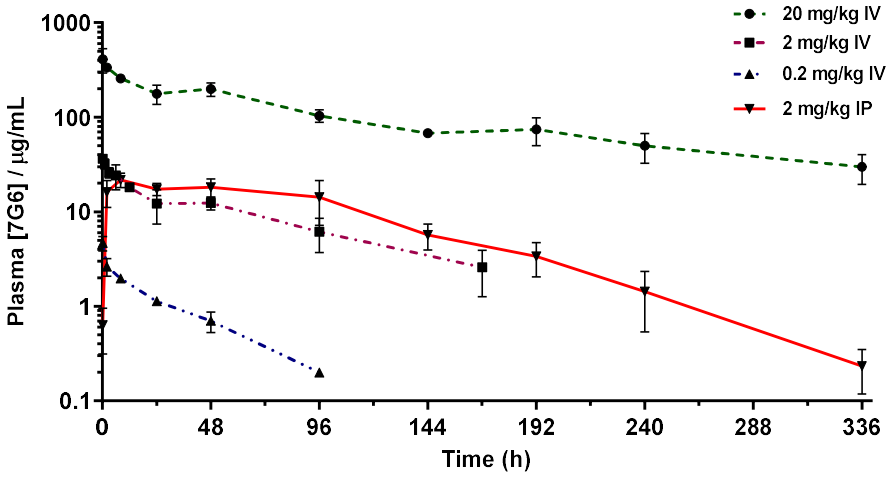

Figure 3.1. Plasma concentration profiles of the rat anti-mouse CD21 mAb 7G6 over two weeks following IV administration at 0.2 (▲), 2 (■) and 20 mg/kg (●) or IP administration at 2 mg/kg (▼) to the male C57BL/6 mouse. Data shown as mean +/- SD (n=3) with a connecting line for illustration.

The 2 mg/kg 7G6 IV bolus dose was performed as part of an initial pilot study ahead of the rest of the pharmacokinetic studies, to assess performance of the study design and trial feasibility of the micro sampling approach. Following the success of this pilot study, the general pharmacokinetic study design was adopted moving forward with the three remaining

7G6 dose groups and the other tool molecules. However, some subtle amendments to the protocol were implemented to improve the quality of the data generated. In the remaining dose groups the sampling times were adjusted to characterise the full plasma concentration profile, with additional samples collected during the terminal phase to replace less critical samples in the early distribution phase. This was driven by the absence of measurable drug in the 336 h plasma sample which left a large portion of the terminal phase undefined, as visible in figure 3.1. A further amendment was to weigh the dosing syringes both prior and following drug administration to allow accurate calculation of the volume of dose solution administered, and to retain and analyse the dose solutions alongside the plasma samples. In lieu of a measured value, the dose administered for the 2 mg/kg IV bolus group was recorded as the nominal dose value.

Table 3.1. Pharmacokinetic parameters for the rat anti-mouse CD21 mAb 7G6, derived following either IV bolus administration at 0.2, 2 or 20 mg/kg or IP administration at 2 mg/kg to the male C57BL/6 mouse (n=3). Parameters presented as mean +/-SD.

PK Parameters Mean (+/- SD)	IV Bolus (n=3)			IP (n=3)
	0.2 mg/kg	2 mg/kg	20 mg/kg	2 mg/kg
Dose (mg/kg)	0.22 (0.00)	2.00 (N/A)	22.56 (1.49)	2.14 (0.06)
C_{max} (µg/mL)	4.6 (0.8)	36.5 (2.4)	412.3 (116.9)	22.8 (3.0)
C_{max} (µM)	0.03 (0.01)	0.24 (0.02)	2.75 (0.78)	0.15 (0.02)
T_{max} (h)*	-	-	-	8 (8-96)
CL_p (mL/h/kg)	2.3 (0.2)	1.3 (0.5)	0.6 (0.1)	-
V_{ss} (mL/kg)	89 (6)	101 (18)	99 (7)	-
$t_{1/2}$ (h)	28 (2)	58 (9)	^[116 (21)]	63 (4)
AUC_∞ (µg.h/mL)	93 (7)	1660 (579)	36484 (5785)	2605 (639)
AUC_∞ /D (h.kg/mL)	0.4 (0.0)	0.8 (0.3)	1.6 (0.2)	1.2 (0.3)
AUC_t (µg.h/mL)	85 (7)	1429 (446)	31593 (3350)	2544 (621)
AUC_t/D (h.kg/mL)	0.4 (0.0)	0.7 (0.2)	1.4 (0.2)	1.2 (0.3)
F % $(AUC_\infty D_{IP})/(AUC_\infty/D_{IV})$	-	-	-	146

*Expressed as median and range. ^$t_{1/2}$ included for comparison only as study duration covers <3 half lives.

The rat IgG2b anti-mouse CD21 mAb 7G6 was well tolerated across each dose concentration tested, with no observed adverse effects. The concentration of the 7G6 dose solution retained following each dosing occasion returned a value within 20% error of the nominal concentration. Consequently, the actual dose administered, calculated from the volume of dose solution administered and the nominal dosing solution concentration, was used for further pharmacokinetic analysis. In accordance, the C_{max} achieved following IV bolus administration increased proportionally with the dose concentration as shown in table 3.1.

Non compartmental analysis (NCA) was performed on the terminal phase of the individual plasma concentration versus time profiles, starting at 24 h post dosing to account for the extended distribution phase that is characteristic of mAbs. The mean plasma clearance (CL_p), volume of distribution (V_{ss}) and half-life ($t_{1/2}$) were derived from this NCA, along with the area under the curve (AUC). These pharmacokinetic parameters are displayed in table 3.1 for each dose group. This analysis demonstrated that the exposure (AUC) and plasma clearance (CL_p) are dose dependent. While the dose increased from 0.2 to 20 mg/kg, the plasma clearance decreased from 2.3 to 0.6 mL/h/kg, resulting in the increased exposure demonstrated by the increase in AUC_∞/D from 0.4 to 1.6 h.kg/mL. This non-linearity in CLp impacts on the half-life ($t_{1/2}$) of 7G6 so that as the dose increased the apparent half-life extended. The study duration was insufficient to fully define the long $t_{1/2}$ calculated from the 20 mg/kg IV dose group because less than three half lives were defined by the terminal phase. The calculated $t_{1/2}$ for the 20 mg/kg group is included in table 3.1 for comparison purposes, to highlight the non-linearity across doses. The calculated volume of distribution is maintained across the dosing range at a mean value of 96 mL/kg.

The plasma exposure of 7G6 following IP administration at 2 mg/kg was greater than that seen via IV bolus administration at the same dose. This can be observed in figure 3.1 where the terminal phase of the IP plasma profile between 96 h and 336 h is parallel to, but greater than, that achieved IV at 2 mg/kg. This greater plasma exposure results in an estimated bioavailability in excess of 100%. The mean C_{max} following IP administration was 22.8 µg/mL, which occurred at a median T_{max} of 8 h post drug administration. This prolonged distribution phase, compared with the equivalent IV bolus dose, is characterised by the lower C_{max} and flatter initial plasma profile between 8 h and 96 h.

3.3.2. Pharmacokinetics of mAb 4B2

The pharmacokinetics of the tool mAb 4B2 were investigated following IV bolus administration at 0.2, 2 and 20 mg/kg and following IP administration at 2 mg/kg. Plasma samples collected over a three week period following drug administration were assayed for mAb, with the resulting plasma concentration profiles displayed in figure 3.2. In a manner similar to that seen with mAb 7G6 (section 3.3.1), mAb 4B2 behaves differently when administered across a concentration range, with the terminal phase of the three IV profiles demonstrating different rates of decline in observed plasma concentration.

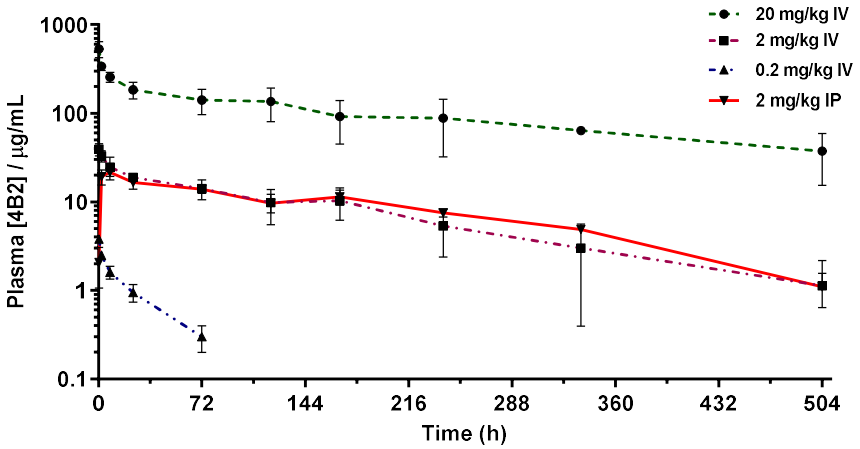

Figure 3.2. Plasma concentration profiles of the mouse anti-mouse CD21 mAb 4B2 (IgG1) over three weeks following IV administration at 0.2 (▲), 2 (■) and 20 mg/kg (●) or IP administration at 2 mg/kg (▼) to the male C57BL/6 mouse. Data shown as mean +/- SD (n=3) with connecting line for illustration.

The mouse IgG1 anti-mouse CD21 mAb 4B2 was well tolerated across each dose concentration tested, with no observed adverse effects following dosing. A consistent C_{max} was observed within each 4B2 dose group, with a dose proportional increase across the 0.2, 2 and 20 mg/kg IV dose levels tested. Dose solutions were analysed alongside plasma samples to confirm the concentration of 4B2 and were found to be within +/-20% of the nominal concentration, with the exception of the low 0.04 mg/mL dose solution used in the 0.2 mg/kg dose group. This dose solution was measured at 70% lower than the nominal value, which does not fit with the linear increase in C_{max} seen between the 0.2 and 2 mg/kg dose groups as shown in table 3.2. The nominal dose solution concentration, along with the volume of dose solution administered, was selected to calculate the dose administered to each animal, with this value used for all further pharmacokinetic analysis. An insufficient volume of blood was collected from mouse 1 at the 24 h time point in the 0.2 mg/kg group, preventing collection of plasma concentration data at this time point. Due to the minimal duration of 4B2 exposure, this resulted in insufficient data points (<3) to define the terminal phase for this animal and the derived pharmacokinetic parameters are therefore the mean of the two remaining animals.

Table 3.2. Pharmacokinetic parameters for the mouse anti-mouse CD21 mAb 4B2 derived following IV bolus administration at 0.2, 2 or 20 mg/kg or IP administration at 2 mg/kg to the male C57BL/6 mouse. Parameters presented as mean +/-SD (n=3).

PK Parameters Mean (+/- SD)	IV Bolus (n=3)			IP (n=3)
	0.2 mg/kg	2 mg/kg	20 mg/kg	2 mg/kg
Dose (mg/kg)	0.21 (0.01)#	2.12 (0.03)	21.10 (1.08)	2.10 (0.03)
C_{max} (µg/mL)	3.8 (0.4)	39.1 (6.2)	532.5 (108.2)	21.6 (2.3)
C_{max} (µM)	0.03 (0.00)	0.26 (0.04)	3.55 (0.72)	0.14 (0.02)
T_{max} (h)*	-	-	-	8 (8-8)
CL_p (mL/h/kg)	2.9 (NC)	0.6 (0.2)	0.4 (0.2)	-
V_{ss} (mL/kg)	91 (NC)	85 (3)	115 (43)	-
$t_{1/2}$ (h)	23 (NC)	102 (29)	^[222 (18)]	99.3 (14.1)
AUC_∞ (µg.h/mL)	75 (NC)	3872 (1488)	NR	4202 (359)
AUC/D_∞ (h.kg/mL)	0.4 (NC)	1.8 (0.7)	NR	2.0 (0.2)
AUC_t (µg.h/mL)	66 (5)	3679 (1286)	46050 (16497)	4024 (289)
AUC_t/D (h.kg/mL)	0.3 (0)	1.7 (0.6)	2.2 (0.8)	1.9 (0.2)
F % $(AUC_\infty D_{IP})/(AUC_\infty/D_{IV})$	-	-	-	110

*Expressed as median and range. #Nominal dose concentration. NC – Not calculated. NR – Not reported. ^$T_{1/2}$ included for comparison only as study duration covers <3 half lives.

Non-compartmental analysis was performed on the terminal phase of the individual plasma concentration versus time profiles, starting at 24 h post dose, with the resulting pharmacokinetic parameters displayed in table 3.2. The exposure (AUC) and plasma clearance (CL_p) of 4B2 were determined to be dose dependent in a similar manner to that seen for 7G6 in section 3.1. As the IV dose increased from 0.2 to 20 mg/kg, the plasma clearance decreased from 2.9 to 0.4 mL/h/kg, resulting in increased exposure demonstrated by the increase in AUC_t/D from 0.3 to 2.2 h.kg/mL. The resulting terminal half-life of 4B2 at the low 0.2 mg/kg dose was < 1 day, which increased to 4.3 days at 2 mg/kg and an estimated 9.3 days at the top dose of 20 mg/kg. The study duration was insufficient to fully characterise the terminal phase of the concentration time profile (<3 half-lives) in the 20 mg/kg group. The calculated $t_{1/2}$ for the 20 mg/kg group is included for comparison purposes to highlight this non linearity across doses. However, the extrapolation beyond the final plasma concentration to generate an AUC_∞ was greater than 20% and for this reason was not reported. The 2 and 20 mg/kg IV bolus dose groups exhibited a greater level of inter individual variability in plasma exposure than other groups, demonstrated by the high standard deviation value for AUC_t.

The IP route of administration was also explored for the mouse tool antibody 4B2 at a dose of 2 mg/kg to assess bioavailability and exposure. The bioavailability from this dosing route was calculated to be in excess of 100% when compared to the 2 mg/kg IV group, which had marginally lower plasma exposure. This can be observed in figure 3.2, where the terminal

phases of the 2 mg/kg IV and IP groups virtually overlay. The mean C_{max} following IP administration was 21.6 µg/mL, which occurred at a median T_{max} of 8 h post drug administration.

3.3.3. Pharmacokinetics of mAb 9E10

The pharmacokinetics of mAb 9E10 was investigated following IV bolus administration at 0.15, 1.5 and 15 mg/kg and following IP administration at 1.5 mg/kg. Plasma samples collected over a three week period following drug administration were assayed for mAb 9E10, with the resulting plasma concentration profiles displayed in figure 3.3.

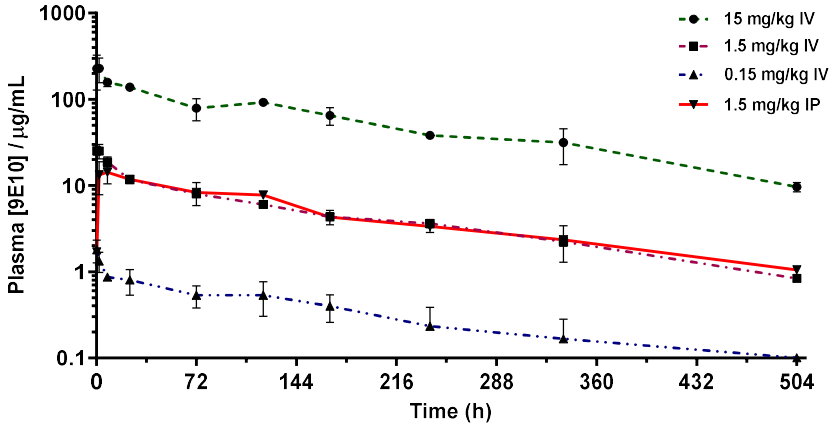

Figure 3.3. Plasma concentration profile of the mouse anti-mouse CD21 mAb 9E10 (IgG1) over three weeks following IV administration at 0.15 (▲), 1.5 (■) and 15 mg/kg (●) or IP administration at 1.5 mg/kg (▼) to the male C57BL/6 mouse. Data shown as mean +/- SD (n=3) with connecting line for illustration.

In contrast to the plasma concentration profiles following IV bolus administration of 7G6 and 4B2 (section 3.3.1 and 3.3.2), mAb 9E10 results in parallel, dose proportional plasma concentration profiles when administered across the range 0.15 to 15 mg/kg. Plasma concentrations of 9E10 were also measurable out to the terminal 504 h sample in all three dose groups. This is in contrast to both 7G6 and 4B2, where the concentrations fell below the assay limit of quantification within 96 h post drug administration at the lowest dose tested of 0.2 mg/kg.

The mouse anti-murine CD21 mAb 9E10 was well tolerated across each dose concentration tested, with no observed adverse effects following dosing. When dosed at 0.15, 1.5 and 15 mg/kg, 9E10 generated a dose proportional increase in C_{max} from 1.8 µg/mL to 283 µg/mL. Dose solutions were analysed alongside plasma samples for confirmation of dosing concentration and found to be within 20% error of the nominal concentration, with the exception of the low 0.15 mg/kg dose solution. This was found to be 90% lower than the nominal concentration of 0.03 mg/mL. Because this value did not fit with the linear increase in C_{max}, nominal dose concentration was selected for further pharmacokinetic analysis.

Table 3.3. Pharmacokinetic parameters for the mouse anti-mouse CD21 mAb 9E10 derived following either IV bolus administration at 0.15, 1.5 or 15 mg/kg or IP administration at 1.5 mg/kg to the male C57BL/6 mouse. Parameters presented as mean +/- SD (n=3).

PK Parameters Mean (+/- SD)	IV Bolus (n=3)			IP (n=2)
	0.15 mg/kg	1.5 mg/kg	15 mg/kg	1.5 mg/kg
Dose (mg/kg)	0.15 (0.002)#	1.15 (0.01)	16.40 (0.54)	1.16 (NC)
C_{max} (µg/mL)	1.8 (0.5)	26.7 (2.3)	283.0 (75.8)	14.4 (NC)
C_{max} (µM)	0.01 (0.003)	0.18 (0.02)	1.89 (0.51)	0.10 (NC)
T_{max} (h)*	-	-	-	2.0, 7.9
CL_p (mL/h/kg)	1.0 (0.4)	0.5 (0.01)	0.6 (0.04)	-
V_{ss} (mL/kg)	187 (48)	85 (5)	109 (5)	-
$t_{1/2}$ (h)	139 (23)	132 (7)	133 (9)	138 (NC)
AUC_∞ (µg.h/mL)	189 (NC)	2437 (36)	28849 (1990)	2501 (NC)
AUC/D_∞ (h.kg/mL)	1.2 (NC)	2.1 (0.04)	1.8 (0.1)	2.2 (NC)
AUC_t (µg.h/mL)	150 (71)	2274 (43)	26836 (1825)	2306 (NC)
AUC_t/D (h.kg/mL)	1.0 (0.5)	2.0 (0.03)	1.6 (0.1)	2.0 (NC)
F % $(AUC_\infty D_{IP})/(AUC_\infty/D_{IV})$	-	-	-	102

*Expressed as range. #Nominal dose concentration. NC – Not calculated.

Pharmacokinetic analysis was again performed using non compartmental analysis of the terminal phase of the individual plasma concentration versus time profiles, starting at 24 h post drug administration, with the resulting pharmacokinetic parameters shown in table 3.3. Unlike 7G6 and 4B2, the other tool anti-CD21 mAbs tested, the dose normalised exposure (AUC/D_∞) and clearance (CL_p) of 9E10 did not demonstrate any dose dependency. As the IV bolus dose was increased from 0.15 to 15 mg/kg, the plasma clearance remained constant, within the range 0.5 – 1.0 mL/h/kg. As a consequence, the dose normalised exposure (AUC/D_∞) remained constant, within the range of 1.2 to 2.1 µg.h/mL. The impact of the linear clearance across the dose range tested is that the $t_{1/2}$ remains constant in each group, with a mean value of 136 h.

The IP route of administration was explored, with the exposure following dosing at 2 mg/kg approximately equal to that seen via IV bolus administration at the same dose, leading to an estimated bioavailability of approximately 100%. The plasma samples from mouse 3 in this group were found to contain concentrations of 9E10 below the limit of quantification of the assay at all time points, despite the dosing syringe weights indicating the animal received the correct dose. This animal was removed from the pharmacokinetic analysis meaning data from this group is reported as n=2. The mean C_{max} following IP administration was 14.4 µg/mL, which occurred at a T_{max} between 2 and 7.9 h post drug administration.

3.4. Discussion

Implementation of the one mouse one PK profile based study design successfully generated high quality data to allow full characterisation of the PK of each surrogate mAb. This dramatically reduced the number of animals compared to a composite study design. This was made possible through a combination of micro sampling and the miniaturisation of the drug bioassay. The Gyrolab xP platform was utilised to facilitate minimisation of the sample volume requirement for bioanalysis of the mAb, in what is quickly becoming the industry standard technique within the discovery setting. A key benefit to this technique is the ability to rapidly develop a fit for purpose ligand binding assay. Here this was achieved using an antigen capture anti-species detect bioanalytical strategy, which provided a robust and adequately sensitive response. In part, assay sensitivity was limited by what appears to be lower than expected binding affinity to the recombinant CD21 capture protein. However, the primary assay limitation was high background noise, caused by the anti-species detection strategy encountering cross reactivity to low affinity background IgG from the mouse. As a consequence, it was found during assay development that direct bioanalysis of diluted blood, as reported by other investigators (Joyce *et al.*, 2014), was unfeasible due to the need for increased dilution of this more difficult matrix. The requirement for plasma to be collected in place of diluted blood directly impacted study design, due to the additional blood volume required to acquire sufficient plasma. This combined with the small size of C57BL/6 mice limited the maximum number of sampling time points to 10 and required mice to have a minimum body weight of 25 g to enter the study. At the time these studies were performed, a suitable capillary tube for collecting small volumes of plasma was unavailable, consequently blood was collected by pipette directly from the tail nick prior to plasma isolation. Logistically

this is a challenging procedure for the operator and the quality of isolated plasma suffered as a result in some cases.

Data was collected for each surrogate mAb across a dose concentration range of two orders of magnitude to confirm PK linearity, whilst bioavailability was assessed following IP administration at the mid dose concentration. The dose range of 9E10 was lowered, compared with the other two mAbs, due to availability of the drug at the time of the study. Each mAb was well tolerated following dosing, with no adverse events observed during the in life phase. Exaggerated pharmacology is often reported as the major cause of toxicity exhibited by mAbs (Vugmeyster *et al.*, 2012). So, it provides confidence to the therapeutic strategy that even at the highest tested dose, where drug levels are expected to far exceed the target level, that the mAbs were well tolerated. This observation is in line with literature, where Kulik *et al.* (2015) report administration of mAb 4B2 at a dose concentration 4-fold higher than tested here, with no reported toxicity. In addition, they noted no appreciable decrease in the total number of B cells following dosing with 4B2, indicative that the mAb does not induce lymphocytopenia (Kulik *et al.*, 2015). This is the mechanism of action of Rituximab, which similarly targets a B cell expressed target in CD20 and depletes the B cell population. CD21 knockout strains of mice are also viable, demonstrating that although CD21 is immunologically important, full prevention of its function is non-fatal (Ahearn *et al.*, 1996).

Comparison of the PK data generated for the three surrogate mAbs clearly identifies that two of the mAbs (7G6 and 4B2) behave similarly, whilst the third (9E10) behaves quite differently. The PK of 9E10 is characteristic of a non-specific IgG1 molecule when administered to the mouse, with a mean half-life of 5.5 days at 15 mg/kg, which remains linear as the dose decreased to 0.15 mg/kg. The half-life of mAbs is often described as predictable, which is a justified description when the mAb tested has irrelevant binding affinity in that species, or in situations where the kinetics or distribution of the target has no bearing on the kinetics of the mAb. In an experiment by Vieira and Rajewsky (1988) to define the serum half lives of different antibody classes and isotypes in mouse, an irrelevant anti-idiotypic antibody was used to define the IgG1 serum half-life as 6 - 8 days. In another experiment by Garg and Balthasar (2007), they showed the half-life of a radiolabelled mouse IgG1 to be in the region of 15 days in the mouse. Whilst this indicates that 9E10 is behaving in the way a typical IgG1 molecule of mouse origin would be expected, it does also indicate quite wide variability in half-life estimates even within an IgG isotype. At the highest dose of 4B2, also an IgG1 molecule of mouse origin, it exhibits a mean $t_{1/2}$ of 9.3 days which similarly falls into the expected range. However, in contrast the PK of 4B2 is non-linear across doses, with the

clearance increasing 7-fold as the dose is reduced to 0.2 mg/kg. This characteristic is also shared by 7G6, an IgG2b molecule of rat origin, which exhibits the same non linearity. The $t_{1/2}$ of 4.8 days derived from the high 20 mg/kg dose reflects that expected for a mAb of IgG2b isotype, with Vieira and Rajewsky (1988) reporting this to be in the range 4 to 6 days, shorter than that of an IgG1 molecule. In addition, the affinity of the rat IgG2b molecule for mouse FcRn is anticipated to be reduced compared with that of a mouse IgG2b mAb based on the work of Ober (2001). It is perhaps expected then that the $t_{1/2}$ would fall into the lower reaches of the 4 to 6 day estimate. The PK is again non-linear across doses, with the clearance increasing 4-fold as the dose is reduced to 0.2 mg/kg. This is a classic characteristic of target mediated drug disposition (TMDD) and acts as confirmation that CD21 targeted mAbs are subject to this phenomenon. By extension, this identifies a difference in the way that 9E10 is interacting with CD21 *in vivo*, that was not highlighted during its *in vitro* characterisation.

Identification of the non-linear clearance that is characteristic of TMDD was not unexpected for high affinity antibodies targeting CD21. It is commonly observed that mAbs targeting membrane bound receptors exhibit TMDD due to internalisation of the mAb receptor complex following binding (Dostalek *et al.*, 2013). In addition the presence of CD21 primarily on B cells and FDCs means that the majority of the target is located in secondary lymphoid tissue, away from the systemic circulation, as demonstrated by Whipple *et al.* (2004) using radiolabelled 7G6. Both these factors lead to a specific route of mAb clearance from the plasma, which is driven by the high affinity target binding. The apparent decrease in clearance at higher drug concentrations observed for 4B2 and 7G6 is as a result of saturation of this specific but limited capacity clearance route. This saturability of binding to splenic B cells was demonstrated by the IV infusion experiment of Whipple *et al.* (2004), who describe binding saturation to cells in the spleen with a 2 μg dose of 7G6 within a 2 h timeframe. It is for this reason that at the highest dose concentration, the PK of both 4B2 and 7G6 return to values typical for an antibody of that class. The pharmacokinetics of both mAbs are hence intimately dependent on the abundance, distribution and kinetics of CD21. In the PK studies described here, at each dose tested the initial amount of mAb administered is estimated to exceed the total amount of CD21 target. However, as the mAb distributes, interacts with the target or is cleared, this excess reduces to the point that the kinetics of the target begin to dictate the behaviour of the total mAb. In the Kulik *et al.* (2015) paper describing the characterisation of 4B2, this impact of target abundance and distribution on mAb plasma exposure is investigated using a CD21 knockout strain of mouse against wild type C57BL/6. In this experiment they describe a curious result showing a 3-fold reduction in plasma mAb exposure 22 hours after IP dosing to the wild type versus receptor knockout mice (Kulik *et al.*, 2015). The

concentrations reported would be expected to be many 1000-fold in excess of receptor abundance and do not align with the linear increase in C_{max} observed in our experiments.

The determined volume of distribution remains within a narrow band across each mAb and dose tested, between 85 and 187 mL/kg. Although this represents a theoretical volume to describe drug partitioning, this equates to a volume range of between 2.1 and 4.7 mL, which is not far removed from the blood volume in a typical 25 g mouse of 2.1 mL. This is consistent with typical estimates of V_{ss} from non compartmental pharmacokinetic analysis of mAbs that indicate limited distribution beyond the systemic circulation, which is a limitation to the use of this approach (Dostalek *et al.*, 2013). Clearly the identification of pronounced TMDD with these anti-CD21 mAbs demonstrates that the mAb is able to distribute to the site of specific clearance in secondary lymphoid tissues. It is therefore likely that the Vss calculated by NCA of the three tool mAbs is an underestimate of the true Vss. It is thought that the discrepancy arises through the assumption in classic non compartmental and mamillary models that the plasma is in rapid equilibrium with the site of tissue elimination, an assumption that does not hold for mAbs (Wang *et al.*, 2008).

Drug administration via the IP route is considered a simpler technique than IV administration in the mouse, where it is complicated by the small and delicate nature of the mouse vasculature. As such it is widely regarded as a more convenient dose administration route for preclinical investigation in mice. The exposure that can be achieved through administration of the surrogate mAbs via this route was explored. In each case the exposure was similar or slightly greater than that seen via IV bolus administration, resulting in an estimated bioavailability of 100% for all three mAbs. Some variability in the plasma exposures achieved between individual animals is likely the underlying factor for the bioavailability calculating in excess of 100%. This is particularly apparent for 7G6 where the mean bioavailability was 146%, however the coefficient of variability (CV%) for the AUC_{∞} observed in the 2 mg/kg IV and IP groups was 35% and 25% respectively.

The rat origin of 7G6 has historically precluded its use in repeat dose studies, due to the potential for formation of anti-drug antibodies (ADA). This was reported by Kulik *et al.* (2015) to occur as soon as after a single administration of 7G6. Although the presence of ADA was not specifically investigated in this study, the plasma profile following IV administration of 2 mg/kg 7G6 shows an indication of an ADA response. The final plasma sample collected on day 14 post 7G6 administration was unexpectedly measured as BLQ when compared with the terminal phase of the 2 mg/kg IP group. An explanation for this increased clearance in the 7G6

2 mg/kg IV group could be the appearance of an ADA response that accelerates clearance of the mAb or interferes with the bioassay.

3.5. Chapter conclusion

CD21 is an immune target that is receiving a great deal of interest both internally within GSK and across the wider scientific community due to its therapeutic potential in a number of autoantibody driven diseases. Whilst the biological function of CD21 and the impact of neutralising its activity have been extensively investigated in mice using the tool antibody 7G6, to date the pharmacokinetics of this molecule have not been reported. This precludes quantitative investigation of the pharmacology and has restricted understanding of the PKPD relationship of this molecule. The experiments within this chapter described characterisation of the pharmacokinetics of 7G6, in addition to two new mouse anti-CD21/CD35 mAbs. This includes the recently reported mAb 4B2 and a new mAb 9E10 raised in house at GSK. It has been identified from these experiments that 7G6 and 4B2 experience TMDD as a consequence of the distribution and kinetics of CD21, the implication of which is twofold. Firstly the non linearity complicates extrapolation of observed plasma exposure data across doses, making dose recommendations for preclinical efficacy studies difficult. Secondly, and more importantly, it indicates that clinical development of human mAbs targeting CD21 are likely to be complicated by non-linear PK. Enhanced understanding of the interplay between drug and target therefore becomes imperative during drug development. Characterisation of the PK of 9E10, a mAb raised in house, identified a stark difference in its behaviour compared with the published tool molecules, in that it does not demonstrate appreciable TMDD. Whilst alone this does not disqualify 9E10 as a useful tool molecule, it does raise questions regarding its binding epitope and functional potential that would require further investigation.

A consideration when reviewing the drug concentration data reported in this chapter is that this represents the drug population that was freely available to bind CD21 and was not cell membrane bound. This is as a consequence of the ligand binding assay format used in bioanalysis, which relies upon binding to recombinant CD21 by at least one free CDR of the full mAb. Accordingly, bivalently bound drug to soluble CD21 in the plasma would be prohibited from detection. Similarly, drug bound to B cells in circulation would be lost during plasma isolation from the blood sample. The impact on estimation of circulating drug concentration would however be low due to the small population of B cells in blood. In both scenarios the impact on the measured drug concentration would be greatest when the

concentration was low and the ratio of drug to target was closer to parity. In the absence of the reagents required to improve the bioassay to determine the total concentration for the murine origin mAbs and the free concentrations for all three mAbs, this limitation in the data must be taken into consideration when making conclusions.

The NCA approach described in this chapter to calculate the principle pharmacokinetic parameters for each mAb has been shown to have limited value when comparing across doses as a consequence of TMDD. Whilst the NCA approach is able to provide sound description of the terminal phase, the prolonged distribution phase that is characteristic of mAbs would better suit two compartmental analysis. This is the commonly adopted approach to assess clinical PK data for mAbs exhibiting linear PK (Dostalek *et al.*, 2013). In instances of non-linear PK, this can be extended to incorporate a saturable route of clearance such as that described by the original one compartmental TMDD model proposed by Mager and Jusko (2001a). The limitation of following this route is that it can only describe the plasma drug concentration. The value of this is reduced when the site of action is considered primarily to reside outside the circulation and when the desire is to investigate interplay between drug and target. A physiologically based modelling approach would have greater applicability here, where physiological values for tissues and flow rates can be incorporated to better describe distribution of the mAb. The benefit of adopting this approach is that it can be employed to make predictions of drug in tissue compartments over time, allowing understanding of concentration at the site of action. Target localisation and kinetics may also then be built into the model to add a peripheral saturable clearance route and a site that can be used to assess target engagement.

The proceeding chapter describes the development of a physiologically based PK model to describe the plasma concentration data generated through the experimental work described here. This model comprised of a combination of literature and experimental data describing physiological compartments, flow rates and distribution coefficients to describe mAb pharmacokinetics. The base model was then extended to include target abundance and kinetic data to describe the saturable clearance route highlighted here as TMDD.

Chapter 4: Development of a physiologically based PK model to describe the kinetic properties of the surrogate murine CD21 specific mAbs

4.1. Chapter introduction

The identification of nonlinear pharmacokinetics for the surrogate anti-CD21 mAbs in mouse, as detailed in chapter 3, resulted in the requirement for a more comprehensive modelling approach to fully describe the mAb's behaviour in mouse and allow extrapolation of the data across doses. Accurate description of the pharmacokinetic behaviour constitutes a cornerstone of the PKPD approach, with extrapolation required to define optimal dosing strategies. Target dependent nonlinear PK for the surrogate mAbs makes integration of the target into the PK model essential to allow description of the saturable target mediated clearance pathway. Integration of target kinetics also allows the PK model to predict target engagement in plasma, and when combined with a physiologically based pharmacokinetic (PBPK) modelling approach, may allow plasma concentration time data to be used to predict tissue distribution and peripheral target engagement. The following results chapter details the development and evolution of a mathematical TMDD PK model, integrated into a minimal PBPK modelling approach, to describe the nonlinear PK of the surrogate mAbs.

4.2. Mathematical model development

Development of a mathematical model to describe the PK of the surrogate CD21 specific mAbs and all model simulations were conducted by the author using Simbiology v5.9, an app within the Matlab R2019b software package (MathWorks). Details of selection and progression of the model structure are detailed here, alongside the source of all model parameters, with the associated model equations detailed in appendix I, II and III.

4.2.1. Development of the mPBPK model structure (PK model v1)

Initially a mPBPK model was developed, based upon the second generation mPBPK model reported by Cao *et al.* (2013) as illustrated in figure 4.1. This model provides a simplified approach to incorporate physiological elements such as compartment volumes and lymphatic flow, to provide PK values with increased practical utility compared with standard two compartmental models (Cao *et al.*, 2013). The model employs a reductionist 'tissue lumping' approach, where all tissues are pooled into two categories; tight tissue (composed of muscle, skin, adipose and brain) and leaky tissue (incorporating all other tissue types) (Cao *et al.*, 2013). The model considers convection as the only distribution pathway using the one pore formalism.

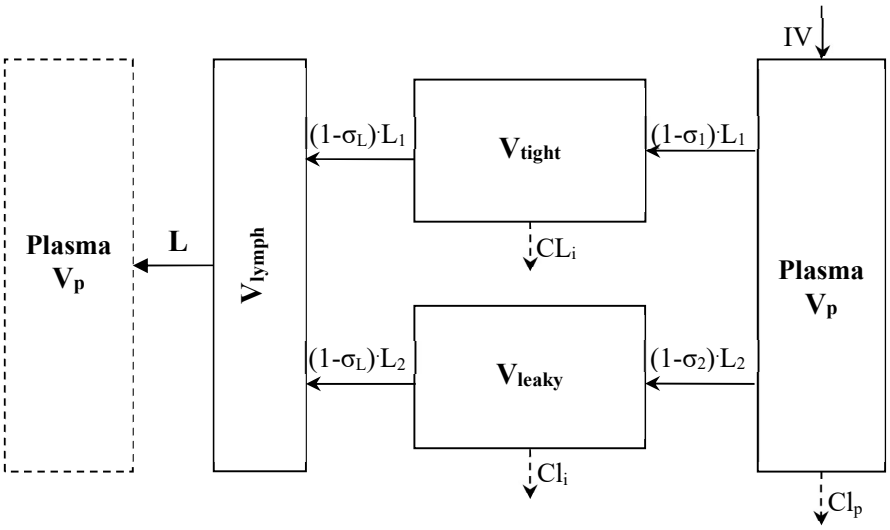

Figure 4.1. Schematic of the minimal PBPK model to describe monoclonal antibody pharmacokinetics, adapted from Cao *et al.* (2013). Parameter descriptions and values are listed in table 4.1. Adapted by permission from Springer Nature.

The model was parameterised using the physiological values for mouse reported by Zhao *et al.* (2015), which were scaled by body weight to represent a 25 g mouse. This represents the typical size of a C57BL/6 male mouse and was the minimum body weight of mice used to define the pharmacokinetics. The relative fraction of lymph flow to the tight and leaky tissue compartments was assumed to be 0.33*L and 0.66*L respectively, based upon reported values used in full PBPK models (Zhao *et al.*, 2015). The volume of interstitial fluid (ISF) in the tight and leaky tissues were assigned according to species specific physiological values, where V_{tight} is described by 0.65*ISF*k_p and V_{leaky} by 0.35*ISF*k_p. The value of k_p represents the available fraction of ISF that the mAb can partition within and is set to 0.8, which represents a value estimated for mAbs of IgG1 isotype (Zhao *et al.*, 2015). The fractions of total ISF assigned to tight (0.65) and leaky (0.35) compartments was again based on full PBPK models (Zhao *et al.*, 2015). Vascular reflection coefficients for tight tissue ($\sigma_1 = 0.908$) and leaky tissue ($\sigma_2 = 0.579$) were taken from Zhao *et al.* (2015) and represent the mean value collected from twelve mAbs. The lymphatic capillary reflection coefficient was also taken directly from Zhao *et al.* (2015) and was set to a value of 0.2. The final parameter in the mPBPK model is Cl_p, which was assigned from the saturating dose in the PK investigation of each mAb in chapter 3. The values of Cl_p were $1.0E^{-5}$ L h^{-1} for 4B2 and $1.5E^{-5}$ L h^{-1} for both 7G6 and 9E10. The final parameters used in the mPBPK model are shown in table 4.1.

Table 4.1. Parameter descriptions and values used to define the minimal PBPK model (PK model v1) with physiological parameter values gained from Zhao *et al.* (2015) and specific mAb clearance rates gained from NCA analysis (chapter 3).

Parameter	Description	Value	Units
L	Total lymph flow rate	$1.5E^{-4}$	$L\ h^{-1}$
L1	Lymph flow rate (tight tissue)	$4.95E^{-5}$	$L\ h^{-1}$
L2	Lymph flow rate (leaky tissue)	$1.005E^{-4}$	$L\ h^{-1}$
σ1	Vascular reflection coefficient (tight tissue)	0.908	n/a
σ2	Vascular reflection coefficient (leaky tissue)	0.579	n/a
σL	Lymphatic capillary reflection coefficient	0.2	n/a
V_{Tight}	Volume tight tissue ISF	$2.808E^{-3}$	L
V_{Leaky}	Volume leaky tissue ISF	$1.512E^{-3}$	L
V_{Plasma}	Plasma volume	$1.0625E^{-3}$	L
V_{Lymph}	Lymph volume	$2.0E^{-3}$	L
Cl_p (4B2)	Plasma Clearance (4B2)	$1.0E^{-5}$	$L\ h^{-1}$
Cl_p (9E10)	Plasma Clearance (9E10)	$1.5E^{-5}$	$L\ h^{-1}$
Cl_p (7G6)	Plasma Clearance (7G6)	$1.5E^{-5}$	$L\ h^{-1}$

4.2.2. Development of the mPBPK model incorporating TMDD with shedding (PK model v2)

To describe the nonlinear clearance of the surrogate CD21 specific mAbs, a TMDD model was incorporated into the mPBPK model (PK model v1). CD21 is a membrane bound receptor which has been reported to be shed into a soluble form (Masilamani *et al.*, 2003a). Therefore the TMDD model including receptor shedding, as described by Li *et al.* (2014) and illustrated in figure 4.2, was adapted and implemented into the mPBPK model structure.

As a consequence of the origin of CD21 and CD35 as splice variants of a single gene, all mAbs directed against CD21 are expected to bind the homologous epitope in CD35. In addition, the two proteins are thought to be co-expressed on the same cell types in mouse, although to differing extents. Consequently, for the purpose of the model, the two proteins are combined to form a single description of the target, denoted T. Expression of CD21 and CD35 in mice is thought to be predominantly on B cells, of which the vast majority are located in easy to

access tissue such as the spleen, lymph nodes and bone marrow (Westermann and Pabst, 1992). In contrast, only minimal B cells are thought to reside in the blood or in hard to access tissues such as the brain or skin (Westermann and Pabst, 1992). The membrane expressed form of target (T,m) was therefore fixed in the model to reside exclusively in the leaky tissue compartment, also acting as the sole site of target synthesis, degradation and shedding.

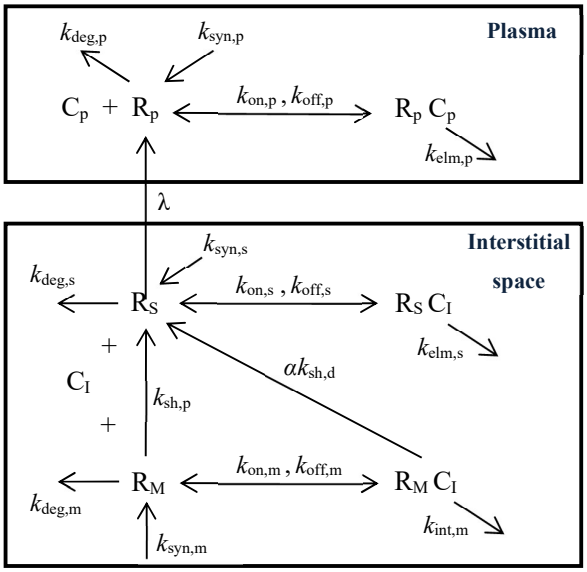

Figure 4.2. Schematic of the target mediated drug disposition model incorporating shedding mechanisms as described by Li *et al.* (2014). Where *C* denotes drug and *R* denotes the target. Subscript letters denote form, where $_p$ is plasma, $_s$ is soluble, $_I$ is interstitial and $_m$ is membrane bound. Reprinted with permission from John Wiley & Sons.

Initial estimates for the concentration of T,m in leaky tissue were based on estimates of the total population of B cells in mice. There is limited published data describing this in mice, however a paper by Morris *et al.* (2005) reports a figure of $2.26E^8$ cells. There are no reports of the number of CD21/35 receptors per B cell in mice, however the number of receptors was measured in cynomolgus monkey to be 10499 per peripheral B cell by flow cytometry (Appendix VIII). The concentration of T,m was then calculated by combining these two values to give the total number of receptor molecules, converting this to moles of receptor utilising Avogadro's constant and then fitting this into the volume of the leaky tissue compartment. This resulted in an initial estimate for T,m of 2.61 nM in the leaky tissue. This initial estimate was subsequently selected as the most sensitive parameter to improve the fit of the model to the observed plasma concentration data, with the final value used displayed in table 4.2.

Binding of antibodies to human CD21 has been reported to promote internalisation of the receptor, with a half-life of 2 h reported by Tessier *et al.* (2007). It is assumed that a similar internalisation event occurs in mouse and as such the rate of internalisation of the bound receptor ($k_{int,m}$) was fixed in the model to the same value, equating to 0.3466 h^{-1}. Internalisation of the native receptor without bound antibody is also assumed to occur, but at a much reduced rate. Receptor expression on the surface of splenic B cells isolated from mice 14 days after treatment with a saturating dose of mAb 7G6 or 4B2 in PKPD study 1, indicated a greater than 10-fold reduction in receptor number, compared with isotype control treated mice. It is assumed that the shedding rate of the receptor is not impacted by binding, thus the difference is solely due to different receptor internalisation rates. To reflect this, the internalisation rate of native receptor ($k_{deg,m}$) was assigned a value 10-fold lower at 0.03466 h^{-1}.

Both CD21 and CD35 exist in plasma as a shorter soluble form of the protein, denoted sCD21 and sCD35. It is assumed that shedding of membrane receptor is the sole source of this soluble form of the proteins and that the rate of shedding is unaffected by antibody binding. In the model, soluble target (T,s) is fixed to be synthesised exclusively in the leaky tissue from shed membrane expressed receptor. Once shed, T,s becomes available to distribute via the lymph to the plasma and other tissue with distribution kinetics that are assumed identical to mAb because of their similar molecular mass. The shed form of CD21 is estimated to be ~126 kDa, compared with ~150 kDa for a typical IgG antibody (Masilamani *et al.*, 2002). There is no experimentally measured value for the tissue or plasma sCD21 / sCD35 concentration in mouse, but plasma sCD21 concentrations have been reported in several studies in human. In a study reported by Masilamani *et al.* (2004), a sCD21 range between 150 and 600 ng/mL was measured in 160 healthy individuals, with a median value of 294 ng/mL. Another study reported by Singh *et al.* (2008) stated a measured range of 100 to 500 ng/mL in 25 healthy individuals with a median value of 330 ng/mL. Whilst a study by Tomita *et al.* (2012) reports a slightly lower range of 30 to 250 ng/mL in a group of 49 healthy individuals. Based on this evidence, a value of 300 ng/mL (2.38 nM) was adopted for the plasma T,s concentration in the model. Plasma clearance of sCD21 /sCD35 can be estimated from a study by Zhang *et al.* (2013), in which the kinetics of recombinant human sCD35 were monitored following dosing to mice, with a reported half-life of 18 h. It is assumed that nonspecific clearance of the soluble target occurs solely in the plasma in a similar manner to unbound mAb, hence the plasma clearance rate ($k_{deg,s}$) was set to 0.03851 h^{-1}.

Estimates for the synthesis rate of the membrane receptor ($k_{syn,m}$) and its shed rate ($k_{shed,m}$) were gained from the model to fit the estimates of soluble and membrane target concentration.

Where the synthesis rate ($k_{syn,m}$) at steady state is the sum of the decay rate constants ($k_{shed,m}$ and $k_{deg,m}$) and the shedding rate ($k_{shed,m}$) was fitted empirically to derive the estimated plasma T,s concentration. Based on this approach, the estimate for $k_{shed,m}$ was set at 0.0193 h^{-1} and $k_{syn,m}$ was set at 0.1805 nM h^{-1}. Initial estimates for the T,s concentration in the leaky tissue, tight tissue and lymph compartments were gained from the model at steady state, with the values shown in table 4.2.

Table 4.2. Model parameters used to define the mPBPK model with TMDD and shedding (PK model v2) in addition to those described in table 4.1.

Parameter	Description	Value	Units
k_a	Absorption rate from IP site of administration	0.0002	L h^{-1}
k_{on}	mAb binding on rate	0.18	nM^{-1} h^{-1}
k_{off}	mAb binding off rate	0.18	h^{-1}
$k_{syn,m}$	Synthesis rate of membrane expressed target	0.1805	nM h^{-1}
$k_{deg,m}$	Native rate of membrane expressed target internalisation	0.03466	h^{-1}
$k_{int,m}$	mAb binding enhanced rate of membrane expressed target internalisation	0.3466	h^{-1}
$k_{shed,m}$	Rate of membrane expressed target shedding	0.0193	h^{-1}
$k_{deg,s}$	Soluble target clearance rate	0.03851	h^{-1}
T,m_{LT}	Concentration of membrane expressed target in the leaky tissue compartment	3.345	nM
T,s_{plasma}	Concentration of soluble target in the plasma	2.381	nM
T,s_{LT}	Concentration of soluble target in the leaky tissue	2.465	nM
T,s_{TT}	Concentration of soluble target in the tight tissue	0.27	nM
T,s_{L}	Concentration of soluble target in the lymph	1.39	nM

Finally, in a modification to the base mPBPK model, a separate IP dosing route was included. This involves an additional dose compartment of arbitrary volume, out of which mAb can reach the blood at a rate defined by the constant k_a. This rate was fixed to achieve a T_{max} at approximately 8 h, to align with the observed data, resulting in a value for k_a of 0.0002 L h^{-1}.

The binding affinity (K_d) of the tool mAbs has not been experimentally measured but is assumed to represent that considered to be typical of a tool rodent mAb of approximately

1 nM. A typical k_{off} value of 0.18 h^{-1} has been assumed, resulting in an estimated k_{on} of 0.18 nM^{-1} h^{-1} to fit the 1 nM K_d affinity. It has been assumed that the mAb binding affinity is equivalent to both the membrane and soluble forms of the target, with only monovalent binding considered in the model. Once mAb bound, soluble target is assumed to inherit the kinetics of the free mAb.

4.2.3. Parameterisation with experimentally determined values (PK model v3)

The initial estimates of target kinetics used to parameterise PK model v2 were a combination of literature values from other species and estimates based on the behaviour of similar proteins. The importance of collecting experimentally determined values to improve PK model performance was highlighted during model development. Three values were identified as high impact and measurable; the concentration of soluble target in plasma (T,s), the number of receptors on splenic B cells (impact on T,m) and the K_d of the antibody to cellular target (k_{off}/k_{on}). These three values have a knock-on impact on $k_{deg,m}$, $k_{int,m}$, $k_{shed,m}$, $k_{syn,m}$ and k_{on}, all of which are critical in characterising the impact of TMDD on the surrogate CD21 specific mAb pharmacokinetics and characterising the extent of target engagement. The base mPBPK model parameters remain the same as those described in section 4.2.1, with the same model structure and assumptions used as described for PK model v2 (section 4.2.2).

The mean number of target receptors expressed per splenic B cell was measured in PKPD study 7 (described in chapter 5) both in naïve and treated mice, resulting in a determined mean receptor number per splenic B cell of 5426. The same approach used previously (section 4.2.2) to calculate an estimate of T,m was again followed, resulting in a new value of 1.347 nM. Once again, T,m was assumed to reside solely in the leaky tissue compartment. The membrane receptor (T,m) can either internalise and degrade ($k_{deg,m}$) or be shed ($k_{shed,m}$) into a soluble form. Internalisation was set to a default value, based on the turnover of similar receptors, with a $t_{1/2}$ of 24 h resulting in a $k_{deg,m}$ value of 0.0289 h^{-1}. Meanwhile, the shedding rate ($k_{shed,m}$) was fixed empirically to derive the measured plasma concentration of soluble target (T,s), based on the assumption that shedding is the sole source of T,s. The mean measured plasma concentration of T,s was 12.8 nM (n=8, isotype control), as measured in PKPD study 7 (described in chapter 5), with a resulting $k_{shed,m}$ value of 0.257 h^{-1}. The synthesis rate of T,m ($k_{syn,m}$) at steady state is equal to the sum of the decay rate constants ($k_{deg,m}$ and $k_{shed,m}$) multiplied by the concentration of target at time zero (T,m_0), resulting in a $k_{syn,m}$ value of 0.385 nM h^{-1}. As previously, T,s was assumed to have the same distribution kinetics as mAb due to their similar

molecular weight, thus T,s equilibrates throughout the tissues. Initial estimates of T,s in each tissue compartment were gained from the model at steady state, with the values shown in table 4.3. It is again assumed that nonspecific clearance of the soluble target occurs solely in the plasma, with a rate ($k_{deg,s}$) set at 0.03851 h^{-1}, based upon the reported kinetics ($t_{1/2}$ of 18 h) of recombinant human soluble CD35 administered to mice (Zhang *et al.*, 2013).

Table 4.3. Parameters defining the TMDD model with shedding (PK model v3) following measurement of soluble and membrane target concentration and mAb binding kinetics.

Parameter	Description	Value	Units
k_a	Absorption rate from IP site of administration	0.0002	L h^{-1}
k_{on}	mAb binding on rate	3.6	nM^{-1} h^{-1}
k_{off}	mAb binding off rate	0.18	h^{-1}
$k_{syn,m}$	Synthesis rate of membrane expressed target	0.385	nM h^{-1}
$k_{deg,m}$	Native rate of membrane expressed target internalisation	0.0289	h^{-1}
$k_{int,m}$	mAb binding enhanced rate of membrane expressed target internalisation	1.386	h^{-1}
$k_{shed,m}$	Rate of membrane expressed target shedding	0.257	h^{-1}
$k_{deg,s}$	Soluble target clearance rate	0.03851	h^{-1}
mAb_Cl_p	mAb (7G6) plasma clearance rate	0.01412	h^{-1}
$k_{deg,s\text{-}mAb}$	mAb – soluble target complex clearance rate	0.03851	h-^{1}
$k_{shed,m\text{-}mAb}$	mAb – membrane target complex shedding rate	0.257	h^{-1}
T,m_{LT}	Concentration of membrane expressed target in the leaky tissue compartment	1.347	nM
T,s_p	Concentration of soluble target in the plasma	12.8	nM
T,s_{LT}	Concentration of soluble target in the leaky tissue	13.25	nM
T,s_{TT}	Concentration of soluble target in the tight tissue	1.47	nM
T,s_L	Concentration of soluble target in the lymph	7.49	nM

The binding affinity (K_d) of mAb 7G6 and 4B2 to native CD21/35 was determined through incubation with murine splenocytes, resulting in calculated values of 0.054 and 1.65 nM, respectively (Appendix V). To describe the affinity of mAb 7G6, the previous estimate of k_{off} was maintained and the k_{on} was increased to 3.6 nM^{-1} h^{-1}. The result of mAb binding to membrane target is assumed to be accelerated receptor internalisation. It is known that

following high dose administration of mAb 7G6 and 4B2, the surface expression of CD21/35 is reduced, as observed in PKPD study 1 and quantified for mAb 7G6 in PKPD study 7 (described in chapter 5). The kinetics are unknown but assumed to be fast, therefore a value (30 min) reported for other fast internalising mAbs was used (Vainshtein *et al.*, 2015), with $k_{int,m}$ set at 1.386 h^{-1}. The other outcome of mAb binding to T,m is shedding ($k_{shed,m\text{-}mAb}$), which was initially assumed to be equal to naïve receptor shedding. Once bound, T,s was initially assumed to inherit the kinetics of the free mAb. The model assumes binding affinity is equivalent to both T,m and T,s, with only monovalent binding considered throughout the model. A list of all the final model parameters can be found in table 4.3.

4.2.4. Alternative model incorporating soluble protein synthesis (PK model v4)

In a fundamental shift in underlying assumption, the model was reconsidered with the source of the soluble target a separate synthesis pathway, instead of resulting from shedding of membrane target. The final PK model v3 structure was modified to remove the shedding component in the leaky tissue ($k_{shed,m}$ and $k_{shed,m\text{-}mAb}$), with a separate synthesis route for T,s created in the leaky tissue compartment, defined by the parameter $k_{T,s}$. This required an alteration to the calculation of $k_{syn,m}$, which is now equivalent to $k_{deg,m}$ multiplied by the concentration of target at time zero (T,m_0), with a new value of 0.0389 nM h^{-1}. The new parameter $k_{T,s}$ was derived empirically to result in the observed steady state plasma concentration of T,s (12.8 nM), resulting in a value of $k_{T,s}$ of 0.334 nM h^{-1}. All other model parameters and assumptions hold true from PK model v3.

4.3. Results

4.3.1. Development of the mPBPK model structure (PK model v1)

The minimal PBPK model as described by Cao *et al.* (2013) was successfully constructed in the Simbiology software package (v5.9) as shown in figure 4.3, with the related parameter values described in table 4.1. The underlying equations of the model are displayed in appendix I.

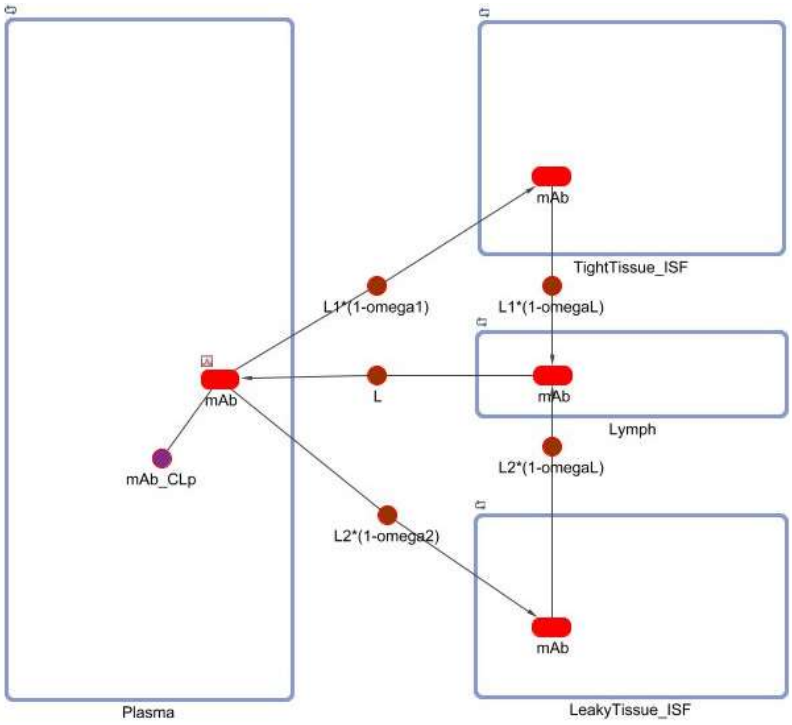

Figure 4.3. Diagrammatic representation of the mPBPK model in Simbiology v5.9. PK model v1 comprises four compartments, with the mAb cycling between the plasma and two lumped tissue compartments denoted tight and leaky, before returning to plasma via lymph.

The mean plasma clearance value calculated from the 20 mg/kg dose group of each mAb in chapter 3, was implemented to describe the nonspecific plasma clearance rate of each mAb. The model was then used to simulate the plasma concentrations that could be achieved in a 25 g mouse following IV dosing of the surrogate mAbs. The resulting simulated profiles have been overlaid onto graphs containing the observed plasma concentration data collected for each mAb at the three different doses tested, as described in chapter 3. The overlaid graphs for mAbs 9E10, 4B2 and 7G6 are shown in figures 4.4, 4.5 and 4.6 respectively.

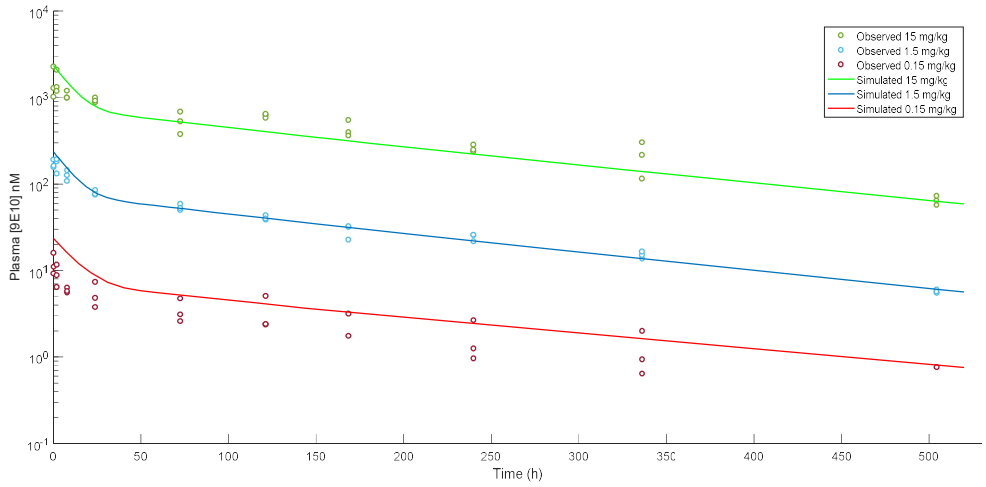

Figure 4.4. Simulated plasma concentration profiles for mAb 9E10 following IV bolus administration at 0.15, 1.5 or 15 mg/kg. Simulation performed using the mouse mPBPK model (PK model v1) and illustrated as solid lines. Overlain are the experimentally observed plasma concentrations following IV bolus administration to the male C57BL/6 mouse at the same doses (open circles).

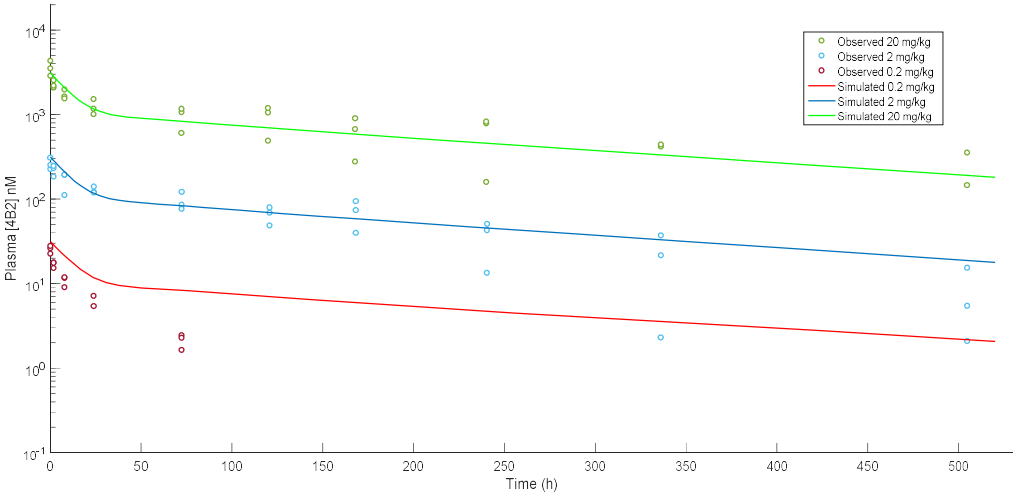

Figure 4.5. Simulated plasma concentration profiles for mAb 4B2 following IV bolus administration at 0.2, 2 or 20 mg/kg. Simulation performed using the mouse mPBPK model (PK model v1) and illustrated as the solid lines. Overlain are the experimentally observed plasma concentrations following IV bolus administration to the male C57BL/6 mouse at the same doses (open circles).

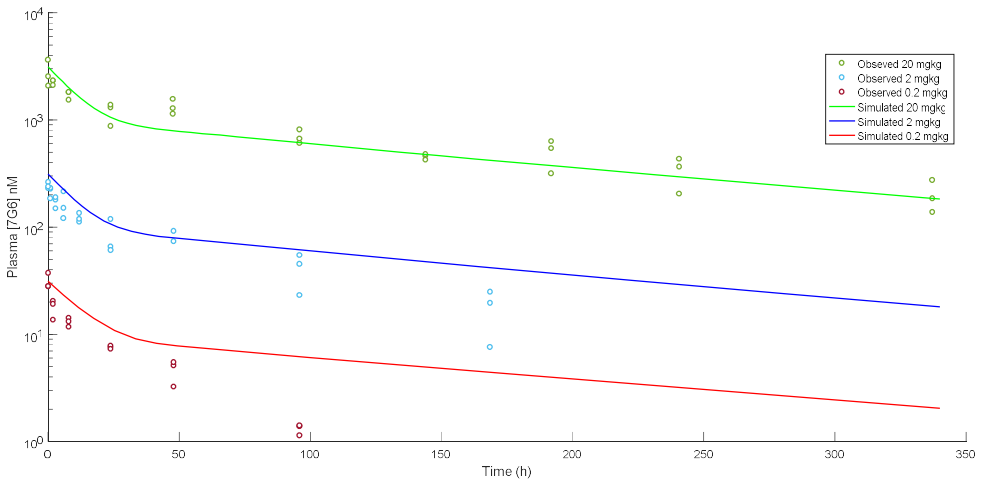

Figure 4.6. Simulated plasma concentration profiles for mAb 7G6 following IV bolus administration at 0.2, 2 or 20 mg/kg. Simulation performed using the mouse mPBPK model (PK model v1) and illustrated as the solid lines. Overlain are the experimentally observed plasma concentrations following IV bolus administration to the male C57BL/6 mouse at the same doses (open circles).

4.3.2. Development of the mPBPK model incorporating TMDD with shedding (PK model v2)

The TMDD model with shedding as described by Li *et al.* (2014) was adapted and extended to describe the properties of the target CD21, prior to successful implementation into the mPBPK model framework using the Simbiology software package (v5.9). An illustration of the model showing the interplay between mAb and target within the compartments of the mPBPK model is shown in figure 4.7, with the related parameter values described in table 4.2. The underlying equations of the model are displayed in appendix II.

The model was again used to simulate the plasma concentrations that could be achieved in a 25 g mouse following IV dosing of the surrogate mAbs 7G6 and 4B2 at 0.2, 2 and 20 mg/kg, or following IP dosing at 2 mg/kg. Because of the visually good fit achieved for mAb 9E10 using just the mPBPK model without target, this mAb has been excluded from further analysis. The simulated profiles have been overlaid onto graphs containing the observed plasma concentration data collected for each mAb at the three different dose concentrations tested, as described in chapter 3. As a consequence of bioassay format, the observed values of drug concentration in plasma include both free drug and soluble target bound drug. Therefore, a

combined value for both the free and soluble target bound drug in the model (Total_mAb) has been used to simulate the plasma concentration. The overlaid graphs for mAbs 4B2 and 7G6 are shown in figures 4.8 and 4.9 respectively.

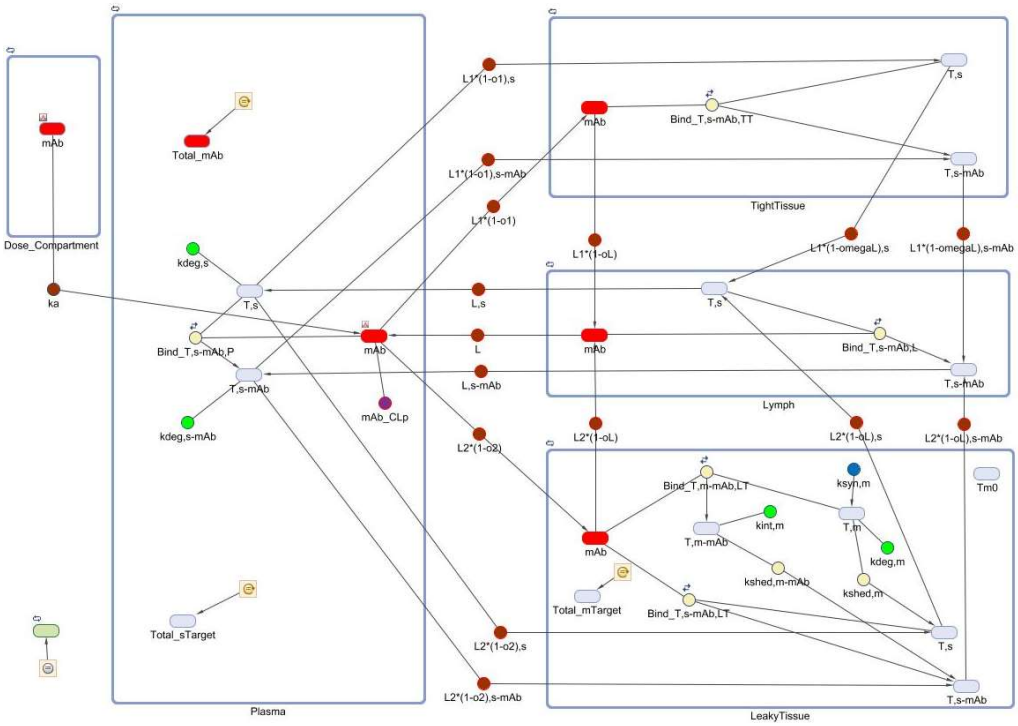

Figure 4.7. Diagrammatic representation of the mPBPK model incorporating TMDD with shedding in Simbiology v5.9. PK model v2 comprises the basic four compartments described in the mPBPK model, with the addition of the membrane target T,m fixed in the leaky compartment and soluble target T,s able to move similarly to mAb.

To assess model performance in accurate simulation of the plasma concentration profile of each drug, the observed AUC_t and the concentration at C_{max} or the earliest measured time point were compared to those predicted by the model. The trapezoidal rule was used to estimate the area under the simulated plasma concentration profile to gain an estimate of AUC_t, whilst observed values are described in chapter 3. To assess the accuracy of the model predicted values, the percentage difference between the observed and simulated values have been calculated. This analysis has been performed for both 4B2 and 7G6, with the results displayed in table 4.4 and 4.5.

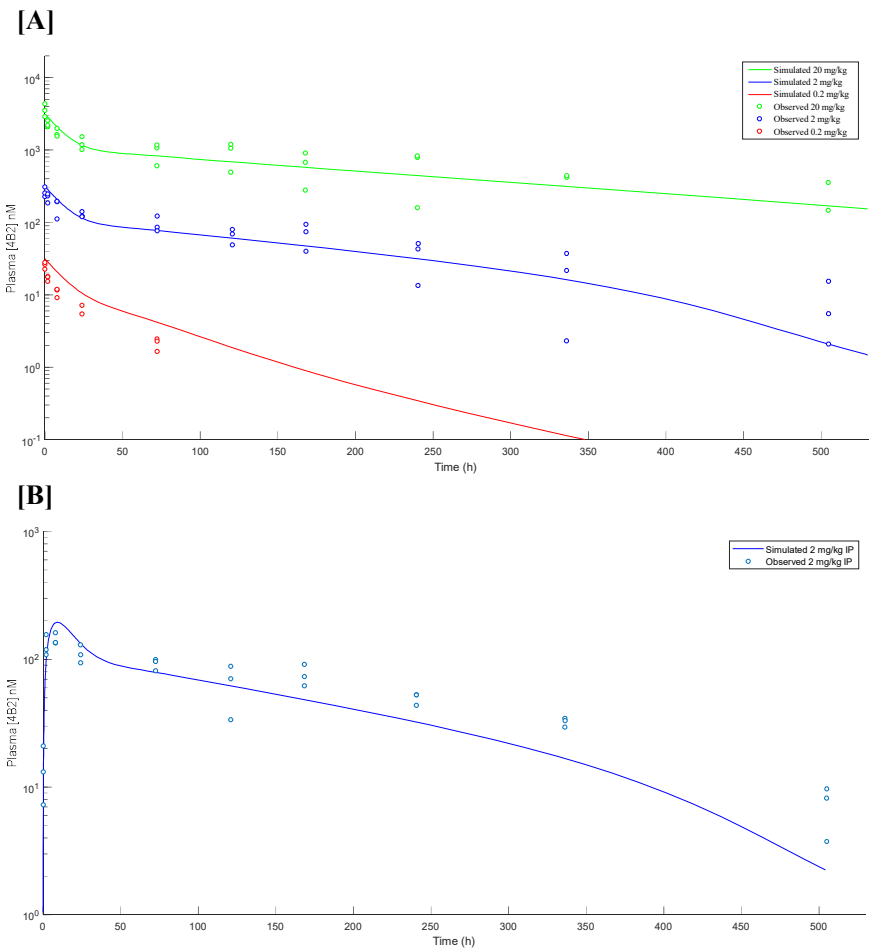

Figure 4.8. Simulated plasma concentration profiles for mAb 4B2 using PK model v2, overlain with the experimental observations (open circles) following administration to the male C57BL/6 mouse (n=3). **[A]** Simulated profile (solid line) following IV bolus administration at 0.2 (red), 2 (blue) or 20 mg/kg (green). **[B]** Simulated profile (solid line) following IP administration at 2 mg/kg.

Table 4.4. PK model v2 performance evaluation, comparison of the simulated AUC_t and maximum concentration for each 4B2 dose against the observed values collected in chapter 3.

Dose Group	AUC_t (µg.h/mL)			C_{max} (C_{10min} IV) (µg/mL)		
	Observed (n=3)	Simulated	Difference (%)	Observed (n=3)	Simulated	Difference (%)
0.2 mg/kg IV	66	113	72	3.8	4.7	24
2 mg/kg IV	3679	3150	-13	39.1	46.6	20
20 mg/kg IV	46050	40243	-12	532.5	466.5	-11
2 mg/kg IP	4024	3138	-21	21.6	29.0	35

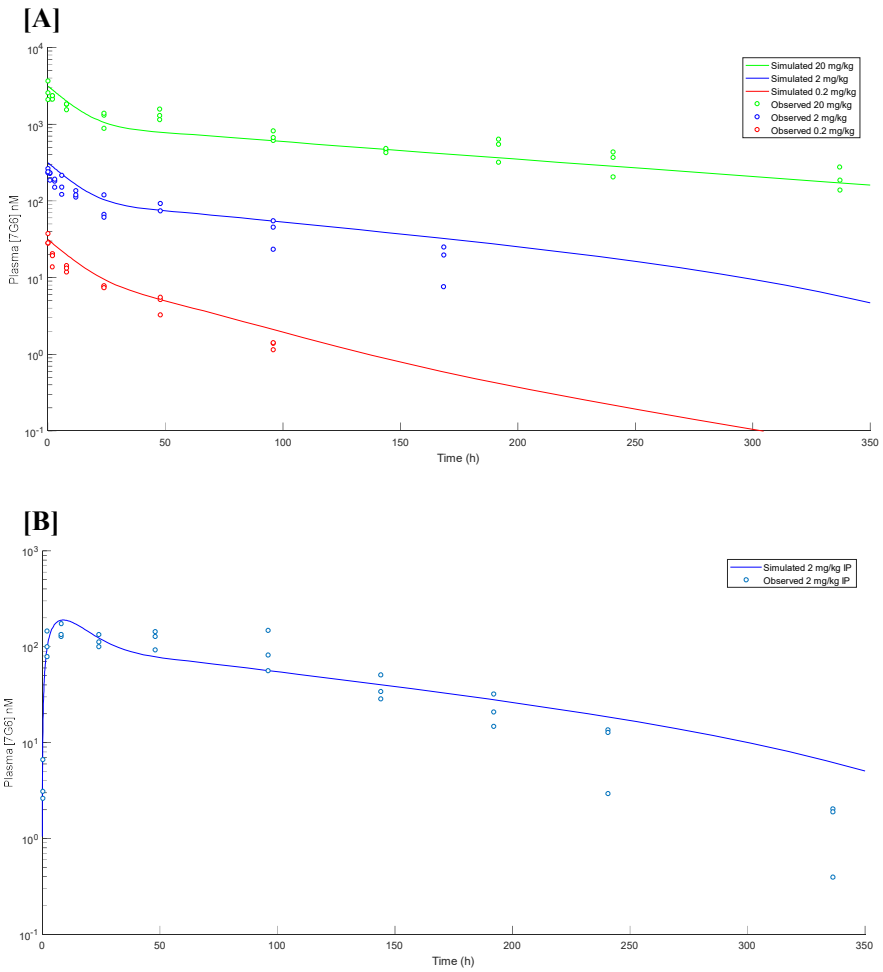

Figure 4.9. Simulated plasma concentration profiles for mAb 7G6 using PK model v2, overlain with the experimental observations (open circles) following administration to the male C57BL/6 mouse (n=3). **[A]** Simulated profile (solid line) following IV bolus administration at 0.2 (red), 2 (blue) or 20 mg/kg (green). **[B]** Simulated profile (solid line) following IP administration at 2 mg/kg.

Table 4.5. PK model v2 performance evaluation, comparison of the simulated AUC_t and maximum concentration for each 7G6 dose against the observed values collected in chapter 3.

Dose Group	AUC_t (µg.h/mL)			C_{max} (C_{10min} IV) (µg/mL)		
	Observed (n=3)	Simulated	Difference (%)	Observed (n=3)	Simulated	Difference (%)
0.2 mg/kg IV	85	112	33	4.6	4.7	2
2 mg/kg IV	1429	1874	32	36.5	46.6	29
20 mg/kg IV	31593	26963	-14	412.3	466.2	14
2 mg/kg IP	2544	2292	-9	22.8	28.4	26

4.3.3. Parameterisation with experimentally determined values (PK model v3)

Experimentally determined values for the concentration of target (soluble and membrane associated) and mAb binding affinity were added into the framework of PK model v2 to improve description of mAb pharmacokinetics and provide a more accurate projection of target engagement. The model structure remained fundamentally the same, with the same basic assumptions but new experimentally derived parameter values. A model diagram is shown in figure 4.7, with the new parameter values listed in table 4.3. The underlying equations of the model remain the same as v2, displayed in appendix II.

To evaluate the performance of the re-parameterised model (PK model v3), simulated mAb 7G6 plasma concentrations following IV administration at 0.2, 2 and 20 mg/kg were compared with the observed data collected in chapter 3 (figure 4.10). The simulated and observed values are both considered to be total drug (Total_mAb), the combination of free (mAb) and soluble target bound drug (T,s-mAb). In addition, the simulated concentration of total membrane receptor (T,m + T,m-mAb) and total soluble target (T,s + T,s-mAb) are illustrated, overlain with the baseline value (dotted line).

The re-parameterised PK model v3 provides poor description of the dose dependent pharmacokinetics of mAb 7G6, as shown in figure 4.10, failing to provide adequate description of the accelerated clearance at low mAb concentrations. The simulated soluble target concentration at each dose deviates from the baseline measurement. This is particularly prevalent at the 20 mg/kg dose, where the simulated concentration reaches a maximum of 16 nM after 2 days, prior to progressive decay to a minimum of 8 nM at day 14. This profile of soluble CD21/35 deviates from baseline in a manner not observed experimentally following analysis of plasma samples from the 20 mg/kg 7G6 PK study (Appendix VII), where the concentration remained approximately constant across an 8 day period following dosing. Additionally, it can be observed from the simulation that at 20 mg/kg the total membrane target concentration is predicted to reduce by 6-fold (83%), whilst data generated at 10 mg/kg Q4D in PKPD study 7 (chapter 5) demonstrates that a much larger reduction would be expected (>99.5% or 200-fold). This analysis clearly highlights that the underlying assumptions of the model do not fit with the observed data, inadequately describing the pharmacokinetics of mAb 7G6 in mouse.

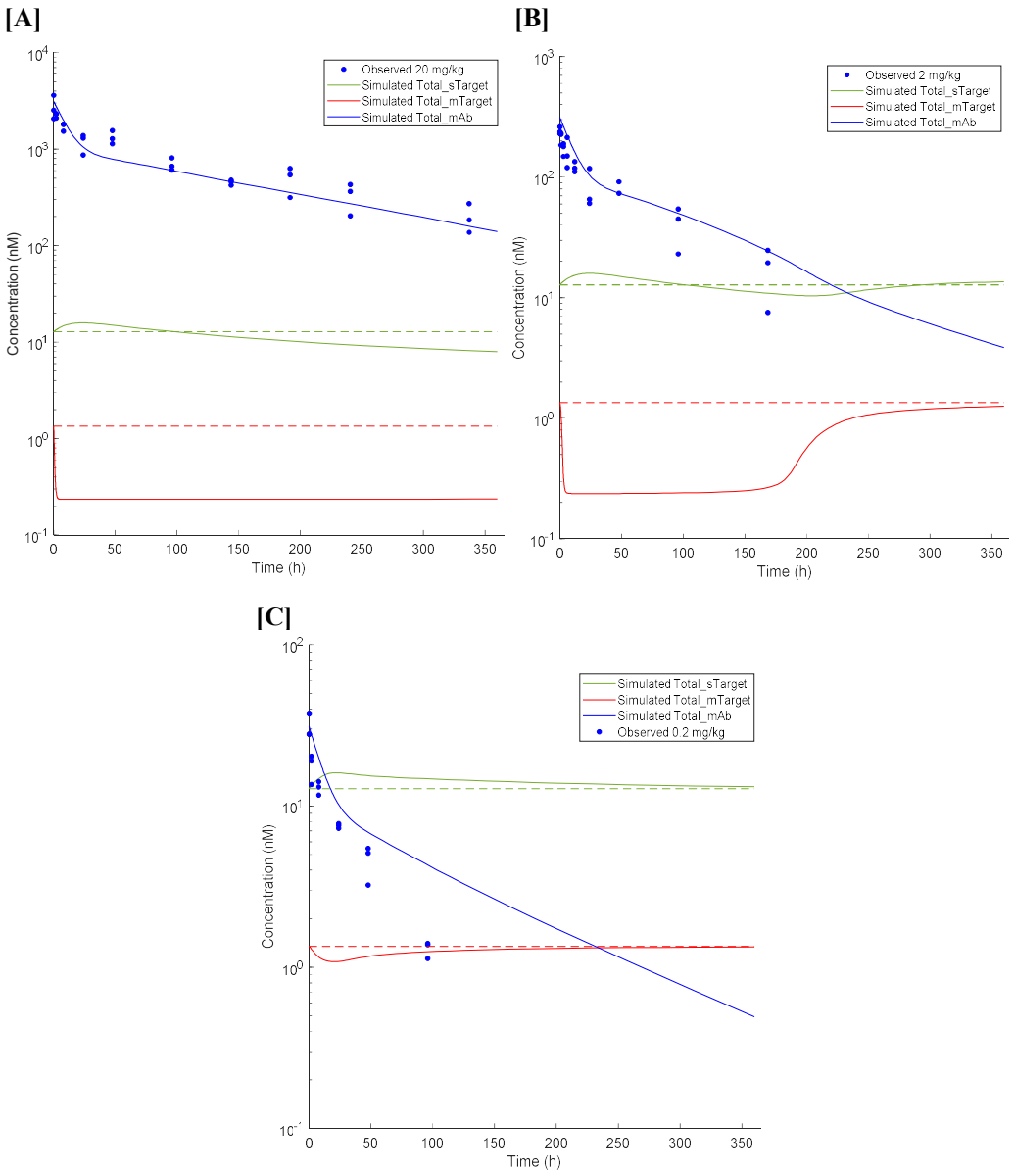

Figure 4.10. Simulated concentration profiles (solid line) of mAb 7G6 in plasma (blue), soluble target in plasma (green) and membrane target in leaky tissue (red), with the baseline values captured as a dashed line. Simulations were performed using PK model v3, following IV bolus administration at **[A]** 20 mg/kg, **[B]** 2 mg/kg and **[C]** 0.2 mg/kg, with the observed plasma 7G6 concentration overlain (blue circle).

4.3.3.1. Scenario modelling to test model assumptions: TMDD mechanism

To investigate the impact of the underlying assumptions that define the description of accelerated target mediated mAb clearance, two scenarios were explored.

1. Receptor internalisation is the primary cause of TMDD.
2. Soluble complex (mAb + soluble target) is the primary cause of TMDD

Currently the model utilises a literature value to describe the internalisation rate ($k_{int,m}$) as result of mAb binding, with a value of 30 minutes to describe fast internalisation of the receptor-mAb complex (figure 4.11A). An extreme value of 1 minute was explored, to ascertain the impact a rapid internalisation rate could have on mAb clearance (figure 4.11B). Alternatively, the impact of clearance of the soluble target-mAb complex was explored, with this complex initially assumed to inherit the kinetics of the mAb. As an alternative scenario, the complex was instead assumed to inherit the kinetics of the soluble protein (18 h vs 49 h), representing a 2.7-fold increase in clearance rate (figure 4.11C). Comparison of the performance of each model scenario in describing the PK following IV administration of mAb 7G6 at 0.2 mg/kg IV to the male C57BL/6 mouse, is shown in table 4.6.

Table 4.6. PK model performance in describing the observed PK following 0.2 mg/kg 7G6 given IV to the C57BL/6 mouse. Comparison of the observed AUC_t (µg.h/mL) vs the simulated values from PK model v2, PK model v3, increasing $k_{int,m}$ to 41.59 h^{-1} or increasing $k_{deg,s-mAb}$ to that of $k_{deg,s}$.

PK model	AUC_t (µg.h/mL) / 0.2 mg/kg 7G6 IV		
	Observed (n=3)	Simulated	Difference (%)
PK model v2	85	112	33
PK model v3 (base values)		133	57
PK model v3 ($k_{int,m}$ = 41.59 h^{-1})		130	54
PK model v3 ($k_{deg,s-mAb}$ = 0.03851 h^{-1})		91	8

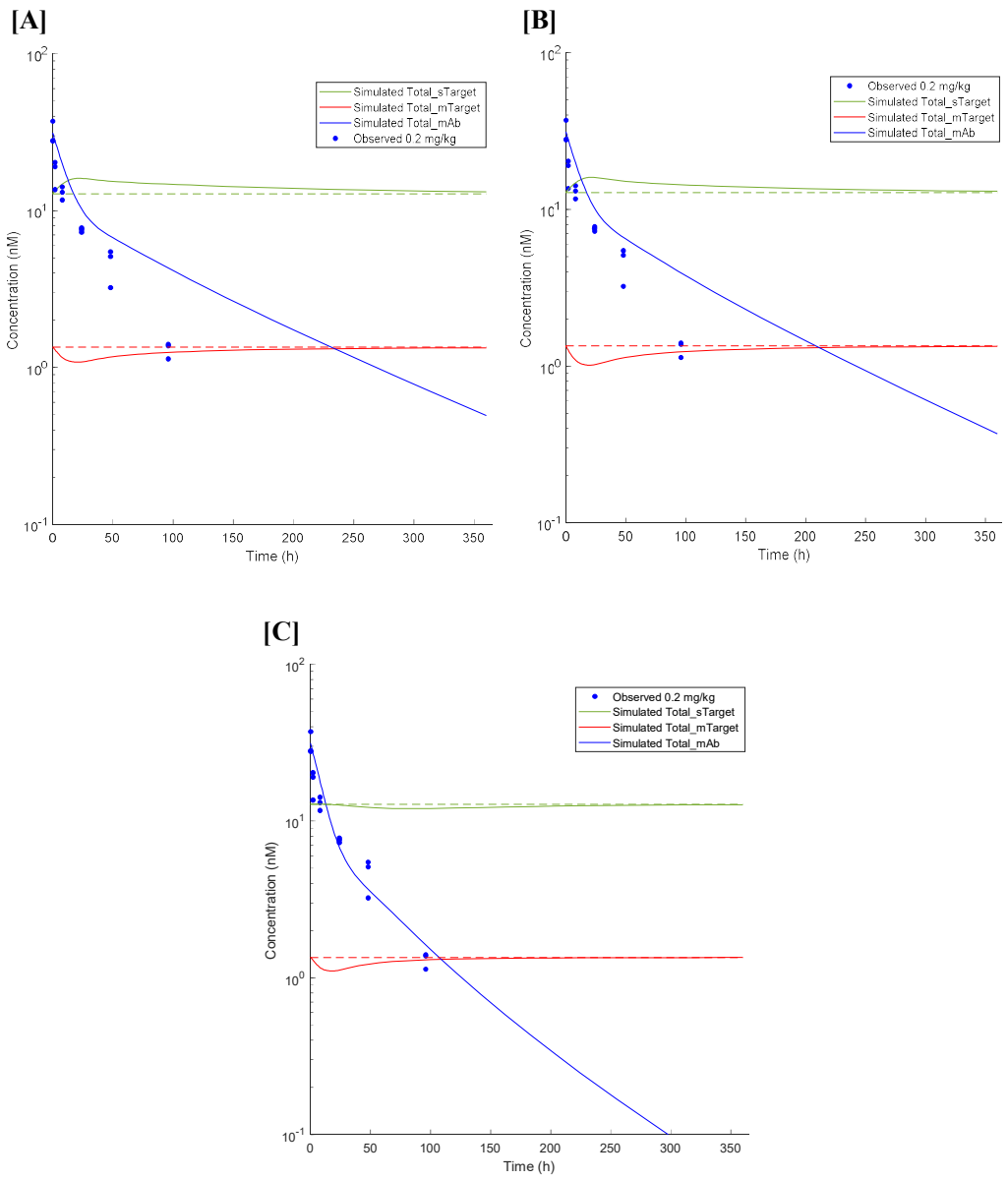

Figure 4.11. Simulations of the impact of two potential mechanisms of TMDD on the fit of PK model v3 to the observed plasma mAb profile following 0.2 mg/kg IV administration of mAb 7G6 to the C57BL/6 mouse. **[A]** PK model v3 with the original parameter values of $k_{int,m}$ 1.3863 h^{-1}, $k_{deg,s\text{-}mAb}$ 0.0141 h^{-1} **[B]** $k_{int,m}$ set to 41.59 h^{-1} **[C]** $k_{deg,s\text{-}mAb}$ set to 0.03851 h^{-1}.

4.3.3.2. Scenario modelling to test model assumptions: Impact of mAb binding

While the modification of PK model v3, to include the changed assumption that soluble target mAb complex inherits the kinetics of the soluble protein, provides an improved description of the observed plasma 7G6 PK, the underlying assumptions do not result in the observed target kinetics. This is demonstrated in figure 4.12A, where following 10 mg/kg Q4D IP administration of mAb 7G6 in PKPD study 7 (chapter 5), PK model v3 is unable to describe the observed soluble target concentration and the greater than 99% reduction in total membrane receptor. Two scenarios were explored with the potential to describe the increased loss in membrane associated target.

1. Binding membrane target causes rapid target internalisation
2. Binding target causes rapid target shedding

These two scenarios were simulated by alteration of the values of $k_{int,m}$ or $k_{shed,m}$ from the standard values in the model to an extremely rapid rate of 41.59 h^{-1}, equivalent to a turnover rate of 1 min. These scenarios were performed individually, with the results shown in figure 4.12.

The results in figure 4.12B illustrate that rapid internalisation of the membrane associated receptor is unable to describe the observed target kinetics. This scenario has a dramatic effect on the availability of membrane receptor for shedding into the pool of soluble target, resulting in a gradual decline in soluble target concentration. In contrast, the scenario where mAb binding results in rapid shedding is able to describe the observed target kinetics (figure 4.12C). This results in both depletion of the membrane associated receptor and maintenance of the soluble target concentration. The improvement in description of target kinetics comes however at the cost of its ability to describe PK at low doses, as illustrated in figure 4.13.

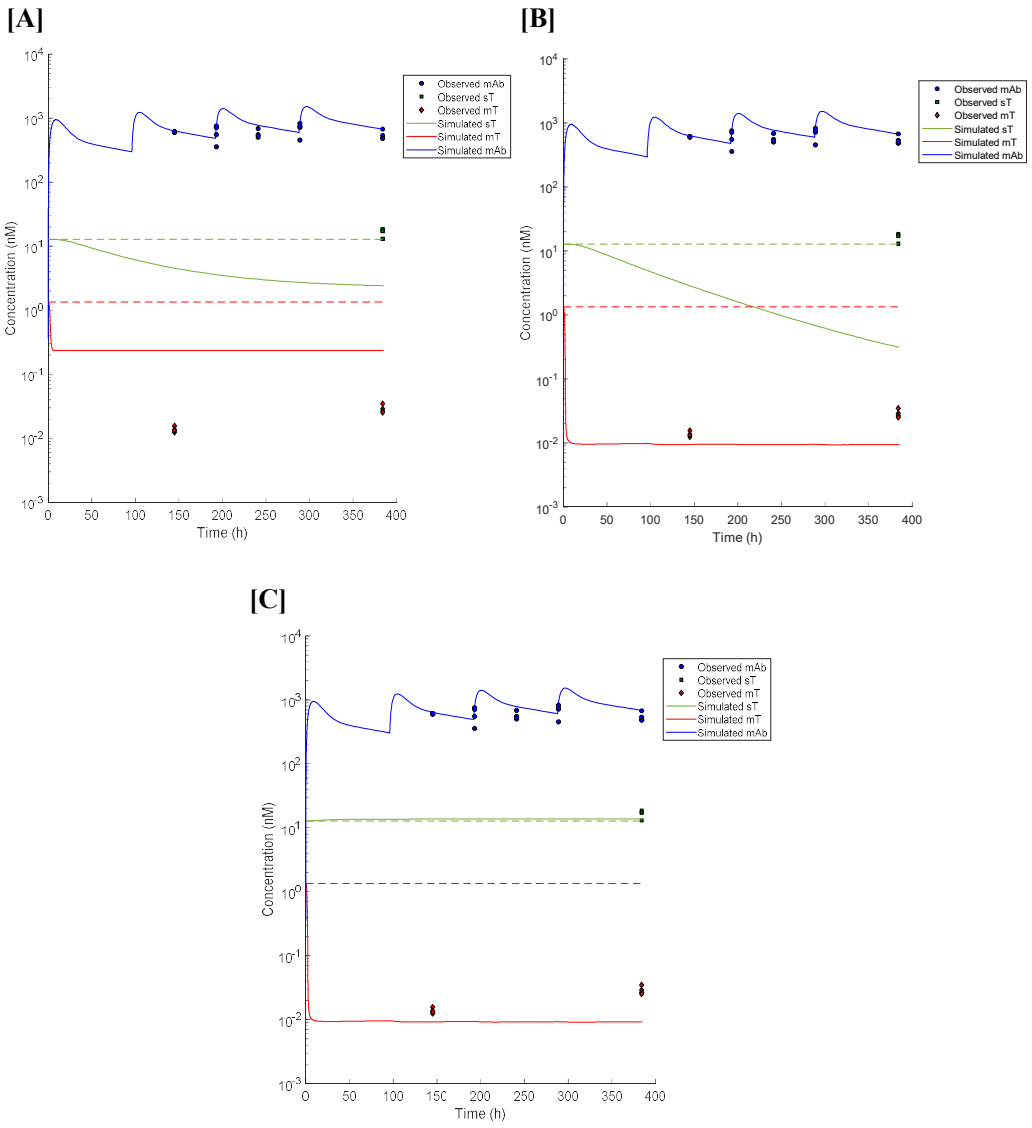

Figure 4.12. Scenario exploration using PK model v3, in comparison with the observed plasma mAb and target concentrations following 10 mg/kg Q4D IP administration of mAb 7G6 to the C57BL/6 mouse (PKPD study 7). **[A]** PK model v3 with original parameter values **[B]** Binding causes rapid internalisation ($k_{int,m}$ = 41.59 h^{-1}) **[C]** Binding causes rapid shedding ($k_{shed,m}$ = 41.59 h^{-1}).

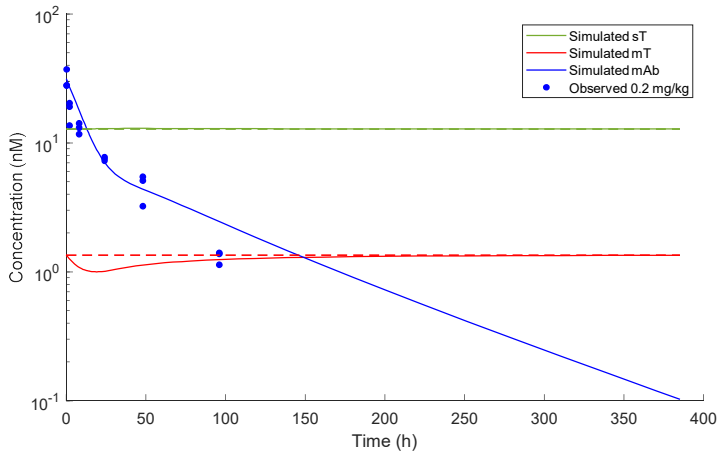

Figure 4.13. Scenario exploration using PK model v3, with the assumption that mAb 7G6 binding causes rapid shedding ($k_{shed,m}$ = 41.59 h^{-1}). Model performance in describing the observed plasma mAb profile following 0.2 mg/kg IV administration of mAb 7G6 to the C57BL/6 mouse.

4.3.4. Alternative model incorporating soluble protein synthesis (PK model v4)

An additional scenario that can be imagined, with potential to impact the kinetics of the membrane associated receptor, is that soluble protein synthesis is via an unrelated pathway as opposed to through receptor shedding. In this scenario, the saturable route of mAb clearance is still a combination of internalisation of the membrane target and clearance of the soluble target-mAb complex. However, in contrast to previous assumptions, mAb binding can trigger target internalisation and loss from the cell surface without the associated impact on soluble target concentration. To model this scenario, PK model v3 was adapted to include a separate synthesis route for soluble target and the shedding routes were removed. A diagram of the model structure is shown in figure 4.14 and the underlying equations are displayed in appendix III.

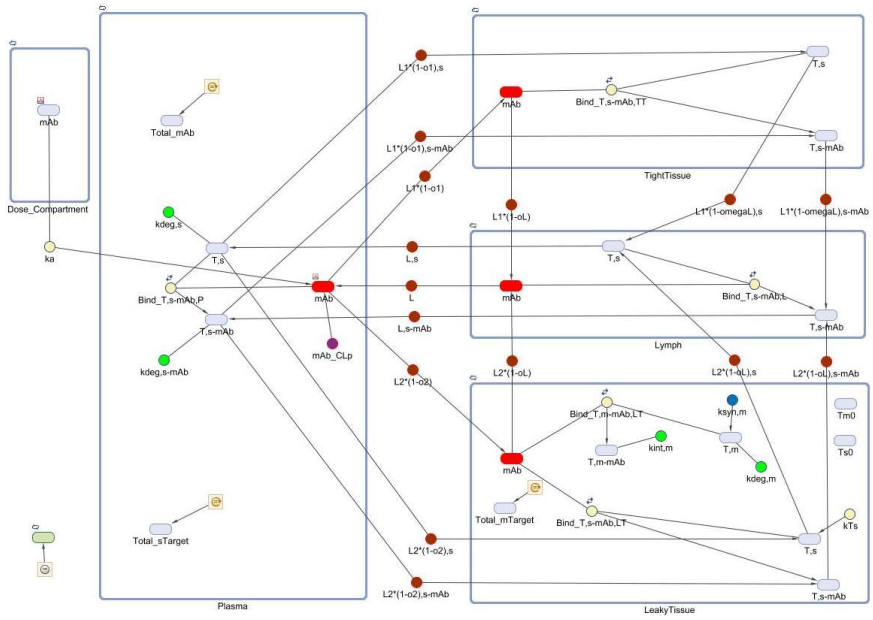

Figure 4.14. Diagrammatic representation of PK model v4, incorporating TMDD with a separate source of soluble target, as built in the Simbiology software package (v5.9).

The results gained simulating the observed data with PK model v4 demonstrates that the model provides an improved description of the dose dependent PK (figure 4.15). This improvement is clearly shown in table 4.7 by a reduction in the difference between the observed and simulated AUCt at the lower two dose concentrations (11% and 24%), when compared with those achieved with PK model v3 (33% and 32%). Indeed, PK model v4 also shows improvement in its performance simulating the measured target kinetics observed following 10 mg/kg Q4D IP administration of mAb 7G6 in PKPD study 7 (figure 4.16).

Table 4.7. Model performance review of the mPBPK model v4 incorporating TMDD. Comparison of the simulated AUC_t and maximum concentration for each dose of 7G6 estimated from the model against the observed values collected in chapter 3.

Dose Group	AUC_t (µg.h/mL)			C_{max} (C_{10min} IV) (µg/mL)		
	Observed (n=3)	Simulated	Difference (%)	Observed (n=3)	Simulated	Difference (%)
0.2 mg/kg IV	85	93	11	4.6	4.7	2
2 mg/kg IV	1429	1765	24	36.5	46.5	28
20 mg/kg IV	31593	26679	-15	412.3	465.7	14
2 mg/kg IP	2544	2039	-19	22.8	28.2	25

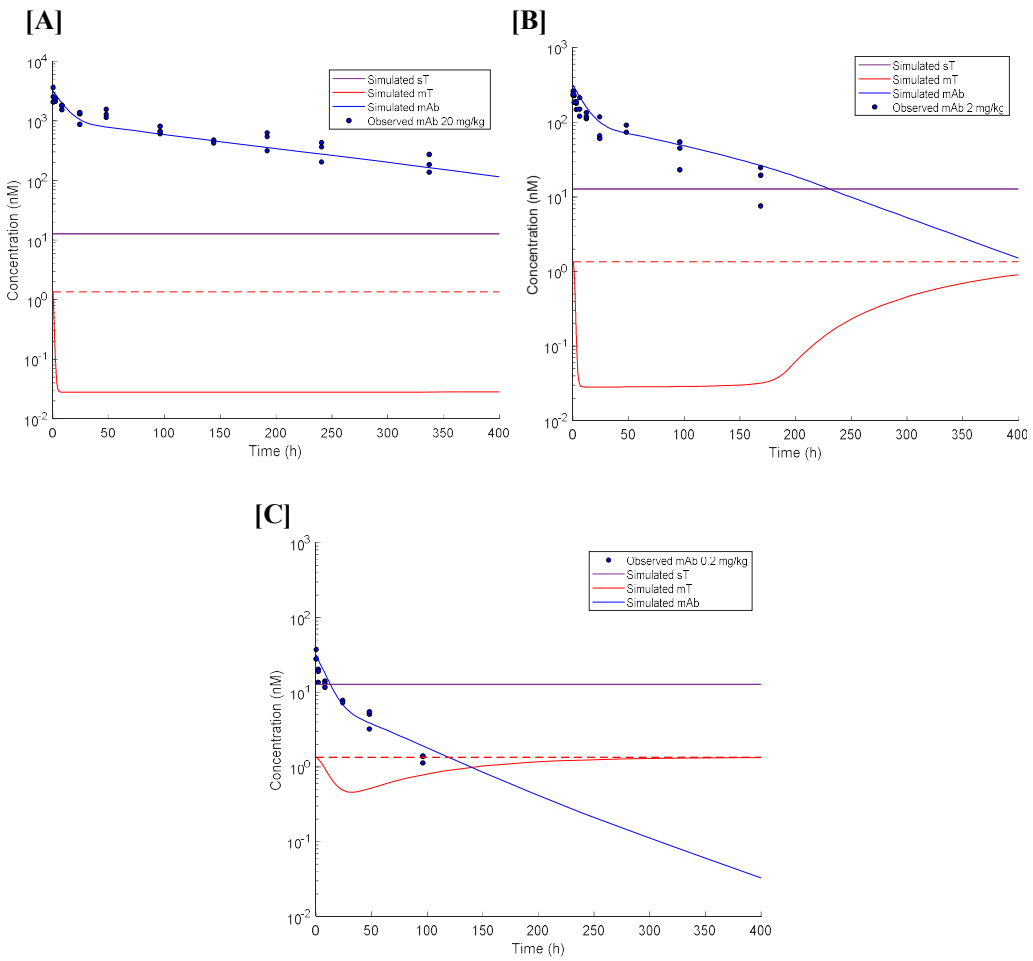

Figure 4.15. Simulated concentration profiles of mAb 7G6 in plasma (blue line), soluble target in plasma (purple line) and membrane target in leaky tissue (red line) using PK model v4, overlain with the baseline value (dashed line). Simulations performed following IV bolus administration of 7G6 at **[A]** 20 mg/kg, **[B]** 2 mg/kg and **[C]** 0.2 mg/kg and overlain with the observed data in the male C57BL/6 mouse.

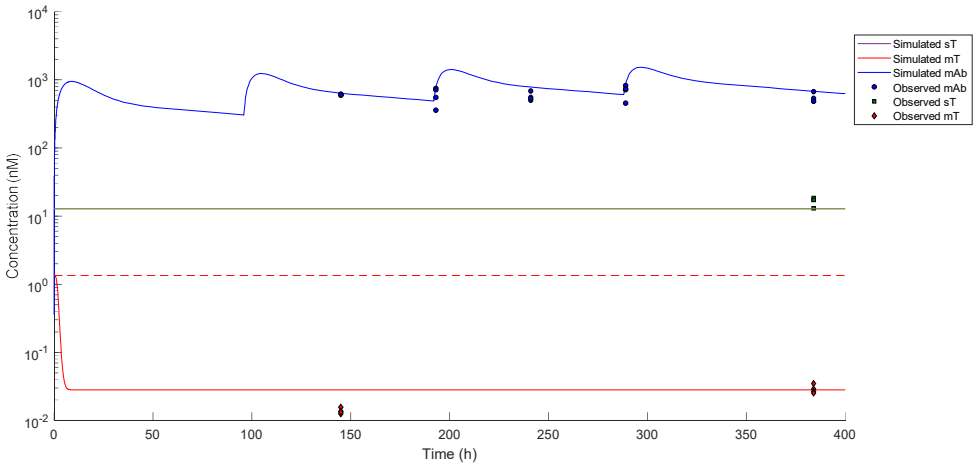

Figure 4.16. Simulation of mAb 7G6 (blue line), soluble target in plasma (green line) and membrane target in leaky tissue (red line) following 10 mg/kg Q4D IP administration using PK model v4. Simulations overlain with the experimentally observed data from PKPD study 7 in the C57BL/6 mouse.

4.4. Discussion

4.4.1. Development of the mPBPK model structure (PK model v1)

The mPBPK model described by Cao *et al.* (2013) was implemented to describe the pharmacokinetics of the surrogate CD21 specific mAbs following IV administration, utilising scaled physiological parameters for mouse. The model incorporated mAb specific values for plasma clearance, derived from the non-compartmental analysis described in chapter 3. In addition, vascular reflection coefficients to describe the restricted access of mAbs to the leaky and tight tissue compartments in mouse were assigned mean values reported by Zhao *et al.* (2015). In each instance, the resulting simulated profiles gave visually good prediction of the observed plasma concentration data for the high dose group. Providing a reasonable estimation of the duration and absolute plasma exposure achieved for each mAb.

It is apparent, that whilst the mPBPK model gives a good prediction of plasma exposure following a high dose of each mAb, this fit degrades when the dose decreases for two of the three surrogate mAbs (4B2 and 7G6). This is in line with the observed nonlinear PK in chapter 3 and consistent with a mAb demonstrating TMDD as a consequence of an additional saturable route of clearance provided by the target. As such, the model retains its ability to

provide a good prediction of the early plasma concentrations following drug administration but is unable to describe the elimination phase due to the absence of the additional clearance route in the model.

The visual goodness of fit of the simulated data for each mAb at the saturating dose provides strong endorsement for application of the mPBPK approach to the description of preclinical mAb PK. The simplified model design condenses the full PBPK model to just four compartments by implementing a tissue lumping approach. Despite this simplification, the results here demonstrate that this is a fit for purpose approach, with the model able to provide a strong prediction of mAb exposure in plasma. The performance of the model is weaker in its description of the initial distribution phase following IV dosing, over the first 8 h of the study. The rate and extent of distribution to the leaky and tight tissue compartments, which define this region of the profile, are dictated by the tissue reflection coefficients (σ1 and σ2). It was selected to use the mean values reported by Zhao *et al.* (2015), which were derived from fitting a group of 12 mAbs. In their analysis it was identified that these fitted reflection coefficients, whilst conserved across species, differed among the antibodies tested (Zhao *et al.*, 2015). This is logical, as the extent of tissue penetration is dependent upon the individual physicochemical properties of the antibody, such as net charge or the extent of glycosylation, which would vary between antibodies (Vugmeyster *et al.*, 2012). The 12 antibodies reported in the paper are all of human or humanised origin and of IgG1 isotype with the exception of Rituximab, which is a mouse/human chimera, and Rilotumumab which is of human IgG2 isotype (Zhao *et al.*, 2015). These two mAbs were both reported to have lower σ1 reflection coefficients than 9/10 of the remaining mAbs and among the lowest σ2 reflection coefficients (Zhao *et al.*, 2015). Thus, indicating that murine origin mAbs and mAbs of IgG2 isotype (such as 7G6) may have easier access to the tissue compartments than currently allowed in the model. One limitation of the data set collected in this thesis is that only sparse samples were taken to define the early phase of the profile. This limits the ability of the collected data to be used to fit mAb specific reflection coefficients to improve model performance in the distribution phase.

The plasma clearance values, calculated from the NCA of each mAb as described in chapter 3, allow the model to give a good prediction of the elongated terminal phase at the highest tested dose. In the case of mAb 9E10, this fit of the terminal phase was retained across each dose level because of the lack of target mediated interference in the clearance. The model does over predict both the C_{max} and the exposure of the 0.15 mg/kg dose of 9E10, however retaining the correct profile shape. This potentially provides confirmation that the 0.15 mg/kg group of mice were in fact under dosed. This perhaps confirms that the observed inaccuracy in measured

dose value was not solely an artefact of the post study storage conditions as postulated but may indicate an inaccurate dose solution concentration because of low concentration overnight storage in a glass container prior to dosing.

In contrast to the linear PK seen with mAb 9E10, the remaining two surrogate mAbs (7G6 and 4B2) were highlighted to have concentration dependent clearance. As a result, although the mPBPK model provides a good prediction of the plasma concentration for the highest dose group, this is lost at the lower two doses. For both 7G6 and 4B2 the model provides a reasonable estimation of the early plasma concentrations achieved. At the 2 mg/kg dose, the distribution phase is reasonably predicted by the model, however for both mAbs the plasma exposure during the terminal phase is over predicted. The model is completely unable to predict the plasma concentration profiles for the 0.2 mg/kg dose of both 7G6 and 4B2. The inability of the model to perform at these lower concentrations is due to the additional high rate but low capacity route of clearance that is presented by the target. To capture this specific route of clearance, an extended TMDD model as described by Li *et al.* (2014) was adapted and incorporated into the mPBPK model structure.

4.4.2. Development of the mPBPK model incorporating TMDD with shedding (PK model v2)

Incorporation of the membrane and soluble forms of the target into the previous mPBPK model structure, allowing reversible binding to occur between drug and target, improved the ability of the model to predict the plasma exposure at the lower dose concentrations. The model now inherits the ability to simulate the concentration dependent clearance due to the addition of a saturable clearance route within the leaky tissues compartment, described by $k_{int,m}$. The result is increasingly rapid clearance of the drug from plasma with decreasing plasma concentration. This phenomenon is demonstrated well for the 2 mg/kg dose of 4B2, where initially the model simulates a terminal phase that remains parallel to the higher 20 mg/kg dose, indicating saturation of the specific clearance route and diminishing its influence. However, at the later stage of the profile, following the 336 h sample, the specific clearance route becomes more important to the overall clearance rate resulting in accelerated plasma clearance. The model, now that it incorporates the target, can give a visually good prediction of the observed plasma concentration for both mAbs at all doses. Comparison of the simulated AUC_t versus the observed AUC_t for 4B2, demonstrates that model performance is within 20% of the observed values at both the 2 and 20 mg/kg dose levels. In a manner similar to the low 9E10 dose, the

simulation of the 0.2 mg/kg dose of 4B2 provides an over estimation of the observed AUC_t at 72% greater than the observed, along with a 24% greater estimated 10 minute concentration. This is perhaps again because of under dosing caused by the preparation and storage of a low concentration protein solution, as indicated by the difficulty in accurately measuring the dose solution concentration post study. 7G6 plasma concentrations are conversely well predicted by the model even at the lowest dose, with the simulated profile within 30% of the observed AUC_t at the 0.2 and 2 mg/kg dose levels and within 15% at the 20 mg/kg level. In this case the dose analysis following the study identified the 0.2 mg/kg dose solution concentration to be within acceptance limits. Overall, model performance in simulating the plasma concentration profiles for 4B2 and 7G6 is good as demonstrated by the low percentage difference to the observed values, providing confidence in the ability of the TMDD model incorporating shedding to describe the additional saturable route of clearance.

The target abundance and kinetics values that were selected to populate the model are based on a mixture of *in vitro* experiments and *in vivo* observations undertaken predominantly in man, with few mouse specific values available. These values however are critical to describe the saturable clearance route, with the abundance and turnover of the membrane target the most critical to the rate of drug internalisation and elimination. Consequently, to improve model performance, the abundance of the target was increased in the final model to 3.345 nM compared with the estimated value calculated as described in the methodology of 2.61 nM. This covers a multitude of possibilities within the parameter estimations to result in an increase in the capacity of the target mediated route of clearance. Clearly the primary determinant of capacity is the total amount of membrane target available, which was estimated from the total B cell population in mouse. Such a value is complicated to measure definitively, with limited published studies describing this in man, with even fewer in preclinical species. The value reported by Morris *et al.* (2005) of $2.26E^8$ used in the calculations here, was the most extensive study found in mouse. The value was based upon measuring the number of cells in processed cell suspensions from a subset of mouse organs and then combining the individual tissue values to give a total body population. An alternative method of gaining a total B cell value could be explored, such as scaling a more reliable estimate from another species based on body weight. The total target estimation could also be crucially impacted by an under appreciation of the importance of CD21 / CD35 expression on T cells and FDCs, which have been excluded as irrelevant in the model. The model also ignores the kinetics and turnover of the B cells themselves, with the assumption that they remain a stationary pool within the leaky tissue compartment. Clearly this is a significant simplification and the natural turnover of B cells would contribute to the $k_{deg,m}$ and $k_{int,m}$ values. B cells are also fairly mobile and move

throughout the body. For the purpose of the model, because the population of B cells present in the blood at a single snapshot in time is <2% of the total population, the contribution of the blood borne B cells was ignored (Westermann and Pabst, 1992). However, although the blood contains only a small population of lymphocytes at any one time, a volume estimated to be equivalent to the entire population of lymphocytes in the body travel through it per day (Westermann and Pabst, 1992). Thus, likely acting as a key contributor to accessibility of the target to the mAb. It should also be considered that the tissue lumping simplification that so successfully describes the distribution of the mAb away from the plasma, may actually underestimate the accessibility of the mAbs to the B cells located in tissues such as the spleen and lymph nodes. These highly perfused tissues contain the majority of the B cell population and are fairly easily accessed by circulating mAb (Westermann and Pabst, 1992). However, the mean reflection coefficients used in the lumped tissue compartments may lead to an underestimation of the accessibility of the target.

The soluble form of the target (T,s) plays a crucial role in the model, however no reliable estimates of the concentration of T,s were reported for mouse in the literature. To assign values for the rate of receptor shedding (k_{shed}) and the rate of membrane receptor synthesis ($k_{syn,m}$), the model is fixed to a theoretical value of T,m, but also critically to a fixed value of plasma T,s. The value selected was a median value of 300 ng/mL, taken from a study in healthy human subjects with a plasma concentration range of 150 to 600 ng/mL (Masilamani *et al.*, 2004). The k_{shed} estimate was then set by empirically altering the value to achieve the fixed plasma target concentrations at steady state. Thus, the value of T,s directly leads to k_{shed}, playing a role in creating a pool of soluble target, but also crucially in estimating the $k_{syn,m}$ rate, hence directly influencing clearance. A related assumption in the model is that upon mAb binding, soluble target takes on the clearance attributes of the mAb. The result of which is that upon mAb binding the clearance rate of soluble target ($k_{deg,s\text{-}mAb}$) decreases from 0.03851 h^{-1}, to either 0.01412 h^{-1} for 7G6 or 0.00941 h^{-1} in the case of 4B2. The impact of this is that the total pool of soluble target increases following drug administration, which is not an uncommon phenomenon for mAb therapeutics against soluble proteins. The difference here however is that the soluble target is almost the same molecular mass as the mAb, perhaps making this an over simplification of the impact on soluble target clearance. Indeed, the underlying assumption would be that the interaction of the mAb with FcRn acts to protect the soluble target from degradation and that binding between mAb and target has no pH dependency. The reverse scenario, where soluble target-mAb complex acquires the kinetics of the soluble target, would result in an additional saturable route of accelerated clearance for the mAb and could contribute to the observed terminal phase.

A knock-on effect of the soluble form of the target and the potential accumulation of its mAb bound form, is that it impacts the plasma mAb concentration. Indeed, because of the assay technique used, the measured value of plasma mAb concentration represents a composite of free mAb and partially bound mAb. This is because of the bivalent nature of mAb binding and the requirement for only a single free CDR on the mAb to elicit a signal in the bioassay. To account for this in the simulated profiles, the free mAb and bound mAb concentrations have been combined to give a single value denoted total mAb. In the model, mAb binding is only considered as a monovalent reaction with the consequence that the model may actually overestimate the measurable mAb concentration due to the contribution of bivalent binding. The largest impact of this would be felt by samples with low mAb concentrations, such as those in the lowest dose group or in the terminal phase of the profiles where the ratio of mAb to soluble target decreases. The impact in reality is considered minimal due to the large dilutions used to prepare the plasma samples for bioanalysis and the energetically unfavourable nature of bivalent binding compared with monovalent binding in a dilute solution.

When comparing the model fit across both mAbs, it can be noticed that the model provides a slight under estimate of the terminal phase and resulting AUC_t for mAb 4B2 at 2 mg/kg, with a 13% lower AUC_t compared to the observed value. Whilst for mAb 7G6 at the same dose level, the model provides an over estimate in the terminal phase and resulting AUCt, with a 32% higher AUC_t compared to the observed value. This perhaps provides an insight into the relative affinities of the two mAbs for the target, because in both cases the model provides a good fit of the 20 mg/kg dose profile, where target is expected to be fully saturated. The affinity (K_d) of both these mAbs was set to 1 nM in the model to represent a good preclinical tool molecule, in the absence of a measured value, along with estimated values for k_{on} and k_{off}. Clearly a difference in the actual affinity of the tool molecules would exist because of the different ways in which they were originally raised, with the data indicating 7G6 as the higher affinity mAb.

4.4.3. Parameterisation with experimentally determined values (PK model v3)

The initial estimates used to parameterise PK model v2 were a combination of literature values from other species and estimates based on the behaviour of similar proteins. The importance of collecting experimentally determined values to improve PK model performance was highlighted during the model development phase. In addition, improved description of target

kinetics enhances the translational value of the model and its ability to describe target engagement. Whilst it would be ideal to gather experimental values for all model parameters, in practice it is unfeasible to measure many of the rate constants involved. Therefore, three values in the model were identified as high impact and potentially measurable. These were the concentration of soluble target in plasma, the number of receptors on splenic B cells and the K_d of the antibody to cellular target. These three values have a knock-on impact on $k_{shed,m}$, $k_{syn,m}$ and k_{on}, all of which are critical in characterising the impact of the target on the pharmacokinetics of the drug and the impact of the drug on the kinetics of the target.

With the estimated target concentration identified as the most critical model unknown, considerable effort was applied to the development of analytical methodology to measure these values. These methods are described in chapter 2 and the results of the analysis when applied in PKPD study 7 are described in chapter 5. In addition, the K_d of mAbs 7G6 and 4B2 was determined, confirming the earlier observation that 7G6 is considerably higher affinity (0.05 nM vs 1.65 nM, Appendix V). Once these new measured values of target and kinetics were input into the PK model structure (denoted PK model v3), it quickly became apparent that the underlying assumptions regarding the target and mAb interactions were inconsistent with the observed data. This can be visually observed in figure 4.10, where PK model v3 is unable to describe the accelerated target mediated clearance of mAb 7G6 at lower drug concentrations. The causes of this loss in performance are twofold. Firstly, the mean measured receptor number was lower than the original estimated value, and certainly lower than the tweaked number used to improve PK model v2 performance. Secondly, the higher measured soluble target concentration requires a much higher rate of shedding to maintain it, compensated by a more rapid target synthesis rate. With soluble target clearance remaining unchanged, this results in a large increase in the total amount of soluble target available, acting as a sink for the drug and trapping it within the system. Indeed, this can be visually observed in figure 4.10C where mAb dosing leads to an increase in total soluble target (free + bound) that gradually returns to baseline over 14 days, resulting in a prolonged terminal phase of the total mAb (free + bound) profile.

4.4.3.1. Scenario modelling to test model assumptions: TMDD mechanism

The inability of PK model v3 to describe the observed TMDD of mAb 7G6 highlights that the assumptions defining the mechanism of TMDD may be incorrect. PK model v2 ascribes receptor internalisation as the sole mechanism, with an assumed fast rate of internalisation following mAb binding, lifted from literature describing other similar mAbs (Vainshtein *et*

al., 2015). To challenge this premise, a test scenario was modelled using an extreme $k_{int,m}$ value of 41.59 h^{-1} (figure 4.11B). An alternative route of TMDD, often described for mAbs targeting soluble proteins, occurs due to either clearance of the target-mAb complex as if it were the native soluble protein or phagocytosis of aggregated complexes by macrophage. PK model v2 ignores this route, therefore to test its impact a scenario was modelled where the target-mAb complex inherited the clearance rate of the native soluble target.

Comparison of the performance of the base PK model v3, versus the adapted versions testing the two potential mechanisms of TMDD, clearly demonstrates that the pharmacokinetics of 7G6 at low drug concentrations is dominated by the soluble protein. This is highlighted by the loss of performance (table 4.6), as measured by the AUC_t, when swapping from PK model v2 (+33% vs observed) to the measured parameters in PK model v3 (+57% vs observed), which includes a much higher soluble protein concentration. Changing the underlying assumption of target mediated clearance highlights the importance of soluble protein complex clearance versus internalisation rate in determining 7G6 pharmacokinetics. Little improvement in prediction is observed in the scenario where internalisation rate is an unrealistically high value (54% vs 57%), whereas the scenario where the soluble complex clearance rate is that of the native protein results in a drastic improvement (8% vs 57%). This is a definitive outcome that resulted in an update of the underlying assumptions of PK model v3, with soluble target-mAb complex now retaining the clearance rate of the free soluble protein. However, because the extent of clearance that occurs via internalisation versus soluble clearance cannot be experimentally determined, both routes are now included in the model. The internalisation rate ($k_{int,m}$) retains its fast internalisation description.

4.4.3.2. Scenario modelling to test model assumptions: Impact of mAb binding

Despite the improvement in description of 7G6 pharmacokinetics, the revised PK model v3 still doesn't provide an accurate description of target kinetics following dosing. This is highlighted in figure 4.12A, where following 10 mg/kg Q4D IP administration of mAb 7G6 in PKPD study 7 (chapter 5), whilst 7G6 PK is well characterised the description of soluble target and membrane target are poor. The underlying cause of this is actually the shedding rate used to define the soluble target concentration in plasma. The $k_{shed,m}$ rate must be high to maintain the soluble target pool, resulting in fairly rapid turnover of membrane receptor. When drug is applied to the model system, rather than receptor being shed to maintain soluble target, it can now be rapidly internalised instead, resulting in a reduction in the observed total soluble

target concentration. This scenario can be confirmed through simulation of an extreme internalisation rate value ($k_{int,m}$ of 41.59 h^{-1}), with exacerbation of the impact on soluble target observed (4.12B), albeit to the benefit of fitting the measured reduction in total membrane target.

An alternative hypothesis was modelled, whereby mAb binding increases the rate of receptor shedding, a reported characteristic of other mAbs. Again, an extreme value was tested ($k_{shed,m}$ of 41.59 h^{-1}), which on first observation appears to resolve the issue (figure 4.12C). The simulated profiles of both the soluble and membrane target can describe the observed data well. However, this new assumption comes at the cost of the description of TMDD, conversely this time due to the impact on membrane receptor availability, minimising the role of internalisation on 7G6 PK. Whilst this may indicate soluble complex clearance as the primary driver of TMDD, such a model requires a number of bold assumptions to fit the observed data, including rapid shedding and rapid clearance of the soluble target-mAb complex. These assumptions would be extremely challenging to confirm experimentally, devaluing the validity of the model.

4.4.4. Alternative model incorporating soluble protein synthesis (PK model v4)

One assumption that up to this point has not been considered, is the origin of the soluble form of target. While reports have indicated the origin to be shed receptor, this is not definitively proven, opening the possibility that a separate synthesis pathway exists. Certainly, other similar targets have reported a combination of shedding and secretion as the source of the soluble form. Once again, an extreme approach was taken to explore this assumption, removing the shedding route from PK model v3 and replacing it with a separate soluble target synthesis rate (k_{Ts}) in the leaky tissue compartment (figure 4.14). The synthesis rate k_{Ts} was empirically fitted to achieve the observed steady state concentration of soluble target in plasma. The scenario where all soluble target originates from a secreted source, whilst all membrane receptor is internalised was then tested for its performance in simulating the observed data.

The performance of PK model v4 was initially tested through its ability to describe the observed pharmacokinetics of mAb 7G6. The results demonstrated that PK model v4 provides a good description of mAb 7G6 pharmacokinetics at all tested doses, with performance on a par with the revised PK model v3 (figure 4.15). Improvement in the description of AUC_t following 0.2 mg/kg IV administration was demonstrated to within 11% of the observed value, versus 33% for model v2 (table 4.7). Model performance was then tested in its ability to

describe both the PK and observed target effects in PKPD model 7, following 10 mg/kg IP Q4D administration (chapter 5). This analysis showed that PK model v4 can also describe the observed impact of mAb 7G6 on both the soluble and membrane associated target (figure 4.16). This improved performance is because the model can balance the impact of drug on membrane receptor, without the associated impact on soluble target synthesis. This potentially provides evidence for the existence of a separate soluble target synthetic route. However, whilst this assumption provides the best fit of the currently observed data set, the reality is almost certainly more complex and is most likely a combination of both shedding and secretion.

4.5. Chapter conclusion

The application of a modelling approach has successfully allowed simulation of the nonlinear PK demonstrated by two of the three surrogate mAbs. The simplified mPBPK model design provides a fit for purpose method for describing the distribution and kinetics of the mAbs in mouse, while resulting in physiologically relevant lumped tissue concentrations. In addition, incorporation of the target into this model structure allowed description of the nonlinear PK experienced by two of the mAbs. As a direct consequence of its simplified nature, the model does contain several limitations which could be addressed by moving to a full PBPK model. This includes aspects such as tissue accessibility which defines the early distribution phase, along with over simplified target abundance and expression characteristics. However, the large number of unknowns regarding the target would render parameterisation of such a full PBPK model abject, significantly reducing the value gain over the simpler approach described here.

The base mPBPK model implemented here remained little changed from that reported by Cao *et al.* (2013) with parameters for mouse taken from a more recent publication released by the same research group (Zhao *et al.*, 2015). Overall performance of the base model was good in its description of the kinetics of mAb 9E10, which was untroubled by target mediated clearance. The exception to this was the fit of the initial distribution phase which the model overstates, likely due to an under estimation of the rate of distribution away from the plasma. To improve this, mAb specific values for the reflection coefficients σ1 and σ2 could be gained from fitting data. This approach is however limited by the sparse data collected in the early phase following drug administration. Physiological limitations of mice mean that a standalone pharmacokinetic study would be required to elaborate this phase further and collect sufficient

data to fit. The base model was extended to cater for drug administered via intraperitoneal injection, which is a less technically challenging administration route for preclinical studies in mice. This was achieved through addition of a dosing compartment with a rate limited entrance into the circulation, defined by k_a. Bioavailability was previously identified in chapter 3 to be 100% via the IP route for each of the three surrogate mAbs, with a T_{max} of approximately 8 hours that was used to fix k_a. Clearly description of T_{max} is limited by the sampling regimen used in the PK studies, thus a further standalone pharmacokinetic study would be required to elaborate the rate of absorption from the IP dosing site further.

Models constantly evolve over time as further evidence and knowledge is collected, as aptly demonstrated in this work, however several key refinements are required to enhance the performance of the model further. While collection of experimental values for the concentration of target provided a massive step forward in model performance, description of target kinetics is still based on numerous unexplored assumptions. Refinement of the kinetics of target synthesis and turnover would provide significant benefit to the description of target engagement. However, the *in vitro* experiments required to elaborate these rates would be a daunting technical prospect to pursue and exists beyond the scope of the current work. Whilst use of the model to predict plasma exposure following varying dosing regimens is useful, its real value comes from linking this to biological engagement of the target to begin to inform questions related to target coverage and effect.

The models described in this chapter have been utilised in the design of the PKPD experiments described later. PK model v2 was used to predict the optimal dosing strategy to achieve maintenance of mAb exposure in PKPD study 7 (described in chapter 5). Despite its limitations at the time, regarding its potential description of target kinetics, the model performance was strong for the estimation of total mAb exposure in plasma. This resulted in the Q4D IP dosing regimen selected to provide optimal maintenance of 7G6 exposure over the proposed 16-day study period. The model was also used to extend the pre-treatment time to two days to ensure maximum target coverage within the tissue prior to the immune challenge. It was also used to identify the optimal use of the minimal number of available sampling occasions to gain maximum data coverage in the PKPD study. Later improvements in the model resulted in PK model v4, which was implemented for the interpretation of the data generated in PKPD study 7 and the creation of a mathematical PKPD model as described in chapter 6.

Chapter 5: Exploration of the *in vivo* pharmacology of CD21 neutralising mAbs in an acute mechanistic pharmacodynamic model of humoral immunity in mice

5.1. Chapter introduction

Acute, mechanistic pharmacodynamic models are a popular experimental approach for characterising the primary pharmacology of novel investigational drugs, in a relatively simple, short duration *in vivo* study design. This project applied such a mechanistic PKPD strategy to expand understanding of the pharmacology of CD21 neutralisation by therapeutic mAbs, using the three murine specific surrogates (7G6, 4B2 and 9E10). Whilst a few literature reports describe the phenotypic impact of CD21 knockout or therapeutic blockade in mice, none have moved beyond testing full knockdown or a single high dose that saturates the target. Consequently, data describing the extent and duration of target engagement required to elicit a significant downstream pharmacological effect on the T-dependent antigen response is currently absent. Whilst logic would dictate that a CD21 neutralising mAb, as a receptor antagonist, would require high target coverage to drive effect, this has not been demonstrated to date. Additionally, due to the complex biological role and restricted cellular expression of CD21, it represents an onerous target for *in vitro* investigation, augmenting the importance of *in vivo* experimentation.

The following results chapter details the investigation of three murine surrogate mAbs (7G6, 4B2 and 9E10) using T-dependent immunisation of mice as an acute model of humoral immunity. Initial investigation was conducted using an established T-dependent immunisation protocol requiring adjuvant. But with greater alignment to the underlying biology of CD21 sought, the chapter details the development, qualification and application of a non adjuvant driven model to explore CD21 pharmacology.

5.2. *In vivo* study overview

Seven *in vivo* studies were performed in total, as summarised in table 5.1. The objective of the initial study was to confirm the efficacy of the three surrogate CD21 specific mAbs in a classic TDAR experimental model and assist selection of the best tool to take forward into further experiments. A set of studies were then performed to develop and optimise an alternative TDAR model design for improved alignment with target biology and qualify the approach using gold standard therapies. Finally, the pharmacology of CD21 neutralisation was explored in the new TDAR experimental model using a surrogate mAb to generate enhanced understanding of the concentration effect relationship and facilitate mathematical PKPD modelling.

Table 5.1. Overview of the seven *in vivo* studies performed to support the mechanistic PKPD strategy, with reference to the results section for each study.

Study Ref.	Study Title	TD Challenge	Study Objective	Results Section
PKPD study 1	7G6, 4B2, 9E10 head to head comparison at 20 mg/kg	IP immunisation at 100 µg/kg (TNP-KLH 1:1 Alum)	Compare relative efficacy of the three tool antibodies	5.4.1
PKPD study 2	IV KLH TDAR pilot	IV immunisation at 10 µg/mouse (soluble KLH)	Explore feasibility of IV immunisation, excluding adjuvant requirement	5.4.2
PKPD study 3	IV KLH TDAR pilot 2	IV immunisation at 10 or 30 µg/mouse (Imject KLH)	Explore IV immunisation with high molecular weight KLH. No adjuvant	5.4.2
PKPD study 4	IV KLH protocol development	IV immunisation at 30 or 100 µg/mouse (Imject KLH)	Extend challenge dose range, confirm reproducibility	5.4.2
PKPD study 5	IV KLH TDAR qualification	IV immunisation. Imject KLH at 1.2 mg/kg	Qualify the experimental model with clinically validated therapies. Identify a model positive control	5.4.3
PKPD study 6	Fingolimod concentration effect	IV immunisation. Imject KLH at 1.2 mg/kg	Fingolimod dose response as a training data set for mathematical model development	5.4.4
PKPD study 7	Evaluation of 7G6 concentration effect	IV immunisation. Imject KLH at 2.4 mg/kg	Generate dose response data with mAb 7G6 for mathematical PKPD modelling	5.4.5

5.3. *In vivo* and analytical methodology

An in-depth description of the full experimental protocol and reasoning for each *in vivo* study is located in chapter 2, including description of the materials and drug molecules involved. Chapter 2 also includes full description of the analytical methodology used to generate all experimental endpoint data described in this report.

5.4. Results

The pharmacology of CD21 neutralisation by surrogate murine mAbs was explored as part of a mechanistic PKPD strategy using a T-dependent immunisation experimental model in mouse. Initial experimentation was to confirm the efficacy of the three surrogate CD21 neutralising antibodies and select the best mAb to take forward into further characterisation (5.4.1). This study ultimately led to the development of a new experimental TDAR model format, with improved alignment to target biology and an enhanced sampling strategy to facilitate mathematical PKPD modelling of key biomarker endpoints (5.4.2). Gold standard therapies were tested to provide external qualification of the reformatted experimental model and explore its translational potential for clinical projection (5.4.3 and 5.4.4). Finally, the preclinical mechanistic PKPD strategy was applied to exploration of the pharmacology of CD21 neutralisation by the surrogate mAb 7G6 (5.4.5).

5.4.1. PKPD study 1: Mouse TDAR (IP TNP-KLH): 7G6, 4B2 and 9E10 head to head comparison

To characterise the relative efficacy of the three surrogate CD21 neutralising antibodies 7G6, 4B2 and 9E10, a head to head study was initiated in an *in vivo* TDAR experimental model in the C57BL/6 mouse. The objective was to confirm literature data describing the impact of CD21 neutralisation on the humoral immune response, provide experimental data to support target validation and identify the best molecule to progress into further investigation. Of the three mAbs tested, the internal GSK tool mAb 9E10 (murine IgG1) was the only molecule without prior confirmation of efficacy *in vivo*. The murine IgG1 mAb 4B2 was published by Kulik *et al.* (2015), confirming functional inhibition of the TDAR to the classic TD antigen SRBC. Direct comparison of the efficacy of these two murine IgG1 mAbs to the commercial rat IgG2b mAb 7G6 was highly desirable, in view of the 10-fold higher dose reported for mAb 4B2 (2 mg/mouse) compared with that of 7G6 (0.2 mg/mouse). At the time of study initiation, comparative *in vitro* binding data was unavailable.

The study successfully implemented the well characterised TNP-KLH IP immunisation protocol in the male C57BL/6 mouse. Due to insufficient drug material, one mouse in the 7G6 treatment group was not dosed, reducing the treatment group size to n=5. Primary endpoints were plasma drug exposure and TNP specific antibody concentration (IgG and IgM) on study days 1, 10 and 14, alongside B cell populations in the spleen on the study day 14. A crude measurement of target engagement constituted a secondary exploratory endpoint, identifying CD21 expression on splenic B cells using a panel of labelled CD21/35 antibodies.

5.4.1.1. Tool mAb pharmacokinetics

The measured plasma exposure of the murine CD21 specific mAbs 7G6, 4B2 and 9E10 following IP administration at 20 mg/kg are shown in figure 5.1, providing confirmation of the magnitude and maintenance of drug exposure. Bioanalytical assay performance was in line with acceptance criteria, with a limit of quantification (LLQ) after dilution of 2 µg/mL for mAbs 7G6 and 4B2 or 1 µg/mL for mAb 9E10. Where the plasma concentration was measured below the assay LLQ, in the case of two animals in the 7G6 group, a value of half LLQ was plotted for illustrative purposes but the sample was excluded from the group mean. The systemic plasma concentration at 24 h post dose was almost identical for each of the three tested mAbs, measured at 183, 186 and 169 µg/mL for mAbs 7G6, 4B2 and 9E10 respectively. The inter-individual variability at this C_{max} (24 h) concentration was low, with a coefficient of

variation (CV%) of 10%, 5% and 24% for mAbs 7G6, 4B2 and 9E10, respectively. Thus, demonstrating consistency in dose formulation, administration and ultimately absorption from the dosing site between the different mAbs.

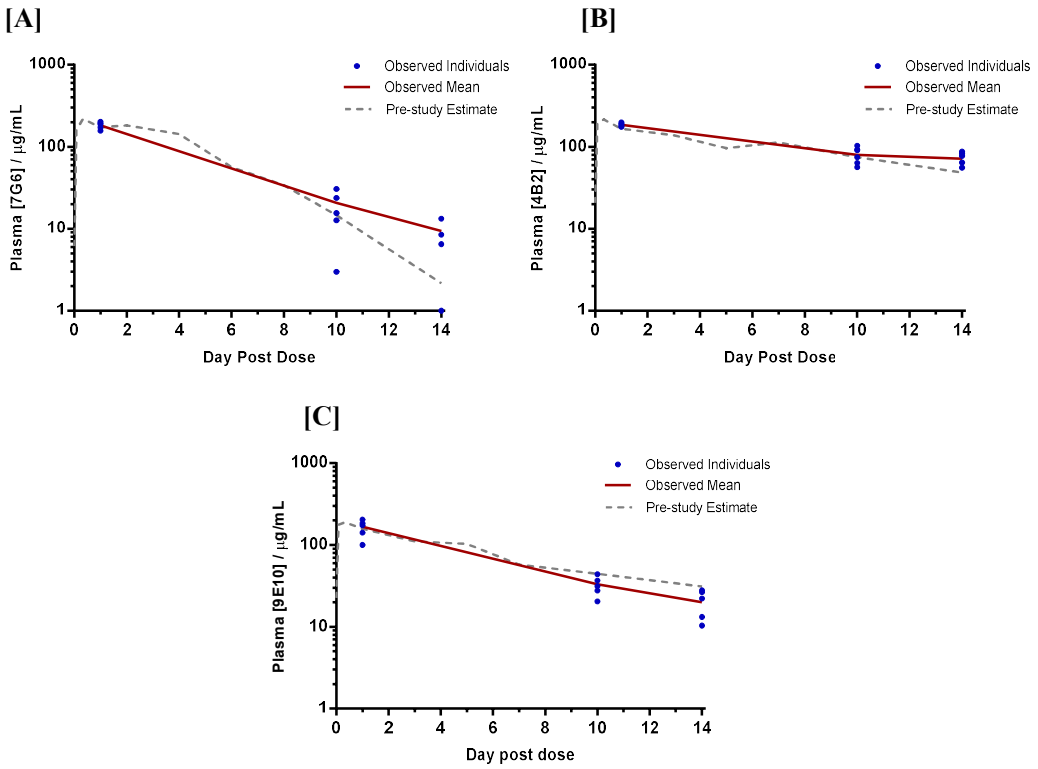

Figure 5.1. Surrogate mAb plasma concentrations observed in the TNP-KLH TDAR head to head study (PKPD study 1), when the following mAbs were administered IP at 20 mg/kg to the male C57BL/6 mouse. **[A]** 7G6, **[B]** 4B2 and **[C]** 9E10. Data represented as individual concentration (blue circles), group mean (red solid line) and the pre-study estimate (grey dashed line).

The observed plasma concentration of each mAb is overlain with the pre-study estimate (figure 5.1), based upon linear scaling of the pharmacokinetic characterisation data described in chapter 3. For each tested mAb, the observed exposure showed strong correlation with this pre-study estimate, indicating consistency in study performance. There was one exception to this, with the mean plasma exposure of 7G6 diverging from the pre-study prediction at the terminal time point. In addition, the 7G6 plasma concentration measured in two mice fell below the limit of quantification on day 14, in contrast to the three remaining mice in the group, despite fitting within the group at 24 h post dose.

5.4.1.2. Tool mAb pharmacodynamics

The plasma concentration of TNP specific IgG1 and IgM was measured at baseline (study day 0), on day 10 and following termination on day 14, with the results illustrated in figure 5.2. Immunisation with TNP-KLH in this study resulted in a 20-fold increase in TNP specific IgG1 in the control treatment group on day 14. With this antigen specific response defined as the fold increase from baseline, which was measured below the assay limit of quantification (0.4 µg/mL). Prophylactic treatment with 20 mg/kg 7G6, 4B2 and 9E10, one day prior to immunisation, resulted in no significant attenuation of the antigen specific IgG1 response. A trend toward inhibition was observed with the commercial mAb 7G6, that was not observed with the remaining two treatments. Inter-individual variability was high, illustrated by the coefficient of variation (CV%) of 86% in control IgG1 response on day 14, with this variance maintained across all treatment groups. The TNP specific IgM assay suffered from a high degree of background interference from low affinity, naïve pool IgM. This resulted in an extremely narrow 7-fold antigen specific IgM response window, between baseline on study day 0 and the terminal day 14 sample. Inter-individual variability was again high, illustrated by the CV% of 43% in control IgM response on day 14. This narrow antigen specific IgM response was not shown to be attenuated by prophylactic treatment at 20 mg/kg with either mAb 7G6, 4B2 or 9E10, when compared against the control treatment group.

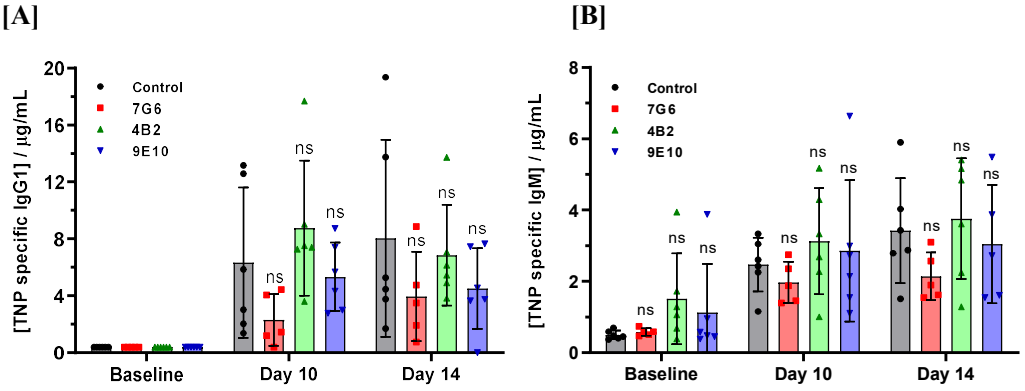

Figure 5.2. TNP specific antibody concentrations **[A]** IgG1 and **[B]** IgM, measured on study days 0, 10 and 14 in PKPD study 1. C57BL/6 male mice were immunisation IP with 100 µg/kg TNP-KLH in PBS formulated 1:1 with Alum (v/v) on study day 1, 24 h after pre-treatment on study day 0 with 20 mg/kg IP of either mAb 7G6, 4B2, 9E10 or an isotype control. Data illustrated as the individual (symbols) and mean ±SD (bars) plasma concentration (n=6), with statistical significance calculated using a one way ANOVA with Dunnett's multiple comparison test to compare with the control group, ns = not significant.

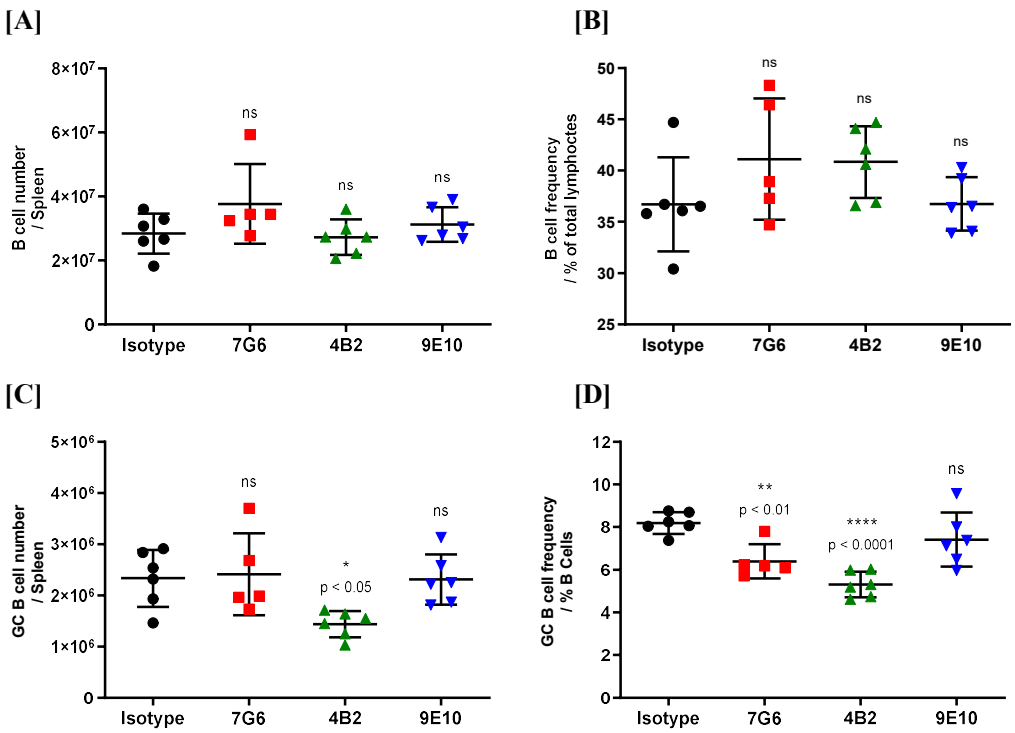

Figure 5.3. Splenic cell populations in the C57BL/6 male mouse measured 13 days post IP immunisation with 100 µg/kg TNP-KLH in PBS formulated 1:1 with Alum (v/v). Mice were pre-treated IP 24 h prior to immunisation with 20 mg/kg of either mAb 7G6, 4B2, 9E10 or an isotype control. **[A]** B cell ($B220^+$) and **[C]** GC B cell ($B220^+$, $GL7^+$, IgD^-) number per spleen. **[B]** B cell ($B220^+$) and **[D]** GC B cell ($B220^+$, $GL7^+$, IgD^-) frequency as a percentage of total lymphocytes. Data illustrated as the individual (symbols) and mean ±SD (line and bar) n=6, with statistical significance calculated using a one way ANOVA with Dunnett's multiple comparison test, * $p < 0.05$, ** $p < 0.01$, **** $p < 0.0001$, ns = not significant.

To evaluate the impact of treatment with anti-CD21 mAbs on the cellular components of the humoral immune response, the B cell and germinal centre B cell populations were measured in the spleen following termination on day 14. Comparison of the resulting B cell and germinal centre B cell number and frequencies are shown in figure 5.3. Importantly, this analysis demonstrates that treatment with anti-CD21 mAbs does not result in depletion of the total number of B cells (figure 5.3A) or the number of B cells as a percentage of total lymphocytes (figure 5.3B). It should also be noted that one animal in the 7G6 treatment group presented with a much higher number of B cells, skewing interpretation of the observed cell number data, emphasising the importance of the frequency analysis for accurate interpretation of the data in this study. Prophylactic treatment with both 7G6 and 4B2 at 20 mg/kg resulted in

significant inhibition of the germinal centre B cell response to the TD TNP-KLH challenge (figure 5.3D). In contrast, treatment with mAb 9E10 at 20 mg/kg resulted in no attenuation of the GC B cell response.

As a crude evaluation of target engagement, a trio of labelled probe antibodies were used to identify the presence of CD21/35 on splenic B cells by flow cytometry (figure 5.4), as described previously by Kulik *et al.* (2015). This assay allows direct comparison of the relative ability of each test article to engage with CD21/35 on the surface of B cells in the target tissue. The trio of probes are; 7G6, which competes for binding with each mAb, 7E9, which is non-competitive with each mAb and 8C12, which binds CD35 only.

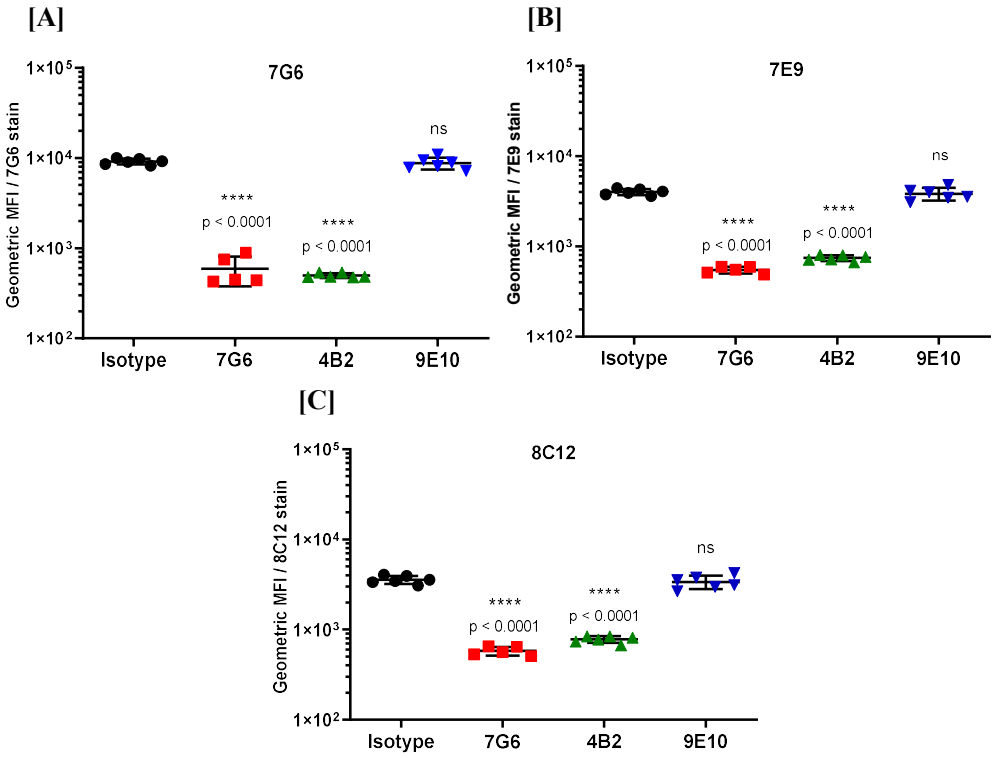

Figure 5.4. Splenic B cells were probed with fluorescently labelled mAbs targeting CD21/35 to investigate the extent of target engagement following termination, 14 days post IP treatment with 20 mg/kg of either mAb 7G6, 4B2, 9E10 or an isotype control, during the mouse TDAR head to head study (PKPD study 1). Splenic B cells probed with **[A]** PE labelled 7G6, specific for CD21/35, **[B]** APC labelled 7E9, specific for CD21/35 but non-competitive with 7G6/4B2, **[C]** BV421 labelled 8C12, specific for CD35 alone. Data illustrated as the individuals (symbols) and mean ±SD (line and bar) n=6, with statistical significance calculated using a one way ANOVA with Dunnett's multiple comparison test, **** p <0.0001, ns = not significant.

The results shown in figure 5.4 demonstrate that prophylactic treatment with both mAb 7G6 and 4B2 at 20 mg/kg resulted in a >10-fold reduction in the measured MFI of each fluorescent probe antibody (7G6, 7E9 and 8C12) on splenic B cells, when compared with the isotype control treated group. This provides direct evidence of target engagement at the site of action within the spleen, as demonstrated by the reduction in 7G6 signal (figure 5.4A). But crucially, also shows that both 7G6 and 4B2 result in a loss of expression of the receptor from the cell surface, as demonstrated by the reduction in 7E9 signal (figure 5.4B). In addition, the phenomenon is replicated at the closely related protein CD35, with the 8C12 signal also reduced (figure 5.4C). In stark contrast, treatment with mAb 9E10 does not result in a change in MFI of any of the trio of fluorescent probes on splenic B cells, when compared with the IgG1 isotype control treated group.

In review, the head to head study confirmed the ability of both 7G6 and 4B2 to engage the target at the level of the spleen, following IP administration at 20 mg/kg. These two mAbs consequently result in inhibition of the humoral immune response to the TD antigen TNP-KLH at the cellular level, through a reduction in GC B cell frequency, but importantly, without depletion of the total B cell population. The in house mAb 9E10 failed to demonstrate target engagement and subsequently did not inhibit the cellular response to the TD antigen. None of the three tested anti-CD21 mAbs resulted in significant inhibition of the TNP specific IgG1 or IgM responses under the experimental conditions used.

5.4.2. PKPD study 2/3/4: Development of an adjuvant free TDAR mouse model

To improve mechanistic alignment with the underlying biology of the complement receptors and to enhance translational value, the mouse *in vivo* TDAR experimental model was redesigned. The objective was to change the route of administration of the TD antigen, whilst removing the requirement for an adjuvant, to result in a subtler immune response in which to test the efficacy of the CD21 neutralising antibodies. The initial IV immunisation pilot experiment (study 2) was carried out with a widely used, soluble form of KLH (Sigma Aldrich), formulated in PBS alone and injected via the tail vein at a dose of 10 µg/mouse. Plasma samples were collected at baseline (prior to immunisation), day 7, 10 and 14 for the measurement of the antigen specific antibody concentration. However, no measurable antigen specific IgG or IgM response was propagated, when compared with the day 0 baseline. This was an unexpected outcome considering the 4-fold higher antigen dose used here compared

with the earlier head to head study (study 1), at 400 µg/kg versus the 100 µg/kg of TNP conjugated KLH administered IP in the presence of the adjuvant Alum in study 1.

A second pilot study was conducted to test alteration of the form and source of KLH to the high molecular weight Imject mcKLH form (ThermoFisher Scientific), which has superior reported immunogenicity when compared to the soluble subunit form used previously (Lebrec *et al.*, 2014a). A pilot experiment (study 3) was performed at 10 µg/mouse, with an additional group challenged at 30 µg/mouse. Subsequently a follow up study was performed to confirm and extend the tested KLH dose range (study 4). The objective was to generate data to guide selection of a KLH challenge that provokes a robust, yet submaximal, immune response as defined by KLH specific IgG and germinal centre B cell endpoints.

The initial feasibility study was completed successfully, with one minor alteration to the intended group size following the untimely death of one mouse between the baseline blood sample collection on study day 0 and administration of the KLH challenge 24 h later. This resulted in a reduction of the PBS control group size to n=2. No adverse reactions were observed following treatment with KLH. Whilst animal welfare was continuously tracked throughout the study by monitoring bodyweight every other day (figure 5.5A). The follow up protocol development study (study 4) tested a repeat of the 30 µg/mouse challenge and a higher 100 µg/mouse challenge, with no adverse reactions to KLH treatment observed. However, the unexplained death of two mice on study resulted in insufficient animals to complete the 300 µg/mouse challenge. Animal welfare was tracked throughout the study with bodyweight recorded every other day (figure 5.5B).

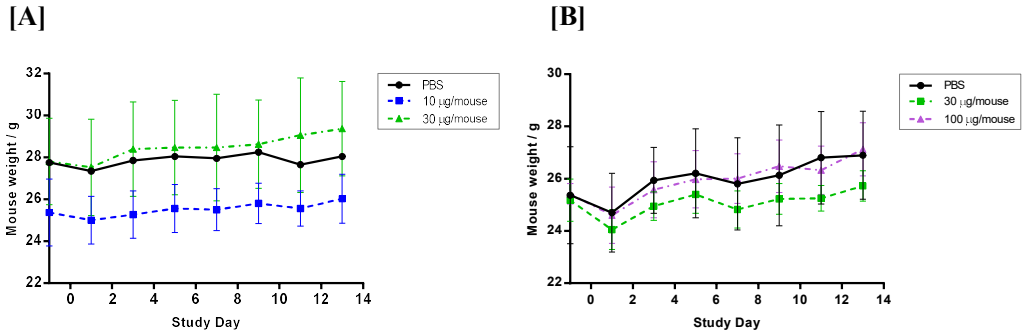

Figure 5.5. Bodyweights of C57BL/6 male mice recorded on alternate days as a marker of animal wellbeing during the pilot IV KLH TDAR studies **[A]** PKPD study 3 and **[B]** PKPD study 4, following IV immunisation on study day 0 with either PBS control, 10 or 30 µg KLH in study 3 or PBS control, 30 or 100 µg KLH in study 4. Data illustrated as the mean (symbol) +/- SD (bar), n=3 (or n=4, 30 and 100 µg).

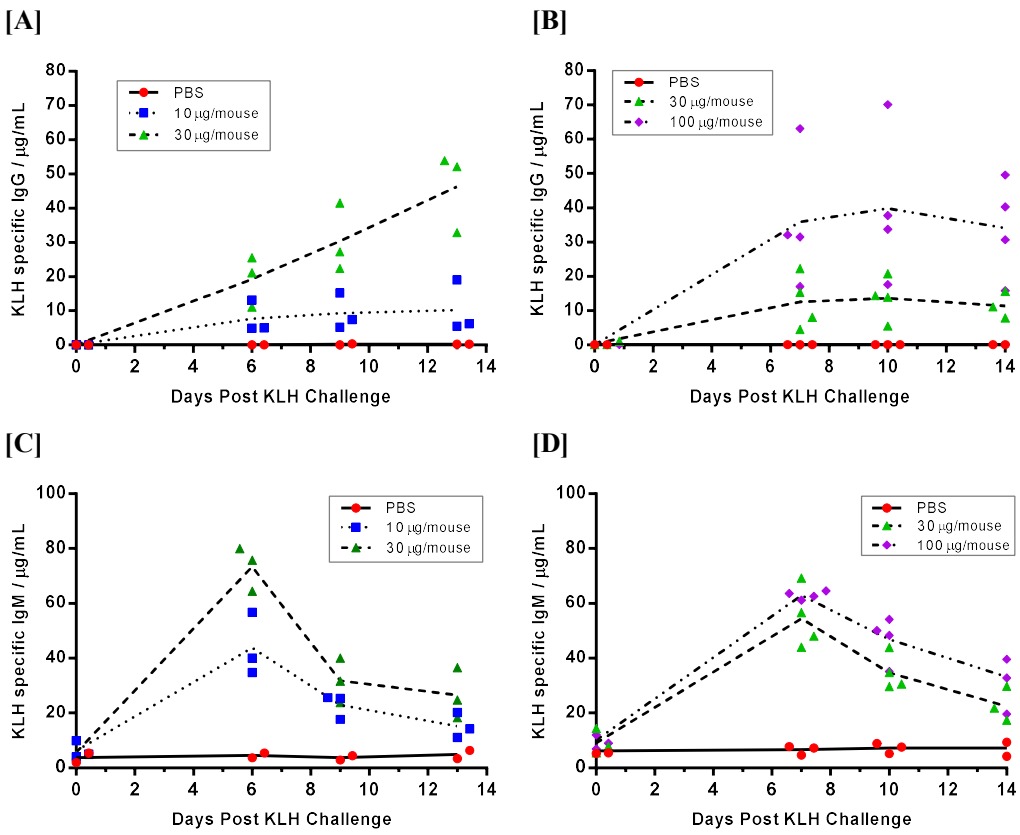

Figure 5.6. KLH specific **[A/B]** IgG and **[C/D]** IgM plasma concentrations in C57BL/6 male mice over the period following IV immunisation with either **[A/C]** PBS, 10 µg or 30 µg KLH per mouse in PKPD study 3 or **[B/D]** PBS, 30 µg or 100 µg KLH per mouse in PKPD study 4. Data illustrated as the individual (symbol) and group mean (dotted line) n=3 (or n=4, 30 and 100 µg).

The plasma concentration of KLH specific IgG and IgM was measured at four time points across the pilot and follow up study (study 3/4), with the resulting plasma profiles shown in figure 5.6. Each of the tested KLH challenge amounts elicited a measurable antigen specific antibody response, that was elevated above baseline, but absent in mice administered PBS alone. A challenge dependent response was demonstrated on each dosing occasion and for both the IgG and IgM endpoints. The KLH specific IgG response window, defined as the difference between the baseline measurement on day 0 and that on day 14, was 52-fold at 10 µg/mouse and 231-fold at 30 µg/mouse in study 3 (figure 5.6A). A lower overall response was observed in study 4, where the response window was 57-fold at 30 µg/mouse and 171-fold at 100 µg/mouse (figure 5.6B). A challenge dependent response window was also observed for the KLH specific IgM antibody response, defined as the difference between the

baseline measurement on day 0 and study day 6 (10/30 µg/mouse) or day 7 (30/100 µg/mouse). This response window was 7-fold at 10 µg/mouse and 13-fold at 30 µg/mouse in study 3 (figure 5.6C), but slightly lower at 6-fold for the 30 µg/mouse and 7-fold for the 100 µg/mouse in study 4 (figure 5.6D). Thus, demonstrating wide inter-study variability in the achieved antibody response on separate dosing occasions. Within a study, the inter-individual variability in the antigen specific antibody response is moderately high, demonstrated by a coefficient of variation (CV%) of 28% and 42% in terminal IgG response at 30 µg and 100 µg KLH challenges respectively (study 4). A lower extent of inter-individual variability is seen for the maximum KLH specific IgM response on day 7, demonstrated by a CV% of 21% and 2% for the 30 µg and 100 µg KLH challenges respectively (study 4).

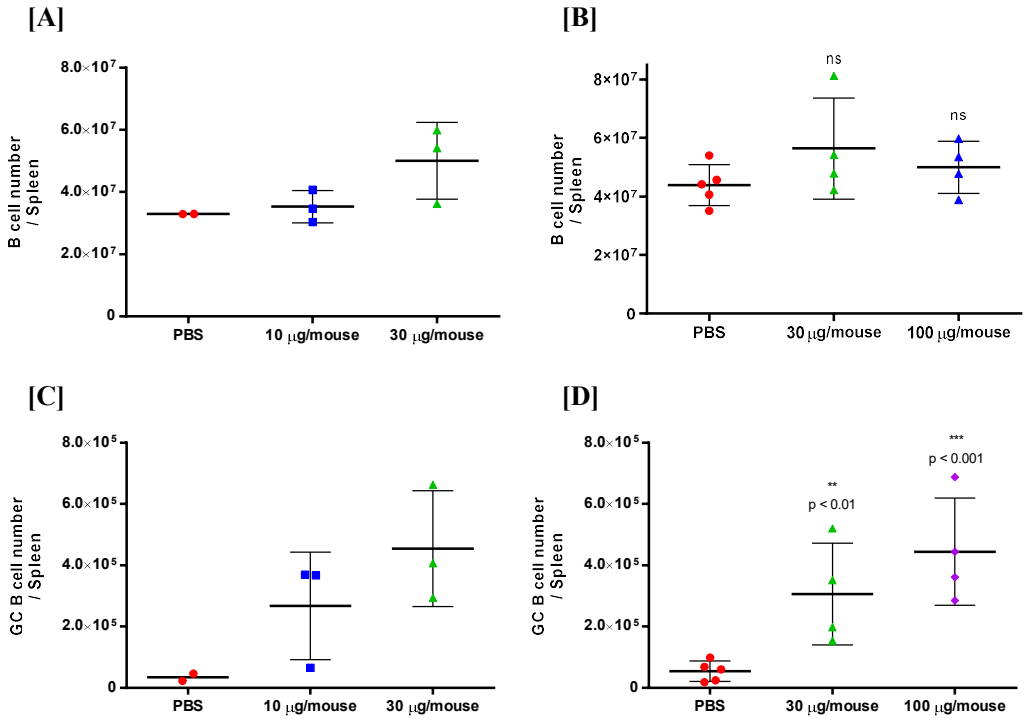

Figure 5.7. Splenic B cell population, **[A/B]** B cell number ($CD45^+$, SSC^{low}, $B220^+$) and **[C/D]** GC B cell number ($CD45^+$, SSC^{low}, $B220^+$, GL7+, PNA+), in the male C57BL/6 mouse on study day 14, following IV challenge on study day 1 with either **[A/C]** PBS, 10 µg or 30 µg KLH per mouse in PKPD study 3 or **[B/D]** PBS, 30 µg or 100 µg KLH per mouse in PKPD study 4. Data illustrated as the individual (symbols) and mean ±SD (line and bar) n=3 (or n=4, 30 and 100 µg), with statistical significance calculated (PKPD study 4) using a one way ANOVA with Dunnett's multiple comparison test, ** p <0.01, *** p<0.001, ns = not significant.

To assess the cellular response to the IV TD KLH challenge, the total number of B cells (figure 5.7A/B) or germinal centre B cells (figure 5.7C/D) per spleen were quantified by flow cytometry. Treatment with KLH did not result in a significant change in the number of B cells per spleen, at any of the KLH challenge amounts tested, when compared with the PBS control (figure 5.7A/B). A KLH challenge dependent increase in the germinal centre B cell number can be observed on each dosing occasion. Resulting in an 8-fold and 13-fold response window at 10 and 30 μg/mouse in study 3 or a 6-fold and 8-fold response window at 30 and 100 μg/mouse in study 4. Insufficient test subjects in study 3 precluded statistical analysis, however in study 4 the challenge induced increase in GC B cells was significant at both tested doses. This provides evidence of a cellular response to the TD challenge and a treatment window to explore in further studies. The successful demonstration of a measurable TD antigen response at both the level of antibody release and instigation of a cellular response, generates confidence that this experimental protocol can be used going forwards.

5.4.3. PKPD study 5: Qualification of the IV KLH TDAR mouse experimental model

In order to evaluate the performance of the reformatted IV KLH TDAR mechanistic experimental model, two clinically validated therapies were tested. The first was the S1P receptor modulator Fingolimod (FTY720). Fingolimod is a clinically validated drug, with known mechanism of action and prior evidence of activity in KLH induced T-dependent immunisation studies, both preclinically (Han *et al.*, 2004) and clinically (Boulton *et al.*, 2012). Thereby, Fingolimod acts not only as an external qualification of the experimental model, but also offers the potential to evaluate its translational value. The second was a surrogate CD20 targeting mAb (SA271G2), selected to mimic Rituximab, a B cell depleting antibody approved for clinical use in haematological cancer and RA.

A small, statistically powered qualification study was performed (PKPD study 5) to confirm the efficacy of Fingolimod and SA271G2. The *in vivo* protocol included several modifications on the initial development studies, to improve data collection and enhance suitability for mathematical modelling. Therefore, this study also acted as an evaluation of the in-life protocol and a test of the overall performance of the experimental model. The study was statistically powered using data collected during the model development studies (PKPD studies 3 and 4), resulting in selection of a group size of n=10. The study protocol included several modifications to facilitate an increase in the number of samples collected to define the drug PK, its pharmacology and the antigen specific antibody response to the KLH challenge.

5.4.3.1. Pharmacokinetics and proof of pharmacology

The in-life phase of PKPD study 5 completed successfully, with no adverse effects to either daily oral administration of Fingolimod or IP administration of SA271G2. Welfare was tracked across the study through daily observations and body weight monitoring. Blood samples were collected at six timepoints across the study, to capture both the PK of each treatment and the resulting impact on the KLH specific antibody response to TD challenge. Fingolimod (FTY720) and Fingolimod Phosphate (FTY720-P) blood concentrations were determined using a specific LC-MS/MS assay, with the resulting data shown in figure 5.8A. SA271G2 plasma concentrations were meanwhile determined using a generic format immunoassay on the Gyrolab platform, with the results shown in figure 5.8B.

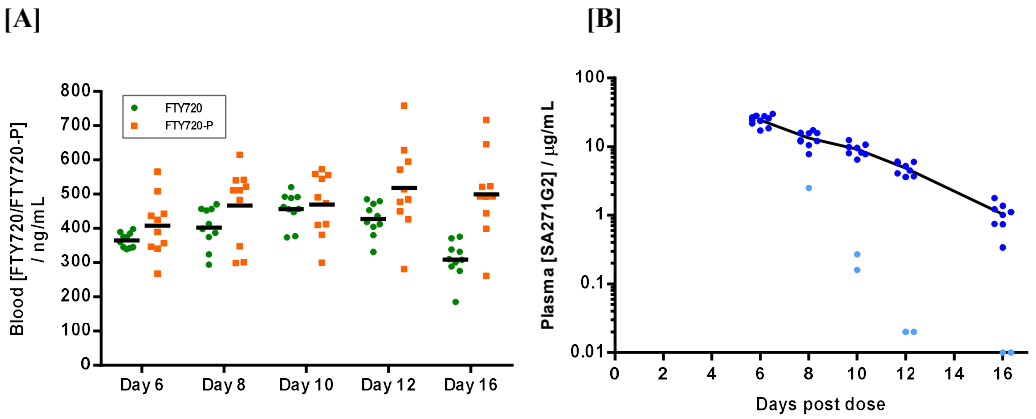

Figure 5.8. Pharmacokinetic exposure data observed in male C57BL/6 mice during the IV KLH TDAR mouse experimental model qualification study (PKPD study 5). **[A]** Fingolimod / FTY720 (green) and Fingolimod phosphate / FTY720-P (orange) blood concentrations at 1 h post dose following daily oral administration at 3 mg/kg. **[B]** SA271G2 (anti-CD20) plasma concentrations following a single IP administration at 10 mg/kg on day 0. Data illustrated as the individual (symbols) and mean (line), n=10, with SA271G2 concentrations in light blue excluded from calculation of the mean.

Following daily oral administration at 3 mg/kg, the Fingolimod blood exposure was consistent across each sampled study day, ranging between 308 ng/mL (day 16) and 457 ng/mL (day 10). Inter-individual variability was low, as described by the CV% ranging between 6 and 18% (figure 5.8A). The active phosphorylated metabolite was detected in blood at marginally higher concentrations than the parent drug, ranging between 408 ng/mL (day 6) and 518 ng/mL (day 12). Inter-individual variability was higher than the parent drug, with a CV% range

between 20 and 25% (figure 5.8A). Meanwhile, a single IP administration of SA271G2 at 10 mg/kg resulted in sustained plasma exposure, as shown in figure 5.8B. In 2 out of 10 treated mice, exposure was not maintained beyond study day 8, with the affected samples excluded from the group mean (highlighted in figure 5.8B). Non-compartmental analysis (NCA) was performed on the terminal phase of the mean plasma concentration versus time profile, resulting in a half-life estimate of 53 h for SA271G2 following IP administration at 10 mg/kg.

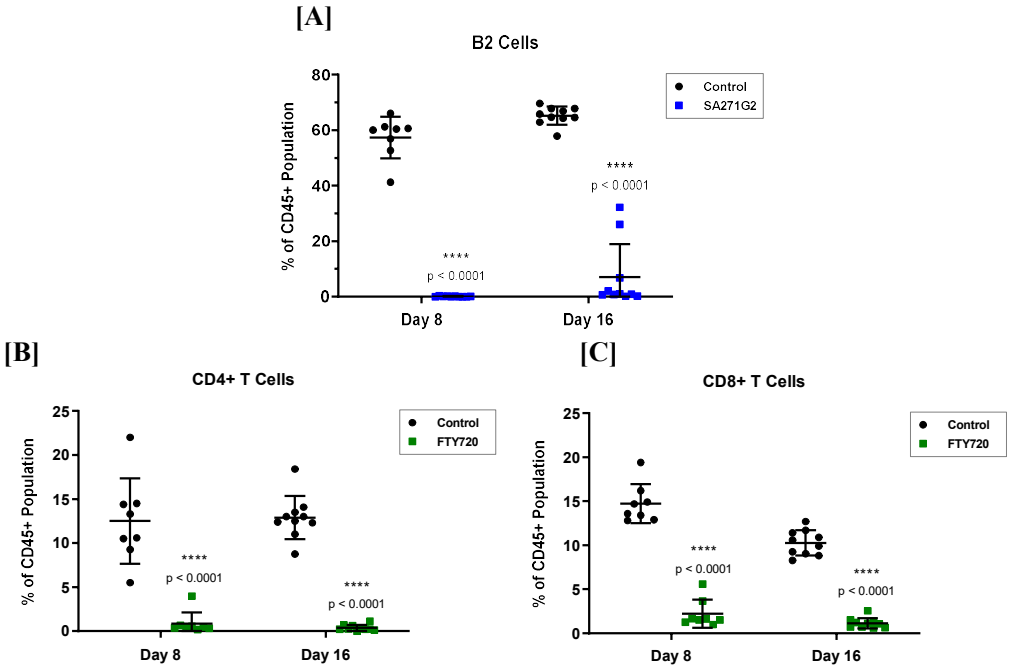

Figure 5.9. Confirmation of Fingolimod and SA271G2 primary pharmacology in PKPD study 5 through assessment of the peripheral lymphocyte population in blood. **[A]** B2 B cells ($CD45^+$, $CD5^-$, $CD19^+$), **[B]** CD4+ T cells ($CD45^+$, $CD3e^+$, $CD4^+$) and **[C]** CD8+ T cells ($CD45^+$, $CD3e^+$, $CD4^+$) as a percentage of the total lymphocyte population ($CD45^+$) in blood, measured on study days 8 and 16. B2 B cell data shown for the group treated with 10 mg/kg SA271G2 IP on day 0, while CD4+ and CD8+ T cell data shown for the group treated with Fingolimod orally QD starting day 0. Data illustrated as individual (symbols) and mean ± SD (line and bar), n=10, with statistical significance calculated using an unpaired t-test versus the control treatment group, **** $p < 0.0001$.

The pharmacological impact of Fingolimod and SA271G2 treatment on the lymphocyte population in blood was evaluated on day 8 and again following termination on day 16. Blood samples taken on these days were analysed by flow cytometry for the CD4+ and CD8+ T cell and B2 B cell population, as a percentage of the total CD45+ lymphocyte population, with the

results shown in figure 5.9. These results show that daily oral administration of Fingolimod at 3 mg/kg results in a 93.1% reduction in CD4+ T cells and a slightly lower 84.9% reduction in CD8+ T cells in blood, when compared to the control. Furthermore, this reduction was mirrored on day 16 (97.1% reduction CD4+, 88.7% reduction in CD8+), indicating maintenance of Fingolimod pharmacology throughout the duration of the 16-day study, in line with the maintained plasma exposure of the active metabolite Fingolimod Phosphate. Treatment with 10 mg/kg SA271G2 IP on day 0 was shown to result in near complete depletion (99.8%) of the B2 B cell population in the blood on study day 8. While the mean extent of B cell depletion had reduced by day 16 (89.1%), this reduced pharmacology was only observed in 3 animals which aligned with the same animals experiencing the lowest plasma exposure of SA271G2 on day 16 (figure 5.8).

5.4.3.2. Pharmacodynamics

The antigen specific antibody response to the TD KLH challenge was monitored in plasma at the same six timepoints previously assayed for plasma PK, providing full coverage of the response profile. The resulting mean concentration-time profiles are shown in figure 5.10, alongside an area under the curve (AUC) analysis of the individual profiles. The mean KLH specific IgG response window, defined as the difference between the baseline measurement on day 0 and that on day 16, was 433-fold in the control treated group (n=10). As a more holistic analysis of the overall antibody response profile, the area under the curve (AUC) of the antigen specific antibody response was determined. This demonstrated a mean KLH specific IgG AUC of 229 μg.day/mL in the control treatment group, with a CV% of 62%. Due to the additional samples collected at earlier timepoints, description of the IgM response profile is better than in the pilot experiments, with the peak KLH specific IgM plasma concentration measured on day 6. This enhances the mean KLH specific IgM response window, with a 67-fold window achieved in the control treatment group between baseline and the peak on day 6. The resulting mean KLH specific IgM AUC was 2283 μg.day/mL, with a CV% of 69%.

Daily oral treatment with Fingolimod at 3 mg/kg resulted in significant ($p < 0.01$) attenuation of the KLH specific IgG response, reducing the mean IgG AUC by 62%, when compared with the control treatment group (figure 5.10). Conversely, the surrogate anti-CD20 mAb SA271G2 resulted in a significant ($p < 0.05$) 68% increase in the mean KLH specific IgG AUC. In contrast to the impact on antigen specific IgG, treatment with Fingolimod resulted in no

inhibition of the antigen specific IgM response, when compared with the control treatment group. Meanwhile, anti-CD20 treatment resulted in significant ($p < 0.01$) inhibition of the antigen specific IgM response, with SA271G2 reducing the mean KLH specific IgM AUC by 83% compared with the control (figure 5.10). Two animals from the SA271G2 group were excluded from this analysis because exposure was not maintained.

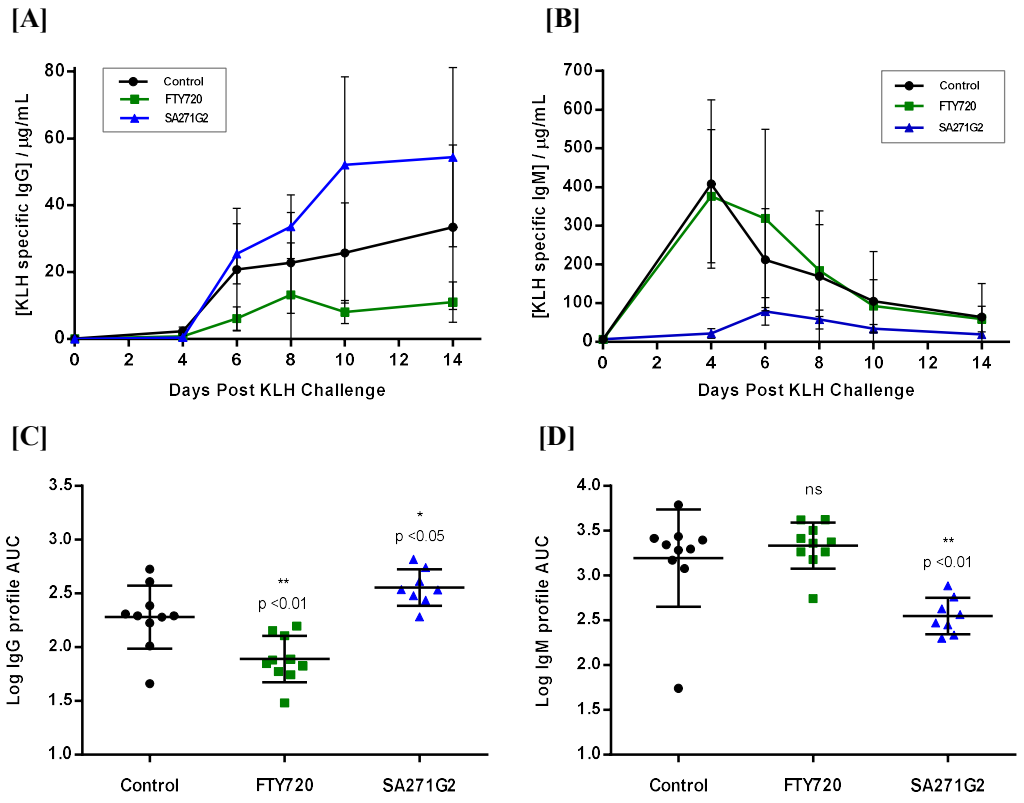

Figure 5.10. KLH specific **[A]** IgG and **[B]** IgM plasma concentrations in male C57BL/6 mice over 14 days following IV KLH immunisation at 1.2 mg/kg on study day 2, when treated orally QD with 3 mg/kg Fingolimod or 1% methylcellulose (control), starting 2 days prior to KLH challenge, or IP one at 10 mg/kg with SA271G2 on study day 0. Data illustrated as the group mean (symbol) ± SD (bar), n=10. The KLH specific antibody data is also presented as the area under the curve (AUC) of the individual **[C]** IgG and **[D]** IgM profiles. Data illustrated as individual (symbols) and mean ± SD (line and bar), n=10, with statistical significance calculated using a one way ANOVA with Dunnett's multiple comparison test, * $p < 0.05$, ** $p < 0.01$, ns = not significant.

The impact of Fingolimod and SA271G2 treatment on the germinal centre B cell response to KLH immunisation was monitored in the spleen following termination on day 16. In addition, certain T and B cell populations were measured in the spleen to evaluate the pharmacology of the two treatments at the site of action. The results of this analysis are illustrated in figure 5.11. This analysis shows that the TD KLH challenge results in a significant increase ($p < 0.0001$) in germinal centre B cell number per spleen, when compared to the naïve untreated control (figure 5.11A) but does not impact the T or B cell populations (figures 5.11B/C/D). This germinal centre response can be attenuated through daily oral treatment with 3 mg/kg Fingolimod, which results in a statistically significant ($p < 0.0001$) 65% reduction in GC B cell number per spleen (figure 5.11A). In line with its primary pharmacology, Fingolimod causes a 32.6% reduction in B cell number per spleen (figure 5.11B) and a 56.9% and 38.7% reduction in CD4+ and CD8+ T cells respectively (figure 5.11C/D). Treatment with 10 mg/kg SA271G2 also significantly ($p < 0.0001$) attenuates the formation of germinal centre B cells in response to KLH TD challenge, with a 68% reduction in the GC B cell number per spleen (figure 5.11A). As would be expected, anti-CD20 treatment results in almost complete depletion (98.4%) of the B cell population within the spleen (figure 5.11B). Interestingly, although anti-CD20 is not thought to directly impact T cells, a significant 71.7% ($p < 0.0001$) increase in the CD8+ T cell number per spleen was observed (figure 5.11D) when compared with the control. Conversely, no impact was observed on the CD4+ T cell population in the spleen following treatment with SA271G2 (figure 5.11C). Two animals from the SA271G2 group were excluded from this analysis because exposure was not maintained.

In summary, Fingolimod was demonstrated to be efficacious in the IV KLH TDAR model at a dose of 3 mg/kg when administered daily by oral gavage. Daily oral dosing maintained systemic exposure of both Fingolimod and its active metabolite Fingolimod phosphate, resulting in the expected impact on both peripheral and splenic T and B cell populations. This pharmacology resulted in a 62% inhibition of the antigen specific IgG response and 65% inhibition of the GC B cell response to the IV KLH challenge. Despite conversely demonstrating no impact on the antigen specific IgM response, 3 mg/kg Fingolimod represents a valuable model positive control to take forward into further studies. Treatment with the surrogate anti-CD20 mAb SA271G2 also demonstrated efficacy when administered IP prophylactically at 10 mg/kg. This provided sustained systemic exposure in 8 out of 10 animals, resulting in near complete depletion of both peripheral and splenic B cells. Similar efficacy (68%) was seen to Fingolimod on inhibition of the GC B cell response to KLH TD challenge. In contrast, SA271G2 treatment resulted in a 68% exacerbation of the KLH specific IgG response, while showing an 83% inhibition of the KLH specific IgM response.

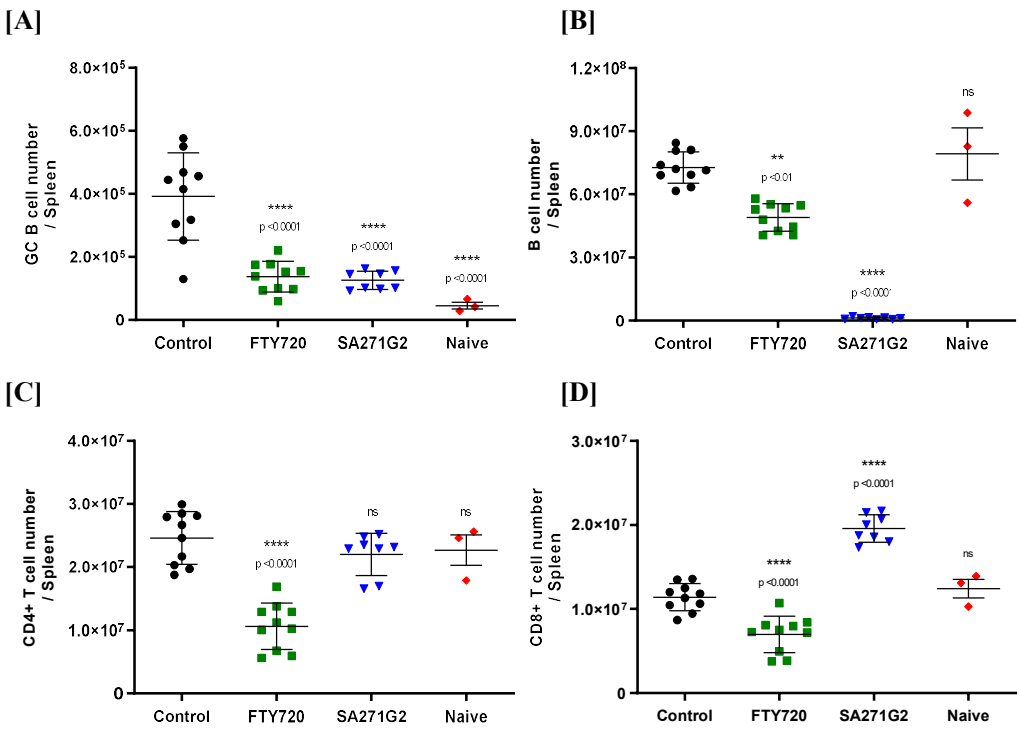

Figure 5.11. Splenic lymphocyte population, **[A]** GC B cell number ($CD19^+$, $CD3e^-$, $GL7^+$, FAS^+), **[B]** B cell number ($CD19^+$, $CD3e^-$), **[C]** CD4+ T cell number ($CD19^-$, $CD3e^+$, $CD4^+$) and **[D]** CD8+ T cell number ($CD19^-$, $CD3e^+$, $CD8^+$) in the male C57BL/6 mouse on study day 16, following IV KLH immunisation on study day 2, in naïve mice or those treated orally QD with 3 mg/kg Fingolimod or 1% methylcellulose (control), or IP once at 10 mg/kg with SA271G2 on day 0. Data illustrated as the individual (symbols) and mean ±SD (line and bar) n=10 (naïve, n=3), with statistical significance calculated using a one way ANOVA with Dunnett's multiple comparison test, ** p <0.01, **** p<0.0001, ns = not significant.

5.4.4. PKPD study 6: Concentration-effect profiling of Fingolimod in the IV KLH TDAR mouse experimental model

To extend the Fingolimod data set beyond simple confirmation of efficacy, toward a concentration effect relationship, a further experiment (study 6) was performed. The study protocol utilised an unconventional design in place of the typical, statistically powered format that investigates only a handful of treatments with a high subject number. Instead, the design used low subject numbers per treatment, but across many treatment groups which cover the expected dose response window. A detailed description of the protocol is included in chapter 2

section 2.3.7. The objective of study 6 was to generate concentration effect data that could be fitted using a mathematical model to estimate an *in vivo* EC_{50}. An initial, rudimentary non-linear regression approach is reported in this chapter, fitting the individual biological response against the average plasma concentration data generated in this study. A more elaborate mathematical PKPD approach with potential for cross species translation was then pursued, as described in chapter 6.

5.4.4.1. Fingolimod pharmacokinetics

Whole blood samples collected across the study were split into two separate samples; a blood:water sample for quantification of Fingolimod and Fingolimod phosphate by LC-MS/MS and a plasma sample for quantification of antigen specific antibodies by ELISA. Additional blood samples were collected at 4, 8, 12 and 24 h post drug administration on study day 10 to generate an intraday pharmacokinetic profile for both Fingolimod and its active metabolite Fingolimod phosphate. The Fingolimod and Fingolimod phosphate blood concentration on each sampling day are shown in figure 5.12, with the intraday pharmacokinetic profile shown in figure 5.13.

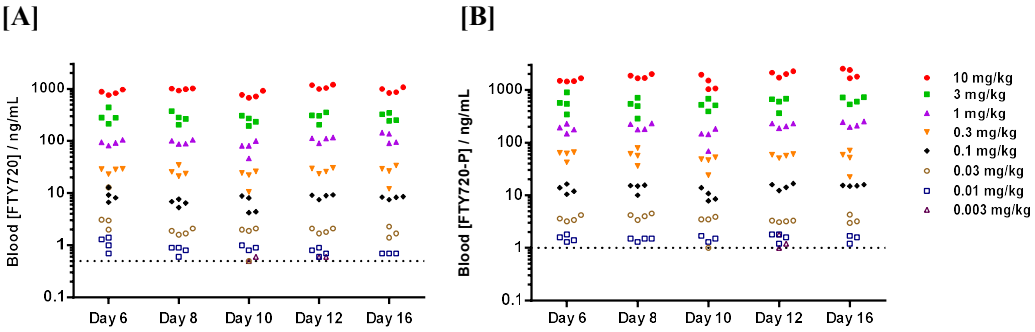

Figure 5.12. Pharmacokinetic exposure data observed following daily oral administration of Fingolimod to the male C57BL/6 mouse at doses of 0.003, 0.01, 0.03, 0.1, 0.3, 1, 3 and 10 mg/kg in the IV KLH TDAR experimental model (PKPD study 6). The blood concentration of **[A]** Fingolimod (FTY720) and **[B]** Fingolimod phosphate (FTY720-P) were measured on day 6, 8, 10, 12 and 16 at 1 h post oral dose, with the assay LLQ of 0.5 ng/mL (Fingolimod) and 1 ng/mL (Fingolimod phosphate) marked with a dotted line. Data illustrated as individual measurements (symbols), with n=4 / treatment.

Following daily oral administration at 3 mg/kg, the mean Fingolimod blood concentration ranged between 252 ng/mL (day 8) and 305 ng/mL (day 6), showing remarkable consistency across each sampled study day (figure 5.12A). Inter-individual variability (n=4) was moderate, described by a CV% range between 18 and 32%. The Fingolimod blood exposure range observed in this study aligns with that seen previously at the same dose level in study 5 (308 to 457 ng/mL). The corresponding mean blood exposure of the active metabolite Fingolimod phosphate ranged between 509 ng/mL (day 8) and 649 ng/mL (day 16), with moderate inter-individual variability shown by a CV% range between 15% and 39% (figure 5.12B). The blood exposure of both Fingolimod and Fingolimod phosphate was shown to be dose proportional across the 1000-fold measurable dose range (0.01 to 10 mg/kg). The lowest Fingolimod dose of 0.003 mg/kg resulted in the majority of samples measuring below the assay cut-off, with an LLQ of 0.5 and 1 ng/mL for Fingolimod and Fingolimod phosphate respectively.

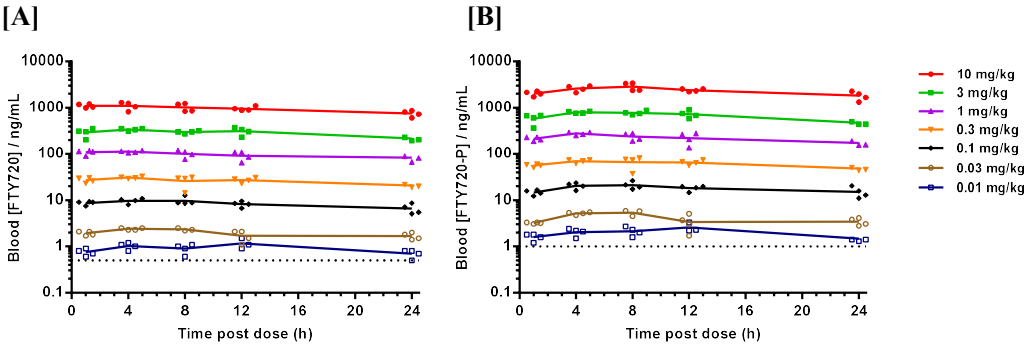

Figure 5.13. Pharmacokinetic exposure profile collected on study day 12 of the IV KLH TDAR experimental model (PKPD study 6) following daily oral administration of Fingolimod to the male C57BL/6 mouse at doses of 0.003, 0.01, 0.03, 0.1, 0.3, 1, 3 and 10 mg/kg. The blood concentration of **[A]** Fingolimod (FTY720) and **[B]** Fingolimod phosphate (FTY720-P) were measured at 1, 4, 8, 12 and 24 h post oral dose, with the assay LLQ of 0.5 ng/mL (Fingolimod) and 1 ng/mL (Fingolimod phosphate) marked with a dotted line. Data illustrated as individual measurements (symbols) and the group mean (line), with n=4 / treatment.

The intraday exposure of Fingolimod (figure 5.13A) and its active phosphorylated metabolite, Fingolimod phosphate (figure 5.13B) was shown to be remarkably prolonged, with little deviation in blood concentration across the measured 24 h period following oral administration. Indeed, the intra-day pharmacokinetics of both Fingolimod and Fingolimod phosphate show exceptional dose linearity, as previously observed between study days (figure 5.12A/B). The observed T_{max} was between 1 and 4 h for Fingolimod, with a slightly

later T_{max} for Fingolimod phosphate of between 4 and 8 h. The prolonged nature of drug exposure following oral administration makes the average blood concentration (C_{av}) a very useful measurement for rudimentary comparison of PK and PD, with the determined C_{av} values at each dose level shown in table 5.2. The C_{av} of the active moiety Fingolimod phosphate is 2.1 to 2.5-fold higher in blood than that of the parent drug Fingolimod (table 5.2).

5.4.4.2. Pharmacodynamics

The primary antigen specific IgG and IgM response to the IV KLH TD challenge was shown to be similar to that observed in previous studies, with the resulting mean concentration time profiles shown in figure 5.14. The mean KLH specific IgG response window, defined as the difference between the baseline day 0 measurement and that on day 16, was 564-fold in the control treatment group (n=8), with a mean KLH specific IgG AUC of 268 µg.day/mL and CV% of 38%. As observed in previous studies, the mean KLH specific IgM response window was smaller, achieving a 28-fold window in the control treatment group (n=8), with a mean KLH specific IgM AUC of 1246 µg.day/mL and CV% of 25%.

Daily oral treatment with Fingolimod showed dose dependent inhibition of both the antigen specific IgG and IgM responses to the IV KLH TD challenge (figure 5.14 and table 5.2). Maximum inhibition was achieved at 10 mg/kg, reducing both the mean KLH specific IgG AUC by 74% and the mean KLH specific IgM AUC by 79%, when compared with the vehicle control. Daily oral treatment with 3 mg/kg Fingolimod once again demonstrated a mean 60% inhibition of the KLH specific IgG AUC, however conversely to study 5 (3.3), showed a mean 51% inhibition of the KLH specific IgM AUC. Despite the small number of animals in each study group, a statistically significant inhibition of the antigen specific IgG and IgM response can be observed at the highest tested Fingolimod doses, in comparison with the control.

The concentration effect relationship of Fingolimod treatment on the germinal centre B cell response to KLH immunisation was monitored in the spleen following termination on day 16. In addition, certain T and B cell populations were also measured in the spleen to evaluate the primary pharmacology following Fingolimod treatment across the tested dose range (figure 5.15). This analysis indicates that Fingolimod exercises full effect against both CD4+ and CD8+ T cell populations in the spleen at doses of 0.03 mg/kg and above, with no impact observed at the lower 0.01 or 0.003 mg/kg doses (figure 5.15C/D). The effect of Fingolimod on T cells manifests as an all or nothing response, with no obvious dose dependent

responsiveness. A similar pattern of effect is seen on the total B cell number per spleen, with maximum effect again observed at doses of 0.03 mg/kg and above, with little observed dose dependency in the magnitude of response (figure 5.15B).

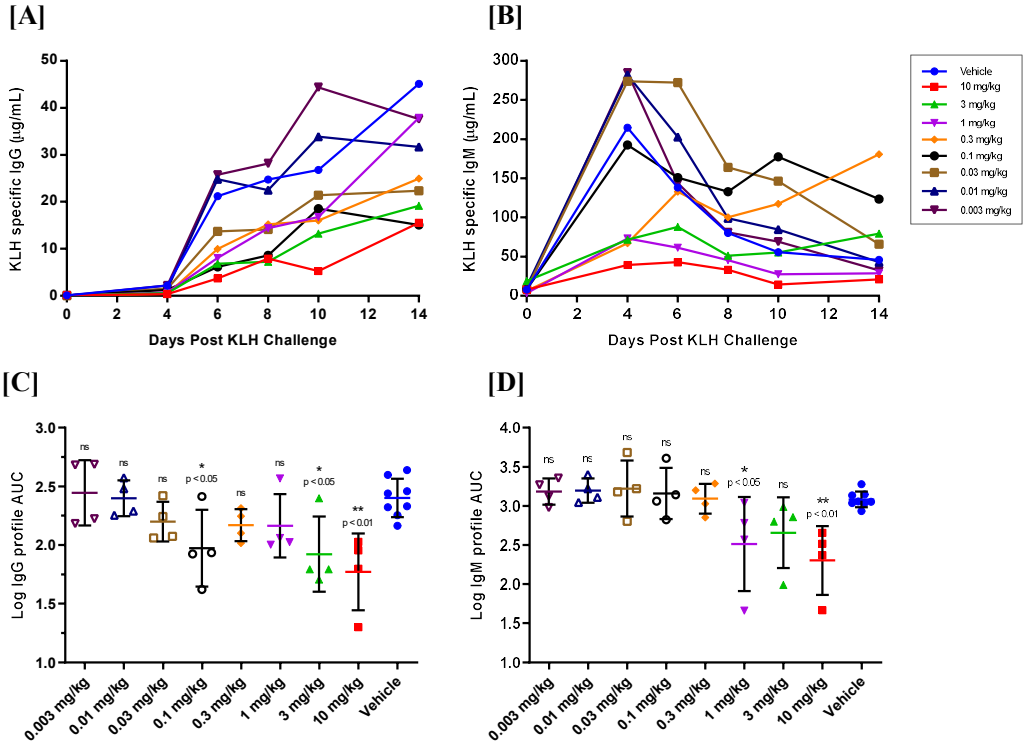

Figure 5.14. KLH specific **[A]** IgG and **[B]** IgM plasma concentrations in male C57BL/6 mice over 14 days following IV KLH immunisation at 1.2 mg/kg on study day 2, when treated orally QD with 1% methylcellulose (control) or Fingolimod across the range 0.003 to 10 mg/kg. Data illustrated as the group mean (symbol), n=4/treatment (control, n=8). The KLH specific antibody data is also presented as the area under the curve (AUC) of the individual **[C]** IgG and **[D]** IgM profiles. Data illustrated as individual (symbols) and mean ± SD (line and bar), n=4/treatment (control, n=8), with statistical significance calculated using a one way ANOVA with Dunnett's multiple comparison test, * p <0.05, ** p<0.01, ns = not significant.

Following TD KLH challenge, the total B cell number per spleen did not significantly change, but a 6-fold increase in germinal centre B cells per spleen was observed, compared with the naïve control (figure 5.15A). Interestingly, a trend toward fewer CD4+ and CD8+ T cells was also observed in the TD challenged mice, although the sample size (n=3) for the naïve treatment group was low (figure 5.15C/D). Converse to the impact of Fingolimod treatment

on total T and B cell numbers, its impact on the germinal centre B cell response showed clear dose responsiveness. Fingolimod concentration dependent inhibition of the GC B cell response can be observed, with maximum inhibition achieved at 10 mg/kg returning the germinal centre B cell population to naïve levels (figure 5.15A).

5.4.4.1. PKPD interpretation

A Fingolimod concentration effect relationship has been demonstrated against both the germinal centre B cell (figure 5.15A) and antigen specific antibody response (figure 5.14A/B) to KLH TD challenge. To coalesce this relationship into a single term of comparative value, the concentration effect data sets were modelled using a non-linear regression fit, as a rudimentary approach to estimate an *in vivo* EC_{50}. This analysis was completed for the AUC of the KLH specific IgG and IgM response profiles and the absolute germinal centre B cell numbers per spleen, using the corresponding Fingolimod blood C_{av} estimated from the day 10 PK profile. Here a four-parameter logistic curve with variable slope, of the form Y = bottom + (top-bottom) / (1+10^((logEC50-X)*Hillslope)), was fitted to the individual observed data. The vehicle treated control group observations were added to anchor the top of the curve with an arbitrary low Fingolimod concentration value. Additionally, the naïve values were added to anchor the bottom of the curve in the germinal centre data set with an arbitrary high Fingolimod concentration value. These groups define the baseline normal KLH induced response and the maximum achievable inhibition of this response, respectively.

Table 5.2. Summary table of the key results from PKPD study 6. Fingolimod and Fingolimod phosphate blood exposure expressed as the mean (±SD) C_{av} following daily oral treatment across the range 0.003 to 10 mg/kg, listed alongside the accompanying mean (±SD) KLH specific IgG and IgM responses (peak and $AUC_{2\text{-}16}$) and the mean (±SD) germinal centre B cell number per spleen. The effect of each treatment on the TD antibody response can be calculated compared with the control treatment group. BLQ: below limit of quantification, n/a: not applicable.

Treatment Group	**KLH specific IgG day 16 peak concentration Mean (±SD) (µg/mL)**	**KLH specific IgG $AUC_{day\ 2–16}$ (±SD) (µg.day/mL)**	**KLH specific IgM day 6 peak concentration Mean (±SD) (µg/mL)**	**KLH specific IgM $AUC_{day\ 2–16}$ (±SD) (µg.day/mL)**	**Mean (±SD) germinal centre B cell number / spleen**	**Fingolimod blood C_{av} (±SD) (nM)**	**Fingolimod phosphate blood C_{av} (±SD) (nM)**
Control	45.1 (26.3)	268 (103)	214.6 (49.2)	1246 (311)	6.6E5 (1.9E5)	n/a	n/a
10 mg/kg	15.6 (9.6)	70 (38)	39.4 (30.7)	266 (172)	9.8E4 (5.7E4)	3085 (421)	6041 (707)
3 mg/kg	19.2 (19.8)	107 (96)	71.7 (40.8)	605 (369)	1.8E5 (1.0E5)	936 (96)	1733 (141)
1 mg/kg	37.9 (36.4)	173 (132)	73.5 (78.7)	531 (442)	2.4E5 (2.3E5)	311 (43)	567 (91)
0.3 mg/kg	24.9 (6.7)	153 (47)	67.2 (58.2)	1327 (538)	3.5E5 (1.6E5)	85 (3)	159 (5)
0.1 mg/kg	15.1 (9.7)	118 (97)	192.7 (54.9)	1824 (1532)	2.3E5 (1.3E5)	27 (4)	47 (8)
0.03 mg/kg	22.3 (8.7)	168 (70)	273.8 (207.1)	2164 (1831)	6.4E5 (2.1E5)	6 (0.5)	10 (1)
0.01 mg/kg	31.7 (15.0)	263 (92)	282.0 (141.7)	1649 (627)	6.5E5 (3.1E5)	3 (0.7)	5 (1)
0.003 mg/kg	37.6 (23.2)	323 (187)	285.2 (158.9)	1609 (585)	4.7E5 (5.4E4)	BLQ	BLQ

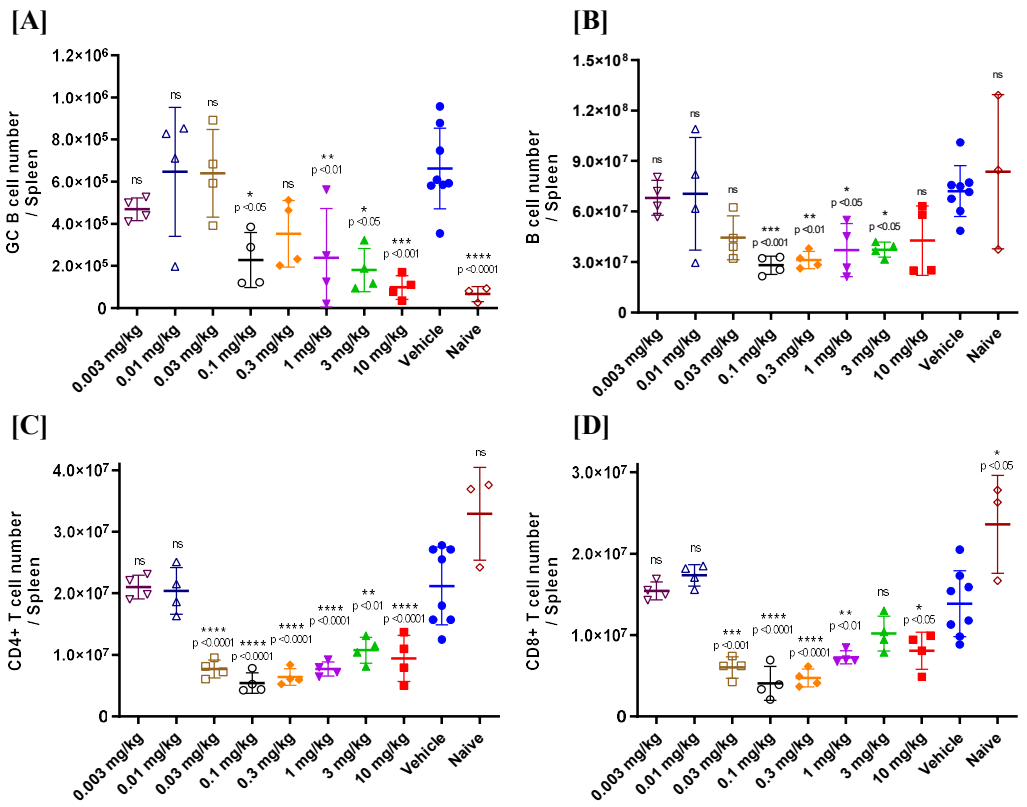

Figure 5.15. Splenic lymphocyte populations, **[A]** GC B cell number ($CD19^+$, $CD3e^-$ $GL7^+$, FAS^+), **[B]** B cell number ($CD19^+$, $CD3e^-$), **[C]** CD4+ T cell number ($CD3e^-$, $CD4^+$) and **[D]** CD8+ T cell number ($CD3e^-$, $CD8^+$) in the male C57BL/6 mouse on study day 16, following IV KLH immunisation on study day 2, in naïve mice or those treated orally QD with either 1% methylcellulose (control) or Fingolimod across the range 0.003 to 10 mg/kg. Data illustrated as the individual (symbols) and mean ± SD (line and bar) n=4/treatment (control n=8, naïve n=3) with statistical significance calculated using a one way ANOVA with Dunnett's multiple comparison test, * p <0.05, ** p<0.01, *** p <0.001, **** p<0.0001, ns = not significant.

Non-linear regression analysis was completed on each concentration effect data set with the resulting curve fit shown for KLH specific IgG (figure 5.16A), IgM (figure 5.16B) and germinal centre B cell number per spleen (figure 5.16C) endpoints. Strikingly analogous *in vivo* EC_{50} estimates were gained for the antigen specific IgG response (16.5 nM) and the germinal centre B cell response (46.0 nM). A slightly higher *in vivo* EC_{50} value was calculated against the antigen specific IgM response of 150.7 nM. Interestingly, the analysis also produced similar (1-(bottom/top)*100) maximum effect estimates of 76%, 77% and 89% for the IgG, IgM and GC B cell endpoints respectively.

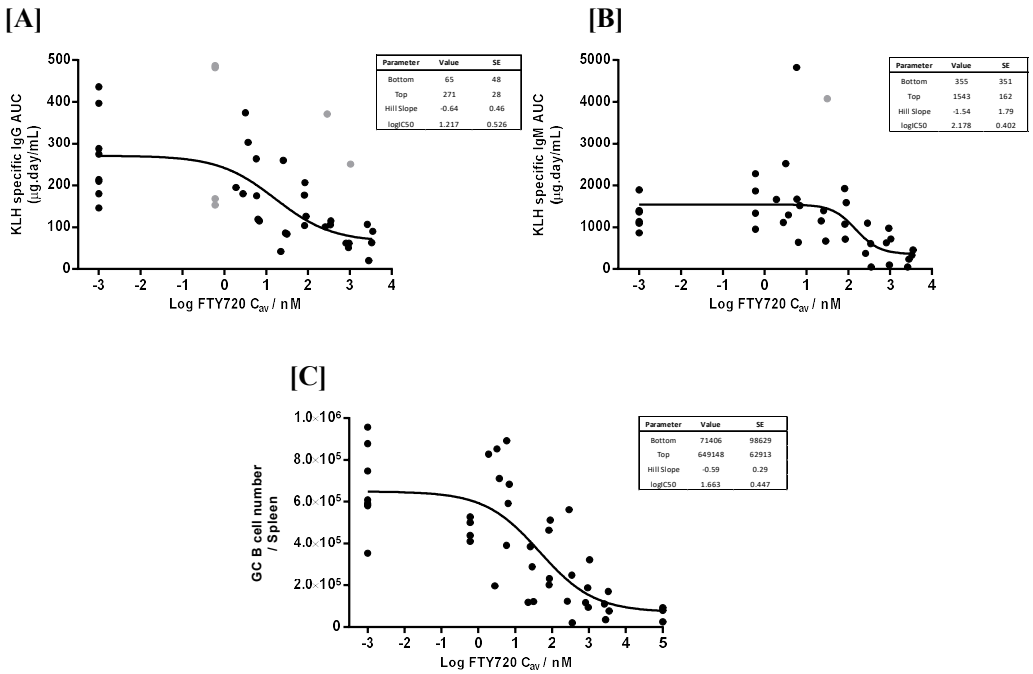

Figure 5.16. Non-linear regression fit of the KLH specific **[A]** IgG response, **[B]** IgM response or **[C]** the germinal centre B cell number against the Fingolimod C_{av}. Data illustrated as individual observations (solid black symbols), with grey symbols representing observations that were excluded from the four-parameter logistic fit curve with variable slope (line). EC_{50} and maximum effect estimates were gained from the curve.

5.4.5. PKPD study 7: Surrogate CD21 specific mAb 7G6 concentration-effect profiling in the IV KLH TDAR mouse experimental model

To explore the therapeutic potential of CD21 neutralisation, the concentration effect relationship of the surrogate mAb 7G6 was explored in the reformatted adjuvant free IV KLH TDAR mouse experimental model. Despite limitation due to the immunogenicity of the rat IgG2b backbone, 7G6 represents the best characterised and highest affinity murine CD21 specific mAb (K_d 0.05 nM – Appendix V), making this the most suitable tool for concentration effect profiling. The objective of the study was to test several distinct concentrations of 7G6, to facilitate interpretation of the extent of drug exposure and target engagement required for efficacy. Whilst typical mAb pharmacokinetics are amenable to achieving this extended plasma exposure, mAb 7G6 suffers the impact of TMDD and resulting accelerated clearance at doses below 2 mg/kg (PK characterisation, chapter 3). Consequently, to achieve

maintenance of low 7G6 plasma exposure, mathematical simulations identified repeated administration every 96 h as the optimal dosing approach (PK model v2, chapter 4). To ensure near maximal distribution of the mAb, a pre-treatment period of 2 days was included in the study design prior to immunisation. A 7G6 dose range between 0.01 and 10 mg/kg was tested, at seven half log unit separations (n=4). A rat IgG2b isotype control mAb of irrelevant binding acted as the study control, administered at 10 mg/kg (n=8). Additional control groups included a Fingolimod positive control at 3 mg/kg (n=4), a PBS only negative control (n=4) and an untreated naïve control (n=3).

5.4.5.1. Dose concentration analysis

Due to concern about the stability and accuracy of the very low mAb 7G6 dose concentrations required in the study, a dose preparation and stability test was performed prior to the start of the study. This involved preparation and storage of mock 7G6 dose solutions, in the lower concentration range, to mimic the process followed on each study dosing day. The results of this analysis are shown in table 5.3. At the 1 mg/kg dose (0.1 mg/mL dose solution concentration), following preparation and storage at 4°C for a period of 2 h, the dose solution was found to be within 1% of the nominal concentration. However, as dose solution concentration reduced, accuracy similarly declined. At the 0.3 and 0.1 mg/kg dose levels (0.03 and 0.01 mg/mL), the accuracy of the dose solution reduced to 70% of the nominal concentration. This reduced further to only 25% of the nominal concentration at the 0.03 and 0.01 mg/kg dose levels (0.003 and 0.001 mg/mL). To account for these differences and because dose solution analysis was unable to be performed during the study, further data interpretation was completed with the doses adjusted according to the values in table 5.3.

Table 5.3. Dose preparation and stability test for mAb 7G6, performed pre-study to mimic the procedure and storage conditions (4°C for 2 h) experienced on each study dosing day. Low concentration dose solutions in the range 0.1 to 0.001 mg/mL (1 to 0.01 mg/kg) were tested.

Nominal 7G6 dose solution concentration (mg/mL)	Measured 7G6 concentration (mg/mL)	Percentage of nominal concentration (%)
0.1	0.1007	1
0.03	0.0213	-29
0.01	0.0071	-29
0.003	0.0007	-77
0.001	0.0003	-74

5.4.5.2. Pharmacokinetics and target engagement

The exposure and pharmacokinetics of both mAb 7G6 and the positive control Fingolimod were monitored across the study period. Fingolimod and Fingolimod phosphate concentrations were measured directly from the plasma by LC-MS/MS, then subsequently converted to blood concentrations using *in vitro* determined blood:plasma ratios of 3.15 and 1.25 respectively (Appendix IX), with the data shown in figure 5.17. The mean converted Fingolimod blood concentration range was between 247 ng/mL (day 10) and 337 ng/mL (day 12) with a CV% range between 7% and 26%, comparing well with previous studies. The resulting Fingolimod phosphate concentration range was between 125 ng/mL (day 12) and 332 ng/mL (day 8) with a CV% range of between 9% and 44%. A drawback of collecting plasma for analysis of Fingolimod is the reduced sample stability compared with blood:water. This issue is highlighted by the slighly lower and more variable Fingolimod phosphate concentration compared to previous studies and the apparent change in Fingolimod phosphate to Fingolimod ratio on day 12 and 16.

The measured plasma concentration of mAb 7G6, at each tested dose level is illustrated in figure 5.18, overlain with the PK model simulated plasma exposure used to design the dosing regimen. Administration of mAb 7G6 at 10 mg/kg resulted in a plasma exposure profile that was in line with this pre-study prediction at all tested time points. However, the quality of the prediction degrades both with decreasing dose and with increasing dosing duration. So, whilst for higher doses at early time points the prediction remains close to the observed plasma concentration, it decreases in quality considerably as the study progresses. This leads to a very poor prediction of the terminal plasma concentration at all but the 10 mg/kg dose, with most samples measured below the assay LLQ. The quality of the prediction also degrades with decreasing dose, fitting poorly at doses of 0.1 mg/kg and below. All samples in the 0.01 mg/kg group were below the limit of quantification, with only the samples taken 1 h post dose on days 8 and 12 resulting in a measurable concentration in the 0.03 mg/kg group. Performance of the immunoassay was in line with acceptance criteria, reporting an assay cut-off of 20 ng/mL (0.13 nM). The day 10 7G6 plasma concentration provides an approximate estimate of the average plasma concentration (C_{av}) achieved in each treatment group across the study duration, falling at 2 days post dose on the third dosing occasion.

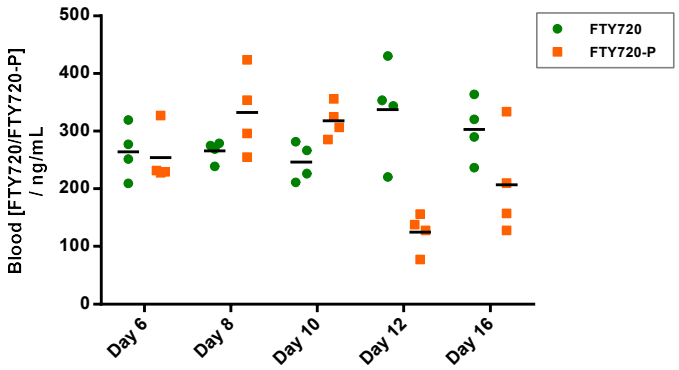

Figure 5.17. Fingolimod exposure following daily oral administration at 3 mg/kg to male C57BL/6 mice as the model positive control during the IV KLH TDAR experimental model (PKPD study 7). Plasma concentrations of Fingolimod (FTY720) and Fingolimod phosphate (FTY720-P) were collected 1 h post dose on study days 6, 8, 10, 12 and 16 and converted to a blood concentration based on a blood:plasma ratio of 3.15 and 1.25 respectively. Data illustrated as the individual (symbols) and mean (line), n=4.

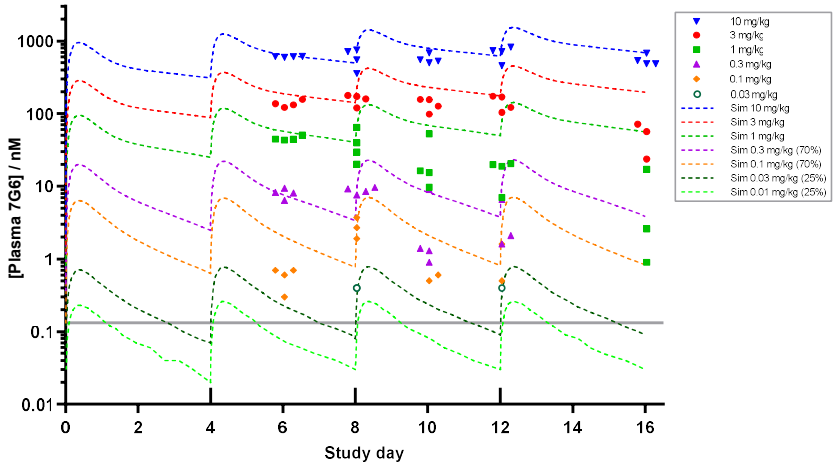

Figure 5.18. Plasma concentration of mAb 7G6 on study days 6, 8, 10, 12 and 16, when administered IP every 96 h at 0.01, 0.03, 0.1, 0.3, 1, 3 and 10 mg/kg to the male C57BL/6 mouse, starting 2 days prior to IV KLH challenge at 2.4 mg/kg. The assay LLQ was 0.13 nM and is depicted with a solid grey line. Data illustrated as the individual (symbol) staggered for clarity (n=4), overlain with the pre-study simulation (dashed line) with dose adjustment for inaccurate preparation below 0.3 mg/kg.

To investigate the unpredicted loss of mAb 7G6 plasma exposure in the terminal sample of many animals, particularly in the mid-range doses, the samples were assayed for the presence of anti-drug antibodies against the rat IgG2b mAb 7G6. To ascertain whether a sample was ADA positive, a signal in excess of the assay cut off must be achieved. This cut-off was defined as double the mean baseline response on day 0, resulting in an assay electrochemiluminescence (ECL) cut-off value of 136. The results are shown in figure 5.19, clearly demonstrating the propagation of an anti-drug antibody response to mAb 7G6, particularly affecting the mid-range doses (0.1 to 3 mg/kg). 15/28 animals (54%) treated with mAb 7G6 are identified as ADA positive on day 16. This ADA response takes time to propagate, in line with the impact observed on the 7G6 plasma exposure in figure 5.18. A lower incidence of ADA positive samples was observed on day 12, with 5/28 (18%) animals treated with 7G6 identified as positive. Only 2/28 (7%) 7G6 treated animals were identified as positive on day 10. There was insufficient sample volume to complete ADA analysis in a small number of cases on days 10 (5 samples) and 12 (11 samples), with minimal impact on study outcome.

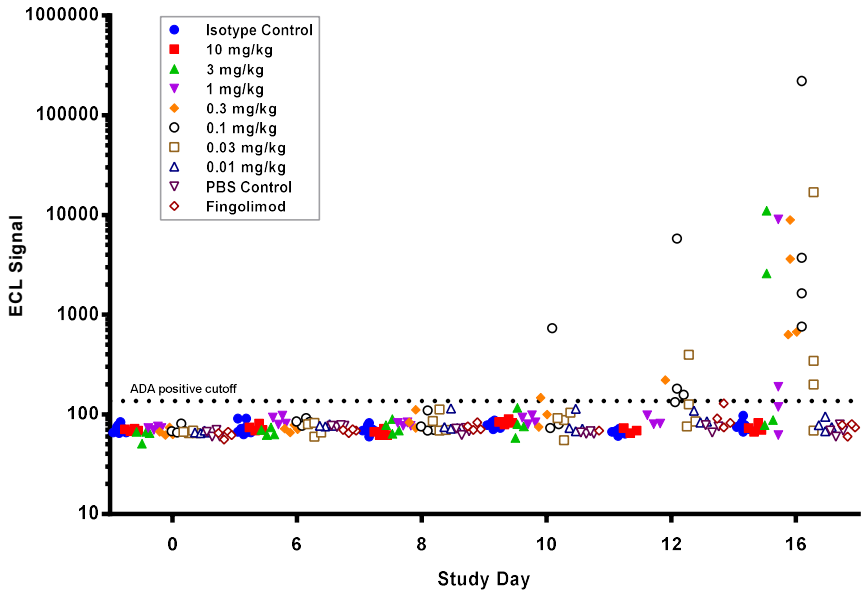

Figure 5.19. Anti-drug antibody (ADA) qualitative results, identifying ADA positive plasma samples as those above the 2x baseline cut-off (dashed line). Plasma samples were collected on study day 6, 8, 10, 12 and 16 following administration of either mAb 7G6 IP every 96 h at 0.01, 0.03, 0.1, 0.3, 1, 3 and 10 mg/kg, isotype control IP every 96 h at 10 mg/kg, PBS control IP every 96 h or 3 mg/kg Fingolimod PO daily to the male C57BL/6 mouse, starting 2 days prior to IV KLH challenge at 2.4 mg/kg. Data illustrated as the individual value (symbol) staggered for clarity, n=4 (isotype control n=8).

To directly quantify the extent of target engagement resulting from mAb 7G6 plasma exposure, the expression of CD21/35 on the surface of peripheral B cells was measured by flow cytometry from blood samples collected on day 6 and again following termination on day 16. The objective was to provide supportive data for mathematical PKPD model progression. Quantibrite bead technology (BD Biosciences) was employed to provide quantitative data, resulting in enumeration of the mean CD21/35 receptor number per B cell. The technique results in measurement of the number of antibodies bound per cell (figure 5.20) which, due to the 1:1 binding stoichiometry of 7G6 on CD21/35, can be interpreted as the number of unbound receptors per cell. The data shown in figure 5.20A/B demonstrates that mAb 7G6 treatment resulted in a reduction in the mean number of CD21/35 receptors present per B cell on day 6 (48 h post dose) at all tested dose levels. Maximum effect on CD21/35 expression (>99% reduction) was observed at doses of 0.3 mg/kg and above, with a dose dependent decrease in effect seen at lower doses. Interestingly, treatment with Fingolimod also results in a reduction in the mean number of CD21/35 receptors per peripheral B cell. The measured mean CD21/35 receptor number on untreated peripheral B cells (day 6) was identified as 4119 receptors / B cell, in the isotype control treated group. In keeping with data generated in study 1, the impact of target engagement with 7G6 was the loss of CD21/35 from the B cell surface, as indicated by the reduction in non-competitive 7E9 MFI signal.

On study day 16 (96 h post dose), the impact of 7G6 treatment on peripheral B cell CD21/35 surface expression was reduced (figure 5.20C/D). Maximum reduction is only observed following treatment at 10 mg/kg at this time point, with no effect observed with doses of 0.1 mg/kg and below. The pattern of loss of treatment impact correlates with the loss of 7G6 plasma exposure at this time point. This exposure loss was previously identified as resulting either through clearance at this later time point (96 h post dose) in the lower dose groups, or as a result of the propagation of an ADA response to 7G6. The measured mean CD21/35 receptor number on untreated peripheral B cells at this later time point (day 16), was in keeping with that measured on day 6 with 4389 receptors / B cell measured in the isotype control treated group (vs 4119 receptors / B cell, on day 6).

The impact of 7G6 treatment on splenic B cell CD21/35 surface expression, measured on study day 16, is an almost mirror image of the effect on peripheral B cells (figure 5.20E/F). Again, maximum reduction was only observed at the 10 mg/kg treatment level, with no effect seen at doses of 0.1 mg/kg and below. The remaining pattern of target engagement mirrors that observed on peripheral B cells, demonstrating a strong correlation between these two measurements. The measured mean CD21/35 receptor number per splenic B cell is however

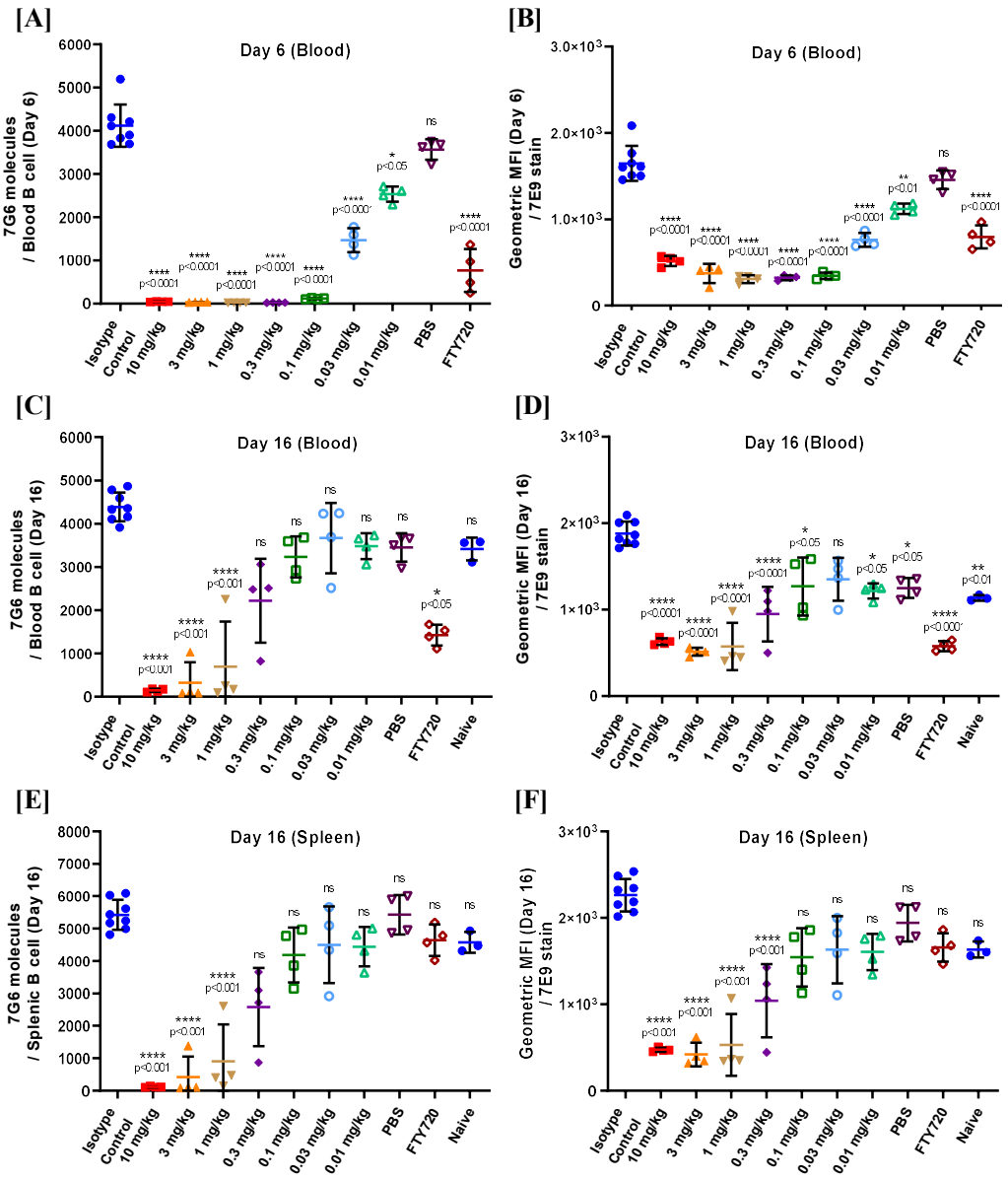

Figure 5.20. Free CD21/CD35 receptor number per B cell ($CD45^+$, $CD19^+$) in the **[A/C]** blood and **[E]** spleen on study day 6 and 16, measured by quantitative flow cytometry. Non-quantitative geometric MFI using labelled 7E9 to confirm impact on total CD21/35 receptor on B cells ($CD45^+$, $CD19^+$) in the **[B/D]** blood and **[F]** spleen. C57BL/6 male mice were treated with mAb 7G6 IP every 96 h at 0.01, 0.03, 0.1, 0.3, 1, 3 and 10 mg/kg, isotype control IP every 96 h at 10 mg/kg, PBS control IP every 96 h or 3 mg/kg Fingolimod PO daily, starting 2 days prior to IV KLH challenge at 2.4 mg/kg. Data illustrated as the individual (symbols) and mean ± SD (line and bar), n=4/treatment (isotype control n=8, naïve n=3), with statistical significance calculated using a one way ANOVA with Dunnett's multiple comparison test, * $p < 0.05$, ** $p < 0.01$, *** $p < 0.001$, **** $p < 0.0001$, ns = not significant.

higher than that observed on peripheral B cells, with values of 5426 receptors / splenic B cell vs 4389 receptors / peripheral B cell. In contrast to the observed impact on CD21/35 expression on B cells in blood, daily oral treatment with Fingolimod at 3 mg/kg did not result in a reduction in the CD21/35 receptor number / splenic B cell (68% reduction on peripheral B cells vs 13% reduction on splenic B cells).

In a similar manner to that reported for other cell surface receptors, the complement receptors CD21 and CD35 coexist in membrane expressed and soluble forms. Plasma samples collected on day 16 were analysed for the concentration of soluble CD21/35 using a novel, LC-MS/MS based, targeted proteomics assay with the results shown in figure 5.21. The baseline sCD21/35 plasma concentration was measured as 14.5 nM in the naïve C57BL/6 male mouse (n=3). No significant difference in this baseline sCD21/35 plasma concentration was observed in the isotype control (n=8) or PBS control (n=4) treatment groups following IV KLH challenge, 12.8 nM and 13.2 nM, respectively. Treatment with mAb 7G6 was shown to evoke no significant change in sCD21/35 plasma concentration at any dose tested. Thus, indicating that high mAb 7G6 exposure does not significantly alter the clearance of the soluble protein, resulting in no accumulation of the target protein in plasma.

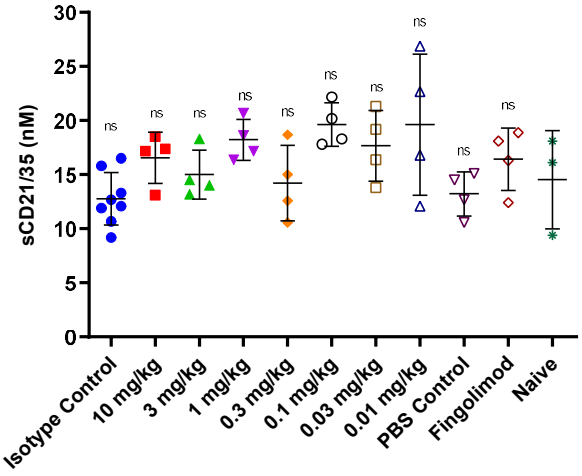

Figure 5.21. Soluble CD21/35 plasma concentration measured on study day 16, following administration of either mAb 7G6 IP every 96 h at 0.01, 0.03, 0.1, 0.3, 1, 3 and 10 mg/kg, isotype control IP every 96 h at 10 mg/kg, PBS control IP every 96 h or 3 mg/kg Fingolimod PO daily to the male C57BL/6 mouse, starting two days prior to IV KLH challenge at 2.4 mg/kg. Data illustrated as the individual (symbols) and mean ± SD (line and bar), n=4/treatment (isotype control n=8, naïve n=3). Statistical significance calculated using a one way ANOVA with Dunnett's multiple comparison test compared to naive, ns = not significant.

5.4.5.3. Pharmacodynamics

The primary pharmacodynamic endpoint of the IV KLH TDAR experimental model is the impact on antigen specific antibody production to the TD challenge, with the data shown in figure 5.22 and table 5.4. In this study, the mean KLH specific IgG response window, defined as the difference between the baseline day 0 measurement and that on day 16, was 318-fold in the vehicle treatment group (n=8). The maximum achieved KLH specific IgG concentration of 10.5 μg/mL in the control treatment group was low when compared to the qualification studies (33 μg/mL and 45 μg/mL in study 4 and 5, respectively). The outcome was a smaller mean KLH specific IgG AUC of 49.3 μg.day/mL than observed previously, with a CV% of 72%. In contrast, the mean KLH specific IgM response window, defined as the difference between baseline and peak response on day 6, was 26-fold in the vehicle treated group (n=8). This resulted in a mean KLH specific IgM AUC of 2037 μg.day/mL and CV% of 72%, which is in line with previous studies.

Treatment with 7G6 resulted in a dose concentration dependent exacerbation of the antigen specific IgG response (figure 5.22 A/C). Maximum impact was observed at 3 mg/kg, resulting in a 674% increase in KLH specific IgG AUC compared with the isotype control. The positive control, 3 mg/kg Fingolimod, in contrast resulted in a 69% inhibition of the KLH IgG AUC, correlating with previous studies. No difference was observed between the isotype and PBS treated control groups, confirming the absence of an isotype effect on the antigen specific antibody response. In stark contrast to the impact of 7G6 on the IgG response to KLH challenge, 7G6 demonstrated a dose concentration dependent inhibition of the antigen specific IgM response (figure 5.22 B/D). Maximum effect was observed at 1 mg/kg, resulting in a 91% inhibition of the KLH specific IgM AUC compared with isotype control. The positive control Fingolimod, once again demonstrated inhibition of the antigen specific IgM response, with a 64% reduction in KLH specific IgM observed compared with the isotype control, in line with previous studies.

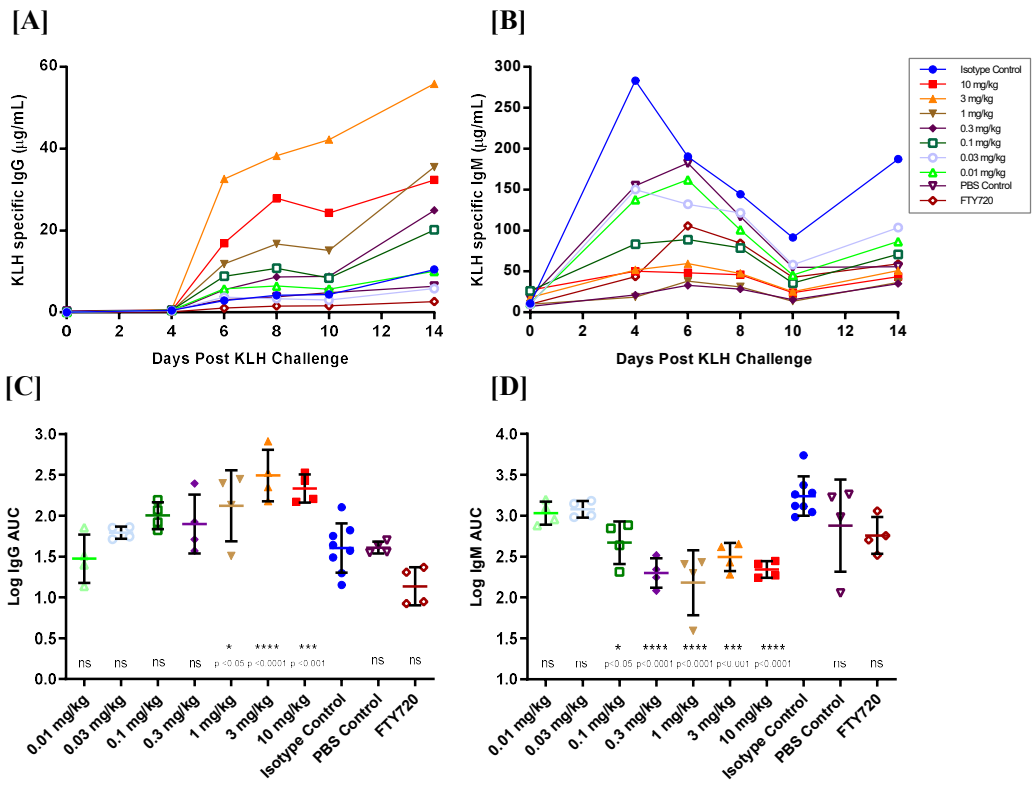

Figure 5.22. KLH specific **[A]** IgG and **[B]** IgM plasma concentrations in male C57BL/6 mice over 14 days following IV KLH immunisation at 2.4 mg/kg on study day 2. Mice were treated with either mAb 7G6 IP every 96 h at 0.01, 0.03, 0.1, 0.3, 1, 3 and 10 mg/kg, isotype control IP every 96 h at 10 mg/kg, PBS control IP every 96 h or 3 mg/kg Fingolimod PO daily, starting 2 days prior to immunisation. Data illustrated as the group mean (symbol), n=4/treatment (isotype control, n=8). The KLH specific antibody data is also presented as the area under the curve (AUC) of the individual **[C]** IgG and **[D]** IgM profiles. Data illustrated as individual (symbols) and mean ± SD (line and bar), n=4/treatment (isotype control, n=8), with statistical significance calculated using a one way ANOVA with Dunnett's multiple comparison test, * p <0.05, ** p<0.01, *** p<0.001, **** p<0.0001, ns = not significant.

To further unravel the observed exacerbation of the antigen specific IgG response following treatment with 7G6, the contribution of each individual antigen specific IgG isoform was explored. This was achieved by quantitative ELISA for the IgG1, IgG2b and IgG3 isotypes and by a relative antibody titre approach for IgG2c, using the day 16 terminal plasma sample. The results of this analysis are shown in figure 5.23, demonstrating that the 7G6 dose dependent exacerbation of the antigen specific IgG response is driven by a substantial increase in antigen specific antibodies of the IgG2 subclass (figure 5.23C/D). This increase is dose

dependent, with a maximum exacerbation achieved at 3 mg/kg and no increase observed at 0.01 mg/kg or below, when compared with the isotype control. The IgG1 and IgG3 responses are not altered from the control response at any dose tested. Treatment with Fingolimod results in a reduction of all KLH specific IgG isotypes, with no clear bias.

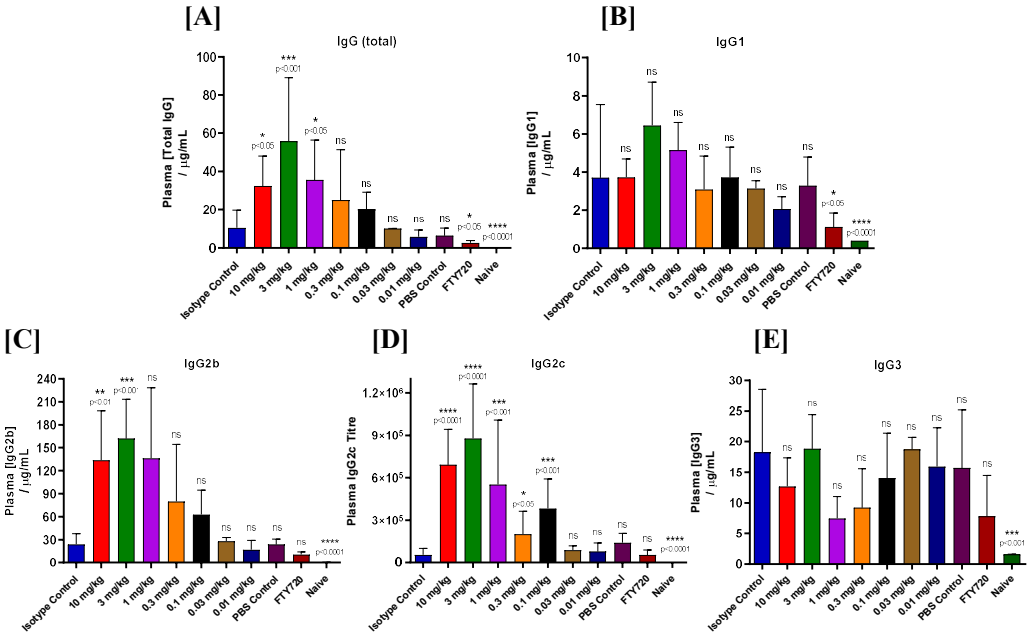

Figure 5.23. KLH specific IgG isotype analysis of plasma on study day 16, showing **[A]** the total IgG concentration and the subdivision of this into KLH specific **[B]** IgG1, **[C]** IgG2b, **[D]** IgG2c and **[E]** IgG3, following IV KLH immunisation at 2.4 mg/kg to male C57BL/6 mice on study day 2. Mice were treated with either mAb 7G6 IP every 96 h at 0.01, 0.03, 0.1, 0.3, 1, 3 and 10 mg/kg, isotype control IP every 96 h at 10 mg/kg, PBS control IP every 96 h or 3 mg/kg Fingolimod PO daily. Data illustrated as the group mean (solid bar) ± SD (error bar), n=4/treatment (isotype control n=8, naïve n=3), with statistical significance calculated using a one way ANOVA with Dunnett's multiple comparison test, * p <0.05, ** p <0.01, *** p <0.001, **** p < 0.0001, ns = not significant.

Counter to all previous studies, a significant increase in the germinal centre B cell number per spleen was not observed following IV KLH TD challenge in this study, when compared with the naïve untreated control (figure 5.24A). Consequently, no KLH specific GC B cell window exists to complete a meaningful analysis of the 7G6 concentration effect relationship. Treatment with mAb 7G6 did not result in a reduction in total splenic B cell number at any dose tested (5.24B), while treatment with the positive control Fingolimod resulted in a

significant reduction in B cell number per spleen. These outcomes are in line with previous studies and the primary pharmacology of the two treatments.

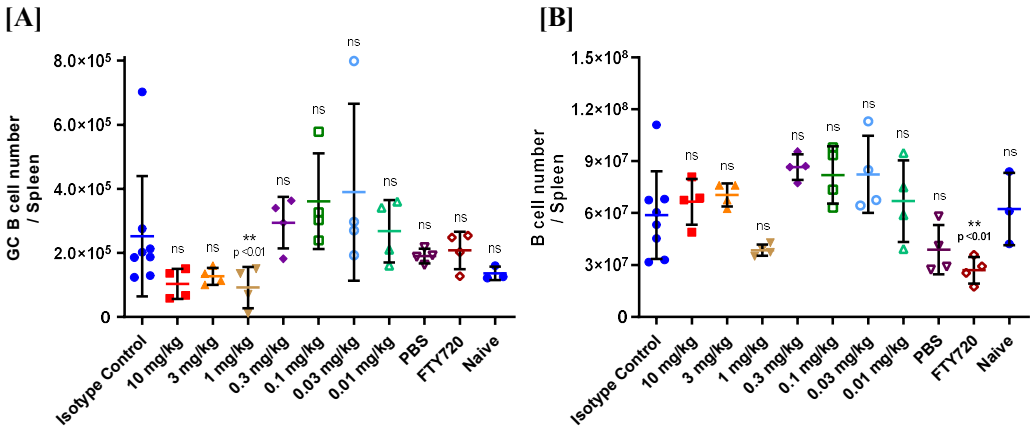

Figure 5.24. Splenic lymphocyte populations, **[A]** GC B cell number ($CD45^+$, $CD19^+$, $GL7^+$, FAS^+) and **[B]** B cell number ($CD45^+$, $CD19^+$) in C57BL/6 male mice on study day 16, following treatment with mAb 7G6 IP every 96 h at 0.01, 0.03, 0.1, 0.3, 1, 3 and 10 mg/kg, isotype control IP every 96 h at 10 mg/kg, PBS control IP every 96 h or 3 mg/kg Fingolimod PO daily, starting two days prior to IV KLH challenge at 2.4 mg/kg. Data illustrated as the individual (symbols) and mean ± SD (line and bar) n=4/treatment (isotype control n=8, naïve n=3) with statistical significance calculated using a one way ANOVA with Dunnett's multiple comparison test, ** p <0.01, ns = not significant.

5.4.5.4. PKPD interpretation

In summary, treatment with mAb 7G6 resulted in a concentration dependent inhibition of the KLH specific IgM response, but unexpectedly caused a concentration dependent exacerbation of the IgG response (figure 5.22A/C). Further exploration of this result identified this to be an IgG2 isotype driven response (figure 5.23C). In both cases, the observed response was dose dependent, indicative that a concentration effect relationship could be obtained. To achieve this, the data sets were modelled using a non-linear regression fit as a rudimentary approach to estimate an *in vivo* EC_{50}, as completed previously with Fingolimod. This analysis was conducted for the AUC of the KLH specific IgG and IgM responses, using the corresponding 7G6 plasma concentration measured on day 10 as a rough estimate of the average drug exposure achieved at each dose level. The resulting graphs are shown in figure 5.25, showing

the four-parameter logistic curve with variable slope, of the form Y = bottom + (top-bottom) / (1+10^((LogEC50-X)*Hillslope)), fit to the individual observed data. The isotype control treatment group observations were added to anchor the curve, utilising an arbitrary low 7G6 concentration value. Estimates of the plasma concentration were used for the 0.03 and 0.01 mg/kg treatment groups, due to the samples falling below the assay limit of quantification.

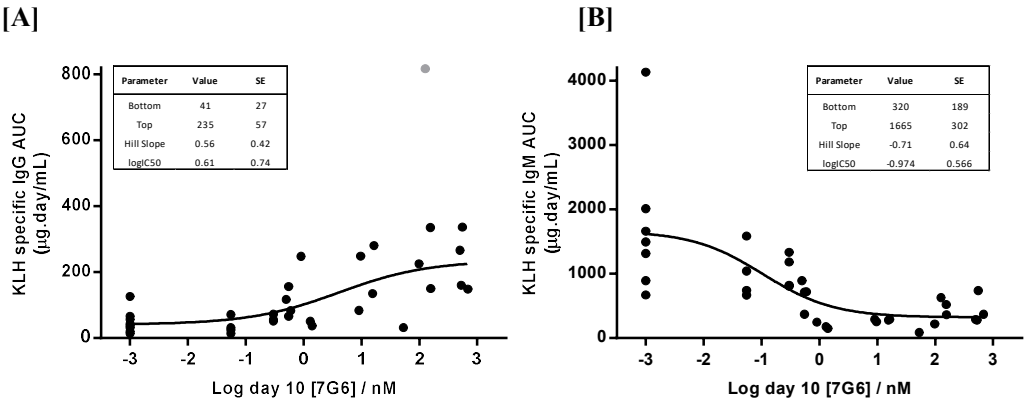

Figure 5.25. Non-linear regression fit of the KLH specific **[A]** IgG response or **[B]** IgM response against the 7G6 concentration on day 10. Data illustrated as individual observations (solid black symbols), with grey symbols representing observations that were excluded from the four-parameter logistic fit curve with variable slope (line). EC_{50} and maximum effect estimates were gained from the curve.

Non-linear regression fit of the KLH specific IgG response data (figure 5.25A) resulted in an estimated *in vivo* EC_{50} of 4.1 nM, with a positive hill slope of 0.56, highlighting that mAb 7G6 drives an exacerbated production of antigen specific IgG, as opposed to inhibition of the response to KLH immunisation. Contrary to this, and more in line with expectation, mAb 7G6 demonstrates a concentration dependent inhibition of the KLH specific IgM response to IV KLH immunisation. Non-linear regression of this concentration effect relationship results in an *in vivo* EC_{50} estimate of 0.1 nM and a maximum inhibitory effect of 81%.

Table 5.4. Summary table of the key results from PKPD study 7. mAb 7G6 plasma exposure expressed as the mean on day 6 (±SD) following IP treatment every 96 h across the range 0.01 to 10 mg/kg, listed alongside the accompanying mean (±SD) KLH specific IgG and IgM responses (peak and $AUC_{2\text{-}16}$), the mean (±SD) germinal centre B cell number per spleen and mean target engagement on peripheral B cells on day 6 (percentage of 7G6 antibodies bound per cell versus control). The effect of each treatment on the TD antibody response can be calculated compared with the control treatment group. n/a: not applicable.

Treatment Group	**KLH specific IgG day 16 peak concentration Mean (±SD) (µg/mL)**	**KLH specific IgG $AUC_{day\ 2–16}$ (±SD) (µg.day/mL)**	**KLH specific IgM day 8 peak concentration Mean (±SD) (µg/mL)**	**KLH specific IgM $AUC_{day\ 2–16}$ (±SD) (µg.day/mL)**	**Mean (±SD) germinal centre B cell number / spleen**	**Day 6 7G6 plasma concentration Mean (±SD) (nM)**	**Target engagement on peripheral B cells on day 6 (%)**
Isotype Control	10.5 (9.3)	49 (36)	190.4 (172.6)	2036 (1473)	2.5E5 (1.9E5)	n/a	n/a
10 mg/kg	32.4 (15.7)	228 (118)	48.3 (13.0)	225 (52)	1.0E5 (4.7E4)	607.1 (7.6)	99.0
3 mg/kg	55.9 (33.1)	382 (225)	59.5 (24.7)	331 (121)	1.3E5 (2.6E4)	136.7 (14.8)	99.2
1 mg/kg	35.5 (20.9)	174 (114)	38.1 (18.7)	191 (106)	9.2E4 (6.4E4)	45.7 (3.3)	99.5
0.3 mg/kg	24.9 (26.4)	105 (75)	33.0 (9.3)	212 (87)	2.9E5 (8.0E4)	8.0 (1.2)	99.5
0.1 mg/kg	20.2 (9.0)	106 (38)	88.8 (26.9)	527 (257)	3.6E5 (1.5E5)	0.6 (0.2)	97.2
0.03 mg/kg	10.0 (0.2)	63 (40)	132.1 (27.4)	1221 (283)	3.9E5 (2.8E5)	<0.13	64.4
0.01 mg/kg	5.8 (3.5)	35 (22)	162.1 (81.3)	1117 (364)	2.7E5 (9.8E4)	<0.13	38.5
PBS Control	6.4 (4.0)	41 (12)	182.4 (151.6)	1140 (780)	1.9E5 (2.3E4)	n/a	n/a
3 mg/kg Fingolimod	2.6 (1.2)	15 (14)	105.7 (49.1)	638 (353)	2.1E5 (5.9E4)	n/a	n/a

5.5. Discussion

5.5.1. Confirmation of tool molecule efficacy

Initial investigation centred on comparison of the three surrogate CD21 specific mAbs, to confirm literature reports on the action and efficacy of these molecules and to identify the one most suitable to proceed into further pharmacological interrogation. The head to head efficacy study (study 1) was performed using a well characterised TD immunisation study design, involving the IP administration of hapten conjugated subunit KLH, precipitated in the mineral adjuvant Alum. This is a routinely used protocol both within GSK and across the wider scientific community (van Ommen *et al.*, 1994), monitoring the formation of antibodies against the otherwise non-immunogenic small hapten TNP.

To confirm maintenance of mAb exposure across the duration of study 1, the plasma concentration of each surrogate mAb was monitored. Prior to initiation of the study, mAb exposure was projected based upon linear scaling of the 2 mg/kg (1.5 mg/kg 9E10) IP plasma profile (illustrated in figure 5.2) achieved during the PK characterisation studies described in chapter 3. The pharmacokinetics of the two murine IgG1 mAbs (4B2/9E10) remain in line with this projection, demonstrating linear PK across this dose range. The rat IgG2b mAb 7G6 adheres to the projected plasma concentration up to day 10. But whilst the observed profile remains declining steadily, the projected profile deviates, with increased clearance occurring from day 10 onward. This highlights the limitation of linear scaling, when the PK demonstrates non-linear dose dependent clearance, and the requirement for the more complex TMDD PK model described in chapter 4. It also highlights that at 20 mg/kg, all three mAbs are likely saturating the target, minimising the impact of TMDD on the pharmacokinetics. Two animals in the mAb 7G6 treatment group deviate from the group mean at the later time points. This is despite the day one drug exposure being consistent within both the treatment group and with the pre-study estimate, thus precluding mis dosing as an explanation. Although not specifically investigated in this study, the rapid acceleration of 7G6 clearance is indicative of an anti-drug antibody response to the rat origin IgG2b mAb. Due to its rat architecture, this is not an entirely unexpected outcome, with anecdotal evidence for the appearance of anti-rat IgG reported by Kulik *et al.* (2015) as soon as after the first 7G6 dosing occasion. Whilst this provides credence to the ADA theory, curiously this was not observed at any dose of 7G6 tested in the pharmacokinetic studies described in chapter 3.

The plasma PK data may demonstrate maintenance of mAb exposure across the 14-day study period, however it is not a direct demonstration of mAb exposure at the site of action, or indeed evidence of pharmacological engagement of the target protein. The site of action in this experimental model is considered to be secondary lymphoid tissue, primarily the draining lymph nodes due to the IP challenge site, but additionally within the spleen. Therefore, as a direct analysis of target engagement at the site of action, the expression of CD21 and CD35 on the surface of splenic B cells was determined by flow cytometry on day 14 (figure 5.4). The spleen was selected because the anatomical size of draining lymph nodes in mice make this a technically challenging tissue to both collect and analyse. Splenic B cell analysis provided evidence that CD21/35 was engaged at the site of action by mAbs 4B2 and 7G6, as demonstrated by the reduction in measured MFI for the competitive, fluorescently labelled 7G6 (figure 5.4A). Furthermore, this reduction in MFI can be identified as a loss of surface expressed receptor, as opposed to epitope masking, through the decrease in measured MFI of the non-competitive, fluorescently labelled 7E9 (figure 5.4B). This loss of surface expression was mirrored by CD35, as indicated by the reduction in measured MFI for the uniquely CD35 specific, fluorescently labelled 8C12 (figure 5.4C). This is a phenomenon observed in previous literature with mAb 4B2 and 7G6 (Kulik *et al.*, 2015, Heyman *et al.*, 1990) and is an often observed characteristic of mAbs targeting cell surface receptors. Whilst the exact mechanism is unknown, potential explanations are proposed for this loss of surface expression; such as receptor internalisation (Tessier *et al.*, 2007), ectodomain shedding (Masilamani *et al.*, 2003a, Hoefer *et al.*, 2008) or possibly down modulation of expression. While receptor internalisation following mAb binding is in itself not a cause of efficacy concern, indeed removing the receptor completely could be considered a preferential approach, it could lead to accelerated elimination of the mAb and an overall reduction in the period of efficacy following dosing. Certainly, an element of receptor internalisation could be attributed to explaining the non-linear pharmacokinetics observed for mAb 7G6 and 4B2 in chapter 3, whereby the mAb and receptor are internalised and destroyed upon binding.

The inability for mAb 9E10 to replicate the on-target behaviour of mAb 7G6 and 4B2 (figure 5.4) is indicative of no target binding, or at least no functional target binding. Whilst this observation contrasts *in vitro* data generated during mAb selection (Appendix IV), it does corroborate with the observed differences in pharmacokinetic behaviour described in chapter 3. Interestingly, despite the non-competitive mAb 7E9 being considered to bind at an epitope distant from the C3d binding site, it has been shown previously to result in downregulation of surface CD21/35 (Kinoshita *et al.*, 1990). This indicates that non-functional

binding may still result in receptor loss, perhaps suggesting that 9E10 does not bind native CD21/35 *in vivo*.

To ascertain the ability of each surrogate mAb to translate the identified target engagement on B cells at the site of action, into a measurable impact on the TD humoral immune response, three key biomarkers were monitored. These were the B cell and germinal centre B cell populations in the spleen and the TNP specific antibody concentration in plasma. Analysis of the B cell and germinal centre B cell populations was conducted on splenic tissue collected post mortem, 13 days after TD immunisation with TNP-KLH. Importantly, the total splenic B cell population (figure 5.3A) demonstrated that maintained CD21 neutralisation by the surrogate mAbs did not result in B cell depletion, a key reported characteristic of these molecules (Heyman *et al.*, 1990, Kulik *et al.*, 2015) and an important differentiator from currently marketed B cell therapies such as Rituximab and Belimumab. In contrast, treatment with mAbs 7G6 and 4B2, but not 9E10, resulted in a significant reduction in the frequency of germinal centre B cells (figure 5.3D) in response to the TD challenge. This impact on germinal centre B cells correlates with the observations of other authors (Heyman *et al.*, 1990, Kulik *et al.*, 2015) and provides a clear link between target engagement and its downstream impact on humoral immunity. Treatment does not however result in complete abrogation of the germinal centre response, but a reduction in magnitude. A similar observation to that of Ahearn *et al.* (1996) who noted that in Cr2-/- mice, while there is a reduction in germinal centre number and size in response to TD challenge, functional germinal centre foci are still formed.

Whilst therapeutic blockade of CD21/35 with 7G6 and 4B2 resulted in an impaired germinal centre response to the TD KLH challenge, there was no significant attenuation of antigen specific antibody production (figure 5.2). This is despite numerous publications describing an impaired primary antibody response to TD challenge, following both genetic knockout of CD21 (Ahearn *et al.*, 1996, Molina *et al.*, 1996) and therapeutic intervention with 7G6 and 4B2 (Heyman *et al.*, 1990, Kulik *et al.*, 2015). These results echo a study by Wu *et al.* (2000) in Cr2-/- mice, in which alum precipitated NP-KLH restored the impaired antibody response seen to NP-KLH alone to within 2-fold of wild type mice, without improvement in GC response development. In addition, the original work by Heyman *et al.* (1990) describing the activity of 7G6, showed that treatment only resulted in complete suppression of the IgG response to HRBC when that challenge was suboptimal. These observations indicate that the experimental TD challenge protocol used in study 1 may not be ideal for interrogation of CD21 pharmacology.

It should be noted that variability in the measured IgG and IgM response has an impact on interpretation of the data in study 1. A very narrow response window was achieved, coupled with high inter individual variability. This narrow response window is in part due to the rarity of the TNP hapten specific antibodies and could be expanded through detection of antibodies against the KLH carrier protein instead. However, it is also caused by the high baseline of natural repertoire antibodies with low affinity binding for the BSA carrier protein in the TNP-BSA capture protein. Whilst all three treatments fail to demonstrate a significant reduction in antigen specific IgG response, there is an observed trend toward inhibition following treatment with mAb 7G6. Two further complicating factors affected the 7G6 treatment group. Firstly, the group size was reduced to n=5 due to limited availability of the drug at the time of the study. While secondly, the impact of the potential ADA interference at later time points in two animals is unknown. Certainly, the two affected animals presented with the highest concentration of TNP specific IgG on day 14, potentially highlighting an impact on the group mean.

5.5.2. Optimisation of a new TDAR experimental model format

The results generated in the head to head comparison of the three surrogate CD21 specific mAbs highlighted a shortcoming in the experimental TD immunisation protocol. Namely that, whilst this protocol results in a strong and robust humoral immune response, the driving force behind this is likely a combination of the adjuvant and immunisation site. Resulting in a response that may be insensitive to CD21 neutralisation. Consequently, an alternative approach was sought, that provided more alignment with the biology of CD21. In the original work by Heyman *et al.* (1990), 7G6 was shown to significantly inhibit the specific IgG response to 10 μg KLH, administered IV via the tail vein. In another study exploring the basis for the impaired humoral immune response in a Cr2-/- mouse strain, Fang *et al.* (1998) reported using a higher dose of 100 μg KLH, again given IV, to which mice deficient in the expression of both CD21 and CD35 show a profound deficit in IgG response. This data became the starting point for developing a suboptimal challenge model with greater alignment to CD21 biology.

The initial pilot (study 2) tested a 10 μg dose of soluble KLH formulated in PBS and administered IV via the tail vein to male C57BL/6 mice. However, in contrast to the Heyman *et al.* (1990) study, IV administration of 10 μg KLH resulted in no measurable KLH specific IgG response and no detectable change in splenic germinal centre B cells after 14 days. A key difference between the studies was the source of KLH, with potential differences in the purity

and composition perhaps explaining the observed differences in response. The 10 μg/mouse KLH dose used in study 2 represents a 4-fold increase compared to that used in study 1 (400 vs 100 μg/kg). These two KLH forms are closely aligned, despite conjugation with the hapten TNP in study 1, demonstrating the importance of the adjuvant in driving the much stronger humoral immune response seen in study 1.

The results of the pilot (study 2) highlighted the importance of inherent antigen immunogenicity in non-adjuvant driven models. A comparison by Lebrec *et al.* (2014a) of the TD response to different forms and sources of KLH demonstrated that these factors were important determinants in the strength and variability of the resulting IgG response. This work highlighted the stronger immunogenicity of high molecular weight forms of KLH, generating log unit increases in IgG response, whilst offering improvement in inter individual variability. High molecular weight KLH is also the more commonly used form for clinical TDAR investigation. These factors drove the decision to switch the challenge to Imject mcKLH (ThermoFisher Scientific), a high purity, responsibly sourced, high molecular weight KLH. The 10 μg challenge amount (0.4 mg/kg) used in the initial pilot, sits at the lower end of the typically reported range of 0.1 to 2 mg (0.4 to 8 mg/kg) in rat immunotoxicology studies (Lebrec *et al.*, 2014b). The challenge range was thus extended to identify a suitable KLH challenge dose. Immunisation with KLH is a widely used technique both in preclinical immunotoxicology studies and in clinical investigation, with an exemplary record of safety and tolerability (Swaminathan *et al.*, 2014). Therefore, these higher challenge amounts were expected to be well tolerated.

The second pilot (study 3) tested challenge amounts of 10 and 30 μg (0.4 and 1.2 mg/kg) of Imject mcKLH (ThermoFisher Scientific) in the male C57BL/6 mouse, to confirm tolerability of the altered form of KLH and define the humoral immune response. The study was successfully completed, with no observed welfare issue at either tested dose and the successful propagation of a measurable immune response to the KLH challenge. This antigen specific IgG response provided a 52-fold window compared with baseline at the 10 μg challenge, extended to a 231-fold window for the higher 30 μg challenge (figure 5.6A). The challenge dependent increase in response indicates that the tested KLH amounts are not resulting in a maximal response, offering scope for further extension of the challenge range. The outcome was mirrored in the antigen specific IgM response to the two challenge doses, with a 7-fold response window at 10 μg KLH and a 13-fold window at 30 μg KLH. The measurement of antigen specific IgM is disrupted by the non-specific, low affinity naïve IgM pool, which results in high assay background interference and the ensuing narrowing in response window.

In alignment with the antigen specific antibody response, increased germinal centre B cell numbers were observed in the spleen, 13 days post KLH immunisation. Although the increase is small in terms of fold change, 8-fold and 13-fold at 10 and 30 μg/mouse respectively, it does indicate a challenge dose dependency. It is likely that 13 days may not represent the ultimate time point post challenge to measure the germinal centre response at its peak, with reports indicating it can reach its maximum between day 10 and 12 (Kelsoe and Zheng, 1993). Whilst an additional study was considered to investigate the optimal time point to measure the GC response, IgG was considered to be the primary study endpoint. As such, a compromise in study duration was sought to minimise animal usage, with sampling at the peak response of both endpoints requiring duplicate treatment groups.

The KLH challenge dose was extended in study 4 toward the upper reaches of the reported range, to test the linearity of response to the challenge and to provide evidence of the repeatability of the study design. Due to the loss of animals on study, insufficient animals were available to complete the planned highest challenge of 300 μg/mouse. However, this was not due to tolerability, with KLH immunisation well tolerated at both the 30 and 100 μg doses. Repeatability of the antigen specific IgG response to KLH was tested through a repeat of the 30 μg challenge amount in study 4, with a lower response observed compared with study 3 (57-fold vs 231-fold). The same reduced response was observed for antigen specific IgM (6-fold vs 13-fold) and for the number of germinal centre B cells (6-fold vs 13-fold), compared with study 3. This outcome demonstrates that there may be a high level of inter-study variability in response, potentially caused by differences in the batch of KLH or the age and litter of mice used. The higher 100 μg dose of KLH once again demonstrated that the response at 30 μg was submaximal, with an increased antigen specific IgG response (171-fold vs 57-fold), antigen specific IgM response (7-fold vs 6-fold) and an increased number of germinal centre B cells in the spleen (8-fold vs 6-fold). Whilst inter-individual variability was moderately high for both IgG (CV% of 28% and 42%) and IgM (CV% of 21% and 2%) endpoints, it presented at a level with potential to be overcome by increased sample size.

These studies have demonstrated that the mouse TDAR experimental protocol can be reformatted into a non-adjuvant driven model with a suboptimal TD challenge, for greater alignment with the underlying biology of CD21. Selection of the KLH challenge dose to progress to further studies was a balance between the suboptimal nature of the challenge and provision of a robust response window in which to test therapeutic inhibition. This led to selection of 30 μg/mouse (1.2 mg/kg) as the Imject mcKLH IV challenge dose for further studies.

5.5.3. Qualification with gold standards

A full protocol qualification was undertaken to demonstrate the performance of the reformatted IV KLH TDAR experimental model. This experimental model qualification was conducted with two clinically validated therapies that target different mechanisms contributing to adaptive immunity. The first was Fingolimod, a S1P receptor modulator that interferes with T cell trafficking and has been demonstrated both preclinically (Han *et al.*, 2004) and clinically (Boulton *et al.*, 2012) to attenuate humoral immunity. The second was a murine surrogate (SA271G2) for Rituximab, a B cell depleting mAb with prior evidence of impacting adaptive immune responses in the clinic (Bingham *et al.*, 2010), with similar results shown preclinically (DiLillo *et al.*, 2007).

The qualification (study 5) experiment was completed successfully, with IV immunisation with Imject mcKLH at 1.2 mg/kg resulting in a mean 433-fold increase in antigen specific IgG on day 16, compared with baseline (figure 5.10). Thus, providing confidence in the ability of the 1.2 mg/kg KLH challenge to generate a robust and repeatable KLH specific IgG response (231-fold and 57-fold in study 3 and 4, respectively). Inter-individual variability was high, illustrated by a 74% CV in the day 16 IgG response. However, because this was anticipated, adequate sample size powering was incorporated into the study design to account for this extent of variability. The KLH specific IgM response window was again similar to previous studies, with a 10-fold window on study day 16 compared to earlier windows of 13-fold and 6-fold in studies 3 and 4 respectively. A naïve control group was included in the study design to act as a negative control for cellular endpoints, with this group demonstrating that the germinal centre B cell number per spleen increases as a result of the IV KLH challenge. The mean number of GC B cells per spleen on day 16 was 3.9×10^5 following 1.2 mg/kg IV KLH challenge, which compares well with prior studies (4.5×10^5 in study 3 and 3.1×10^5 study 4) and provides a 9-fold response window.

Study 5 trialled an increase in the number of plasma samples collected across the study duration, providing data that describes the entire IgG response profile to facilitate further mathematical interrogation. This enables an area under the curve (AUC) analysis of the IgG response profile to be used for the comparison of treatment groups, in place of the previous single timepoint approach. Thus, providing a more accurate analysis of the impact on the overall IgG response and better representing the inherent inter-individual variability in antigen specific IgG response. An added benefit is that it allowed improved description of the earlier IgM response, identifying the peak at day 6 and expanding the response window to 67-fold over baseline.

5.5.3.1. SA271G2

The pharmacokinetics SA271G2 in study 5 were in line with that expected for a rat IgG2b mAb administered IP to the mouse, showing a long mean terminal half-life of 53 h. This is similar to the 63 h half-life of 7G6 observed previously following IP administration at 2 mg/kg (described in chapter 3). Exposure was maintained throughout the 16-day study period in all but two animals, which although initially in line with the treatment group showed accelerated clearance from day 8, resulting in complete loss of exposure by day 16 (figure 5.8). Although not specifically investigated in this study, this is indicative of an anti-drug antibody response to the rat origin mAb, again similar to that seen previously with 7G6 (study 1). Maintenance of SA271G2 plasma exposure resulted in near complete B cell depletion in the blood, demonstrated by the eradication (99.8%) of the B2 cell population on day 8 (figure 5.10). The two animals with diminished drug exposure in the latter half of the study are showing the early stage of a recovery in this B2 cell population by day 16, but full depletion is maintained in the remaining mice. This provides confirmation of the pharmacological activity of SA271G2 as a B cell depleting mAb, as reported by Moyron-Quiroz *et al.* (2016). Importantly, this B cell depletion also manifests in the spleen, with a drastic 98% reduction in B cell number per spleen observed (figure 5.11).

Treatment with 10 mg/kg SA271G2 was shown to result in a 68% reduction in germinal centre B cell number per spleen and near complete abrogation (83%) of the antigen specific IgM response (figure 5.11A and 5.9B, respectively) to TD KLH challenge. Counter intuitively, rather than a coordinated reduction in the antigen specific IgG response, a 68% exacerbation was observed. This outcome contradicts literature evidence for the impact of CD20 mediated B cell depletion on the TD humoral immune response. Preclinically, DiLillo *et al.* (2007) reported that treatment of C57BL/6 mice with a CD20 specific B cell depleting mAb results in inhibition of the primary and secondary IgG and IgM response to the T-dependent antigen DNP-KLH. Clinically, Bingham *et al.* (2010) demonstrated a decreased antibody response to neoantigen KLH following Rituximab treatment in a RA patient population, whilst a similar decreased response was observed to influenza vaccination in Rituximab treated RA patients by Oren *et al.* (2008). Bearden *et al.* (2005) noted a similar decreased primary antibody response to the neoantigen phiX174 following Rituximab treatment in chronic renal failure patients. Whilst each example mentioned showed a decrease in humoral immunity to primary TD immunisation, each report also notes that a measurable response was generated in several tested patients, despite near complete depletion of the B cell population.

Curiously, although treatment with SA271G2 resulted in a 98% reduction in B cell number per spleen, this only transpired to result in a 68% reduction in the germinal centre B cell response to TD challenge, when compared with control. Indeed, treatment did not even return the GC B cell number per spleen to that of the unchallenged naïve control. Baumjohann *et al.* (2013) reported similar inefficient depletion of antigen specific and germinal centre B cells by anti-CD20 treatment in the mouse. Inefficient depletion was also identified in the lymph nodes of renal transplant patients treated with Rituximab by Kamburova *et al.* (2013). This perhaps offers an explanation as to the altered antigen specific IgG response, whereby treatment with Rituximab is unable to clear the small number of resistant remaining B cells which drive the antigen specific response. This explanation is supported by further analysis completed by Kamburova *et al.* (2013), where following *ex vivo* stimulation of B cells isolated from the lymph nodes of the renal transplant patients, Rituximab treatment enhanced IgG production but fully inhibited IgM production. Another explanation could be the strength and route of the KLH challenge. Morsy *et al.* (2013) showed that in a $CD20^{-/-}$ mouse strain, whilst the antigen specific IgM response was reduced to all TD challenge strengths tested, a reduction in IgG response was only noted to a moderate challenge. Another curious result was that SA271G2 treatment induced an increase in CD8+ T cell number per spleen. Perhaps an indication of the inter-dependence of T and B cells and a resulting phenotypic change in both cell types following CD20 mediated B cell depletion.

5.5.3.2. Fingolimod

The pharmacokinetics of Fingolimod, following daily oral administration at 3 mg/kg, resulted in a consistent mean blood exposure across each sampled day (1 h post dose), ranging between 308 and 457 ng/mL, with low inter-individual variability (figure 5.8A). The resulting blood concentration of the active phosphorylated metabolite ranged between 408 and 518 ng/mL at an average Fingolimod Phosphate/Fingolimod ratio of 1.23. Whilst not reported in mouse, the pharmacokinetic behaviour observed here is reminiscent of that reported in rat (Meno-Tetang *et al.*, 2006) and human (David *et al.*, 2012). In human, the reported Fingolimod Phosphate/Fingolimod ratio was 0.89 at C_{max}, following a single dose (David *et al.*, 2012). This may indicate an increased conversion of Fingolimod to its active phosphorylated form in mouse, when compared with other species. Alternatively, this may just result from species differences in the pharmacokinetics of either parent drug or metabolite.

The impact of daily oral Fingolimod treatment (3 mg/kg) on the peripheral blood lymphocyte population is characterised by a 93% reduction in CD4+ T cells and an 85% reduction in CD8+

T cells after eight days, with this reduction maintained through to study day 16 (figure 5.10). This reduction corresponds well with that seen by Han *et al.* (2004) where a 98% and 95% reduction of CD4+ and CD8+ peripheral T cells was observed in mice treated at 1 mg/kg (PO QOD). While similar levels of peripheral T cell reduction were observed by Morris *et al.* (2005), following Fingolimod treatment at approximately 1.25 mg/kg/day administered in drinking water, although the author speculated that this dose resulted in incomplete S1P1 blockade. The impact on lymphocyte population is also seen within the spleen, albeit to a lesser extent, resulting in a 56% CD4+ and 39% CD8+ T cell reduction (figure 5.11). Again this smaller impact on the splenic lymphocyte population is echoed in the study by Han *et al.* (2004), where a 30% CD4+ and 36% CD8+ T cell reduction was observed. This data provides confidence that 3 mg/kg daily oral treatment results in the expected efficacy on T cell populations both in peripheral blood and within the spleen.

The downstream impact of Fingolimod pharmacology is inhibition of the humoral immune response to KLH immunisation, shown by a reduction in both the number of germinal centre B cells in the spleen (65% reduction) and the concentration of antigen specific IgG in plasma (62% reduction). It is generally considered that the Fingolimod mechanism of action is on the mobility of the leukocyte population, preventing egress from lymph nodes, resulting in a shift in steady state and transient lymphopenia (Morris *et al.*, 2005). This reduction in the number and motility of activated T helper cells has been suggested as the mechanism of action in the TD antibody response (Han *et al.*, 2004). In contrast, there is little to no impact on the antigen specific IgM response, in keeping with the data reported by Han *et al.* (2004), but contrary to the clinical observations of Boulton *et al.* (2012).

The data generated with Fingolimod and SA271G2 lends support to the suitability of the reformatted IV KLH TDAR experimental model, providing external qualification and demonstration of its relevance to clinical outcome. Interest was ended in mAb SA271G2 as a model positive control, considering the lack of impact on antigen specific IgG. Instead, Fingolimod was progressed forward as the model positive control due to its exemplary performance on the primary study endpoints. Despite its mechanistic dissimilarity to CD21 neutralisation, in that it primarily targets the T cell as opposed to the B cell component of humoral immunity, it provides an ideal opportunity to test the translational value of the model. This is through the availability of human healthy volunteer TDAR data following KLH immunisation (Boulton *et al.*, 2012).

5.5.3.3. Fingolimod dose response

To extend the Fingolimod data set beyond profiling only maximal effect and to generate a training data set for mathematical PKPD modelling, Fingolimod was explored in the IV KLH TDAR experimental mouse model across a full dose response range (study 6). To facilitate this dose range, an unconventional study design was successfully implemented involving minimal group sizes but multiple dose levels, encompassing both extremes of the sigmoidal concentration effect relationship. Armed with the knowledge that Fingolimod PK is dose linear (David *et al.*, 2012), the study was designed with eight doses across the range 0.003 to 10 mg/kg, at half log unit intervals.

Consistent with prior literature and in line with the previous study, daily oral administration of Fingolimod resulted in dose linear blood exposure (figure 5.12). This exposure was both consistent across the sampled days and within each treatment group. There was also a high degree of consistency with the blood exposure achieved at 3 mg/kg in the earlier study, with a mean blood concentration of 294 ng/mL vs 427 ng/mL on day 12 in study 5 and 6 respectively. The resulting exposure of the active phosphorylated metabolite was also shown to be dose linear, with a slightly higher mean C_{max} Fingolimod Phosphate/Fingolimod ratio of 1.9, compared with 1.2 in study 5. Although the lowest dose tested (0.003 mg/kg) resulted in blood concentrations below the assay cut-off, due to the linearity of exposure across all other tested doses and the consistent Fingolimod Phosphate/Fingolimod ratio, the blood concentrations can be confidently estimated. To further characterise the PK in mouse and to assist in later PK modelling, an intraday PK profile was collected on day 12. This provided confirmation of the long reported half-life of Fingolimod, reported as 7 days in human (Kovarik *et al.*, 2007) and 1 day in rat (Meno-Tetang *et al.*, 2006), which results in an almost flat PK exposure profile in the mouse. However, an additional standalone single oral dose PK study would need to be conducted in mouse to accurately define the pharmacokinetics for comparison across species. The extended exposure profile is mirrored by Fingolimod phosphate, albeit with a later T_{max} of 4-8 h compared with 1-4 h for Fingolimod. As a consequence of the PK characteristics of Fingolimod, the average blood concentration (C_{av}) offers an ideal measurement of drug exposure for concentration effect analysis, with day 12 presenting the opportunity to gain an estimate. Interestingly, the mean C_{av} Fingolimod phosphate /Fingolimod ratio was 2.3, an increase on that observed at C_{max} (1.9) and contrary to human where the AUC ratio of 0.38 is lower than the C_{max} ratio of 0.89 (David *et al.*, 2012). These differences in the active metabolite should therefore be considered when attempting to translate data across species.

The greater than 1000-fold range of distinct Fingolimod blood exposures achieved in this study, provide the ideal platform to test the concentration effect relationship on the humoral immune response to KLH. The baseline antigen specific IgG response to the IV KLH challenge was defined by the control group, demonstrating a mean 564-fold response window (baseline vs day 16) and a mean IgG AUC of 268 μg.day/mL. This response was in line with the qualification study (433-fold/229 μg.day/mL). Inter study repeatability was further confirmed by the 3 mg/kg dose level, which demonstrated 60% inhibition of the antigen specific IgG response AUC, compared with 64% in study 5. These data provide confidence both in the experimental model and in the data generated in this study. A Fingolimod dose, and by extension blood, concentration dependent inhibition of the antigen specific IgG response was observed. The tested dose range provided good description of the Fingolimod concentration that results in no effect, with the 0.03 mg/kg dose providing the first indication of effect on IgG (figure 5.14A). This correlates well with the measure of on target pharmacology, illustrated by the measured T cell population in the spleen, with 0.03 mg/kg the lowest dose to demonstrate a reduction in both CD4+ and CD8+ T cell number (figure 5.15C/D). Intriguingly, no concentration effect relationship exists for the impact on T cell number in the spleen, which appears to be an all or nothing response. Meanwhile, a concentration effect relationship does exist for all other study endpoints, perhaps indicating a disconnect between the impact on T cell number and the impact on formation of a functional adaptive immune response.

In contrast to the qualification study, Fingolimod treatment resulted in a reduction in antigen specific IgM response, with the 3 mg/kg dose demonstrating a 51% inhibition of the mean IgM AUC in the control versus no inhibition observed in study 5. The extent of the baseline antigen specific IgM response in the control group was marginally lower in this study than previously in study 5 (28-fold / 1246 μg.day/mL vs 67-fold/2283 μg.day/mL). Inhibition of the antigen specific IgM response was shown to be Fingolimod concentration dependent, with maximal inhibition (79%) observed at 10 mg/kg, before the effect was lost at 0.3 mg/kg. Consistent with prior studies, an increase in germinal centre B cell number per spleen was observed 14 days post IV KLH challenge ($6.6x10^5$ GC B cell per spleen) compared with the naïve controls ($6.6x10^4$ GC B cell per spleen). A Fingolimod concentration dependent inhibition of the germinal centre response correlated well with the impact on antibody response.

Study 6 was not designed or powered for interpretation of the significance of individual treatment group effects, rather for interrogation of the data set as a whole. As such, to coalesce the individual concentration response data sets into a mathematical relationship, a four-parameter logistic fit curve was fitted to the IgG, IgM and GC response data, plotted against

the logarithm of the Fingolimod average concentration (C_{av} on day 12). This analysis was used to estimate an *in vivo* EC_{50} value for inter-study comparison and an approach to test translation across species. To provide anchor points for curve fitting in the notoriously difficult to characterise no effect range, the control response data was used along with an arbitrary Fingolimod concentration 3 log units below the lowest tested dose. The nascent inter-individual variability in antigen specific antibody response that drove the qualification study to require a sample size of 10, also impacts curve fitting to some extent. A limited number of samples with particularly large variation, compared to the data set as a whole, were removed to facilitate curve fitting, including the 0.003 mg/kg group from the IgG data set.

The resulting *in vivo* EC_{50} were 17 nM for antigen specific IgG, 151 nM for antigen specific IgM and 46 nM for the splenic germinal centre response (figure 5.16). The EC_{50} values for the IgG and GC B cell endpoints are remarkably similar, demonstrating the inextricable link between these endpoints and potentially a single shared point of Fingolimod activity on the T cell help needed to initiate both the extrafollicular and follicular response pathways or to trigger IgG isotype switching. Although T cell help is still required to elicit the extrafollicular IgM response to the TD antigen KLH, previous reports have indicated a lack of Fingolimod efficacy on this endpoint (Han *et al.*, 2004). The results of this experiment perhaps offer some insight, in that this pathway is less sensitive to Fingolimod treatment with a 9-fold higher EC_{50}. Therefore, perhaps the lack of reported efficacy can be attributed to insufficient Fingolimod exposure in these studies, where the dose used was 1 mg/kg PO QOD. Standard error (SE) values were high for each of the parameters, predominantly caused by the high inter-individual variability in humoral immune response. However, weak definition of maximum effect contributed to poor curve fitting in this region as demonstrated by the high SE, with higher doses required to provide additional data.

The data set generated in study 6 provides an ideal platform to progress into mathematical PKPD model development, with the data used to develop the PKPD model described in chapter 6. With the experimental model fully qualified and the experimental protocol finalised, the next stage was to progress to exploration of the pharmacology of the surrogate CD21/35 specific mAb 7G6.

5.5.4. Efficacy of CD21 neutralisation

The concentration effect relationship for CD21 neutralisation in the IV KLH TDAR experimental model was investigated with the commercial tool mAb 7G6. This was selected

as the most suitable surrogate mAb for concentration effect profiling, despite being limited by the inherent immunogenicity of the rat IgG2b backbone, because it is the best characterised and highest affinity murine CD21 specific mAb (7G6 = 0.05 nM, 4B2 = 1.65 nM, Appendix V). The objective was to test several distinct concentration ranges of 7G6, to allow interpretation of the extent of drug exposure and target engagement required for efficacy. Whilst typical mAb pharmacokinetics are amenable to achieving this extended plasma exposure, mAb 7G6 suffers the impact of TMDD and its accelerated clearance at doses below 2 mg/kg, as characterised in chapter 3. Consequently, to achieve maintenance of low 7G6 plasma exposure, repeated administration was predicted to be essential through simulation of the mathematical PK model developed in chapter 4 (model v2).

5.5.4.1. 7G6 pharmacokinetics

The pharmacokinetics of mAb 7G6 (figure 5.18) were well captured by the mathematical PK model (model v2, chapter 4) when administered at the highest tested dose of 10 mg/kg, showing good prediction of the plasma concentration at all tested time points; 1 h post dose (day 8/12), 2 days post dose (day 6/10) and 4 days post dose (day 16). However, the quality of the prediction degraded both with decreasing dose and with increasing time, at all other tested 7G6 dose concentrations. One reason for the poor model performance would appear to be an under estimation of 7G6 plasma clearance. This is particularly demonstrated by the over prediction of mAb exposure at all dose levels on day 10 (2 days post 3rd dose), resulting from an over prediction of drug accumulation. However, more critically the study suffered from two experimental limitations that are discussed in further detail separately.

The first experimental limitation was that by using low mAb dose concentrations, the impact of non-specific binding is increased, primarily because of saturable binding to the vial. This results in decreased dosing accuracy as the dose concentration itself decreases. Whilst this was a predictable problem, and one that was observed in the PK characterisation studies at the 0.1 mg/kg dose, every effort was taken in this study to minimise its impact. This included using low bind plastic vials, storing stock mAb solutions at high concentration and ensuring dose solution preparation was conducted immediately prior to administration. The second experimental limitation was the immunogenicity of the rat IgG2b backbone of mAb 7G6. Whilst the impact of an ADA response was not observed at any tested dose in the PK characterisation studies, 40% of the mice administered 7G6 in study 1 were suspected of developing an ADA response that resulted in a loss of drug exposure. With this in mind, an assay was developed prior to study initiation for the identification of ADA positive mice.

When implemented in study 7, this assay identified a very high incidence (54%) of ADA positive mice on day 16 (15/28 mice). As would be expected, the response took a period of time to manifest, with a lower observed incidence at earlier time points, where 18% (5/28 mice) were affected on day 12 and only 7% (2/28) on day 10. The mid-range doses were also the worst impacted (1 to 0.03 mg/kg). All animals in the 0.3 and 0.1 mg/kg dose groups were identified as ADA positive, with a resulting loss of plasma exposure by day 16. Consequently, adherence was poor to the PK model simulated exposure at the terminal time point, in all but the 10 mg/kg treatment group. Whilst this did not result in the planned linear range of 7G6 plasma exposures (covering 1000-fold), it did still provide a wide range, particularly over the first 10 study days. Therefore, a platform for concentration effect exploration was still created by the dosing regimen used, albeit somewhat compromised at the terminal time point.

5.5.4.2. 7G6 target engagement

A direct measurement of target engagement was provided by the analysis of CD21/35 expression on peripheral and splenic B cells, providing a link between plasma exposure of mAb 7G6 and the modulation of its target. Whilst previous studies report the impact of a single saturating dose on CD21/35 expression (Kinoshita *et al.*, 1990), here a full concentration range was characterised *in vivo* for the first time (figure 5.20). Day 6 offered the most opportune time point for this analysis, providing a good representation of the 7G6 C_{av} (2 days post 2nd dose). Interestingly, some measure of impact on CD21/35 expression was achieved at all dose levels tested, with decreasing levels of target modulation observed with decreasing drug concentration below 0.3 mg/kg. This data indicates that, despite the high reported doses of 7G6 in literature studies, maintenance of a 1000-fold lower drug exposure (0.1 mg/kg IP every 96 h) can still result in greater than 95% reduction in CD21/35 expression on peripheral B cells. As seen in study 1, the impact of 7G6 treatment on CD21/35 is replicated by the non-competing fluorescent marker 7E9, indicating that it is indeed receptor loss and not epitope blockade that occurs following mAb binding at all tested doses (figure 5.20B).

While target engagement on peripheral B cells offers a convenient measurement that can be taken across the study duration, it is likely that target engagement within secondary lymphoid tissue is essential for efficacy. As a gauge of the value of the peripheral data for prediction of target engagement at the site of action, a direct comparison of peripheral B cells and splenic B cells was made on day 16 (figure 5.20C-F). This comparison identified that the relative expression of CD21/35 on blood and splenic B cells are mirrored, indicating that the blood analysis is a strong predictor of B cell target engagement within the spleen. The impact of the

ADA response on 7G6 exposure is clearly illustrated by the CD21/35 expression data on day 16. Animals identified as having low drug exposure due to an ADA response, are shown to be staging a recovery in CD21 expression on both peripheral and splenic B cells. Whilst not an endpoint expected to be impacted by treatment with the positive control Fingolimod, on both day 6 and 16 the average expression of CD21 on peripheral B cells appears to be reduced. Although not directly measured in this experiment, this is thought to be due to a change in the population of circulating peripheral B cells toward one with a lower CD21 expression. This theory is strengthened by the lack of impact on the CD21/35 expression on splenic B cells.

There is limited reported data describing the expression and kinetics of CD21, particularly following therapeutic intervention, with a complete dearth of quantitative information available in the mouse. To this end, a secondary study objective was to collect quantitative data for both CD21/35 expression on peripheral and splenic B cells and the concentration of the soluble form of CD21/35 in plasma. This information is invaluable for the progression of the mathematical PK model, to provide better predictions of mAb exposure. The first of these objectives was achieved through an alteration in the flow cytometry methodology to allow quantification of the number of CD21/35 receptors present per B cell, through application of Quantibrite bead technology (BD Biosciences). This analysis allows conversion of the typical MFI type data into an average number of bound antibodies per cell which, when antibody binding stoichiometry is 1:1, can be converted into a number of receptors per cell. The binding epitope for mAb 7G6 on murine CD21 has been characterised and mAb – receptor binding stoichiometry is known to be 1:1 (Martin *et al.*, 1991, Molina *et al.*, 1995). As such, this approach was used to enumerate the mean CD21/35 expression on peripheral B cells to be 4389 per cell, with a slightly higher mean of 5426 per splenic B cell. These values are lower than the estimates of CD21 expression on human tonsillar B cells of 12000 per cell reported by Tooze and Bevan (1991) and the cynomolgus monkey estimate on peripheral B cells of 10499 per cell (Appendix VIII), but indicates that CD21 receptor number per cell is reasonably conserved across species.

The second of these objectives was to quantify the plasma concentration of soluble CD21/35, a previously overlooked protein in mouse with no literature reported concentration. The addition of a mAb targeting soluble protein can often drastically alter the kinetics of the typically smaller target protein following mAb binding, resulting in a shift in the total plasma concentration (reviewed in Wang *et al.*, 2008). An entirely novel LC-MS/MS methodology was developed to quantify the concentration of sCD21/35 in the terminal plasma samples, with a value of 12.8 nM determined in the isotype control treatment group. The sCD21/35 plasma

concentration was not impacted by treatment with either mAb 7G6 or Fingolimod, with no impact also observed between the animals receiving the TD KLH challenge and those from the naïve control. This would appear higher than the sCD21 concentration reported in man, with a number of studies reporting this to be in the range of 100 to 600 ng/mL (Masilamani *et al.*, 2004, Singh *et al.*, 2008, Tomita *et al.*, 2012) with median value of approximately 300 ng/mL or 2.38 nM, assuming the shed form has a molecular mass of approximately 126 kDa (Masilamani *et al.*, 2002). The difference is potentially due to the additional sCD35 protein in mouse which cannot be differentiated from sCD21.

5.5.4.3. 7G6 impact on TD immune response

The baseline antigen specific IgG response to the IV KLH challenge was defined by the control treatment group, demonstrating a mean 318-fold response window (baseline vs day 16) and a mean IgG AUC of 49.3 µg.day/mL. This was considerably lower than that observed in the model qualification studies (433-fold / 229 µg.day/mL in study 5, 564-fold / 268 µg.day/mL in study 6), despite the higher 2.4 mg/kg KLH challenge erroneously administered in this study. In contrast, the IgM response window was similar to that observed previously, with a 26-fold response window (baseline vs day 6) and a mean IgM AUC of 2037 µg.day/mL (67-fold / 2283 µg.day/mL in study 5, 28-fold / 1246 µg.day/mL in study 6). An error in the administered volume of the IV challenge from 5 mL/kg to 10 mL/kg, not only resulted in a higher KLH challenge than used previously (2.4 mg/kg) but also an increased volume of PBS. The impact of this difference in challenge is not known but may have resulted in the observed difference in adaptive immune response. Any impact of the isotype control mAb on the antigen specific IgG response can be disregarded by the inclusion of a PBS treated control group in this study, which demonstrated the same diminished IgG response (41.0 µg.day/mL). Despite the lower antigen specific IgG response observed in this study, the positive control demonstrated maintenance of experimental model performance. With daily oral administration of the positive control Fingolimod at 3 mg/kg resulting in a 69% inhibition of the antigen specific IgG response AUC (vs 60% in study 5) and a 66% inhibition of the IgM response AUC (vs 51% in study 5).

Contrary to previous literature (Heyman *et al.*, 1990) and indeed contrary to the data generated in study 1, treatment with mAb 7G6 resulted in a dose dependent exacerbation of the antigen specific IgG response to IV KLH TD challenge (figure 5.22). At its maximum, treatment with 3 mg/kg 7G6 every 96 h resulted in a 674% increase in antigen specific IgG AUC, when

compared with the isotype control. To further unravel this observed exacerbation of the IgG response, the individual contribution of each IgG isoform to the total IgG response was investigated (figure 5.23). This analysis demonstrated that it is antibodies of the IgG2 subclass that are driving this exacerbated response, with considerably enhanced production of both KLH specific IgG2b and IgG2c in mice treated with high dose 7G6, when compared with the isotype control. In contrast, there is no significant difference in the concentrations of KLH specific IgG1 or IgG3 subclass antibodies following treatment with 7G6 at any tested dose. Fingolimod on the other hand appears to inhibit the production of all IgG isotypes equally.

The breakdown of the individual contribution of each IgG isotype to the total antigen specific antibody response does offer one explanation for the apparent absence of IgG exacerbation in study 1. In that the analytical methodology used in study 1 only provided detection of IgG1 class antibodies, showing consistency in the inability of high dose 7G6 to impact the antigen specific IgG1 response in both studies. In contrast to the results of this experiment, in the original work by Heyman *et al.* (1990), treatment with 200 µg 7G6 per mouse (approximately 10 mg/kg) resulted in inhibition of the antigen specific total IgG response to both HRBC and KLH, following IV administration in PBS. Kulik *et al.* (2015), during characterisation of mAb 4B2, demonstrated partial inhibition of the antigen specific IgG1 response to SRBC. Impaired antigen specific antibody production, of all IgG isotypes, was reported in CD21/35 knockout mice in response to TD antigens (Molina *et al.*, 1996, Donius *et al.*, 2013). With this exacerbation of the TD antibody response a unique observation, it was pertinent to question if this was an experimental issue or a true representation of CD21/35 pharmacology. Therefore, to provide confirmation, mAb 4B2 was tested in the same IV KLH TDAR experimental model at 20 mg/kg (Appendix VI). The same exacerbation of the KLH specific IgG response was observed (17-fold increase), driven by an increase in IgG2 subclass antibodies, demonstrating this was not an experimental error and was not unique to the tested mAb.

Whilst being cautious not to over speculate based on limited data, the results of this study do indicate a direct relationship between the anti-CD21/35 mAb and the exacerbation of the KLH specific IgG2 response, that is disconnected from the effect on other endpoints such as the germinal centre B cell response. A potential mechanism that could be imagined is that engagement and/or the subsequent loss of CD21/35 on the B cell (or perhaps even T cell) surface results in a redirection of the immune response to a T-helper type 1 (Th1) polarised response, that is associated with the release of IFNγ from CD4+ T cells and the induction of IgG2. Perhaps occurring in conjunction with a switch to a predominantly extrafollicular rather than germinal centre response. However, further investigation of the mechanisms of this result

would require considerable further experimentation beyond the scope of the present work to explore B and T cell biology in the spleen in the context of KLH immunisation and anti-CD21 treatment. Although the specific IgG isotype breakdown was not investigated at the time, the result is reminiscent of the KLH specific IgG exacerbation seen with the B-cell depleting mAb SA271G2. This similarity perhaps supports the idea that disruption of B cell regulation of T-helper cell differentiation is at the heart of this unexplained result, as proposed for B cell depletion following treatment with anti-CD20 mAbs by Yanaba *et al.* (2008).

In contrast to the impact on antigen specific IgG, prophylactic treatment with mAb 7G6 resulted in a dose dependent inhibition of the antigen specific IgM response to KLH challenge. Maximum inhibition was observed at a dose of 1 mg/kg, resulting in a 91% decrease in antigen specific IgM compared with the isotype control. Inhibition of the primary antigen specific IgM response to TD antigens was observed in the original work with 7G6 by Heyman *et al.* (1990) and was also demonstrated in CD21/35 knockout mice (Molina *et al.*, 1996, Donius *et al.*, 2013). In contrast, Kulik *et al.* (2015) showed the antigen specific IgM response to SRBC was unchanged from control following treatment with 4B2. In agreement with the data generated in study 7 with 7G6, 4B2 was also shown to inhibit (46%) the primary antigen specific IgM response to KLH when administered prophylactically at 20 mg/kg in the IV KLH TDAR experimental model (Appendix VI).

A lower baseline germinal centre B cell response was observed in the spleen in this study, 14 days post IV KLH challenge, compared with the qualification studies ($2.5x10^5$ GC B cells per spleen vs $6.6x10^5$ in study 6). This resulted in no significant difference between naïve and the isotype control, providing no KLH specific response window in this study. The lack of a challenge response in germinal centre B cell number per spleen was replicated in the PBS control. Thus, despite a trend existing toward a reduction in GC B cell number per spleen in the high 7G6 dose groups, no further analysis of this endpoint can be completed. The cause of this smaller GC response is unknown but may be related to the larger immunisation volume in this study, with all previous iterations of the study design having resulted in a significant response.

As proven in study 6, interrogation of the data set as a whole using a nonlinear four-parameter logistic fit relationship, provides a useful approach to coalesce the data set into a single *in vivo* EC_{50} value. Once again, the data for the KLH specific IgG and IgM response was plotted against the logarithm of the 7G6 day 10 plasma concentration, as an approximation of C_{av}. To provide anchor points for curve fitting, the isotype control response data was used along with an arbitrary low 7G6 concentration. The resulting *in vivo* EC_{50} values were 0.1 nM for antigen

specific IgM, along with a value of 4.1 nM for the exacerbated antigen specific total IgG response.

5.6. Chapter conclusion

A mechanistic preclinical PKPD strategy was successfully implemented to expand the known data set describing the *in vivo* pharmacology of CD21 neutralisation in a TD immunisation experimental mouse model. The overarching objective was to produce a data set with which to test the underlying assumptions governing the efficacy and durability of treatment with mAbs that neutralise the function of CD21. The strategy initially focussed on confirmation of efficacy on key translatable endpoints in a classic T-dependent immunisation experimental mouse model. This approach provided confirmation of target engagement by mAb 7G6 and 4B2 on B cells at the site of action in the spleen. However, engagement of the target was only shown to translate into a moderate impact on germinal centre formation, with no observed impact on the primary antibody response to the TD antigen TNP:KLH. The lack of target engagement and efficacy with mAb 9E10 resulted in no further interest in this particular mAb, providing confirmation of earlier observations during PK characterisation in chapters 3 and 4.

The data generated in PKPD study 1 highlighted the limitations of the experimental model format. Not only did the challenge generate a very strong humoral immune response, but interpretation of any impact on this response was restricted to a yes/no scenario that is unsuitable for concentration effect analysis. The strong nature of the response is highlighted by the high percentage of germinal centre B cells identified in the spleen 14 days after challenge, with approximately 8% of the total B cell population identified as GC B cells. This is likely a consequence of the co-administered adjuvant Alum, which primes the immune system to elicit a maximal response. Whilst typically this type of maximal response provides a robust platform with which to test broad spectrum immunosuppressants, it does not align well with the subtle biology of CD21 involvement in B cell activation. Again, whilst TNP conjugation typically provides a handle to measure a fairly uniform antibody response to the small TNP epitope, it resulted here in an extremely narrow response window in which to operate. This, combined with the poor quality reagents available for quantification of TNP specific antibodies in mice, severely hampered the antibody endpoints of the experimental model. With these factors considered, it was identified that a new experimental TDAR model design was required, resulting in a shift in strategy.

The new PKPD strategy involved optimisation of a new experimental format, inclusive of a number of modifications designed to facilitate a mathematical modelling approach to integrate dose, effect and durability (discussed further in chapter 6). The experimental and mathematical models were then qualified using clinically validated tool molecules to confirm performance, prior to application to exploring the *in vivo* pharmacology of CD21 neutralisation. The new experimental approach selected to replace the IP TNP KLH immunisation is actually an adaption of an old experimental approach, inspired by literature from the early 1990's describing the murine CD21 specific mAb 7G6. Here, the original studies used an IV immunisation route combined with a highly immunogenic protein, administered at low challenge doses, to result in a suboptimal TD immune response. The objective was to provide alignment with the unique biology of CD21 which can be considered to behave, in combination with complement, as an immune adjuvant itself. The model reformatting was a success, providing a weaker overall humoral immune response (approximately 1% splenic B cells identified as GC B cells), but with an increased antibody response window in which to test drug efficacy (231/171-fold IgG window at 30 μg/mouse in studies 3 and 4 versus 20-fold IgG1 window in study 1).

The experimental and mathematical models were qualified using the clinically validated treatments Fingolimod and a surrogate of Rituximab. These two treatments target separate strands of the humoral immune response, with Fingolimod primarily targeting the T cell component and Rituximab targeting the B cell component. Drugs targeting the T cell contribution to humoral immunity has become a well explored approach clinically, with a number of recently published clinical trials describing efficacy of T cell targeted therapies on the primary TD neoantigen response. (Examples CD40 / CD28 / ICOSL). Indeed, in the present work, the efficacy of Fingolimod on the humoral immune response was amply demonstrated in the reformatted IV KLH TDAR model, providing an external qualification of the experimental model. Drugs targeting the B cell component of humoral immunity are less well explored, with Rituximab the best described clinically, albeit with a debated level of success on the primary endpoints of the TD neoantigen response. The same is true of the present work, where although the surrogate mAb SA271G2 results in B cell depletion and efficacy on the germinal centre B cell number per spleen and the production of a KLH specific IgM in response to IV KLH immunisation, it also results in exacerbation of the KLH specific IgG response. A number of speculative theories for this inconclusive outcome exist, such as incomplete depletion of certain resistant B cell populations in the secondary lymphoid tissues and changes in the phenotype of the T cell population in response to B cell depletion. However, further exploration of the underlying pharmacology of this response in the mouse TDAR

model are required but remain outside the scope of the current work. Interest in SA271G2 as a model positive control was ultimately ended due to its poor efficacy against the primary model endpoint of antigen specific IgG.

Exploration of the efficacy of Fingolimod in the IV KLH TDAR mouse model was taken further, investigating pharmacology across a wide dose range. This acted as a trial of the study design slated to be applied to expanding the known pharmacology of CD21 neutralisation, testing multiple dose levels with minimal group size. This is a very different study design to that typically used in preclinical studies, with its application in this work an unbridled success. The study successfully generated a valuable data set with which to develop and test a mathematical PKPD model, as discussed in depth in chapter 6. It additionally allowed a simpler modelling approach through curve fitting of the concentration effect data set, providing an estimated *in vivo* EC_{50} for Fingolimod against the primary study endpoints. This revealed the stark similarity in EC_{50} versus the IgG and GC B cell endpoints, but an apparent drop in sensitivity of the IgM endpoint to Fingolimod treatment. This perhaps contextualises other preclinical data claiming limited effect against IgM production as merely insufficient drug exposure. Further experimental work would be required to elaborate this further, particularly considering the contrasting results observed at 3 mg/kg in PKPD study 5, but this resides outside the scope of the current work.

The well characterised rat IgG2b mAb 7G6 was selected over mAb 4B2 for investigation in the qualified IV KLH experimental model to elaborate target pharmacology. This selection was based on the higher measured affinity of 7G6 and the greater body of supporting literature. The study design used to elaborate 7G6 pharmacology closely followed that initially proven with Fingolimod, testing seven distinct dose levels. The study design included a number of additional endpoints aimed at elaborating the effect of mAb treatment on target kinetics to support the mathematical PK model. This yielded several previously unpublished observations, including quantified values of baseline target abundance both membrane associated and soluble, alongside quantification of *in vivo* target engagement across a greater than 1000-fold drug concentration range. These experimentally determined values were implemented into the PK model described in chapter 4, providing previously undescribed insight into the kinetics of CD21/35 in mice. Despite the known risk of immunogenicity with mAb 7G6 going into the study, the incidence of anti-drug antibodies was higher than observed in prior studies, resulting in an undefined impact on study outcome. However, this impact was considered to be confined to the later stages of the study duration, therefore avoiding

compromising the impact of 7G6 treatment on the initiation and propagation of the primary TD antibody response.

In contrast to previously reported literature, in this study treatment with mAb 7G6 was shown to result in a dose concentration dependent exacerbation of the antigen specific IgG response to the TD KLH challenge. This response was identified to be driven by isotypes of the IgG2 subclass, with no impact observed on the IgG1 or IgG3 response. The mechanism by which this unexpected pharmacology occurs is unknown and previously unreported but is speculated to be through a redirection of the immune response to a T-helper type 1 (Th1) polarised response, perhaps as a consequence of changes to the regulatory function of B cells. This unexpected exacerbation is not mirrored in the antigen specific IgM response, which is inhibited in a dose concentration dependent manner, insinuating that treatment with CD21/35 neutralising mAbs does result in a measurable impact on humoral immunity under the test conditions used. To confirm that this is a mechanism driven outcome as opposed to a molecule specific phenomenon, the murine mAb 4B2 was tested under the same experimental conditions using a single prophylactic IP administration at 20 mg/kg, with the same exacerbation of KLH specific IgG observed (Appendix VI). It is important to discover whether this mechanism is unique to the test conditions used in the present work or connected intrinsically to therapeutic modulation of the target. However, this requires considerable further investigation and remains beyond the scope of the present work.

In summary, the data generated from the preclinical PKPD strategy described in this chapter provides a valuable resource to further elaborate the pharmacology of CD21/35 neutralisation in the mouse. Despite the identification of some unexpected biology, the approach generated target kinetics data to support development of a mathematical PK model, as described in chapter 4, whilst providing a data set suitable to develop an integrated PKPD modelling relationship, as described in chapter 6.

Chapter 6:
Development of a mathematical PKPD model to describe the antigen specific antibody response to an IV KLH challenge.

6.1. Chapter introduction

The culmination of the PKPD modelling strategy described in this thesis was the development of an integrative PKPD model that describes the impact of the two tested immunosuppressants, Fingolimod and the surrogate anti-CD21 mAb 7G6, on the progression of the humoral immune response to the T-dependent antigen KLH. Thus in terms of PKPD modelling, there are two distinct elements that require mathematical description; the production of an antigen specific antibody response to KLH immunisation in the absence of drug and the impact of drug on progression of this response following dosing.

In terms of mechanistic understanding, the kinetics of the biological events following KLH challenge are poorly understood. However, it can be roughly outlined as a series of interlinked biochemical and cellular events resulting in the delayed observation of antigen specific antibodies in plasma. This time dependent transduction of the KLH challenge to the observable effect (antibody response) lends itself to a transit compartment modelling approach. A derivation of the basic transit compartment model was described by Yang *et al.* (2015) for this very purpose during the development of the CD28 receptor antagonist, BMS-931699 (Lulizumab pegol). The published work demonstrated that a transit compartment PD model structure could indeed provide an excellent description of the delayed antigen specific IgG response following TD challenge, both in mouse and cynomolgus monkey. Additionally, Yang *et al.* (2015) demonstrated that by linking drug PK via receptor occupancy to the propagation of the effect signal in the PD model, the inhibitory effect of BMS-931699 could be predicted, with strong agreement shown across both species. This led Bristol-Myers Squibb to adopt this PKPD modelling approach to integrate their preclinical knowledge of the drug and target to predict the FTIH starting dose. The Yang *et al.* (2015) signal transduction model was consequently adopted as the starting point in the present work, with the model extended to describe the IV KLH TDAR mouse experimental model data described in chapter 5.

In addition to the time lag in the observed PD response, distribution of the surrogate CD21/35 neutralising mAb (7G6) to the effect site can also be considered to represent a rate limiting step in the present work. Whilst equilibrium between plasma and secondary lymphoid tissue can be considered as rapid for Fingolimod, resulting in no discernible need for an effect compartment, the long distributional time and complex target binding kinetics of 7G6 add the need for effect compartment consideration. To this end, the minimal PBPK model for mAb 7G6 developed in chapter 4 was adopted to mechanistically account for the distributional time to target and provide a suitable PK model with which to link to PD. In addition, due to the

differential modalities and mechanisms of Fingolimod and mAb 7G6, alternative approaches to integration of PK with the PD model were considered. Whilst a measurement of receptor occupancy in plasma was a valid strategy to link the PK of BMS-931699 to PD, this was applicable due to the nature of the drug target and the distributional characteristics of the smaller pegylated dAb. A more complex receptor occupancy strategy may therefore be required to link mAb 7G6 PK to PD. Meanwhile, Fingolimod may be more amenable to an indirect response element using the plasma concentration directly, as a consequence of its rapid equilibrium with the target tissue and rapid interconversion to the active phosphorylated form.

The following results chapter details the evolution of a mathematical PKPD model to describe the impact of Fingolimod and mAb 7G6 on the progression of the TDAR in mouse following primary immunisation with KLH. The concept of model translation to predict clinical effect is also explored, using available clinical data with Fingolimod.

6.2. Mathematical model development

The development of an integrated mathematical PKPD model and all model fitting and simulation was conducted by the author using Simbiology v5.9, an app within the Matlab R2019b software package (MathWorks). Details of selection and progression of the model structure are detailed here, alongside the source of all parameters and the associated equations.

6.2.1. Development of a pharmacodynamic model to describe the KLH induced TDAR

The pharmacodynamic response, defined here as the extent of KLH specific antibodies (IgG or IgM) detected in plasma following TD challenge with KLH, was modelled using Simbiology v5.9, an app within the Matlab R2019b software package (MathWorks). The underlying model structure was based on a signal transduction PKPD model, similar to that published by Yang *et al.* (2015) describing inhibition of the TDAR to KLH in cynomolgus monkey by a surrogate CD28 receptor antagonist for BMS-931699 (Lulizumab pegol). The signal transduction model approach provides a neat method to introduce a time lag between administration of the TD challenge and the appearance of antigen specific antibodies in plasma. The model functions through the administration of an arbitrary stimulus (Stim), producing an effect signal (E1) which can cascade through a series of transit compartments before resulting in the final observed IgG / M response. This series of hypothetical compartments act as a surrogate for the undefined biological processes that occur between TD

challenge and the observed antigen specific antibody response. The transit time between each compartment is defined by τ, with the hypothetical compartment volume fixed as 1 L.

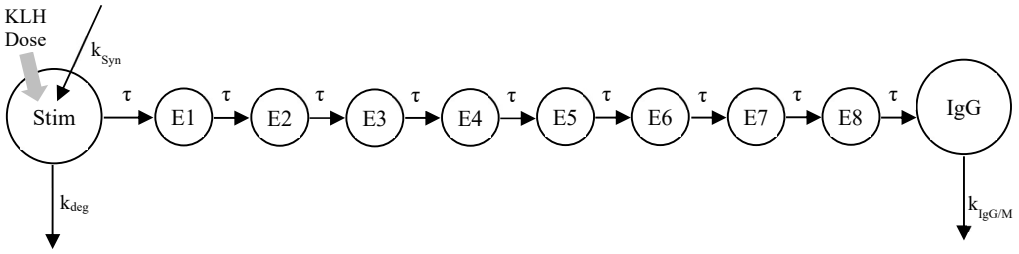

Figure 6.1. Diagram of the transit compartment PD model structure to describe the TD antibody response (IgG / M) in plasma following TD immunisation.

The present work extended this base model structure to expand its utility. To facilitate description of basal non-specific IgG / M, a synthesis route was included for the stimulus (k_{syn}) to allow stable t=0 baseline conditions to be set. Subsequently, this change enables the use of a delayed TD challenge time, paving the way for variable drug pre-treatment periods to be included in an integrated PKPD model. To enhance the relevance of the model and avoid issues relating to the sparse data describing the terminal phase of the IgG response, a literature IgG / M clearance rate (k_{IgG} / k_{IgM}) was applied to the final effect compartment. Finally, due to incomplete understanding of the concentration effect relationship of the KLH TD challenge and the lack of a reliable methodology to monitor its kinetics, an arbitrary stimulus amount was adopted to trigger the effect signal, in a similar manner to that described by Yang *et al.* (2015). Equations 6.1, 6.2, 6.3 and 6.4 define the PD model, with an illustration of the model structure shown in figure 6.1.

Equation 6.1 $$\frac{dStim}{dt} = -\left(\frac{Stim}{\tau}\right) - k_{deg} + k_{syn}$$

Equation 6.2 $$\frac{dE_1}{dt} = \frac{Stim \quad E_1}{\tau}$$

Equation 6.3 $$\frac{dE_{(n)}}{dt} = \frac{E(n-1)-E(n)}{\tau}$$

Equation 6.4 $$\frac{dIgG}{dt} = \frac{E_8}{\tau} - k_{IgG}$$

Where, n = transit compartment number (2 to 20)

Model development was performed using the KLH specific IgG response data generated in PKPD study 5 (chapter 5, 5.3.3). Observed IgG concentrations were interconverted between μg/mL and nM assuming a standard molecular weight of 150 kDa (or 970 kDa for IgM, where required). In the initial phase of PD model development, the number of transit compartments was set to five, as reported by Yang *et al.* (2015), with the reported τ value used as an initial estimate. The initial value of k_{deg} was set to a realistic estimate of 0.12 h^{-1}, equivalent to a 6 h plasma $t_{1/2}$. Initial model conditions (t=0) were defined through modulation of k_{syn}, via an iterative steady state simulation process to achieve the observed basal concentration of KLH specific IgG (0.515 nM). The t=0 conditions for Stim and $E_{(n)}$ were then fixed to the resulting values achieved at steady state, thus providing a stable IgG baseline. The arbitrary KLH TD challenge dose was identified through an iterative process to achieve a value which provides a suitable description of the observed magnitude of the IgG response in study 5. In line with its administration as an IV bolus, the TD stimulus is instantly available, with an arbitrary dose amount of 1000 nmoles used.

The second phase of model development was to optimise the number of transit compartments. Individual models were built including between 2 and 20 transit compartments to interrogate the optimal number, with goodness of fit assessed through visual fit, minimisation of loglikelihood, Akaike information criteria (AIC) and Bayesian information criteria (BIC). Model fitting was performed as a 3-step process using the pooled control data from PD study 5. Initially t=0 conditions were fixed, as described previously, by modulation of k_{syn} via an iterative steady state simulation process using initial estimates of k_{deg} and τ. A constrained nonlinear least squares problems estimation method (lsqnonlin), with a proportional error model, was then used to fit the observed pooled control data to gain model estimates for k_{deg} and τ. Finally, the t=0 conditions were reset using the new estimates of k_{deg} and τ to gain final model values. The visual fit and model fit statistics of the various iterations were then compared to select the optimal compartment number.

6.2.2. Integrated PKPD analysis of Fingolimod in the mouse IV KLH TDAR experimental model

6.2.2.1. Integrated PKPD model development

To describe the inhibitory effect of Fingolimod on the TDAR to KLH, the PD model (section 6.2.1) was linked to the pharmacokinetics of Fingolimod. This was achieved through an indirect response element (equation 6.5) against the transfer rate of the effect signal into the first effect compartment (E1). This effectively installs a 'valve' parameter into the equation defining transmission of the effect signal created by the TD challenge, allowing drug exposure to control the resulting downstream response. In the absence of drug this valve parameter equates to 1, imposing no restriction on transmission of effect. In the presence of drug, as concentration increases the value of this element decreases toward zero, controlled by the parameters E_{max} and EC_{50}.

Equation 6.5

$$\frac{dE}{dt} = \frac{Stim}{\tau}\left(1 - \left(\frac{E_{max} \times drug\_central}{EC_{50} + dr \quad \_central}\right)\right) - \frac{E}{\tau}$$

Description of the pharmacokinetics of Fingolimod was achieved using a simple one compartment PK model, inclusive of oral administration. This employs clearance (Cl_Central), apparent volume of distribution (V_Central), a first order absorption rate constant (ka) and bioavailability (F) to describe the observed blood concentrations of Fingolimod as a function of time. Oral bioavailability (F) was fixed to a value of 0.82, whilst values for Cl_Central, V_Central and ka can be estimated from suitable observed data. The PK model is described through two ODE's (equation 6.6 and 6.7), with the model structure graphically illustrated in figure 6.2. A description of each model species and parameter can be found in table 6.1, listing its source and value (where fixed).

Equation 6.6

$$\frac{d(drug\_central)}{dt} = \left((ka\_central \times dose\_central) - (ke\_central \times drug\_central \times V\_Central)\right) \Big/ V\_Central$$

Equation 6.7

$$\frac{d(dose\_central)}{dt} = -(Cl_{oral} \times dose\_central) - (ka\_central \times dose\_central)$$

Where ka_central = F*ka, ke_central = Cl_central / Central, Cl_Oral = (1-F)*ka

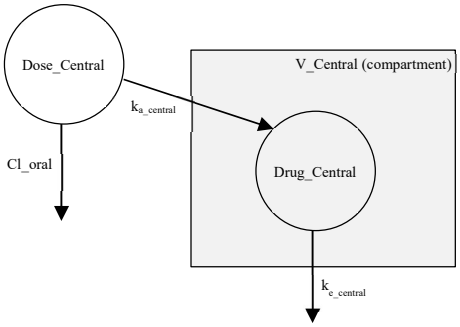

Figure 6.2. Diagram of the one compartment PK model used to describe Fingolimod pharmacokinetics.

Table 6.1. List of parameters and species used to describe the transit compartment and PK models.

Parameter	Value	Unit	Function	Source
PD model parameters				
k_{syn}	-	nM h^{-1}	Rate of baseline Stim formation	Iteratively fit to achieve observed basal KLH specific IgG / M
k_{deg}	-	h^{-1}	Rate of Stim elimination	Modelled value
Stim	-	nmole	TD stimulus	(t_0) steady state simulation
τ	-	h	Transit time of effect signal between compartments	Model estimate, fitted to control group response
k_{IgG} / k_{IgM}	0.0037 / 0.0138	h^{-1}	IgG / M plasma elimination rate	Fixed: Literature $t_{1/2}$ naive murine IgG1 (7.8 d), IgM (2.1 d) (Vieira and Rajewsky, 1988)
$E_{(n)}$	-	nM	Effect signal transit compartment	(t_0) steady state simulation
IgG / M	-	nM	KLH specific IgG signal	(t_0) observed day 0 mean baseline value
KLH challenge dose	1000	nmole	KLH immunisation applied to Stim	Arbitrary assigned value
PK model parameters				
Cl_Central	-	L h^{-1}	Observed blood clearance rate	Modelled value
ka	-	h^{-1}	Oral absorption rate constant	Modelled value
V_Central (compartment)	-	L	Volume of distribution (Vd)	Modelled value
F	0.82		Oral bioavailability	Fixed
$k_{e\_Central}$	Cl_Central / Central	h^{-1}	Drug elimination rate	Model rule
$k_{a\_Central}$	F*ka	h^{-1}	Oral absorption rate	Model rule
Cl_Oral	(1-F)*ka	h^{-1}	Unabsorbed dose elimination rate	Model rule
PKPD model parameters				
E_{max}	-		Maximum inhibitory effect	Modelled value
EC_{50}	-	nM	Concentration of half maximal inhibition	Modelled value

6.2.2.2. Integrated PKPD analysis of Fingolimod (PKPD study 6)

Whilst model development was performed using IgG response data alone, the IgM response is assumed to follow the same general kinetic profile, albeit with a shorter lag time and a faster clearance rate. Consequently, the same model was used to fit both data sets. Initially, to calibrate the model, unique system specific parameters (k_{syn}, k_{deg}, τ and t=0 conditions) were fit to the observed KLH specific IgG / M response achieved in the control group following KLH immunisation at 49 h (chapter 5, 5.3.4). This process was performed in three steps. Initial conditions (t=0) were set to achieve the observed basal concentration of KLH specific IgG / M measured on day 0, through modulation of k_{syn} via an iterative steady state simulation process. A constrained nonlinear least squares problems estimation method (lsqnonlin) with a proportional error model was then used to gain model estimates of k_{deg} and τ, through fitting the observed control data as a naïve pool. Finally, the t=0 conditions were fine tuned to the new estimates of k_{deg} and τ. System parameters were fixed for all further analysis, with these calibrated to the baseline TDAR to KLH immunisation in this experiment.

PKPD analysis of the observed data from PKPD study 6 (chapter 5, 5.3.4) was performed through fitting the concentration effect data set as a naïve pool using a constrained nonlinear least squares problems estimation method (lsqnonlin) with a proportional error model. Initial PK parameter estimates (Cl_central, V_Central, ka) were supplied to ensure robust model fitting, using published rat parameters (Meno-Tetang *et al.*, 2006), as suitable prior PK data in mouse was unavailable. Fingolimod dosing was applied in the model as a daily oral dose at nominal concentration starting on study day 0. The model was initially fit to the observed KLH specific IgG data sets as a naïve pool to gain estimates of Cl_central, V_Central, ka, E_{max} and EC_{50}. This could not be replicated for the IgM data set due to restricting the period of analysis and therefore excluding the intraday PK profile on study day 12. Therefore, the estimates of Cl_Central, V_Central and ka were taken from the IgG PKPD analysis of the same samples and fixed in the model to allow estimation of E_{max} and EC_{50} alone.

6.2.2.3. Integrated PKPD model - clinical translation assessment

Assessment of the translational value of the PKPD model was conducted using the reported clinical data by Boulton *et al.* (2012), where the authors investigated the pharmacodynamic effect of steady state Fingolimod treatment on the TDAR to KLH immunisation in healthy volunteers. The publication provides details of the dosing regimen, a PD profile of KLH specific IgG and IgM over an 8-week period and description of the peak and trough

Fingolimod PK. This provides a useful data set with which to simulate direct translation of the PKPD model, with a caveat that the immunisation protocol differs from that used in the mouse.

The first stage was to identify a set of PK parameters with which to simulate the blood exposure of Fingolimod. The limited nature of the PK reported from the Boulton *et al.* (2012) study, made this data set unsuitable for model fitting. Therefore as an alternative, data was used from an oral, single ascending dose, pharmacokinetic, safety and tolerability study of Fingolimod in healthy volunteers (study FTY720A 2215) reported in the original NDA 22527 submission (CDER). The data was extracted from the reported figure using WebPlotDigitizer (available at https://automeris.io/WebPlotDigitizer. Accessed August 2019) to attain the concentration time data set (dose range 5 to 40 mg) and model fitting was performed to gain estimates of Cl, Vd and ka using a one compartment PK model (figure 6.2 and equations 6.6/6.7). Model estimation was performed using a constrained nonlinear least squares problems estimation method (lsqnonlin) with a proportional error model to fit the mean observed blood concentration data. Bioavailability (F) was set to 0.93, gained from literature reported human PK (David *et al.*, 2012). PK model performance was assessed through its ability to estimate the reported peak and trough Fingolimod concentrations in the Boulton *et al.* (2012) study.

Concentration time values for the KLH specific IgG / M responses reported in Boulton *et al.* (2012) were extracted using WebPlotDigitizer (available at https://automeris.io/ WebPlotDigitizer. Accessed August 2019). System parameters and initial conditions for the PD model were calibrated to achieve the observed KLH specific IgG / M response in the control treatment group. This followed the same process described previously (section 2.2.2), modulating k_{syn} to achieve the observed baseline IgG / M concentration at steady state and fixing the conditions to describe t=0, prior to fitting values for k_{deg} and τ. Due to the different KLH immunisation protocol used in the clinical study, involving three lower dose SC immunisations in adjuvant at one week intervals, and the extended monitoring period, the description of IgG and IgM elimination was altered. The ongoing nature of the response prevents simplification of this elimination rate to that of typical IgG / M as used previously. Therefore, the rate of IgG / M elimination (k_{IgG} / k_{IgM}) was also fitted simultaneously to the observed data. To capture the lower KLH challenge dose and the lower magnitude of the overall response in human, the arbitrary model value for the KLH challenge was reduced to 100 nmoles. Model estimation was again performed using a constrained nonlinear least squares problems estimation method (lsqnonlin) with a proportional error model to fit the observed KLH specific IgG / M data sets as a naïve pool.

6.2.3. Integrated PKPD analysis of 7G6 in the mouse IV KLH TDAR experimental model

6.2.3.1. Integrated PKPD model development

The signal transduction model, successfully developed in section 6.2.1 to describe the TDAR to KLH, was combined with the PK model developed in chapter 4 (PK model v4) to form an integrated PKPD model. To provide a link between PK and PD, the modelled plasma concentration of mAb 7G6 (total) was linked to propagation of the PD effect signal (E_1) via an indirect response element, as previously used for Fingolimod (section 6.2.2). This can be described by a single ordinary differential equation (equation 6.8) allowing drug concentration to regulate the TD antibody response through the drug specific parameters E_{max} and EC_{50}. All other model parameters describing the PK and PD remained as outlined previously, with the integrated model structure graphically illustrated in figure 6.3.

Equation 6.8 $$\frac{dE}{dt} = \frac{Stim}{\tau} * \left(1 - \left(\frac{E_{max} \times Total\_mAb}{EC_{50} + Tot \quad \_mAb}\right)\right) - \frac{E_1}{\tau}$$

Where Total_mAb (plasma) = (free) mAb + (complex) T,s-mAb

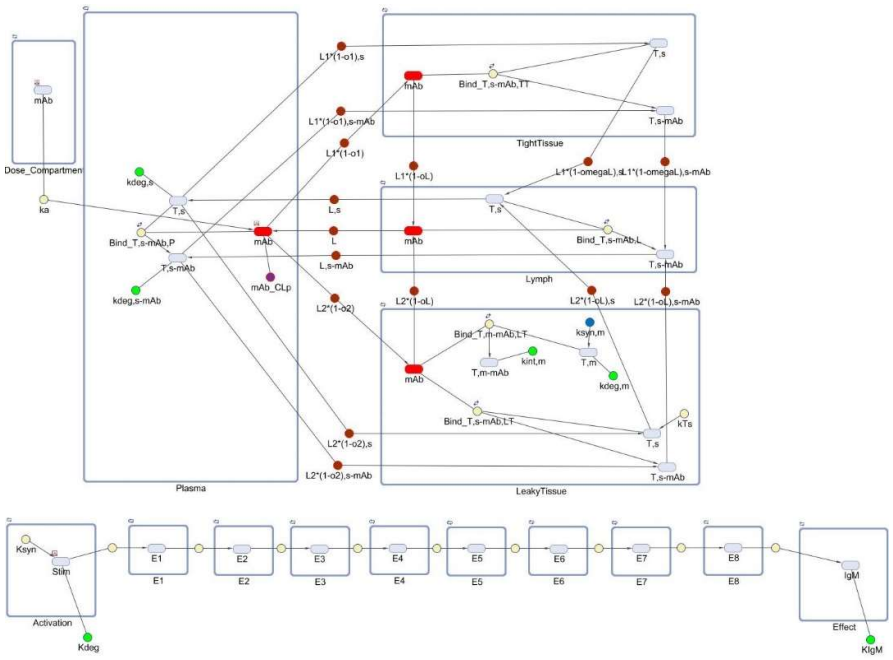

Figure 6.3. Integrated PKPD model diagram, as seen in the Simbiology software package (v5.9) model viewer. Model to describe the PK of mAb 7G6 and its impact on the antigen specific IgM response following TD immunisation.

6.2.3.2. Integrated PKPD analysis of mAb 7G6 (PKPD study 7)

Due to the unexpected IgG response observed in the mAb 7G6 treated groups of PKPD study 7 (chapter 5: 5.3.5), and the unknown translatability of this outcome, PKPD analysis was conducted on the IgM data set alone. Initially, to calibrate the model, unique system specific parameters (k_{syn}, k_{deg}, τ and t=0 conditions) were fit to the observed KLH specific IgM response achieved in the control group following KLH immunisation at 49 h. This process was conducted as described previously for analysis of the Fingolimod data set (section 6.2.2.2). System parameters were fixed for all further analysis, with the model calibrated to describe the baseline response to KLH immunisation in this experiment. The PK of mAb 7G6 was also fixed, as previously described in chapter 4, due to the complexity of the PK model and the sparse nature of PK sampling in this experiment.

PKPD analysis of the observed data from PKPD study 7 (chapter 5: 5.3.5) was conducted to gain model estimates of E_{max} and EC_{50}, through simultaneous fitting of the entire data set. 7G6 dosing was applied in the model as an IP dose every 96 h starting on day 0, using the adjusted doses described in chapter 5. Model estimation was performed using a constrained non-linear least squares problems estimation method (lsqnonlin) with a proportional error model to fit the observed KLH specific IgM data as a naïve pool.

To facilitate the link between EC_{50} concentration and receptor occupancy, a four-parameter logistic fit relationship was established (GraphPad Prism v8.1.2) between total mAb 7G6 plasma concentration and observed receptor occupancy on peripheral B cells in blood on day 6. In the absence of observed mAb 7G6 plasma concentrations for the 0.03 and 0.01 mg/kg dose groups, due to falling below the assay limit of quantification, model simulated values were used instead. The percentage receptor occupancy corresponding to the determined EC_{50} concentration was extrapolated from this relationship.

6.3. Results

6.3.1. Development of a pharmacodynamic model to describe the IV KLH induced TDAR in mice.

A transit compartment based pharmacodynamic model was developed to describe the observed concentration profile of antigen specific IgG in plasma following TD antigen challenge in the mouse. Model development was performed using the control group data generated in PKPD study 5 (chapter 5, 5.3.3), with particular focus on providing description of the basal IgG

concentration, the time delay between challenge and antibody response and the magnitude of the antibody response. Optimisation of the number of transit compartments that comprise the model is a critical element in description of this time delay. Therefore, model iterations were tested containing between 2 and 20 compartments to identify the optimal number. Goodness of fit was evaluated through visual fit of the data, minimisation of loglikelihood, Akaike and Bayesian information criteria (AIC and BIC), as illustrated in figure 6.4 and summarised in table 6.2.

Optimisation of the transit compartment number identified that model performance in description of the delayed onset of the IgG response could be improved through inclusion of additional compartments above the initial five, as confirmed by visual fit and minimisation of loglikelihood (figure 6.4 and table 6.2). Visually, optimal performance is achieved at eight to ten transit compartments, maximising the time delay but retaining fit of the profile up to day 16. Although continued minimisation of loglikelihood, AIC and BIC can be achieved with transit compartment numbers up to sixteen, this additional complexity yields incrementally smaller improvements and a slow degradation of visual fit (table 6.2). Consequently, eight transit compartments were selected to be included in the final model as a compromise between complexity and performance. The model estimates of k_{deg} and τ, following fitting to the control IgG response data, were 0.0946 h^{-1} (SE 0.0234) and 21.4 h (SE 2.1) respectively. All other final model parameters are shown in table 6.3.

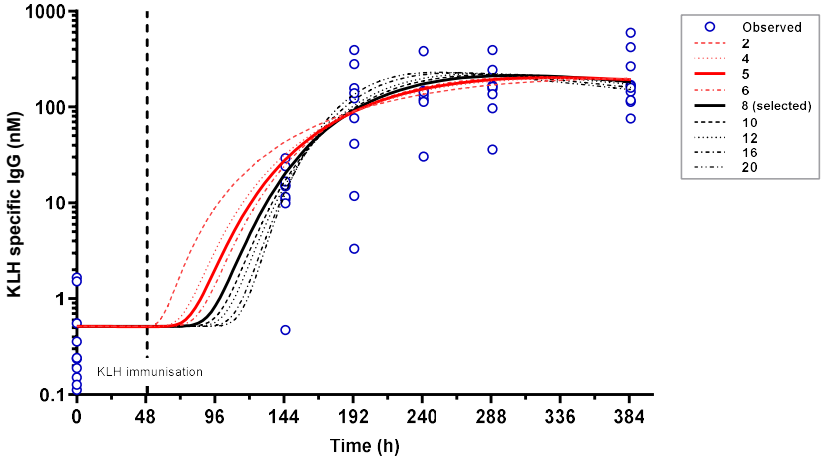

Figure 6.4. Graphical illustration of the impact of transit compartment number on the fit of the PD model to the observed KLH specific IgG response data from PKPD study 5, following IV KLH immunisation at 1.2 mg/kg to the male C57BL/6 mouse. Simulations were performed with model iterations containing between 2 and 20 transit compartments, illustrated as simulation (lines) overlain with the observed individual KLH specific IgG concentration.

Table 6.2. Fit comparison statistics for the model iterations containing an increasing number of transit compartments, including visual fit, loglikelihood, AIC and BIC.

No. Transit Compartments	Loglikelihood	AIC	BIC	Visual Fit
2	-292.6	589.1	593.2	Poor
4	-289.9	583.8	587.9	Moderate
5	-288.7	581.4	585.5	Moderate
6	-287.6	579.1	583.2	Moderate
8	-285.6	575.2	579.3	Good
10	-284.2	572.4	576.5	Good
12	-283.3	570.5	574.6	Good
16	-282.7	569.4	573.4	Moderate
20	-283.0	570.0	574.1	Moderate

The finalised PD model was used to simulate the KLH specific IgG response profile for comparison with the observed data (figure 6.5). This highlights that the model provides a good fit of the IgG response across the full time profile and is thus considered to be fit for purpose. The PD model also achieves description of the basal IgG concentration (0.515 nM), providing the desired model utility to allow for the delayed IV KLH immunisation at 49 h. Figure 6.5 additionally illustrates the high inter-individual variability in observed IgG response, confirming the need for a large control group size to provide sufficient antibody response data for model fitting. This is supported by the low CV% for the model estimates of k_{deg} (25%) and τ (10%).

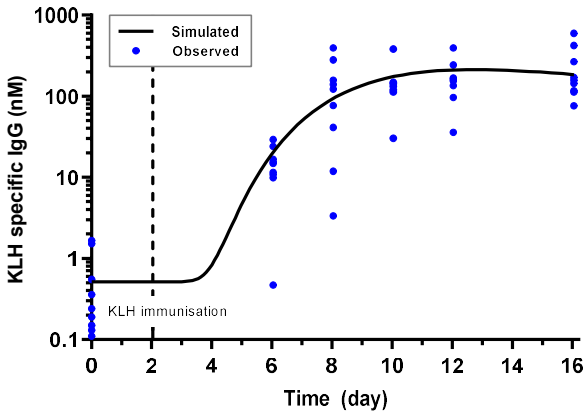

Figure 6.5. Simulation of the IgG response to KLH immunisation at 49 h in the C57BL/6 mouse, using the final PKPD model. Data illustrated as the simulated profile (line) overlain with the observed individual concentrations of KLH specific IgG from PKPD study 5 (symbols).

Table 6.3. PD model parameters and initial conditions to describe the KLH specific IgG response in the control treatment group of PKPD study 5.

Parameter	Unit	Source	Value	Standard Error
k_{syn}	nM h^{-1}	Simulated	0.00576	-
k_{deg}	h^{-1}	Model Estimate	0.0946	0.0234
Stim (t=0)	nM	Simulated	0.0408	-
τ	h	Model Estimate	21.4	2.05
k_{IgG}	h^{-1}	Fixed (literature)	0.0037	-
$E_{(n)}$ (t=0)	nM	Simulated	0.0408	-
IgG	nM	Observed	0.515	-
KLH challenge dose	nmole	Fixed (arbitrary)	1000	-

6.3.2. PKPD model qualification with Fingolimod

6.3.2.1. Integrated PKPD analysis of Fingolimod in the mouse IV KLH TDAR experimental model (PKPD study 6)

An integrated PKPD analysis of the efficacy of Fingolimod in the mouse IV KLH TDAR experimental model was performed (PKPD study 6). System parameters were initially calibrated to describe the KLH specific IgG / M response achieved in the study control group, defining initial conditions and estimating values of k_{deg} and τ, with the final parameter values listed in table 6.4.

Table 6.4. Calibrated PD model parameters and initial conditions to describe the KLH specific IgG / M response in the control treatment group of PKPD study 6.

Parameter	Unit	Source	Value (IgG / IgM)	Standard Error (IgG / IgM)
k_{syn}	nM h^{-1}	Simulated	0.00452 / 0.296	-
k_{deg}	h^{-1}	Model Estimate	0.0528 / 0.198	0.0120 / 0.0181
Stim (t=0)	nM	Simulated	0.0471 / 0.950	-
τ	h	Model Estimate	23.2 / 8.83	1.61 / 0.566
k_{IgG} / k_{IgM}	h^{-1}	Fixed (literature)	0.0037 / 0.0138	-
$E_{(n)}$ (t=0)	nM	Simulated	0.0471 / 0.950	-
IgG / M	nM	Observed	0.549 / 7.80	-
Dose: KLH immunisation	nmole	Fixed (arbitrary)	1000	-

The calibrated model was then used to simulate the IgG / M response profiles to IV KLH immunisation (49 h), with the resulting profiles compared against the observed control group data in figure 6.6. This demonstrates that the calibrated PD model provides a good prediction of the observed mean profiles for both KLH specific IgG (figure 6.6A) and IgM (figure 6.6B), capturing the time delay in the observed response and the shape of the response profile. Due to the observed increase in IgM response on day 16, consistent with observations in other studies, the data for this time point was excluded from analysis.

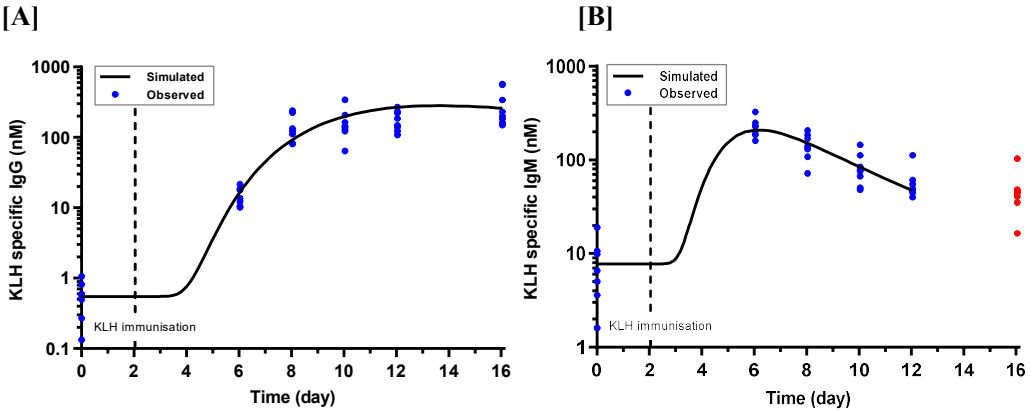

Figure 6.6. Simulation of the calibrated PD model to describe the observed control group KLH specific **[A]** IgG and **[B]** IgM concentration in plasma following IV KLH challenge at 49 h (n=8) in PKPD study 6. Data illustrated as the model simulated profile (line) overlain with the observed individual concentrations of KLH specific IgG / M from PKPD study 6 (symbols), with red symbols indicating excluded samples.

PKPD analysis of the Fingolimod dose response data set was completed separately for IgG and IgM, through simultaneous fitting of all dose groups using a naïve pooled approach. Through fitting the IgG data set, the model was used to gain estimates of clearance (Cl_Central), volume (V_Central), absorption rate (k_a), EC_{50} and E_{max} (table 6.5). Analysis of the IgM data set was restricted to 289 h (12 days), therefore the PK parameter estimates (Cl_Central, V_Central and k_a) from fitting the IgG dataset were used to estimate the E_{max} and EC_{50} only. The resulting model fit plots are shown in figure 6.7A (IgG) and 6.7B (IgM), showing predicted versus observed at each individual dose level and demonstrating the strong performance of the model across the full dose range. The resulting EC_{50} and E_{max} estimates were 4.59 nM (SE 3.09) and 0.639 (SE 0.122) respectively for IgG, 408 nM (SE 210) and 1.00 (SE 0.00002) respectively for IgM. Model estimated PK and PKPD parameters values are shown in table 6.5.

[A]

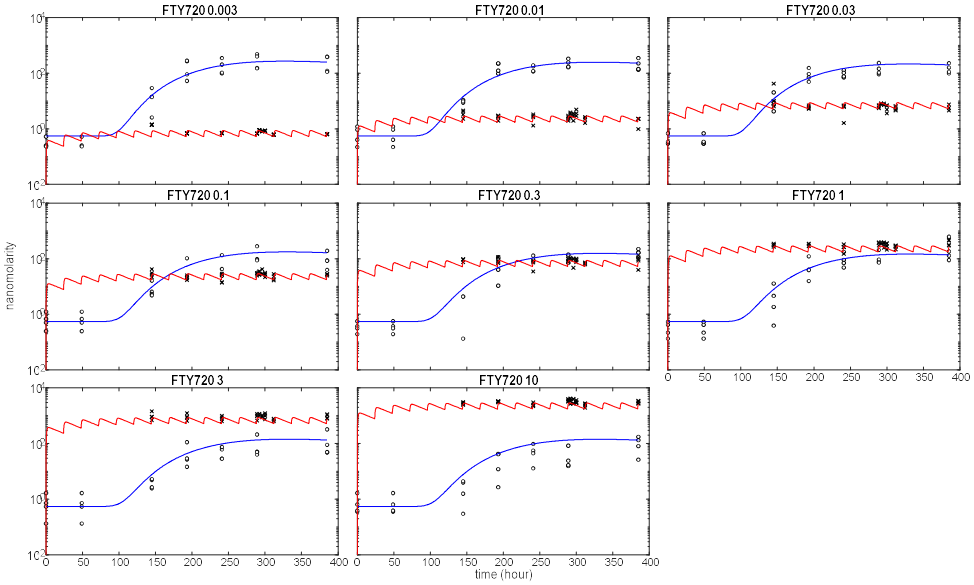

[B]

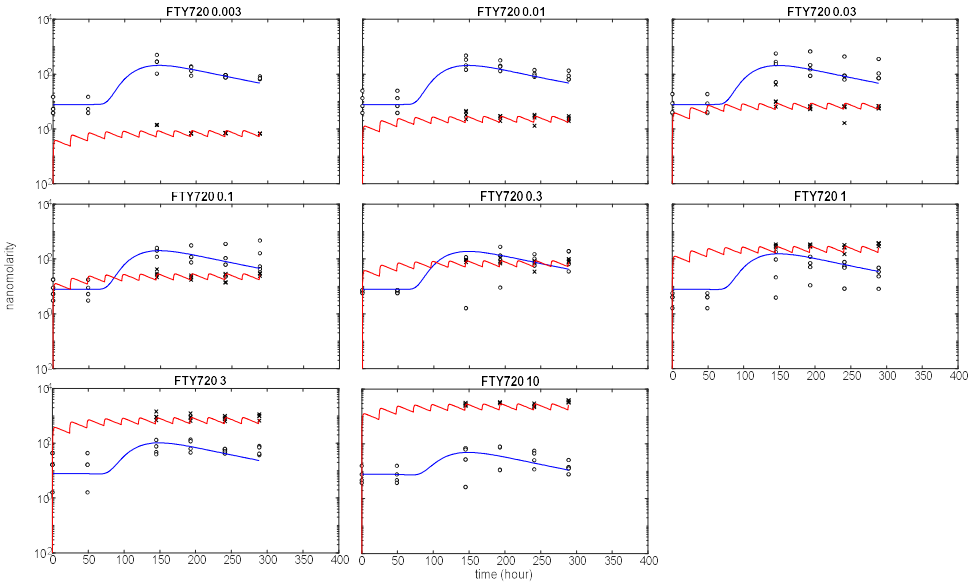

Figure 6.7. Model fit plots depicting the predicted (line) versus observed (symbol) data for Fingolimod blood exposure (red) and KLH specific antibody concentration in plasma (blue) for **[A]** IgG and **[B]** IgM. Observed data (symbols) from PKPD study 6.

Table 6.5. Fingolimod PK and PKPD model estimated parameter values following daily PO treatment in the IV KLH TDAR mouse experimental model.

Parameter	Unit	Source	Value (IgG / IgM)	Standard Error (IgG / IgM)
Cl_Central	L h^{-1}	Model Estimate	0.0119	0.0002
k_a	h^{-1}	Model Estimate	1.09	0.155
V_Central (compartment)	L	Model Estimate	0.484	0.0629
E_{max}	-	Model Estimate	0.639 / 1.00	0.122 / 0.00002
EC_{50}	nM	Model Estimate	4.59 / 408	3.09 / 210

Model performance was assessed through visual inspection of the profiles, residual error and comparison of the predicted versus observed data. This assessment highlighted the strong model prediction of the observed Fingolimod blood concentration, maintained across the 3000-fold tested dose range. The vast majority of the predicted Fingolimod concentration values fall within 2-fold of the observed value (figure 6.8A). Despite high inter-individual variability in the observed KLH specific IgG response data, model performance was also strong in providing simulated IgG concentrations that were mostly within 2-fold of the observed values (figure 6.8B).

The observed KLH specific IgM response data contained a much larger extent of inter-individual variability, resulting in a wider spread of residual error. Despite this and the lack of data in the early part of the IgM response, the model provides a good fit of the observed plasma profiles across all dose levels (6.7B). When the model simulated values are plotted against the observed data (figure 6.8C) model performance can be visualised, with the simulated values largely within 2-fold of the observed.

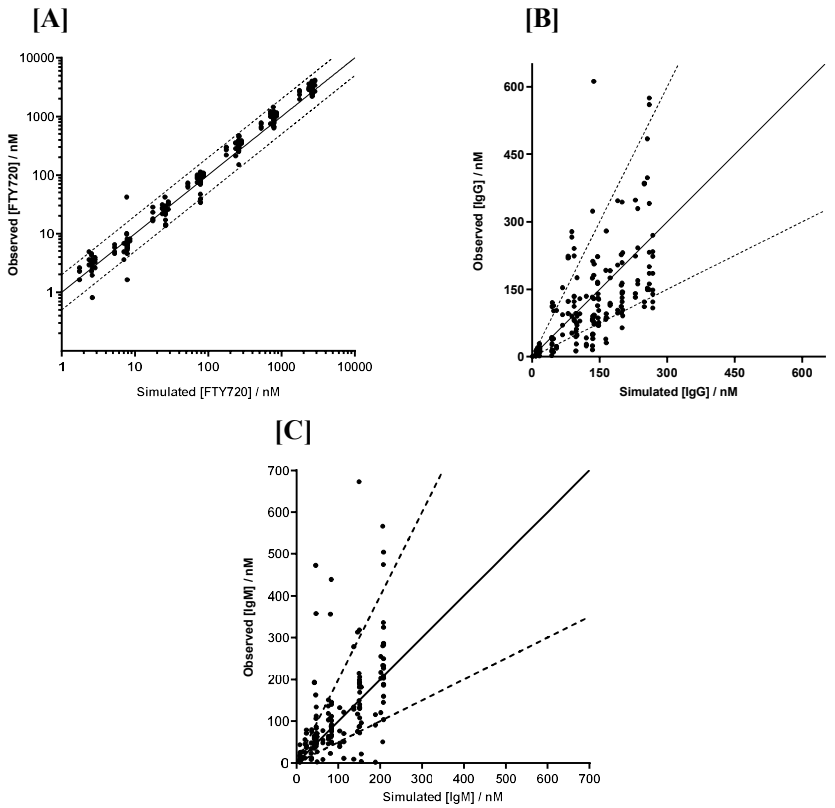

Figure 6.8. Observed data versus model simulated estimates of **[A]** Fingolimod blood concentration **[B]** KLH specific IgG **[C]** KLH specific IgM plasma concentration. Line of unity (solid), 2X and 0.5X (dotted). Observed data from PKPD study 6.

The simulated KLH specific IgG / M profiles at each dose level (figure 6.9A/B) were evaluated using the area under the effect curve (AUEC) for comparison with the mean observed AUEC from PKPD study 6 (figure 6.9C/D). This provides an integrated illustration of the performance of the model in describing the observed inhibition of KLH specific antibody production by Fingolimod. While model description of the baseline IgG response in the control group is strong, visually it would appear to underpredict the maximum observed effect (E_{max}) at the higher tested Fingolimod doses (figure 6.9C). In contrast, the model underpredicts the true IgM baseline, despite providing good description of the control group data (figure 6.9D). This would appear to be because of the high inter-individual variability, with the ineffective low Fingolimod dose groups having higher mean observed AUEC than the control. However, model description of the overall profile of inhibition of the IgM AUEC is reasonable, with a higher model estimate of E_{max} (1.00) when compared with IgG (0.639).

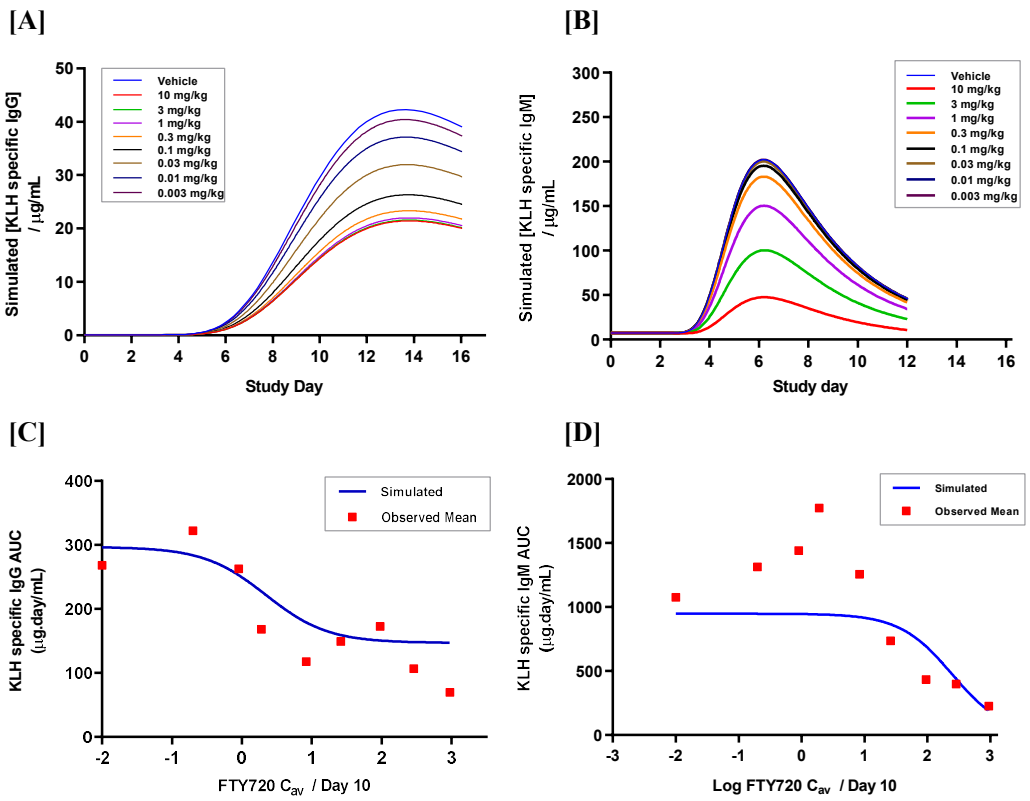

Figure 6.9. PKPD model simulations of the KLH specific **[A]** IgG and **[B]** IgM response profiles following daily PO treatment with Fingolimod across the range 0.003 to 10 mg/kg in the IV KLH TDAR mouse experimental model (PKPD study 6). Further analysis of the same data by calculating the area under the effect curve (AUEC) of **[C]** IgG and **[D]** IgM versus the log10 mean concentration of Fingolimod on day 10. Data illustrated as mean AUEC (symbol) n=4 from PKPD study 6 versus the PKPD model simulated AUEC (line).

The merit of the presented PKPD model, along with the strength of the E_{max} and EC_{50} estimates, were evaluated through cross validation against PKPD studies 5 and 7, which included Fingolimod treatment groups (3 mg/kg, PO daily). Cross validation was achieved by firstly calibrating the PD model system parameters to the observed control group, prior to simulating the Fingolimod treatment outcome using the PK parameters and estimates of E_{max} and EC_{50} obtained from analysis of PKPD study 6, presented in table 6.5. The resulting model simulations are compared against the observed plasma concentrations of KLH specific IgG and IgM in figure 6.10. This cross validation clearly demonstrates the predictive value of the IgG model, with the observed result overlaying the simulation for both PKPD study 5 (figure 6.10A) and PKPD study 7 (figure 6.10B). Disappointingly this predictive power is not mirrored by the IgM model, with poor prediction of the results from PKPD study 7

(figure 6.10D), whilst no effect was observed in PKPD study 5 following 3 mg/kg daily PO Fingolimod treatment (figure 6.10C).

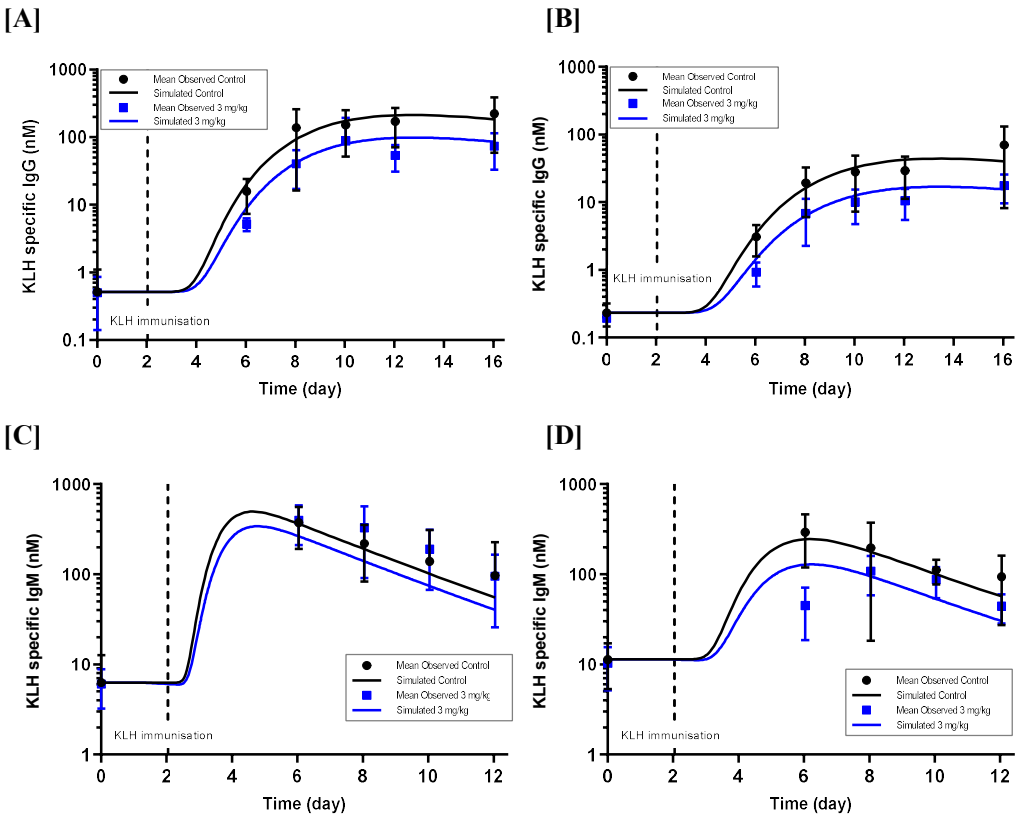

Figure 6.10. Cross validation of the PKPD model and the estimates of E_{max} and EC_{50} through simulation of the KLH specific IgG / M response to IV KLH immunisation following treatment with 3 mg/kg Fingolimod in PKPD study 5 **[A/C]** and PKPD study 7 **[B/D],** overlain with the observed mean KLH specific IgG / M plasma concentrations in these studies. Simulation illustrated as the solid line, overlain with the observed mean (symbol) ± SD (bar).

6.3.2.2. Translational value of the integrated PKPD model

The predictive and translational value of the preclinical mouse model was assessed through its ability to predict clinical outcome. Clinical evaluation of the pharmacodynamic effects of daily oral Fingolimod treatment on TD antibody response in healthy volunteers has been reported previously by Boulton *et al.* (2012), providing the ideal data set to explore. This reported data set was digitised and evaluated using the integrated PKPD model. Initially the PD model was

calibration against the IgG / M response observed in the control treatment group, prior to model simulation using human PK estimates and the derived E_{max}/EC_{50} values gained in the preclinical experiments (table 6.5).

In the absence of Fingolimod blood concentration time profiles alongside the reported PD in Boulton *et al.* (2012), a PK model was required to provide a means to estimate the observed Fingolimod exposure. To achieve this, reported data from an oral, single ascending dose, pharmacokinetic, safety and tolerability study in healthy volunteers (CDER, 2009) was used to gain parameter estimates for a one compartment PK model. The fit of the resulting model to the observed data at each reported dose level (5 to 40 mg) are shown in figure 6.11, with the model estimates of clearance (Cl_Central), volume of distribution (V_Central) and the absorption rate constant (k_a) listed in table 6.6. A one compartment PK model was found to provide a good fit of the observed healthy volunteer PK data (CDER, 2009), capturing both the initial absorption and terminal phases of the Fingolimod blood concentration profile across all tested dose concentrations (figure 6.11). Based on the goodness of fit, a more complex PK model was deemed unnecessary.

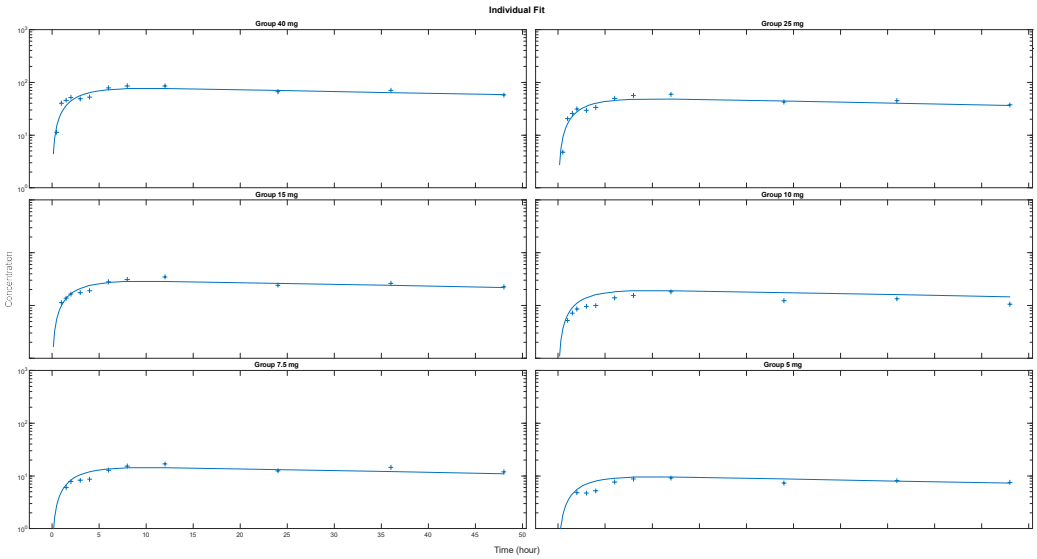

Figure 6.11. Model fit plots depicting the predicted (line) versus observed (symbol) Fingolimod blood concentration data using a one compartment PK model to describe the observed data from an oral, single ascending dose, pharmacokinetic, safety and tolerability study in healthy volunteers. Data digitised from the Fingolimod new drug application (NDA) submission 22-527 (CDER, 2009).

Table 6.6. One compartment PK model parameter estimates to describe the blood exposure of Fingolimod following oral administration to healthy volunteers.

Parameter	Unit	Source	Value	Standard Error
Cl_Central	L h^{-1}	Model Estimate	11.4	2.2
k_a	h^{-1}	Model Estimate	0.382	0.038
V_Central (volume)	L	Model Estimate	1450	63
F		David *et al.* (2012)	0.93	-

The reported plots of KLH specific IgG / M response from Boulton *et al.* (2012) were again digitised and PKPD model fitting was conducted to the extracted data. Model system parameters were again calibrated to the control group IgG / M responses, to define the initial conditions and estimate values of k_{deg} and τ. The clinical repeat challenge protocol does result in a differing terminal phase of the IgG / M responses when compared with the mouse, with a model fitted elimination rate constant (k_{IgG} / k_{IgM}) replacing the literature value of typical IgG / M clearance. Model performance in simulation of the observed control response is illustrated in figure 6.12, demonstrating excellent description of both the magnitude of the response and the prolonged terminal phase. The model is limited by the available data to fit the early phase of the TDAR, however still provides a reasonable description of the observed time lag to response onset. Final model parameters and initial conditions are shown in table 6.7.

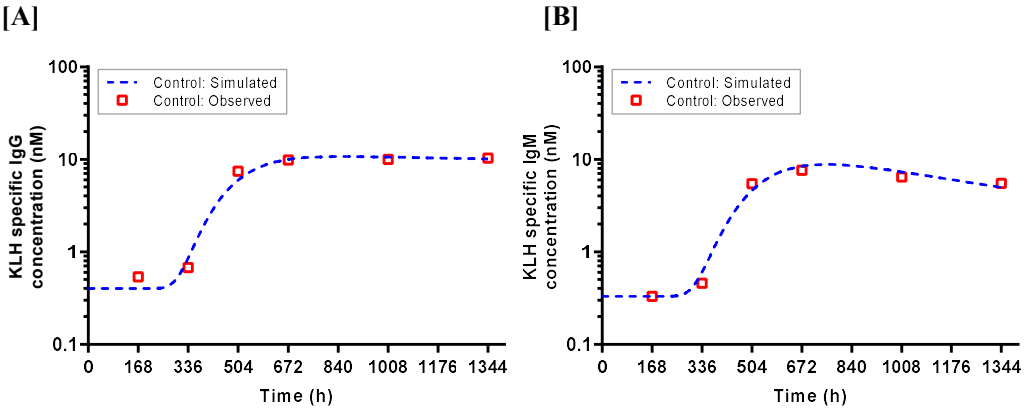

Figure 6.12. Calibrated PD model description of the observed KLH specific IgG **[A]** or IgM **[B]** responses to TD immunisation in healthy volunteers. Observed data obtained by digitising the plots of mean plasma IgG / M response reported in Boulton *et al.* (2012), with permission from John Wiley & Sons.

Table 6.7. Calibrated PD model parameters and initial conditions, describing the specific IgG / M response in control treated healthy volunteers following KLH immunisation (Boulton *et al.*, 2012).

Parameter	Unit	Source	Value (IgG / IgM)	Standard Error (IgG / IgM)
k_{syn}	nM h^{-1}	Simulated	0.000546 / 0.00338	-
k_{deg}	h^{-1}	Model Estimate	0.190 / 0.151	0.055 / 0.024
Stim (t=0)	nM	Simulated	0.00256 / 0.0197	-
τ	h	Model Estimate	42.7 / 48.0	4.7 / 6.4
k_{IgG} / k_{IgM}	h^{-1}	Model Estimate	0.000149 / 0.0012	0.000267 / 0.000228
$E_{(n)}$ (t=0)	nM	Simulated	0.00256 / 0.0197	-
IgG / M	nM	Observed	0.402 / 0.331	-
KLH challenge dose	nmole	Fixed (arbitrary)	100	-

Integration of the calibrated PD model with the parameterised one compartment PK model was achieved via an indirect response relationship, as described for the preclinical model. This integrated model was used to simulate the impact of daily oral Fingolimod treatment on the antigen specific IgG / M response to KLH immunisation in healthy volunteers, using the mouse derived E_{max} and EC_{50} values of 0.639 / 4.59 nM and 1.0 / 408 nM for IgG and IgM respectively. The resulting simulations, shown in figure 6.13, were overlain for comparison with the mean observed plasma concentrations of IgG or IgM, digitised from Boulton *et al.* (2012). The integrated PKPD model was shown to provide a reasonable description of the limited Fingolimod blood concentration data in the Boulton *et al.* (2012) study, with the model predicted values within 2-fold of the observed concentrations (figure 6.13C). Where at 672 h (4 weeks) the predicted versus observed values were 5.13 nM versus 8.46 nM at the 0.5 mg dose and 12.83 nM versus 25.37 nM at the 1.25 mg dose. In addition, the model provides a reasonable projection of the observed impact on the KLH specific IgG response at each dose (figure 6.13A), but underpredicts the observed impact at the 1.25 mg dose. However, the model cannot predict the observed impact on KLH specific IgM (figure 6.13B), with no effect predicted at either dose.

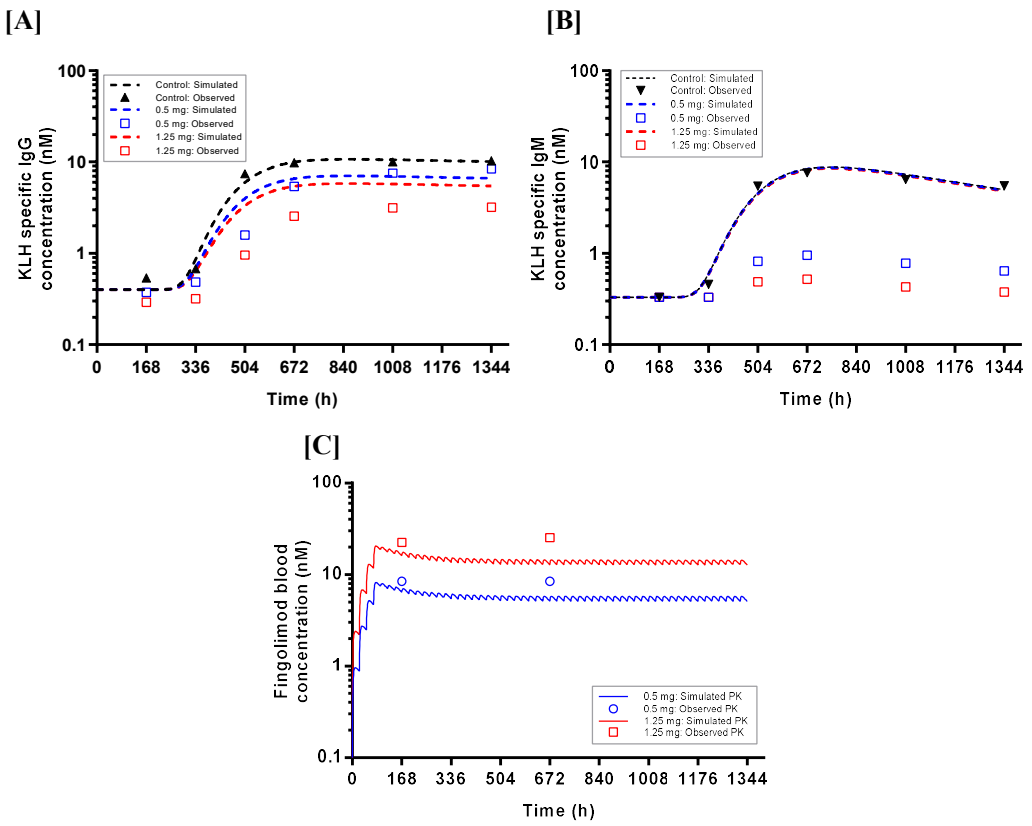

Figure 6.13. PKPD model simulated KLH specific **[A]** IgG or **[B]** IgM plasma response to KLH immunisation in healthy volunteers when treated with either control (black), 0.5 mg (blue) or 1.25 mg (red) oral Fingolimod daily. **[C]** PKPD model simulated Fingolimod blood exposure. Data illustrated as the model simulations (lines), overlain with the observed data (symbols), digitised from Boulton *et al.* (2012) with permission from John Wiley & Sons.

For comparison, reported values of Fingolimod EC_{50} (3.9 nM) and E_{max} (0.903) were used to evaluate model performance, gained from the reported PKPD analysis of peripheral lymphocyte reduction in clinical studies (CDER, 2009). This analysis, shown in figure 6.14, clearly shows that the impact on IgG response can be well predicted using the mechanistic human EC_{50}/E_{max} values, providing improved description of the maximal effect at the 1.25 mg dose. Conversely, the magnitude of the antigen specific IgM response remains unpredicted by the model when using these parameter estimates.

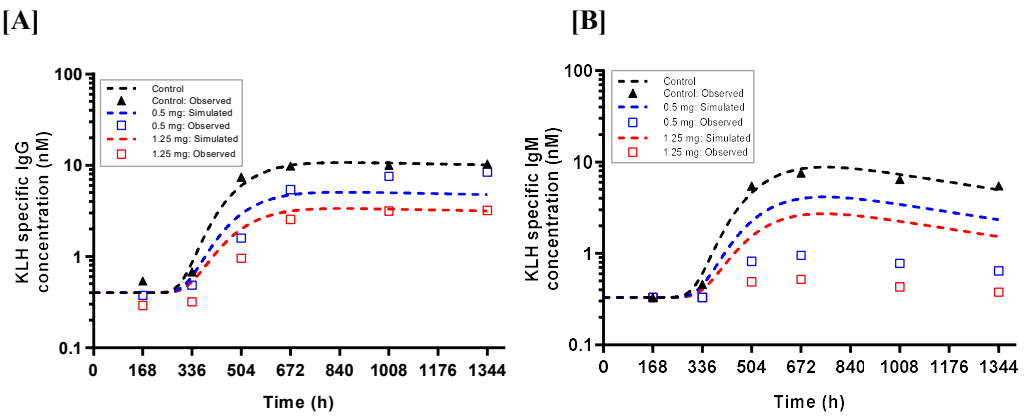

Figure 6.14. Human E_{max} / EC_{50} values (0.903 / 3.9 nM) substituted into the PKPD model to simulate the KLH specific **[A]** IgG or **[B]** IgM plasma response to KLH immunisation in healthy volunteers, when treated daily with either control (black), 0.5 mg (blue) or 1.25 mg (red) oral Fingolimod. Data illustrated as the model simulation (lines), overlain with the observed data (symbols), digitised from Boulton *et al.* (2012) with permission from John Wiley & Sons.

6.3.3. Integrated PKPD model to describe the effect of mAb 7G6 in the mouse IV KLH TDAR experimental model (PKPD study 7)

An integrated PKPD analysis of the efficacy of the murine surrogate anti-CD21/35 mAb 7G6 in the mouse IV KLH TDAR experimental model was performed (PKPD study 7, chapter 5 5.3.5). The analysis was conducted on the IgM dataset alone, due to the unexpected IgG response in that study. System parameters were once again calibrated to describe the KLH specific IgM response achieved in the study control group, defining initial conditions and estimating values of k_{deg} and τ, with the parameter values listed in table 6.8. The calibrated base PD model provided a good prediction of the observed mean KLH specific IgM profile following KLH immunisation (49 h), capturing the extent and profile of the response (figure 6.15). Consistent with earlier studies, day 16 data were excluded due to the observed increase in response. The model estimates of k_{deg} (0.155 h^{-1}) and τ (8.77 h) agreed with those identified for PKPD study 6 in section 6.3.2 (k_{deg} = 0.198 h^{-1} and τ = 8.83 h). Thus, demonstrating the repeatability of the experimental model, with a consistent TDAR to the IV KLH immunisation achieved across studies.

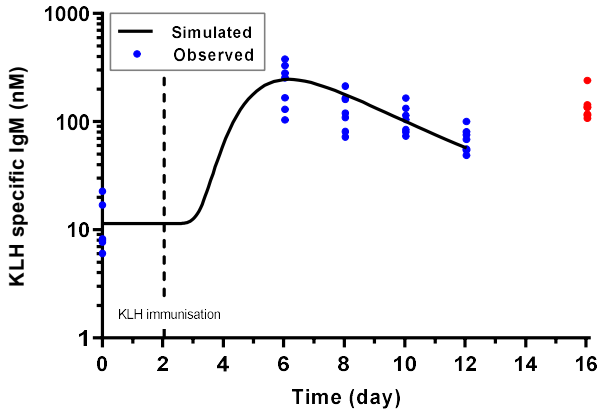

Figure 6.15. Simulation of the calibrated PKPD model to describe the observed control KLH specific IgM plasma response in the C57BL/6 mouse following IV KLH challenge at 49 h. Data illustrated as the model simulated profile (line) overlain with the observed individual concentrations of KLH specific IgM from PKPD study 7 (symbols), with red symbols indicating excluded samples.

Table 6.8. Calibrated PD model parameters and initial conditions to describe the observed KLH specific IgM response to IV KLH immunisation in the control treated group (isotype control) of PKPD study 7.

Parameter	Unit	Source	Value (IgM)	Standard Error (IgM)
k_{syn}	nM h^{-1}	Simulated	0.372	-
k_{deg}	h^{-1}	Model Estimate	0.155	0.0224
Stim (t=0)	nM	Simulated	1.38	-
τ	h	Model Estimate	8.77	0.848
k_{IgM}	h^{-1}	Fixed (literature)	0.0138	-
$E_{(n)}$ (t=0)	nM	Simulated	1.38	-
IgM	nM	Observed	11.44	-
KLH challenge dose	nmole	Fixed (arbitrary)	1000	-

The complexity of the pharmacokinetic model for mAb 7G6 and the sparsity of plasma concentration data collected in PKPD study 7, due to welfare restrictions on procedure number, meant it was unfeasible to fit the observed plasma PK. Consequently, all parameters pertaining to mAb pharmacokinetics were fixed to those described in chapter 4 (PK model v4, table 4.3). Additional PK complexity was delivered by the observed ADA formation to 7G6,

which resulted in severely impaired plasma exposure in most treatment groups by study day 16. This, combined with the increase in IgM response on day 16 in the control group, led to PKPD analysis being restricted to the first 12 days. With the PK parameter values fixed, the model was used to gain estimates of EC_{50} and E_{max} through fitting of the KLH specific IgM data from PKPD study 7 as a naive pool. The resulting simulated versus observed plots at each individual dose level are shown in figure 6.16. The integrated PKPD model provided a reasonable estimation of the observed plasma exposure of mAb 7G6 across the tested dose range. Albeit while underpredicting the impact of target mediated clearance, exemplified by the increasingly poor estimation of day 10 exposure with decreasing dose. The model also provides strong prediction of the observed plasma KLH specific IgM concentration at all tested dose levels. Resulting estimates of EC_{50} and E_{max} were 0.125 nM (SE 0.020) and 0.852 (SE 0.002), respectively (table 6.9).

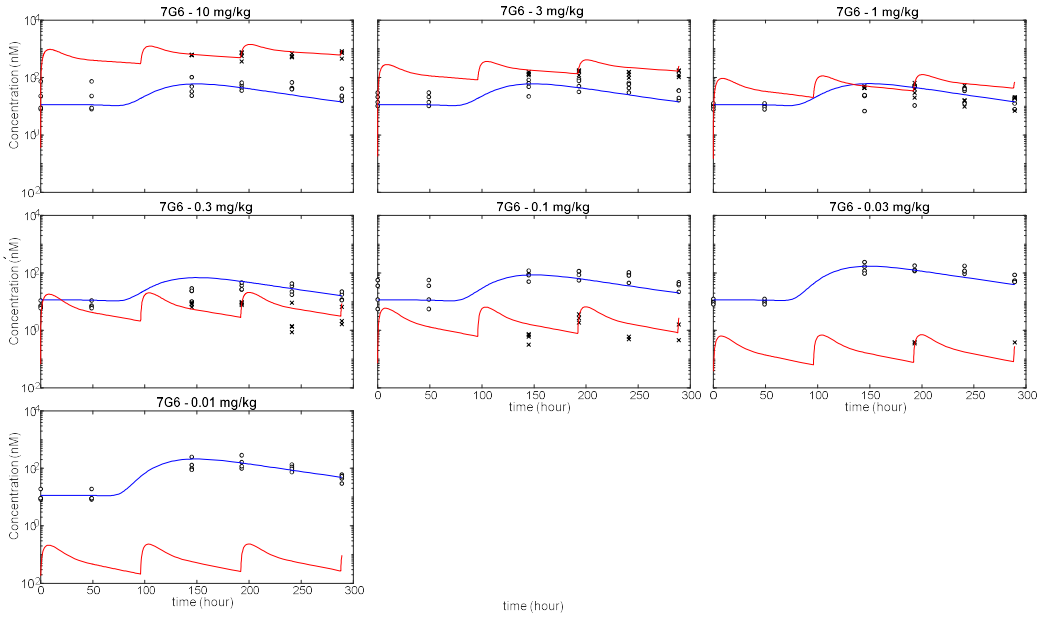

Figure 6.16. Model fit plots depicting the predicted (line) versus observed (symbol) data for 7G6 plasma exposure (red) and KLH specific IgM concentration in plasma (blue). Observed data (symbols) from PKPD study 7.

Table 6.9. Estimated PKPD parameter values for mAb 7G6 against the antigen specific IgM response in the IV KLH TDAR mouse experimental model.

Parameter	Unit	Source	Value (IgM)	Standard Error (IgM)
E_{max}	-	Model Estimate	0.852	0.002
EC_{50}	nM	Model Estimate	0.125	0.020

Model performance was assessed through visual inspection of the profiles, residual plots and comparison of the predicted versus observed data. The PK model used to describe the plasma concentration of mAb 7G6 tends to over predict compared with the observed values, as illustrated in figure 6.17A, with this over prediction more prevalent at lower doses and later time points. Noting that due to falling below the assay limit of quantification, observed values were not gained at the 0.03 and 0.01 mg/kg dose levels. The model prediction of the observed KLH specific IgM concentration was remarkably good, with the simulated values largely within 2-fold of the observed data (figure 6.17B). There was also no obvious bias in model fit across the IgM profile (figure 6.16), albeit with the profile limited to just the elimination phase.

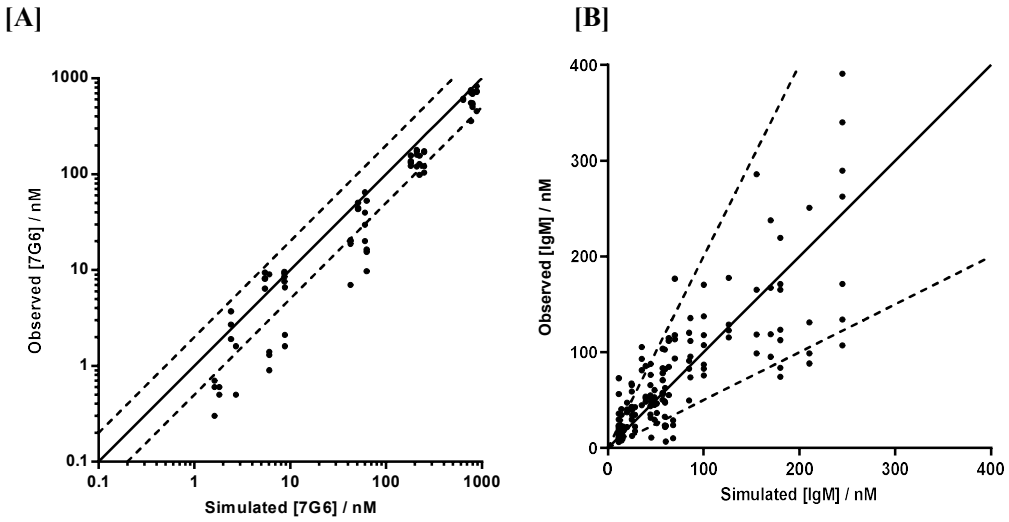

Figure 6.17. Observed data versus model simulated estimates of **[A]** mAb 7G6 plasma concentration **[B]** KLH specific IgM plasma concentration. Line of unity (solid), 2X and 0.5X (dotted). Observed data from PKPD study 7.

Simulated KLH specific IgM profiles (figure 6.18A) at each dose level were evaluated using the area under the effect curve (AUEC), calculated for comparison with the mean observed AUEC from PKPD study 7 (figure 6.18B). This provides an integrated evaluation, demonstrating the excellent model performance in describing the observed inhibition of KLH specific IgM production by mAb 7G6. The model provides a good description of both the slope and the observed maximum effect (E_{max}).

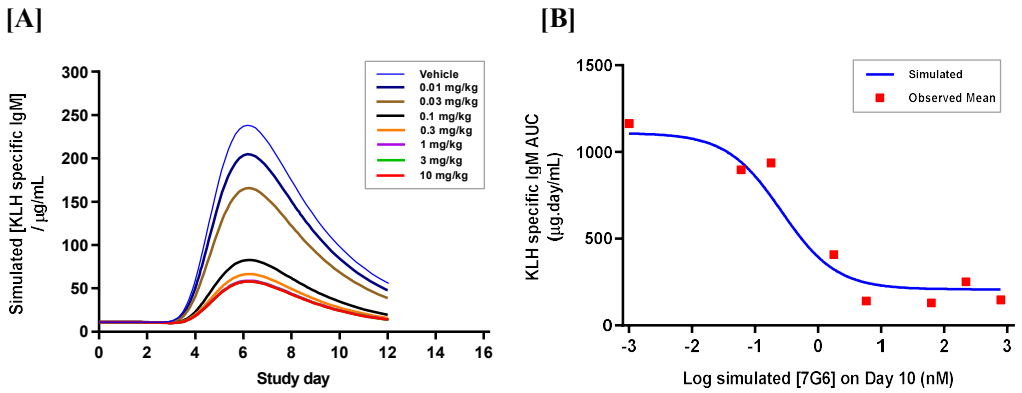

Figure 6.18. **[A]** PKPD model simulations of KLH specific IgM profiles, following IP administration of mAb 7G6 every 96 h across the range 0.01 to 10 mg/kg in the IV KLH mouse experimental model (PKPD study 7). **[B]** Further analysis of the same data by calculating the area under the IgM effect curve (AUEC) versus the log10 simulated 7G6 plasma concentration on day 10. Data illustrated as mean AUEC (symbol) n=4 from PKPD study 7 versus the PKPD model simulated AUEC (line).

6.3.3.1. Exploration of the disconnect between observed and predicted receptor occupancy

Despite reasonable performance in prediction of the total plasma 7G6 concentration (figure 6.17A), the current version of the PK model (PK model v4) is limited in its capacity to predict observed receptor occupancy. This disconnect between the model prediction and the observed receptor occupancy is illustrated in figure 6.19, where an approximately 20-fold shift in apparent receptor occupancy exists. To facilitate a link between the EC_{50} concentration and receptor occupancy, the relationship between observed mAb 7G6 plasma concentration and observed receptor occupancy in blood on day 6 was used. This relationship allowed estimation

of the percentage receptor occupancy corresponding to the determined EC_{50} concentration, in the absence of a reliable model estimate. The estimated EC_{50} concentration of 0.125 nM, for inhibition of antigen specific IgM production, corresponds to a 60% reduction in available receptor (CD21/35) on peripheral B cells in the blood on day 6.

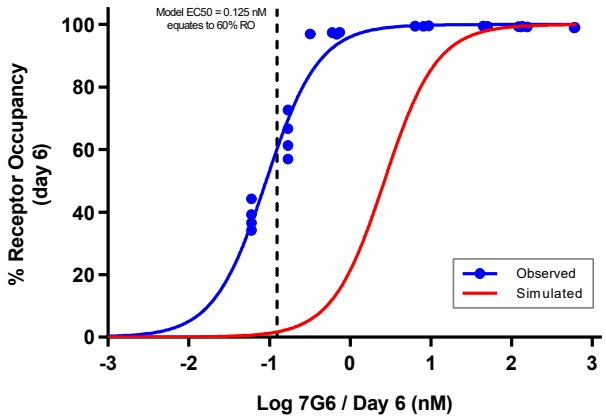

Figure 6.19. Observed receptor occupancy of CD21/35 on peripheral B cells versus the plasma concentration of mAb 7G6 on study day 6 (symbols). Data fitted with a constrained four parameter logistic fit curve (blue line) to allow extrapolation of the receptor occupancy achieved at the *in vivo* derived EC_{50} value (0.125 nM). Overlain with the PKPD model simulated receptor occupancy versus the simulated day 6 7G6 plasma concentration (red line).

To provide further insight into the underlying components contributing to the poor model prediction of receptor occupancy, a parameter sensitivity analysis was conducted. This identified three estimated parameters which directly impact model description of receptor occupancy, these are; mAb affinity to soluble target, membrane receptor turnover and soluble target turnover. Each of these parameters are defined by an assumption without supporting experimental data. Sensitivity analysis was conducted on each parameter individually, simulating the impact of a significant but realistic parameter value change on description of receptor occupancy. The parameter values tested are shown in table 6.10, alongside the fold shift in simulated receptor occupancy driven by this parameter change. The results are also graphically illustrated in figure 6.20, with the altered scenarios highlighted by the dashed lines. This sensitivity analysis indicates that the model is indeed sensitive to each parameter. A change in mAb affinity (K_d) for soluble target from 0.05 to 1 nM, results in a 4.3-fold shift in

simulated receptor occupancy. Altering the turnover rates of the membrane target ($k_{deg,m}$ from 0.0289 to 0.0072 h^{-1}) and soluble target ($k_{deg,s}$ from 0.0385 to 0.0193 h^{-1}) results in a 3.0 and 1.8-fold shift in receptor occupancy respectively. Within the set test boundaries, the most sensitive parameter was the affinity of mAb 7G6 to soluble target.

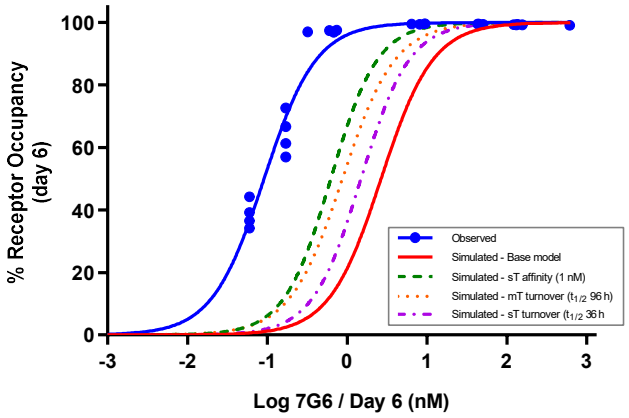

Figure 6.20. Observed receptor occupancy of CD21/35 on peripheral B cells versus the plasma concentration of mAb 7G6 on study day 6 (symbols) plotted against the model simulation (red line), alongside parameter sensitivity analysis showing the impact of decreased soluble target affinity from 0.05 to 1 nM (green dashed), decreased membrane target turnover from a $t_{1/2}$ of 24 h to 96 h (orange dashed) and decreased soluble target turnover from a $t_{1/2}$ of 18 h to 36 h (purple dashed) on the model prediction of receptor occupancy.

Table 6.10. Parameter values tested during sensitivity analysis of the PKPD model, showing the original model value, the alternative value and the resulting impact on the prediction of receptor occupancy.

Parameter	Unit	Original Value	Test Value	RO Fold shift
K_d (T,s)	nM	0.05	1.00	4.3
$k_{deg,s}$	h^{-1}	0.0385	0.0193	3.0
$k_{deg,m}$	h^{-1}	0.0289	0.0072	1.8

6.4. Discussion

The present chapter details the development of a mathematical PKPD model that describes the effect of immunosuppressants on the KLH induced TDAR in mice, as a preclinical model of humoral immunity to support progression of novel therapies. The empirical PD model described by Yang *et al.* (2015) was adopted as a starting point, comprising a transit compartment structure that describes the time lag to appearance of antigen specific antibodies following TD immunisation. This transit compartment approach is a popular mathematical method to insert a time delay between signal and response, acting as a surrogate for a poorly defined biological cascade that takes time to occur. Definition of the time delay is achieved through the number of transit compartments used and the mean transit time between them (τ), which both act to slow progression of the signal to the final effect compartment. An analysis of the optimal number of compartments (2 to 20) to describe the IgG response delay was performed using the KLH specific IgG data generated in PKPD study 5 (figure 6.4 / table 6.2). Whilst increasingly improved mathematical fit can be achieved by increasing the number of transit compartments from 2 up to 16 (defined as minimisation of loglikelihood, AIC and BIC), beyond approximately 8 to 10 compartments, this results in degradation of the visual fit. The loss of visual fit is predominantly through an overestimation of the observed concentration at 241 h (10 days) and a steeper elimination phase that increasingly results in an underestimation of the concentration at 385 h (16 days) with higher compartment number. This outcome is limited by the restricted sampling, with increased data in the early response phase and an extended study timeframe required to discernibly differentiate between models. Because model performance is not overly sensitive to compartment number beyond eight, to provide a compromise between complexity and performance this was selected for the final model. In a similar analysis performed by Yang *et al.* (2015) during their own model development phase, five transit compartments was selected as the optimal compromise for their data set, showing reasonable consistency. A compartment number analysis could not be completed for IgM, due to the lack of any data describing the initial phase, therefore the same model structure used for IgG was extended to analysis of IgM. This approach was latterly shown to provide a good fit of the observed antigen specific IgM response profiles.

To provide further model utility, the transit compartment PD model was extended to include definition of basal IgG / M, the baseline natural antibody repertoire with low KLH affinity that result in low level noise in the bioassay. To facilitate description of this basal IgG / M, a synthesis route was added for the stimulus, denoted k_{syn}. Although this cannot be attributed to any biological mechanism, it provides a neat way to add a constant baseline response, which

can then be calibrated to the observed baseline concentration through manipulation of this synthesis rate (k_{syn}). A lack of knowledge of the pharmacokinetics of KLH results in the stimulus in the model being reduced to an arbitrary amount, rather than using a more desirable mechanistic approach with a direct effect model linked through KLH concentration. This is because a suitable analytical method to quantify KLH in biological samples has yet to be developed, due to the various issues imparted by the heterogeneity of the KLH protein. However, even should an analytical method be identified, the complexity of antigen processing and retention mechanisms in immune cells would likely render a direct response approach simplistic in any case. A final addition to the base PD model structure was a biologically relevant IgG / M clearance rate gained from literature, offering a translational element to description of the response. This additionally overcomes the limited characterisation of the IgG response elimination phase, caused by restricting the study duration to 14 days post immunisation. The value gain of the described model amendments is the ability to delay the KLH challenge but retain description of the observed stable baseline. However, the draw back to the simplistic approach described here is that drug can impact basal IgG / M through modulation of τ, where PK is integrated through an indirect response element against this transfer rate. An alternative approach could be to add a static baseline species of IgG / M to the final effect compartment, with the experimentally measured value assumed to be the sum of this static value and any newly produced IgG /M.

PD model performance to describe the observed KLH specific IgG / M response profile to KLH immunisation is illustrated in the simulated versus observed plots of the control data for each study. In each case the calibrated PD model provides an excellent description of the observed IgG / M response in the control treatment group (figures 6.5, 6.6 and 6.10). The observed response data in the control groups of each study (PKPD study 5, 6 and 7) show remarkable consistency in response time and overall response magnitude, illustrated by the consistency in fitted values of τ and k_{deg}. The values of τ were 21.4, 23.2 and 23.8 h for IgG, 4.9, 8.8 and 8.8 h for IgM, in PKPD studies 5, 6 and 7, respectively. This consistency is logical, because the value of τ is a surrogate for the time between immunisation and observation of a response, representing a series of defined biological processes that must occur to result in antibody formation. It would by extension be safe to assume this value of τ may also be species dependent. Certainly, analysis of the human data reported in Boulton *et al.* (2012) identified τ values of 42.7 and 48.0 h for IgG and IgM, respectively (table 6.7). Meanwhile, in a KLH immunisation study in healthy volunteers reported by Poirier *et al.* (2016), using the same form of KLH (Immucothel) and same route of administration as the Boulton study, the value of τ can be estimated as 42.1 h for IgG. Immunisation route and form may also play a role in

determining τ, due to accessibility and presentation of the antigen. However, due to the often sparse collection of quantitative IgG / M response data in these types of studies, both in the clinic and in preclinical studies, a full analysis of the impact of species and route/form of KLH is not possible. As a note of caution, the derived values of τ in the present work, potentially alongside its apparent consistency, may be biased by the study design and its limited sampling times. In much the same way as for the compartment number analysis, poor characterisation of the early phase of the IgG / M responses may additionally contribute to the observed outcome.

Whilst KLH immunisation in the mouse consistently resulted in a measurable antigen specific antibody response, the magnitude of the observed IgG / M responses in the control group varied between studies. The magnitude of the response is predominantly controlled in the PD model by k_{deg}, with values for IgG of 0.095, 0.053 and 0.555 h^{-1} and for IgM of 0.075, 0.199 and 0.155 h^{-1}, in PKPD studies 5, 6 and 7 respectively. The higher value of k_{deg} in study 7 for the IgG model, is a result of the much lower response measured in this study when compared with studies 5 and 6, despite the higher challenge amount. This variation in response between studies highlights the need to calibrate the model with a well characterised control group. This was achieved through the approach of increasing the number of animals in the control group to ensure collection of a robust data set despite the high inter-individual variability.

It was consistently observed across studies that the measured concentration of IgM increased on day 16, despite the trend between day 6 and 12 being of the response fading. The exact underlying cause of this increase is unknown, but three potential theories are plausible. The simplest being that it is an analytical artefact caused by the change in sampling conditions from in life tail nick sampling to cardiac sampling under terminal anaesthesia on day 16, a difference owing to welfare restrictions regarding procedure number. Indeed, the analytical methodology itself may instead be the cause. The measured response in an immunoassay format is not strictly governed by concentration alone, but also influenced by affinity. Typically, the affinity of the analyte would not alter over time and so would not be considered relevant. However, this does not hold true in this scenario, where ongoing progression of the humoral immune response means affinity maturation is selectively producing higher affinity clones with time. Finally, it may be plausible that day 16 falls into a secondary phase of the antibody response, following presentation of retained KLH antigen to primed B cells resulting in a surge in antibody response. Due to these complicating factors, it was decided to unilaterally exclude day 16 from the analysis of the IgM data sets.

In summary, the modified transit compartment based mathematical PD model was shown to provide an excellent description of both the IgG and IgM responses to T-dependent immunisation. Thus, providing a suitable modelling framework with which to apply to quantitative assessment of immunosuppressants. To confirm the value of this approach, the model system was qualified using a clinically validated treatment, with Fingolimod selected for this task.

6.4.1. PKPD model qualification with Fingolimod

PKPD model development and qualification was completed with the clinically validated immunosuppressant Fingolimod. This required the pharmacokinetics of Fingolimod to be integrated within the PD model, to allow description of its effect on the TD antibody response over time and across doses. The pharmacokinetics of Fingolimod are actually quite complex. The parent drug can be considered as a prodrug, with the active form Fingolimod phosphate reversibly produced *in vivo* through phosphorylation by sphingosine kinases (Brinkmann *et al.*, 2010). The two forms can rapidly interconvert resulting in an equilibrium, with drug concentrations often being reported alongside a ratio of Fingolimod phosphate / Fingolimod. The reported volume of distribution of Fingolimod in human is very high at 1200 – 1700 L, which combined with strong protein binding leads to a very long reported half-life of 6 to 9 days (David *et al.*, 2012). Plasma protein binding is conserved across species, with reported values ranging between 99.74 and 99.87% bound for mouse, rat, dog, cynomolgus monkey and human (Meno-Tetang and Lowe, 2005). Indeed, experimentally the fraction unbound of Fingolimod in blood was measured in mouse at <0.001 (Appendix IX), which compares favourably with reported values in dog and human of 0.0002 and 0.0004, respectively (Meno-Tetang and Lowe, 2005). Consequently, the whole blood Fingolimod concentration provides a suitable value to track Fingolimod PK and does not require conversion to free for translational purposes. Indeed, the PKPD analysis by Meno-Tetang *et al.* (2006) reports that despite Fingolimod being the inactive form, the rapidity of equilibrium between forms allows the parent drug to describe the observed PD well. This simplifies the requirements of the PK arm of the model, with a one compartment PK model found to provide adequate description of the observed Fingolimod blood concentration data. Although more complex PK models have been reported, such as two compartment models (CDER, 2009) or more mechanistic PBPK models (Meno-Tetang and Lowe, 2005), the simplistic approach described here provides a fit for purpose prediction of observed exposure in mice. This fit is illustrated by the plot of observed versus simulated values in figure 6.8A. Here, the one compartment PK model,

fitted to the observed Fingolimod blood concentration data in PKPD study 6, provided simulated values within 2-fold of the observed. At the time of writing, the pharmacokinetics of Fingolimod in the mouse have not been published.

Integration of the PK model to the PD model was achieved through an indirect response element against the transfer rate (τ) of the effect signal into the first effect compartment (E_1). The biological mechanism of Fingolimod results in a reduction in circulating lymphocytes, caused by internalisation and degradation of S1P1 receptors and a consequent reduction in S1P-S1P1 dependent egress of lymphocytes from lymph nodes (Brinkmann *et al.*, 2010). This effect takes time, but is drug concentration dependent, therefore fits with an indirect type response. Prior PKPD modelling of the effects of Fingolimod have been carried out using blood lymphocyte count as the biomarker of effect, with indirect response models providing a good description of the pharmacodynamics (Meno-Tetang and Lowe, 2005). It is assumed that the impact on lymphocyte trafficking is the mechanism by which Fingolimod impacts the TD immune response, reducing the number of activated T-helper cells and thus reducing the response generated to TD immunisation (Han *et al.*, 2004). Consequently, an indirect response relationship was selected to describe inhibition of antigen specific IgG / M by Fingolimod in the present PKPD model.

The integrated PKPD model was explored using the concentration effect data set generated in PKPD study 6, demonstrating strong performance in description of the observed impact of Fingolimod on the antigen specific IgG response to KLH immunisation. Performance of the model is illustrated in the plot of simulated versus observed concentration in figure 6.8B. Model performance was strong in description of the effect of Fingolimod on IgG with low observed residual error and the majority of predicted values falling within 2-fold of observed. The model estimate of EC_{50} was 4.59 nM (E_{max} 0.639) against the IgG endpoint, with high standard error (3.09). This error is likely a consequence of the limited number of observations (n=4 / treatment) and the high variability observed in IgG response. Model estimation of E_{max} was visually weak, appearing to underestimate the observed maximum effect (figure 6.9C). A combination of variability in the observed response and the limits of the tested dose range prevent formalisation of the entire response curve, each contributing to poor description of the extremes of the curve. To provide confidence in the predictivity of the model, cross validation was performed using the estimates of EC_{50} and E_{max} to simulate the impact of 3 mg/kg QD PO Fingolimod in PKPD study 5 and 7 (figure 6.10). This analysis provides confidence both in the predictivity of the model and the repeatability of the experimental study, with the KLH

specific IgG response data in both PKPD study 5 (n=10) and PKPD study 7 (n=4) well predicted.

Comparison of the model estimated Fingolimod EC_{50} in mouse versus those derived in other species against circulating lymphocyte count, shows remarkable consistency. An in depth PKPD analysis of Fingolimod activity by Meno-Tetang and Lowe (2005) derived EC_{50} values of 0.29 nM in rat and 1.32 nM in cynomolgus monkey. These compare favourably with the value of 4.59 nM derived in the present work against the downstream biomarker IgG. PKPD analysis of the oral single ascending dose study in healthy volunteers has also been reported (CDER, 2009), again using the peripheral lymphocyte count as the mechanistic biomarker, deriving a Fingolimod EC_{50} value of 3.9 nM (E_{max} 0.903). This comparable activity across species provides confidence that the preclinical PKPD model could be directly translated to project clinical efficacy.

The plasma KLH specific IgG / M responses in healthy volunteers reported by Boulton *et al.* (2012) visually follow a similar trend to that observed in the mouse, in that an initial delay exists between immunisation and response, but that once initiated quickly reaches its maximum. This similarity is despite the different immunisation protocols used, with three KLH challenges at one-week intervals given SC in an adjuvant formulation, compared with a single IV immunisation in mouse. As such, the transit compartment model developed for the mouse was considered eligible to fit the clinical data. To test this claim, the PKPD model was calibrated to describe the observed clinical IgG / M response to KLH immunisation reported in Boulton *et al.* (2012). The model was indeed found to provide a reasonable description of the time delay in the IgG / M response, however could not describe the terminal phase when human estimates of native antibody clearance were introduced. Allowing the model to estimate these clearance values instead, provided a means to an excellent description of the control response to KLH immunisation (figure 6.12). This difference in apparent antibody clearance rate is likely a consequence of the immunisation route and form used in the clinical study versus the mouse experiments. With the SC route and adjuvant driving a slower but longer lived response than IV immunisation. Certainly the IgG profiles reported in Boulton *et al.* (2012) and Poirier *et al.* (2016) result in similar estimates of IgG clearance when assessed in a similar manner, with k_{IgG} estimates of $1.49E^{-4}$ h^{-1} and $3.03E^{-4}$ h^{-1} respectively.

The clinical study outcome, at the 0.5 and 1.25 mg daily oral doses reported by Boulton *et al.* (2012), was simulated using the calibrated PKPD model. To achieve this, a PK model was first generated to describe the pharmacokinetics of Fingolimod in human, utilising the reported PK data from the oral single ascending dose study in healthy volunteers (CDER, 2009). A simple

one compartment PK model was again able to provide a reasonable fit of the observed data across the dose range of 5 to 40 mg (figure 6.11), as observed for mouse. A linear increase in exposure was observed with dose, providing confidence that at the 10-fold lower therapeutic dose (0.5 mg) the PK model should still provide a reasonable description of the observed data. Indeed, this plays out in the simulation of the reported dosing regimen, consisting of a series of four escalating loading doses prior to daily oral treatment at 0.5 or 1.25 mg (figure 6.13C). The simulated profiles slightly under predict the reported Fingolimod blood concentration on week 1 and 4 but remain within 2-fold of the observed value. This underprediction is likely a consequence of the inaccuracy of the simplistic PK model in describing the terminal phase, highlighted by the overshoot of the loading doses. However, the model provides a fit for purpose prediction of the PK. The resulting outcome of Fingolimod treatment on IgG response was projected using the mouse estimates of E_{max} and EC_{50} (figure 6.13A). This projection provides a reasonable estimate of the observed impact on the magnitude of the KLH specific IgG response, with an overprediction of effect on IgG response at 0.5 mg and an underprediction of effect at 1.25 mg. For both doses, description of the early phase of the IgG response is poor, with the extent of flattening of early response progression poorly captured. This is likely due to the impact of the repeated challenge on progression of the response, as it is not observed in the single IV challenge studies. However, this would require further preclinical experimental work to understand whether a similar protocol in mouse may elicit the same response profile, with these beyond the scope of the present work.

In contrast to the effect of Fingolimod on the IgG response, the effect on IgM was less well defined in the preclinical experiments. As before, application of the integrated PKPD model was explored using the concentration effect data set generated in PKPD study 6. Here a Fingolimod dose response was observed with maximum inhibition of KLH specific IgM achieved at 10 mg/kg. The PKPD model demonstrated adequate performance in description of this observed impact on the antigen specific IgM response to KLH immunisation, illustrated in the plot of simulated versus observed concentration in figure 6.8C. Residual error was higher than that observed for the IgG model as a consequence of the considerably higher inter-individual variability in observed IgM concentration. This variability is particularly highlighted in figure 6.9D, where the mean calculated AUEC is higher in the lowest four dose groups than in the study control. It can also be seen in the wider spread of data around the line of unity in figure 6.8C. Performance of the model was seen to deteriorate at day 12, often underpredicting the observed IgM concentration at this later time point, possibly as an extension of the experimental limitations described earlier for day 16. The model provided EC_{50} and E_{max} estimates of 408 nM and 1.0, respectively. The EC_{50} estimate had reasonably

high standard error (210 nM) reflecting the variability of the data set and weaker model fit. While the limited data describing maximum effect restricts fitting of E_{max}, resulting in convergence with the upper limit (1.0). The less potent EC_{50} value against the IgM endpoint, when compared with IgG, is consistent with the reduced effect of Fingolimod on IgM reported in mouse by other authors (Han *et al.*, 2004). Once again, to provide confirmation of model performance, a cross validation of the model estimates of EC_{50} / E_{max} was performed through simulation of 3 mg/kg QD PO Fingolimod in PKPD studies 5 and 7 (figure 6.10). This analysis demonstrates inconsistency in the performance of Fingolimod to inhibit KLH induced IgM production, with no effect seen in study 5 (figure 6.10C) and a different profile of effect seen in study 7 (figure 6.10D). The mathematical PKPD model was unable to provide accurate prediction of the observed outcome of either study.

To further compound the poor cross validation of the IgM model, there is an apparent disconnect between the impact of Fingolimod on IgM production in human, where enhanced effect is observed compared with IgG, versus mouse where the scenario is reversed. Consequently, the model is unable to describe the impact of Fingolimod on the clinical KLH specific IgM response, when implementing the preclinical estimates of E_{max} and EC_{50} (figure 6.13B). Indeed equally, when supplementing the model with human derived E_{max} and EC_{50} values for lymphocyte depletion, the observed outcome remains unpredicted (figure 6.14B). This is despite the addition of human estimates improving model performance in the prediction of the clinical KLH specific IgG response (figure 6.14A). Ultimately, this indicates a mechanistic disconnect, both between the preclinical and clinical data and between the observed impact on peripheral lymphocytes and the downstream effect on IgM response to a T-dependent challenge. A key difference between the preclinical and clinical study designs is the form and route of KLH challenge administration. The clinical subcutaneous adjuvant driven model is likely to result in local immune activation and direction of the humoral immune response predominantly to the draining lymph nodes. Whereas, in the preclinical IV administration model, the major site of humoral immune response is likely to be the spleen, with little recruitment of localised responses in tissue. In this experimental detail may lie the mechanistic factors complicating the efficacy of Fingolimod, resulting in the observed disconnect between human and mouse.

6.4.2. PKPD analysis of mAb 7G6

Analysis of the concentration effect relationship of mAb 7G6 on the antigen specific antibody response to TD immunisation was achieved through integration of the PK model described in

chapter 4 (PK model v4) with the PD model described in this chapter. This integration was achieved via an indirect response element, as used previously for the Fingolimod model. However, in contrast, the plasma EC_{50} value alone is of rather limited translational value. This is due to the complexity of translating an EC_{50} across species when it was generated with a surrogate antibody, exhibiting not only differential PK, but also differences in target binding. As such, relating the extent of mAb exposure to effect is more typically conducted via receptor occupancy, a term which connects drug exposure with target binding. Disappointingly, despite reasonable performance in prediction of the total plasma 7G6 concentration (figure 6.17A), the current version of the PK model (PK model v4) is limited in its capacity to predict the observed receptor occupancy (figure 6.19). With this disconnect resulting in an approximately 20-fold shift between the predicted and observed values. To provide a bridge between these data, a relationship was established between 7G6 exposure and the measured receptor occupancy value on day 6. Receptor occupancy was measured using peripheral B cells as an easily accessible surrogate for splenic B cells, with this shown to be a reliable correlate in chapter 5. The PKPD model was used to estimate an EC_{50}, before converting this into a more translatable receptor occupancy value using the exposure vs receptor occupancy relationship (figure 6.19).

PKPD analysis was performed on the concentration effect data set generated in PKPD study 7, providing a reasonable description of the observed 7G6 plasma concentration and an excellent fit of the resulting IgM response. The limitations of the PK model have been discussed previously (chapter 4), however in spite of this, the model provides a reasonable prediction of the observed plasma concentration (figure 6.17A). Albeit with this prediction an overestimate at the lower doses and later timepoints. This overprediction is in part due to an under appreciation of the target mediated clearance pathway, illustrated by a consistent overprediction of day 6 and 10 plasma concentrations (2 days post dose), with increasing disparity observed with reducing dose. The 7G6 plasma concentration is also overpredicted at all doses on day 12, an outcome possibly due to this underappreciation of clearance, but also perhaps early evidence of immunogenicity. The impact of the immune challenge on the pharmacokinetics of mAb 7G6 is unknown but may present one explanation for the discrepancy with the standalone PK experiments in naïve mice (chapter 4). To further hamper modelling of mAb 7G6 exposure, nonspecific binding resulted in not only limiting the tested dose range but also the accuracy of the administered dose. Whilst this was accounted for with a correction factor based on a pre-study test described in chapter 5, it impacted the half log unit dose separation, affecting definition of the lower region of the concentration effect curve. Despite these PK model limitations, the integrated PKPD model still provides a reasonable

description of the mean 7G6 exposure and an excellent description of its impact on the KLH specific IgM response. Fitting the model to the observed data resulted in estimates of EC_{50} and E_{max} of 0.125 nM and 0.852 respectively, with low standard error (0.020 nM and 0.002). The majority of the predicted values fall within 2-fold of the observed result (figure 6.17B) with no directional bias. This was aided by lower inter-individual variability compared with that observed in previous experiments.

Comparison of the model prediction of receptor occupancy on splenic B cells and the measured receptor occupancy in study 7 highlighted a 20-fold discrepancy. This disconnect is likely caused by a combination of factors. However, first and foremost it is paramount to consider that the model employs a vast simplification of host physiology, condensing the body down to two lumped tissue compartments, connected via lymph and plasma. This simplification results in a marked under appreciation of the accessibility of drug to the membrane expressed target, with the target reduced to a static population within the tissue. However, even using a full PBPK approach, description of cellular flux would require considerable additional complexity to be added, providing only a small situational gain in utility. In any case, detailed modelling is limited by the sparse information available describing the abundance and kinetics of the target cells and target protein (CD21/35), particularly in the mouse. The current version of the PK model is parameterised using a variety of estimates, as discussed in detail in chapter 4. To review the impact of these parameter estimates on the prediction of receptor occupancy, a sensitivity analysis was performed on three parameters defining the target; mAb affinity to soluble target, membrane target turnover ($k_{deg,m}$) and soluble target turnover ($k_{deg,s}$).

The affinity of mAb 7G6 for the soluble target (sT) was previously assumed to be equal to that experimentally measured against the native cell associated receptor (K_d of 0.05 nM). This assumption does not consider the beneficial impact of avidity in the cellular assay, or the potential that the truncated soluble form may be sterically different due to differential folding or post translational modifications. Certainly, the existence of different soluble versus membrane affinities draws support from the difficulty encountered measuring binding when using a full length soluble recombinant protein. To test model sensitivity, mAb affinity for soluble target was lowered, with a 20-fold drop off simulated (K_d of 1 nM). This assumption change results in a 4.3-fold leftward shift in the model simulated concentration required to drive 50% receptor occupancy. The soluble target is essentially acting as a saturable drug sink, so a reduction in affinity increases the availability of free 7G6 in the system, which can then encounter the tissue constrained target. Model sensitivity to the turnover rates of both membrane associated and soluble target was also tested. These parameter values are also

estimates, anchored using literature data for degradation of similar proteins and fixed to achieve the experimentally determined concentrations of target (see chapter 4). A slower rate of membrane receptor turnover is feasible, with a 4-fold slower rate (turnover $t_{1/2}$ of 96 h) tested in this sensitivity analysis. This change led to a 3-fold leftward shift in the simulated receptor occupancy curve (figure 6.20), caused by the reduced appearance of newly synthesised receptor. The soluble protein clearance rate was similarly defined, with a 2-fold reduction in clearance a feasible extreme to test (turnover reduced to $t_{1/2}$ 36 h). This resulted in a 1.8-fold leftward shift in simulated receptor occupancy (figure 6.20). These parameters are each shown to impact the model definition of receptor occupancy, but individually this impact remains small, indicating it is unlikely to be a single parameter driving the underprediction.

To overcome the limitation of the PKPD model in describing receptor occupancy, an alternative approach was taken to link the effective concentration, described by the model estimate of EC_{50}, and the extent of receptor occupancy. This was achieved through fitting a four parameter logistic fit relationship to the observed receptor occupancy on study day 6 against the measured mAb 7G6 plasma concentration. Interpolation of the model EC_{50} of 0.125 nM from this relationship results in a corresponding estimate of 60% receptor occupancy needed to achieve a 50% reduction in the observed antigen specific IgM response to KLH challenge. Whilst not an exhaustive proof of the relationship between target occupancy and downstream effect, this outcome does support the notion of a direct relationship between the availability of CD21/35 and propagation of an antigen specific IgM response. Therefore, the analysis performed here would indicate that targeting a high level of receptor occupancy could achieve a high level of reduction in antigen specific IgM.

6.5. Chapter conclusion

A PKPD modelling framework was successfully developed to quantitatively interrogate the efficacy of the murine surrogate CD21/35 neutralising mAb 7G6 in the mouse IV KLH TDAR experimental model of humoral immunity. This PKPD modelling framework extended a transit compartment based model to describe the TDAR to the neoantigen KLH in mice, inspired by the published PKPD model of Yang *et al.* (2015). Whilst predominantly empirical in nature, this model provided strong description of the delayed antibody response to KLH immunisation, capturing both the IgM and IgG responses well. System specific parameters were identified, with an indication of species and challenge dependency in the values of τ and

$k_{IgG/M}$. Further work would be required to determine the scalability of these parameters, however in the present work calibration to observed data was considered a valid approach to tether the PD model to the control group response. Integration of drug PK was achieved via an indirect response element against the transfer rate of the effect signal, acting as a valve constant to stem progression of the response to KLH immunisation. This results in two estimated drug specific parameters, EC_{50} and E_{max}, which are considered directly translatable where no species differences in target or target binding exist.

The PKPD model was qualified by exploring the concentration effect relationship of Fingolimod, a clinically validated treatment. Integrated PKPD analysis of the IgG response resulted in an EC_{50} estimate of 4.59 nM, correlating well with published values from modelling of peripheral lymphopenia across species. However, the model estimate of E_{max} of 0.639 was lower than the published values, likely because of limitations in the experimental data which provides inadequate description of maximal effect. Clinical translation was demonstrated through projection of Fingolimod efficacy in a healthy volunteer TDAR study (Boulton *et al.*, 2012), using the preclinical estimates of EC_{50} / E_{max}. This approach provided reasonable predictivity of the observed inhibition of antigen specific IgG in healthy volunteers following immunisation with KLH. Predictivity was improved by switching to the clinical estimate of EC_{50} / E_{max}, driven largely through the higher E_{max} value.

The present work confirmed the literature observation that Fingolimod is less efficacious against the IgM response to T-dependent immunisation in mice compared with the IgG response, with this observation manifesting as a drop off in EC_{50} to 408 nM. This indicates an apparent disconnect between the impact of Fingolimod on lymphocytes and the downstream impact on the IgM response to TD immunisation. However, this lower efficacy does not play out in the clinic, with Fingolimod efficacy demonstrated against the IgM response to T-dependent immunisation. Consequently, the preclinical estimates of EC_{50} / E_{max} do not predict the observed clinical efficacy. However, additionally neither do the clinical estimates of EC_{50} / E_{max} from lymphopenia modelling, indicating these biomarkers are not mechanistically aligned. This perhaps highlights that it is the mechanism of the drug that is failing to translate across model systems, potentially due to the influence of the different immunisation protocol designs. It stands to reason that further characterisation of the IgM endpoint may be required, using an alternative clinically validated drug of a differentiated mechanism. In spite of this, the model qualification package provided confidence in the value of the PKPD modelling framework to provide quantitative assessment of the efficacy of immunosuppressants for projection of clinical dose.

The PKPD modelling framework was implemented to quantitatively assess the efficacy of the murine surrogate CD21/35 mAb 7G6 in the mouse IV KLH TDAR experimental model. The objective being to provide confidence in a receptor occupancy / exposure target that results in a meaningful change in antibody response to a TD antigen, to guide prediction of a therapeutic human dose. Through integration of the mechanistic mPBPK model (PK model v4), via receptor occupancy, to the transit compartment based PD model, it was anticipated this relationship could be directly inferred. However, limitations of current knowledge of CD21/35 abundance and kinetics result in a flawed prediction of receptor occupancy *in vivo*, with an approximately 20-fold discrepancy in predicted versus observed. Consequently, a two-step approach was used as a compromise, gaining an EC_{50} / E_{max} value via the PKPD model and then converting this to a receptor occupancy estimate using the observed receptor occupancy vs concentration relationship. Whilst providing an adequate approach to estimate the target receptor occupancy in this instance, this really highlights the need to generate better understanding of target protein kinetics early in the lifecycle of drug discovery projects. This becomes especially important where the target is estimated to have an impact on drug exposure or where target behaviour is expected to be complex. Nevertheless, the PKPD modelling strategy successfully provided evidence that receptor occupancy and impact on the early IgM response to TD antigens are closely correlated, with an EC_{50} estimate of 0.125 nM, translating to 60% receptor occupancy. Due to the unexplained exacerbation of the IgG response to KLH immunisation following 7G6 treatment, PKPD analysis was limited to the impact on IgM response. This is because there is limited knowledge of the translational nature of this outcome. However, the response could be modelled using only a minor alteration of the current indirect response equation, converting it from inhibitory to stimulatory.

In summary, the present work described the successful development of a PKPD model to quantitatively assess the impact of immunosuppressants on the T-dependent antibody response to KLH. This approach was applied to investigate the concentration effect relationship of the murine surrogate CD21/35 neutralising mAb 7G6 in the mouse IV KLH experimental model. Providing confidence that receptor occupancy correlates with a disease relevant biomarker and therefore represents a suitable parameter with which to project clinical efficacy.

Chapter 7: Conclusion

7.1. Overall conclusion

The work presented in this thesis described the application of mechanistic PKPD modelling, early in the preclinical drug discovery environment, using a surrogate mAb as a tool with which to explore the pharmacology of the novel drug target CD21. A target that is receiving interest as a novel mechanism by which to treat autoimmune conditions characterised by the aberrant production of destructive autoantibodies. Mechanistic PKPD has become the state of the art for the integration of preclinical data to improve early projection of clinical efficacy, and here it was successfully applied to gain new insights into the pharmacology of therapeutic mAbs targeting CD21. The evolution of the PKPD modelling strategy navigated three core objectives; to identify and characterise the PK of a suitable surrogate CD21 neutralising mAb, to design and qualify an experimental model of humoral immunity aligned to CD21 biology, and to mathematically model the concentration effect relationship of the surrogate mAb.

Identify and characterise the PK of a suitable surrogate mAb to use as an investigative tool.

Three potential surrogate mAbs targeting the murine form of CD21 (and its longer splice variant CD35) were identified (7G6, 4B2 and 9E10) and assessed for suitability as an investigative tool, through characterisation of the PK, target affinity and confirmation of efficacy. The widely published mAb 7G6 was subsequently selected to proceed to further in depth PKPD interrogation, due to its higher affinity and confirmed efficacy. Despite its original discovery and disclosure in 1988 (Kinoshita *et al.*, 1988) and subsequent use in numerous published works, this represents the first report of mAb 7G6 target affinity (K_d 0.05 nM) and pharmacokinetics in mouse. It is consequently the first definitive evidence that mAb 7G6 exposure is non-linear with dose, a characteristic symptomatic of target mediated clearance and demonstrated to be shared with the more recently disclosed murine mAb 4B2 (Kulik *et al.*, 2015). This outcome is in agreement with evidence of reduced 4B2 exposure in WT vs cr2-/- mice reported by Kulik *et al.* (2015) and consistent with other membrane expressed protein targets.

To mathematically describe the non-linear PK of the mAbs, the kinetics of the target protein were integrated into the mathematical PK model, as popularised by Mager and Jusko (2001a). A minimal PBPK model reported by Cao *et al.* (2013) was selected as the most appropriate model of PK, incorporating lumped tissue compartments to describe the distributional behaviour of the mAb. The membrane and soluble forms of the target CD21 were added to the relevant compartments and parameterised using literature estimates of abundance and kinetics.

This resulted in a semi-mechanistic PK model, which while able to provide adequate description of the observed PK across doses, highlighted the dearth in reliable quantitative evidence of CD21 abundance and kinetics across species. To address this knowledge gap, considerable effort was applied to the quantification of membrane and soluble forms of CD21/35, which are previously unreported in mouse. This effort revealed there to be approximately 5400 CD21/35 receptors per splenic B cell and 12.8 nM of sCD21/35 in the plasma of healthy male C57BL/6 mice, approximately half that reported in human (12000 per tonsillar B cell) (Tooze and Bevan, 1991) and cynomolgus monkey (10500 per B cell, Appendix VIII). Conversely, the sCD21/35 concentration in mouse plasma was considerably higher than the range of 0.8 to 4.8 nM reported in human (Masilamani *et al.*, 2004).

Design, test and qualify a suitable experimental mouse model of humoral immunity, aligned to both target biology and clinical strategy.

The importance of CD21 in the development of a normal humoral immune response has been well established through the use of murine T-dependent immunisation models (Heyman *et al.*, 1990, Molina *et al.*, 1996). To provide a suitable experimental model with which to investigate CD21 pharmacology, KLH was selected here as the immunogen, as an archetypal T-dependent antigen with clinical relevance. However, as a consequence of the role of CD21 in the B cell co-receptor complex and its involvement in antigen retention by FDCs, the typical adjuvant driven hapten conjugated subunit KLH immunisation models commonplace in industry are poorly aligned with target biology. Consequently, an IV immunisation protocol was optimised as a replacement, using a suboptimal dose of high molecular weight KLH formulated in PBS. Further protocol optimisation was conducted to facilitate the collection of suitable data for PKPD modelling, through maximising simultaneous collection of PK and PD data over time from a single animal. This was achieved through a combination of in-life micro sampling and biomarker assay miniaturisation. The result was a novel, ethical, data rich experimental design, suited to the generation of data for PKPD modelling.

Two gold standard, clinically validated therapeutics were used to qualify the optimised IV KLH TDAR experimental mouse model (Fingolimod and an anti-CD20 mAb), with prior evidence of efficacy on key endpoints both in mice and man. Fingolimod demonstrated the expected primary pharmacology in mice, characterised by a reduction in peripheral CD4+ and CD8+ T cells, with a similar but lower magnitude reduction in the splenic lymphocyte population, in line with prior literature (Morris *et al.*, 2005). This resulted in the expected downstream impact on humoral immunity, with a reduction in the germinal centre B cell

response to TD immunisation and inhibition of antigen specific IgG, providing external qualification of the experimental model. Across studies the impact of Fingolimod on antigen specific IgM was reduced and inconsistent when compared with IgG, in keeping with literature in mouse (Han *et al.*, 2004) but contrary to clinical observations (Boulton *et al.*, 2012).

Treatment with SA271G2, a surrogate anti-CD20 mAb, led to the expected near complete depletion of peripheral B cells, with a similar near complete reduction in splenic B cells, as reported by Moyron-Quiroz *et al.* (2016). The downstream impact was a reduced germinal centre B cell response to TD immunisation and near complete abrogation of the antigen specific IgM response, again providing external qualification of the experimental model. Counter intuitively, rather than a coordinated reduction in antigen specific IgG, an approximately 70% exacerbation of the response was observed. This outcome contradicted literature evidence in mice following CD20 immunotherapy (DiLillo *et al.*, 2007) but is speculated to be due to inefficient depletion of antigen specific and germinal centre B cells, in line with the work of Baumjohann *et al.* (2013).

Investigate the concentration effect relationship of the surrogate mAb in the qualified mouse model and develop a translational mechanistic PKPD model to integrate the data.

Integrated analysis of the rich data sets provided by the IV KLH mouse experimental model was accomplished through the development of a mathematical PKPD model. Description of both the magnitude and time delay observed in the progression of the TDAR was achieved through an empirical transit compartment based PD model, in agreement with similar analysis of cynomolgus monkey TDAR data by Yang *et al.* (2015). This model system was demonstrated to provide an excellent description of both the antigen specific IgG and IgM responses. Integration of drug effect was achieved through an indirect response element, that effectively installs a valve constant through which drug can control propagation of the downstream antibody response.

The integrated PKPD model was tested using the Fingolimod dose response data set (PKPD study 6), allowing estimation of an *in vivo* EC_{50} against the primary endpoints of antigen specific IgG and IgM. Fingolimod PK in mouse was well described using a simple compartmental model, with Fingolimod acting as a suitable surrogate for the active phosphate metabolite, as reported previously (Meno-Tetang *et al.*, 2006). The caveat being that the Fingolimod phosphate/Fingolimod ratio was measured in mouse to be greater than that reported in human, C_{av} ratio 2.3 / C_{max} ratio 1.9 versus AUC ratio 0.38 / C_{max} ratio 0.89 in

human (David *et al.*, 2012). The resulting *in vivo* EC_{50} estimate versus the antigen specific IgG response was 4.59 nM (SE 3.09), showing remarkable similarity to the reported *in vivo* EC_{50}'s across species (Meno-Tetang and Lowe, 2005, CDER, 2009). This suggests direct correlation between the impact of Fingolimod on lymphocyte trafficking and its downstream suppression of the TDAR. To confirm the translational potential of the PKPD model, the clinical outcome was projected for daily oral Fingolimod treatment on a KLH induced TDAR reported by Boulton *et al.* (2012). This was achieved using the reported clinical PK, supplemented with the E_{max} and EC_{50} estimates gained from the mouse PKPD model, providing a reasonable estimation of the observed clinical efficacy on the KLH specific IgG response.

The culmination of the project was the application of the optimised experimental model and mechanistic PKPD modelling strategy to interrogate CD21 pharmacology using the selected surrogate mAb 7G6. An integrated PKPD analysis of the resulting data was achieved through assimilation of the empirical PD model with the semi-mechanistic PK model developed for 7G6. To facilitate this integration, quantitative target engagement assays were developed to provide measured receptor occupancy data. Initial efforts looked to link 7G6 PK to the downstream effect on the TDAR through the fraction of occupied receptors. However, the model prediction of membrane target occupancy was some 20-fold lower than the measured value. This is almost certainly a consequence of the poor quality target information available to parameterise the PK model. As an alternative approach, PK was linked via an indirect response element using the total plasma concentration of mAb 7G6 to enable estimation of an *in vivo* EC_{50}, as used previously with Fingolimod. This analysis identified that mAb 7G6 has an *in vivo* EC_{50} versus antigen specific IgM of 0.125 nM (SE 0.02 nM). Direct translation of this EC_{50} is complicated by affinity differences that may exist between therapeutic mAbs and across species. Therefore, the extent of target engagement related to this EC_{50} was estimated using the measured receptor number on peripheral B cells as a translational bridge, suggesting this concentration relates to approximately 60% target occupancy. This implies a direct correlation between CD21 target occupancy and the downstream impact on the IgM TDAR, indicating that maintenance of high levels of target occupancy are required to drive efficacy.

Contrary to published reports of the efficacy of 7G6 in various TD immunisation models and in opposition to the observed impact on the antigen specific IgM response in this study, treatment with mAb 7G6 resulted in a dose dependent exacerbation of the antigen specific IgG response to IV KLH immunisation. Further analysis of this unexpected response identified this to be an IgG2 subclass driven outcome, with no observed impact on the antigen specific IgG1 or IgG3 response. Counter intuitively considering the impact on IgG, but in line with published

data, treatment with 7G6 resulted in a trend toward inhibition of the germinal centre B cell response at the higher tested doses. To confirm that this was a mechanism driven outcome rather than a molecule specific one, the murine mAb 4B2 was tested under the same experimental conditions and resulted in the same observations (Appendix VI). In both cases, B cell numbers in blood and spleen were not significantly altered following mAb treatment, despite the outcome being reminiscent of the observations with the anti-CD20 mAb SA271G2. The mechanism by which this unexpected pharmacology occurs is unknown and previously unreported, but is speculated to be through a redirection of the immune response to a T-helper type 1 (Th1) polarised response, perhaps as a consequence of changes to the regulatory function of B cells.

7.2. Future perspectives

The mechanistic PKPD modelling conducted in this thesis provided invaluable new insights into the behaviour and pharmacology of CD21 on the one hand, but on the other highlighted the dearth in reliable quantitative evidence of its expression and kinetics. Prior to starting the project it was anticipated that CD21 would pose a fairly straightforward therapeutic target, contributing only minimal impact on mAb PK. However, the data presented with the surrogate mAbs indicate that CD21 may be a more complex drug target than originally thought, highlighting the need for considerable further investigation to unravel its kinetics.

Mechanistic PK modelling of mAb 7G6 in this thesis appears to challenge the general perception that the sole source of sCD21 is ectodomain shedding of membrane receptor, primarily from B cells. The model predicts that saturating doses of anti-CD21 mAbs, which are previously reported to result in a loss of CD21 expression on B cells (Kulik *et al.*, 2015), would directly impact the plasma concentration of sCD21. Either through accumulation of sCD21 following a mAb induced shedding mechanism or through loss of sCD21 following a mAb induced internalisation and degradation mechanism which robs sCD21 of its sole source. However, no alteration of sCD21 concentration was observed following high doses of mAb 7G6 in the experiments reported in this thesis, despite reducing CD21 expression on peripheral B cells by over 99%. The simplest explanation is that the dominant route of sCD21 synthesis in mouse is in fact a previously undescribed secretory mechanism and not ectodomain shedding. Such a mechanism would additionally help to explain the paradox that is the high sCD21 concentration but conflicting low reported turnover of membrane CD21. Further study is required to understand the interlinked kinetics of the membrane and soluble forms of CD21, both in the resting state and following the addition of a CD21 targeted antibody, building upon

previous literature and likely forming an entire research project in its own right. The model parameters that describe the kinetics of CD21 are critical to the performance of the mechanistic PK model and are the key to its further improvement.

A series of *in vitro* experiments using primary B cells could be imagined that may begin to untangle and quantify the mechanisms that dominate CD21 turnover kinetics. These could initially use simple flow cytometry based techniques to monitor the loss of fluorochrome labelled antibody bound to the receptor, under varying incubation conditions. Combined with techniques to inhibit internalisation and shedding or elute membrane bound protein (such as hyperosmolar sucrose, metallo-protease inhibitors or acidification, respectively), such studies could begin to tease out dominant mechanisms and whether these alter following mAb binding. The true value of mAb 9E10, that bound but did not appear to functionally modulate CD21, could be realised in this series of experiments as a non activating control. Corresponding sampling of the cell incubation media for sCD21 may subsequently be used to reveal if an alternative source of soluble CD21 exists, one that cannot be reconciled by shedding or internalisation mechanisms. An additional interesting avenue would be to explore if the mechanisms of CD21 turnover kinetics are conserved across all cell types (i.e. B cells, FDCs and T cells). Whilst collecting target kinetic data in mouse would help to progress the current mechanistic PK model, the real value lies in collecting data across species to enable translational modelling.

Another intriguing observation from mechanistic PK modelling of 7G6 was the implication that different binding affinities exist for the soluble and membrane bound forms of CD21, with sensitivity analysis demonstrating the importance of soluble CD21 as a saturable drug sink. Further *in vitro* binding experiments to understand any discrepancy between mAb binding to soluble and membrane forms of CD21 would be important to improve the predictivity of the mechanistic PK model. Soluble protein clearance was another parameter shown by sensitivity analysis to impact free drug availability, with its experimental determination in mouse via administration of a labelled recombinant sCD21 an interesting prospect.

Mouse TDAR model

Exacerbation of the antigen specific IgG response to IV KLH immunisation following treatment with the B cell targeted therapies SA271G2 (anti-CD20) and 7G6 (anti-CD21), was an unexpected and curious observation. Not only does this represent an undesired drug effect, but it contradicts published data. Understanding this discrepancy therefore represents a critical

avenue for further investigation. The key question here is, could such a result translate to man or is it simply a unique consequence of the experimental design. Differences exist in one or all of; the TD antigen, immunisation route and strain of mouse, between the present IV KLH experimental protocol and the key literature supporting the efficacy of 7G6 and 4B2 on the T-dependent antibody response. Each of these aspects could impact the phenotype of the resulting immune response, perhaps leading to differences in the way that CD21 is involved in propagating the response. A starting point could be to compare the phenotype of the T-dependent antibody response from different immunisation routes (IV, IP and SC), with and without adjuvant, comparing the IgG isoform profile and Th1 / Th2 balance by isolating and stimulating Th cells *ex vivo* to compare the induced cytokine profile. It would also be interesting to explore whether these variables also alter the kinetics of the IgG or germinal centre B cell responses.

Consideration should also be given to the relevance of the mouse experimental model, considering the differences in genetic origin and function of CD21 between mouse and man. With closer homology to human, a TD immunisation study in cynomolgus monkey with an appropriate therapeutic antibody perhaps provides a more predictive efficacy model. From a purely translational viewpoint, conducting studies in both species would provide the ideal dataset with which to explore the mathematical PKPD model and increase confidence in its predictive value. An approach followed by Yang *et al.* (2015) during the preclinical development of lulizumab pegol (BMS-931699). A notable additional limitation of the present experimental approach is that investigation has been restricted to primary immunisation of neoantigen. Whilst this represents a valuable model system, a secondary recall immunisation model is likely to better represent chronic autoimmune disease.

PK and PKPD modelling

Detailed characterisation of the interlinked kinetics of membrane and soluble CD21 are key to the further development of the mechanistic PK model describing the murine anti-CD21 mAbs. In turn, this enhanced understanding of CD21 kinetics may facilitate simplification of the mathematical model structure to describe only the dominant distributional and elimination mechanisms. An avenue not pursued in the present work, but with potential benefits in model simplification and identifiability, is to explore replacing the description of reversible mAb binding kinetics with the quasi steady state (QSS) approximation. The QSS approximation employs the measured K_d alone to define receptor binding under the steady state assumption,

replacing the k_{on}/k_{off} estimates used presently and reducing the overall number of model parameters.

The initial translational analysis conducted in this thesis with Fingolimod, to explore the potential of the integrated TDAR PKPD model to project clinical efficacy, provided some confidence in the approach but requires further assessment. Fingolimod was an excellent clinical exemplar, but the available data package was limited by the lack of full reported PK, whilst the clinical and preclinical TDAR protocols were not perfectly aligned. This led to some discrepancies between the effect of Fingolimod in mouse and man, and between different phases of the humoral immune response, that are perhaps attributable to differences in the TD immunisation protocol and would be interesting to explore further. However, to provide a definitive assessment of the translational potential of the PKPD model, analysis of data with multiple other experimental drugs would be required. Early phase clinical data, containing TD immunisation as a proof of mechanism readout, are gradually appearing in the public domain for several novel experimental drugs targeting the T cell component of humoral immunity. This includes the anti-CD40 mAb Iscalimab / CFZ533 (Espie *et al.*, 2020) and the anti-CD28 dAb lulizumab pegol / BMS-931699 (Shi *et al.*, 2017), amongst others. Investigation of this rich emerging data set would be a really interesting and valuable scientific endeavour, building confidence in the PKPD model and the translational potential of preclinical data where published.

References

Ahearn, J.M., Fischer, M.B., Croix, D., Goerg, S., Ma, M., Xia, J., Zhou, X., Howard, R.G., Rothstein, T.L. and Carroll, M.C. (1996) 'Disruption of the cr2 locus results in a reduction in B-1a cells and in an impaired B cell response to T-dependent antigen'. *Immunity,* 4 (3), pp. 251-262.

Aichem, A., Masilamani, M. and Illges, H. (2006) 'Redox regulation of CD21 shedding involves signaling via PKC and indicates the formation of a juxtamembrane stalk'. *Journal of Cell Science,* 119 (14), pp. 2892.

Allen, C.D.C., Okada, T. and Cyster, J.G. (2007) 'Germinal-center organization and cellular dynamics'. *Immunity,* 27 (2), pp. 190-202.

Andersson, P., Jesson, G., Kylberg, G., Ekstrand, G. and Thorsén, G. (2007) 'Parallel nanoliter microfluidic analysis system'. *Analytical Chemistry,* 79 (11), pp. 4022-4030.

Arrowsmith, J. and Miller, P. (2013) 'Trial watch: Phase II and phase III attrition rates 2011-2012'. *Nature Reviews: Drug Discovery,* 12 (8), pp. 569.

Artimo, P., Jonnalagedda, M., Arnold, K., Baratin, D., Csardi, G., De Castro, E., Duvaud, S., Flegel, V., Fortier, A., Gasteiger, E., Grosdidier, A., Hernandez, C., Ioannidis, V., Kuznetsov, D., Liechti, R., Moretti, S., Mostaguir, K., Redaschi, N., Rossier, G., Xenarios, I. and Stockinger, H. (2012) 'ExPASy: SIB bioinformatics resource portal'. *Nucleic Acids Research,* 40 (Web Server issue), pp. W597-603.

Awate, S., Babiuk, L.A. and Mutwiri, G. (2013) 'Mechanisms of action of adjuvants'. *Frontiers in Immunology,* 4 114-114.

Batista, F.D. and Harwood, N.E. (2009) 'The who, how and where of antigen presentation to B cells'. *Nature Reviews: Immunology,* 9 (1), pp. 15-27.

Baumjohann, D., Preite, S., Reboldi, A., Ronchi, F., Ansel, K.M., Lanzavecchia, A. and Sallusto, F. (2013) 'Persistent antigen and germinal center B cells sustain T follicular helper cell responses and phenotype'. *Immunity,* 38 (3), pp. 596-605.

Bearden, C.M., Agarwal, A., Book, B.K., Vieira, C.A., Sidner, R.A., Ochs, H.D., Young, M. and Pescovitz, M.D. (2005) 'Rituximab inhibits the in vivo primary and secondary antibody response to a neoantigen, bacteriophage phix174'. *American Journal of Transplantation,* 5 (1), pp. 50-57.

Bingham, C.O., 3rd, Looney, R.J., Deodhar, A., Halsey, N., Greenwald, M., Codding, C., Trzaskoma, B., Martin, F., Agarwal, S. and Kelman, A. (2010) 'Immunization responses in rheumatoid arthritis patients treated with Rituximab: Results from a controlled clinical trial'. *Arthritis & Rheumatism,* 62 (1), pp. 64-74.

Bouillie, S., Barel, M. and Frade, R. (1999) 'Signaling through the EBV/C3d receptor (CR2, CD21) in human B lymphocytes: Activation of phosphatidylinositol 3-kinase via a CD19-independent pathway'. *The Journal of Immunology,* 162 (1), pp. 136.

Boulton, C., Meiser, K., David, O.J. and Schmouder, R. (2012) 'Pharmacodynamic effects of steady-state Fingolimod on antibody response in healthy volunteers: A 4-week, randomized, placebo-controlled, parallel-group, multiple-dose study'. *The Journal of Clinical Pharmacology,* 52 (12), pp. 1879-1890.

Brambell, F.W., Hemmings, W.A. and Morris, I.G. (1964) 'A theoretical model of gamma-globulin catabolism'. *Nature,* 203 1352-1354.

Brinkmann, V., Billich, A., Baumruker, T., Heining, P., Schmouder, R., Francis, G., Aradhye, S. and Burtin, P. (2010) 'Fingolimod (fty720): Discovery and development of an oral drug to treat multiple sclerosis'. *Nature Reviews Drug Discovery,* 9 883.

Bueters, T., Gibson, C. and G Visser, S.A. (2015) 'Optimization of human dose prediction by using quantitative and translational pharmacology in drug discovery'. *Future Medicinal Chemistry,* 7 (17), pp. 2351-2369.

Cao, Y., Balthasar, J.P. and Jusko, W.J. (2013) 'Second-generation minimal physiologically-based pharmacokinetic model for monoclonal antibodies'. *Journal of Pharmacokinetics and Pharmacodynamics,* 40 (5), pp. 597-607.

Carel, J.C., Myones, B.L., Frazier, B. and Holers, V.M. (1990) 'Structural requirements for C3d,g/Epstein-barr virus receptor (CR2/CD21) ligand binding, internalization, and viral infection'. *Journal of Biological Chemistry,* 265 (21), pp. 12293-12299.

Carroll, M.C. (1998) 'CD21/CD35 in B cell activation'. *Seminars in Immunology,* 10 (4), pp. 279-286.

Carroll, Michael c. and Isenman, David e. (2012) 'Regulation of humoral immunity by complement'. *Immunity,* 37 (2), pp. 199-207.

Cder, C.F.D.E.a.R. (2009) *Application number: 22-527. Clinical pharmacology and biopharmaceutics review(s).* . Available at: http://www.accessdata.fda.gov/drugsatfda_docs/nda/2010/022527Orig1s000clinpharmr.pdf (Accessed: August 22nd 2020).

Chaudhury, C., Mehnaz, S., Robinson, J.M., Hayton, W.L., Pearl, D.K., Roopenian, D.C. and Anderson, C.L. (2003) 'The major histocompatibility complex-related Fc receptor for IgG (FcRn) binds albumin and prolongs its lifespan'. *Journal of Experimental Medicine,* 197 (3), pp. 315-322.

Clemenza, L. and Isenman, D.E. (2000) 'Structure-guided identification of C3d residues essential for its binding to complement receptor 2 (CD21)'. *The Journal of Immunology,* 165 (7), pp. 3839-3848.

Collins, A.M. (2016) 'IgG subclass co-expression brings harmony to the quartet model of murine IgG function'. *Immunology and Cell Biology,* 94 (10), pp. 949-954.

Cook, D., Brown, D., Alexander, R., March, R., Morgan, P., Satterthwaite, G. and Pangalos, M.N. (2014) 'Lessons learned from the fate of Astrazeneca's drug pipeline: A five-dimensional framework'. *Nature Reviews: Drug Discovery,* 13 (6), pp. 419-431.

Cozzani, E., Drosera, M., Gasparini, G. and Parodi, A. (2014) 'Serology of lupus erythematosus: Correlation between immunopathological features and clinical aspects'. *Autoimmune Diseases,* 2014 321359.

Danhof, M., De Lange, E.C., Della Pasqua, O.E., Ploeger, B.A. and Voskuyl, R.A. (2008) 'Mechanism-based pharmacokinetic-pharmacodynamic (PK-PD) modeling in translational drug research'. *Trends in Pharmacological Sciences,* 29 (4), pp. 186-191.

David, O.J., Kovarik, J.M. and Schmouder, R.L. (2012) 'Clinical pharmacokinetics of Fingolimod'. *Clinical Pharmacokinetics,* 51 (1), pp. 15-28.

Dayneka, N.L., Garg, V. and Jusko, W.J. (1993) 'Comparison of four basic models of indirect pharmacodynamic responses'. *Journal of Pharmacokinetics and Biopharmaceutics,* 21 (4), pp. 457-478.

De Silva, N.S. and Klein, U. (2015) 'Dynamics of B cells in germinal centres'. *Nature Reviews Immunology,* 15 137.

Delves, P.J. and Roitt, I.M. (2000) 'The immune system. First of two parts'. *New England Journal of Medicine,* 343 (1), pp. 37-49.

Dempsey, P.W., Allison, M.E., Akkaraju, S., Goodnow, C.C. and Fearon, D.T. (1996) 'C3d of complement as a molecular adjuvant: Bridging innate and acquired immunity'. *Science,* 271 (5247), pp. 348-350.

Deng, R., Jin, F., Prabhu, S. and Iyer, S. (2012) 'Monoclonal antibodies: What are the pharmacokinetic and pharmacodynamic considerations for drug development?'. *Expert Opinion on Drug Metabolism & Toxicology,* 8 (2), pp. 141-160.

Derendorf, H. and Meibohm, B. (1999) 'Modeling of pharmacokinetic/pharmacodynamic (PK/PD) relationships: Concepts and perspectives'. *Pharmaceutical Research,* 16 (2), pp. 176-185.

Dickinson, B.L., Badizadegan, K., Wu, Z., Ahouse, J.C., Zhu, X., Simister, N.E., Blumberg, R.S. and Lencer, W.I. (1999) 'Bidirectional FcRn-dependent IgG transport in a polarized human intestinal epithelial cell line'. *Journal of Clinical Investigation,* 104 (7), pp. 903-911.

Dilillo, D.J., Hamaguchi, Y., Ueda, Y., Yang, K., Uchida, J., Haas, K.M., Kelsoe, G. and Tedder, T.F. (2007) 'Maintenance of long-lived plasma cells and serological memory despite mature and memory B cell depletion during CD20 immunotherapy in mice'. *The Journal of Immunology,* 180 (1), pp. 361-371.

Dimasi, J.A., Grabowski, H.G. and Hansen, R.W. (2016) 'Innovation in the pharmaceutical industry: New estimates of r&d costs'. *Journal of Health Economics,* 47 20-33.

Donius, L.R., Handy, J.M., Weis, J.J. and Weis, J.H. (2013) 'Optimal germinal center B cell activation and T-dependent antibody responses require expression of the mouse complement receptor CR1'. *Journal of Immunology,* 191 (1), pp. 434-447.

Dostalek, M., Gardner, I., Gurbaxani, B.M., Rose, R.H. and Chetty, M. (2013) 'Pharmacokinetics, pharmacodynamics and physiologically-based pharmacokinetic modelling of monoclonal antibodies'. *Clinical Pharmacokinetics,* 52 (2), pp. 83-124.

Dua, P., Hawkins, E. and Van Der Graaf, P.H. (2015) 'A tutorial on target-mediated drug disposition (TMDD) models'. *CPT: pharmacometrics & systems pharmacology,* 4 (6), pp. 324-337.

Ecker, D.M., Jones, S.D. and Levine, H.L. (2015) 'The therapeutic monoclonal antibody market'. *MAbs,* 7 (1), pp. 9-14.

Emotte, C., Deglave, F., Heudi, O., Picard, F. and Kretz, O. (2012) 'Fast simultaneous quantitative analysis of FTY720 and its metabolite FTY720-P in human blood by on-line solid phase extraction coupled with liquid chromatography–tandem mass spectrometry'. *Journal of Pharmaceutical and Biomedical Analysis,* 58 102-112.

Espie, P., He, Y., Koo, P., Sickert, D., Dupuy, C., Chokote, E., Schuler, R., Mergentaler, H., Ristov, J., Milojevic, J., Verles, A., Groenewegen, A., Auger, A., Avrameas, A., Rotte, M., Colin, L., Tomek, C.S., Hernandez-Illas, M., Rush, J.S. and Gergely, P. (2020) 'First-in-human clinical trial to assess pharmacokinetics, pharmacodynamics, safety, and tolerability of Iscalimab, an anti-CD40 monoclonal antibody'. *American Journal of Transplantation,* 20 (2), pp. 463-473.

Ezan, E. (2013) 'Pharmacokinetic studies of protein drugs: Past, present and future'. *Advanced Drug Delivery Reviews,* 65 (8), pp. 1065-1073.

Fang, Y., Xu, C., Fu, Y.-X., Holers, V.M. and Molina, H. (1998) 'Expression of complement receptors 1 and 2 on follicular dendritic cells is necessary for the generation of a strong antigen-specific IgG response'. *The Journal of Immunology,* 160 (11), pp. 5273-5279.

Fearon, D.T. and Carroll, M.C. (2000) 'Regulation of B lymphocyte responses to foreign and self-antigens by the CD19/CD21 complex'. *Annual Review of Immunology,* 18 393-422.

Fraley, K.J., Abberley, L., Hottenstein, C.S., Ulicne, J.J., Citerone, D.R. and Szapacs, M.E. (2013) 'The gyrolab immunoassay system: A platform for automated bioanalysis and rapid sample turnaround'. *Bioanalysis,* 5 (14), pp. 1765-1774.

Frémeaux-Bacchi, V., Aubry, J.P., Bonnefoy, J.Y., Kazatchkine, M.D., Kolb, J.P. and Fischer, E.M. (1998) 'Soluble CD21 induces activation and differentiation of human monocytes through binding to membrane CD23'. *European Journal of Immunology,* 28 (12), pp. 4268-4274.

Frey, A., Di Canzio, J. and Zurakowski, D. (1998) 'A statistically defined endpoint titer determination method for immunoassays'. *Journal of Immunological Methods,* 221 (1-2), pp. 35-41.

Garg, A. and Balthasar, J.P. (2007) 'Physiologically-based pharmacokinetic (PBPK) model to predict IgG tissue kinetics in wild-type and FcRn-knockout mice'. *Journal of Pharmacokinetics and Pharmacodynamics,* 34 (5), pp. 687-709.

Ghetie, V., Hubbard, J.G., Kim, J.K., Tsen, M.F., Lee, Y. and Ward, E.S. (1996) 'Abnormally short serum half-lives of IgG in beta 2-microglobulin-deficient mice'. *European Journal of Immunology,* 26 (3), pp. 690-696.

Grilo, A.L. and Mantalaris, A. (2019) 'The increasingly human and profitable monoclonal antibody market'. *Trends in Biotechnology,* 37 (1), pp. 9-16.

Han, S., Zhang, X., Wang, G., Guan, H., Garcia, G., Li, P., Feng, L. and Zheng, B. (2004) 'FTY720 suppresses humoral immunity by inhibiting germinal center reaction'. *Blood,* 104 (13), pp. 4129-4133.

Hay, M., Thomas, D.W., Craighead, J.L., Economides, C. and Rosenthal, J. (2014) 'Clinical development success rates for investigational drugs'. *Nature Biotechnology,* 32 (1), pp. 40-51.

Hayashida, K., Bartlett, A.H., Chen, Y. and Park, P.W. (2010) 'Molecular and cellular mechanisms of ectodomain shedding'. *Anatomical record (Hoboken, N.J. : 2007),* 293 (6), pp. 925-937.

Hebell, T., Ahearn, J.M. and Fearon, D.T. (1991) 'Suppression of the immune response by a soluble complement receptor of B lymphocytes'. *Science,* 254 (5028), pp. 102.

Heyman, B., Wiersma, E.J. and Kinoshita, T. (1990) 'In vivo inhibition of the antibody response by a complement receptor-specific monoclonal antibody'. *The Journal of Experimental Medicine,* 172 (2), pp. 665-668.

Hoefer, M.M., Aichem, A., Knight, A.M. and Illges, H. (2008) 'Modulation of murine complement receptor type 2 (CR2/CD21) ectodomain shedding by its cytoplasmic domain'. *Molecular Immunology,* 45 (8), pp. 2127-2137.

Holers, V.M. (2014) 'Complement and its receptors: New insights into human disease'. *Annual Review of Immunology,* 32 433-459.

Iyer, S.B., Hultin, L.E., Zawadzki, J.A., Davis, K.A. and Giorgi, J.V. (1998) 'Quantitation of CD38 expression using quantibrite™ beads'. *Cytometry,* 33 (2), pp. 206-212.

Jacobson, A.C. and Weis, J.H. (2008) 'Comparative functional evolution of human and mouse CR1 and CR2'. *The Journal of Immunology,* 181 (5), pp. 2953-2959.

Joyce, A.P., Wang, M., Lawrence-Henderson, R., Filliettaz, C., Leung, S.S., Xu, X. and O'hara, D.M. (2014) 'One mouse, one pharmacokinetic profile: Quantitative whole blood serial sampling for biotherapeutics'. *Pharmaceutical Research,* 31 (7), pp. 1823-1833.

Junghans, R.P. and Anderson, C.L. (1996) 'The protection receptor for IgG catabolism is the beta2-microglobulin-containing neonatal intestinal transport receptor'. *Proceedings of the National Academy of Sciences,* 93 (11), pp. 5512-5516.

Jusko, W.J., Ko, H.C. and Ebling, W.F. (1995) 'Convergence of direct and indirect pharmacodynamic response models'. *Journal of Pharmacokinetics and Biopharmaceutics,* 23 (1), pp. 5-8; discussion 9-10.

Kagan, L., Gershkovich, P., Mendelman, A., Amsili, S., Ezov, N. and Hoffman, A. (2007) 'The role of the lymphatic system in subcutaneous absorption of macromolecules in the rat model'. *European Journal of Pharmaceutics and Biopharmaceutics,* 67 (3), pp. 759-765.

Kagan, L., Turner, M.R., Balu-Iyer, S.V. and Mager, D.E. (2012) 'Subcutaneous absorption of monoclonal antibodies: Role of dose, site of injection, and injection volume on Rituximab pharmacokinetics in rats'. *Pharmaceutical Research,* 29 (2), pp. 490-499.

Kamburova, E.G., Koenen, H.J.P.M., Borgman, K.J.E., Ten Berge, I.J., Joosten, I. and Hilbrands, L.B. (2013) 'A single dose of Rituximab does not deplete B cells in secondary lymphoid organs but alters phenotype and function'. *American Journal of Transplantation,* 13 (6), pp. 1503-1511.

Kaplon, H., Muralidharan, M., Schneider, Z. and Reichert, J.M. (2020) 'Antibodies to watch in 2020'. *mAbs,* 12 (1), pp. 1703531.

Kaplon, H. and Reichert, J.M. (2019) 'Antibodies to watch in 2019'. *mAbs,* 11 (2), pp. 219-238.

Keizer, R.J., Huitema, A.D., Schellens, J.H. and Beijnen, J.H. (2010) 'Clinical pharmacokinetics of therapeutic monoclonal antibodies'. *Clinical Pharmacokinetics,* 49 (8), pp. 493-507.

Kelsoe, G. and Zheng, B. (1993) 'Sites of B-cell activation in vivo'. *Current Opinion in Immunology,* 5 (3), pp. 418-422.

Kim, Y.U., Kinoshita, T., Molina, H., Hourcade, D., Seya, T., Wagner, L.M. and Holers, V.M. (1995) 'Mouse complement regulatory protein Crry/p65 uses the specific mechanisms of both human decay-accelerating factor and membrane cofactor protein'. *The Journal of Experimental Medicine,* 181 (1), pp. 151-159.

Kinoshita, T., Takeda, J., Hong, K., Kozono, H., Sakai, H. and Inoue, K. (1988) 'Monoclonal antibodies to mouse complement receptor type 1 (CR1). Their use in a distribution study showing that mouse erythrocytes and platelets are CR1-negative'. *The Journal of Immunology,* 140 (9), pp. 3066-3072.

Kinoshita, T., Thyphronitis, G., Tsokos, G.C., Finkelman, F.D., Hong, K., Sakai, H. and Inoue, K. (1990) 'Characterization of murine complement receptor type 2 and its immunological cross-reactivity with type 1 receptor'. *International Immunology,* 2 (7), pp. 651-659.

Kovarik, J.M., Slade, A., Voss, B., Schmidli, H., Riviere, G.J., Picard, F., Sugita, Y., Kawai, R., Mee-Lee, D. and Schmouder, R.L. (2007) 'Ethnic sensitivity study of Fingolimod in white and asian subjects'. *International Journal of Clinical Pharmacology and Therapeutics,* 45 (2), pp. 98-109.

Kulik, L., Chen, K., Huber, B.T. and Holers, V.M. (2011) 'Human complement receptor type 2 (CR2/CD21) transgenic mice provide an in vivo model to study immunoregulatory effects of receptor antagonists'. *Molecular Immunology,* 48 (6-7), pp. 883-894.

Kulik, L., Hewitt, F.B., Willis, V.C., Rodriguez, R., Tomlinson, S. and Holers, V.M. (2015) 'A new mouse anti-mouse complement receptor type 2 and 1 (CR2/CR1) monoclonal antibody as a tool to study receptor involvement in chronic models of immune responses and disease'. *Molecular Immunology,* 63 (2), pp. 479-488.

Kuo, T.T. and Aveson, V.G. (2011) 'Neonatal Fc receptor and IgG-based therapeutics'. *MAbs,* 3 (5), pp. 422-430.

Kurtz, C.B., Paul, M.S., Aegerter, M., Weis, J.J. and Weis, J.H. (1989) 'Murine complement receptor gene family. II. Identification and characterization of the murine homolog

(CR2) to human CR2 and its molecular linkage to Crry'. *The Journal of Immunology,* 143 (6), pp. 2058-2067.

Larcher, C., Kempkes, B., Kremmer, E., Prodinger, W.M., Pawlita, M., Bornkamm, G.W. and Dierich, M.P. (1995) 'Expression of Epstein-barr virus nuclear antigen-2 (EBNA2) induces CD21/CR2 on B and T cell lines and shedding of soluble CD21'. *European Journal of Immunology,* 25 (6), pp. 1713-1719.

Lebrec, H., Hock, M.B., Sundsmo, J.S., Mytych, D.T., Chow, H., Carlock, L.L., Joubert, M.K., Reindel, J., Zhou, L. and Bussiere, J.L. (2014a) 'T-cell-dependent antibody responses in the rat: Forms and sources of keyhole limpet hemocyanin matter'. *Journal of Immunotoxicology,* 11 (3), pp. 213-221.

Lebrec, H., Molinier, B., Boverhof, D., Collinge, M., Freebern, W., Henson, K., Mytych, D.T., Ochs, H.D., Wange, R., Yang, Y., Zhou, L., Arrington, J., Christin-Piché, M.S. and Shenton, J. (2014b) 'The T-cell-dependent antibody response assay in nonclinical studies of pharmaceuticals and chemicals: Study design, data analysis, interpretation'. *Regulatory Toxicology and Pharmacology,* 69 (1), pp. 7-21.

Levy, G. (1994) 'Pharmacologic target-mediated drug disposition'. *Clinical Pharmacology and Therapeutics,* 56 (3), pp. 248-252.

Li, L., Gardner, I., Rose, R. and Jamei, M. (2014) 'Incorporating target shedding into a minimal PBPK-TMDD model for monoclonal antibodies'. *CPT: pharmacometrics & systems pharmacology,* 3 e96.

Liu, R., Pillutla, R., Desilva, B. and Zhang, Y.J. (2013) 'Rapid development of multiple 'fit-for-purpose' assays on an automatic microfluidic system using a streamlined process in support of early biotherapeutics discovery programs'. *Bioanalysis,* 5 (14), pp. 1751-1763.

Lobo, E.D., Hansen, R.J. and Balthasar, J.P. (2004) 'Antibody pharmacokinetics and pharmacodynamics'. *Journal of Pharmaceutical Sciences,* 93 (11), pp. 2645-2668.

Lowe, J., Brown, B., Hardie, D., Richardson, P. and Ling, N. (1989) 'Soluble forms of CD21 and CD23 antigens in the serum in B cell chronic lymphocytic leukaemia'. *Immunology Letters,* 20 (2), pp. 103-109.

Lowe, P.J., Tannenbaum, S., Wu, K., Lloyd, P. and Sims, J. (2010) 'On setting the first dose in man: Quantitating biotherapeutic drug-target binding through pharmacokinetic and pharmacodynamic models'. *Basic & Clinical Pharmacology & Toxicology,* 106 (3), pp. 195-209.

Luckheeram, R.V., Zhou, R., Verma, A.D. and Xia, B. (2012) 'Cd4(+) T cells: Differentiation and functions'. *Clinical and Developmental Immunology,* 2012 925135.

Luu, K.T., Kraynov, E., Kuang, B., Vicini, P. and Zhong, W.Z. (2013) 'Modeling, simulation, and translation framework for the preclinical development of monoclonal antibodies'. *The AAPS journal,* 15 (2), pp. 551-558.

Luxembourg, A.T. and Cooper, N.R. (1994) 'Modulation of signaling via the B cell antigen receptor by CD21, the receptor for C3dg and EBV'. *Journal of Immunology,* 153 (10), pp. 4448-4457.

Lyubchenko, T., Dal Porto, J., Cambier, J.C. and Holers, V.M. (2005) 'Coligation of the B cell receptor with complement receptor type 2 (CR2/CD21) using its natural ligand C3dg: Activation without engagement of an inhibitory signaling pathway'. *Journal of Immunology,* 174 (6), pp. 3264-3272.

Maclennan, I.C.M., Toellner, K.-M., Cunningham, A.F., Serre, K., Sze, D.M.-Y., Zúñiga, E., Cook, M.C. and Vinuesa, C.G. (2003) 'Extrafollicular antibody responses'. *Immunological Reviews,* 194 (1), pp. 8-18.

Mager, D.E. and Jusko, W.J. (2001a) 'General pharmacokinetic model for drugs exhibiting target-mediated drug disposition'. *Journal of Pharmacokinetics and Pharmacodynamics,* 28 (6), pp. 507-532.

Mager, D.E. and Jusko, W.J. (2001b) 'Pharmacodynamic modeling of time-dependent transduction systems'. *Clinical Pharmacology and Therapeutics,* 70 (3), pp. 210-216.

Martin, D.R., Yuryev, A., Kalli, K.R., Fearon, D.T. and Ahearn, J.M. (1991) 'Determination of the structural basis for selective binding of Epstein-barr virus to human complement receptor type 2'. *Journal of Experimental Medicine,* 174 (6), pp. 1299-1311.

Masilamani, M., Apell, H.-J. and Illges, H. (2002) 'Purification and characterization of soluble CD21 from human plasma by affinity chromatography and density gradient centrifugation'. *Journal of Immunological Methods,* 270 (1), pp. 11-18.

Masilamani, M., Kassahn, D., Mikkat, S., Glocker, M.O. and Illges, H. (2003a) 'B cell activation leads to shedding of complement receptor type II (CR2/CD21)'. *European Journal of Immunology,* 33 (9), pp. 2391-2397.

Masilamani, M., Nowack, R., Witte, T., Schlesier, M., Warnatz, K., Glocker, M.O., Peter, H.H. and Illges, H. (2004) 'Reduction of soluble complement receptor 2/CD21 in systemic lupus erythomatosus and Sjogren's syndrome but not juvenile arthritis'. *Scandinavian Journal of Immunology,* 60 (6), pp. 625-630.

Masilamani, M., Von Kempis, J. and Illges, H. (2003b) 'Decreased levels of serum soluble complement receptor-II (CR2/CD21) in patients with rheumatoid arthritis'. *Rheumatology,* 43 (2), pp. 186-190.

Meibohm, B. and Derendorf, H. (1997) 'Basic concepts of pharmacokinetic/pharmacodynamic (PK/PD) modelling'. *International Journal of Clinical Pharmacology and Therapeutics,* 35 (10), pp. 401-413.

Meno-Tetang, G.M., Li, H., Mis, S., Pyszczynski, N., Heining, P., Lowe, P. and Jusko, W.J. (2006) 'Physiologically based pharmacokinetic modeling of FTY720 (2-amino-2[2-(-4-octylphenyl)ethyl]propane-1,3-diol hydrochloride) in rats after oral and intravenous doses'. *Drug Metabolism and Disposition: The Biological Fate of Chemicals,* 34 (9), pp. 1480-1487.

Meno-Tetang, G.M.L. and Lowe, P.J. (2005) 'On the prediction of the human response: A recycled mechanistic pharmacokinetic/pharmacodynamic approach'. *Basic & Clinical Pharmacology & Toxicology,* 96 (3), pp. 182-192.

Molina, H., Holers, V.M., Li, B., Fung, Y., Mariathasan, S., Goellner, J., Strauss-Schoenberger, J., Karr, R.W. and Chaplin, D.D. (1996) 'Markedly impaired humoral

immune response in mice deficient in complement receptors 1 and 2'. *Proceedings of the National Academy of Sciences of the United States of America,* 93 (8), pp. 3357-3361.

Molina, H., Perkins, S.J., Guthridge, J., Gorka, J., Kinoshita, T. and Holers, V.M. (1995) 'Characterization of a complement receptor 2 (CR2, CD21) ligand binding site for C3. An initial model of ligand interaction with two linked short consensus repeat modules'. *Journal of Immunology,* 154 (10), pp. 5426-5435.

Morgan, P., Brown, D.G., Lennard, S., Anderton, M.J., Barrett, J.C., Eriksson, U., Fidock, M., Hamrén, B., Johnson, A., March, R.E., Matcham, J., Mettetal, J., Nicholls, D.J., Platz, S., Rees, S., Snowden, M.A. and Pangalos, M.N. (2018) 'Impact of a five-dimensional framework on R&D productivity at Astrazeneca'. *Nature Reviews Drug Discovery,* 17 (3), pp. 167-181.

Morgan, P., Van Der Graaf, P.H., Arrowsmith, J., Feltner, D.E., Drummond, K.S., Wegner, C.D. and Street, S.D. (2012) 'Can the flow of medicines be improved? Fundamental pharmacokinetic and pharmacological principles toward improving phase ii survival'. *Drug Discovery Today,* 17 (9-10), pp. 419-424.

Morris, M.A., Gibb, D.R., Picard, F., Brinkmann, V., Straume, M. and Ley, K. (2005) 'Transient T cell accumulation in lymph nodes and sustained lymphopenia in mice treated with FTY720'. *European Journal of Immunology,* 35 (12), pp. 3570-3580.

Morsy, D.E.D., Sanyal, R., Zaiss, A.K., Deo, R., Muruve, D.A. and Deans, J.P. (2013) 'Reduced T-dependent humoral immunity in CD20-deficient mice'. *The Journal of Immunology,* 191 (6), pp. 3112.

Moyron-Quiroz, J.E., Lin, L., Oida, T., Garcia-Mojica, S. and Yang, X. (2016) 'Kinetic study of B cell-depletion with a novel mab anti-mouse CD20, clone SA271G2'. *The Journal of Immunology,* 196 (1 Supplement), pp. 209.223.

Neuber, T., Frese, K., Jaehrling, J., Jäger, S., Daubert, D., Felderer, K., Linnemann, M., Höhne, A., Kaden, S., Kölln, J., Tiller, T., Brocks, B., Ostendorp, R. and Pabst, S. (2014) 'Characterization and screening of IgG binding to the neonatal Fc receptor'. *mAbs,* 6 (4), pp. 928-942.

Nilsson, L.B., Ahnoff, M. and Jonsson, O. (2013) 'Capillary microsampling in the regulatory environment: Validation and use of bioanalytical capillary microsampling methods'. *Bioanalysis,* 5 (6), pp. 731-738.

Nimmerjahn, F. and Ravetch, J.V. (2008) 'Fcgamma receptors as regulators of immune responses'. *Nature Reviews: Immunology,* 8 (1), pp. 34-47.

Nirogi, R., Padala, N.P., Ajjala, D.R., Boggavarapu, R.K. and Kunduru, P. (2017) 'Incurred sample reanalysis of Fingolimod and Fingolimod phosphate in blood: Stability evaluation and application to a rat pharmacokinetic study'. *Bioanalysis,* 9 (7), pp. 565-577.

Ober, R.J. (2001) 'Differences in promiscuity for antibody-FcRn interactions across species: Implications for therapeutic antibodies'. *International Immunology,* 13 (12), pp. 1551-1559.

Oren, S., Mandelboim, M., Braun-Moscovici, Y., Paran, D., Ablin, J., Litinsky, I., Comaneshter, D., Levartovsky, D., Mendelson, E., Azar, R., Wigler, I., Balbir-Gurman, A., Caspi, D. and Elkayam, O. (2008) 'Vaccination against influenza in patients with rheumatoid arthritis: The effect of Rituximab on the humoral response'. *Annals of the Rheumatic Diseases,* 67 (7), pp. 937-941.

Pannu, K.K., Joe, E.T. and Iyer, S.B. (2001) 'Performance evaluation of quantibrite phycoerythrin beads'. *Cytometry,* 45 (4), pp. 250-258.

Patton, A., Mullenix, M.C., Swanson, S.J. and Koren, E. (2005) 'An acid dissociation bridging ELISA for detection of antibodies directed against therapeutic proteins in the presence of antigen'. *Journal of Immunological Methods,* 304 (1), pp. 189-195.

Paul, S.M., Mytelka, D.S., Dunwiddie, C.T., Persinger, C.C., Munos, B.H., Lindborg, S.R. and Schacht, A.L. (2010) 'How to improve R&D productivity: The pharmaceutical industry's grand challenge'. *Nature Reviews: Drug Discovery,* 9 (3), pp. 203-214.

Pepys, M.B. (1974) 'Role of complement in induction of antibody production in vivo'. *The Journal of Experimental Medicine,* 140 (1), pp. 126-145.

Phan, T.G., Green, J.A., Gray, E.E., Xu, Y. and Cyster, J.G. (2009) 'Immune complex relay by subcapsular sinus macrophages and noncognate B cells drives antibody affinity maturation'. *Nature Immunology,* 10 (7), pp. 786-793.

Poirier, N., Blancho, G., Hiance, M., Mary, C., Van Assche, T., Lempoels, J., Ramael, S., Wang, W., Thepenier, V., Braudeau, C., Salabert, N., Josien, R., Anderson, I., Gourley, I., Soulillou, J.-P., Coquoz, D. and Vanhove, B. (2016) 'First-in-human study in healthy subjects with FR104, a pegylated monoclonal antibody fragment antagonist of CD28'. *The Journal of Immunology,* 197 (12), pp. 4593-4602.

Porter, C.J. and Charman, S.A. (2000) 'Lymphatic transport of proteins after subcutaneous administration'. *Journal of Pharmaceutical Sciences,* 89 (3), pp. 297-310.

Proc, J.L., Kuzyk, M.A., Hardie, D.B., Yang, J., Smith, D.S., Jackson, A.M., Parker, C.E. and Borchers, C.H. (2010) 'A quantitative study of the effects of chaotropic agents, surfactants, and solvents on the digestion efficiency of human plasma proteins by trypsin'. *Journal of Proteome Research,* 9 (10), pp. 5422-5437.

Prueksaritanont, T. and Tang, C. (2012) 'ADME of biologics-what have we learned from small molecules?'. *The AAPS journal,* 14 (3), pp. 410-419.

Reilly, R.M., Domingo, R. and Sandhu, J. (1997) 'Oral delivery of antibodies. Future pharmacokinetic trends'. *Clinical Pharmacokinetics,* 32 (4), pp. 313-323.

Ristov, J., Espie, P., Ulrich, P., Sickert, D., Flandre, T., Dimitrova, M., Muller-Ristig, D., Weider, D., Robert, G., Schmutz, P., Greutmann, B., Cordoba-Castro, F., Schneider, M.A., Warncke, M., Kolbinger, F., Cote, S., Heusser, C., Bruns, C. and Rush, J.S. (2018) 'Characterization of the in vitro and in vivo properties of CFZ533, a blocking and non-depleting anti-CD40 monoclonal antibody'. *American Journal of Transplantation,* 18 (12), pp. 2895-2904.

Roman, J., Qiu, J., Dornadula, G., Hamuro, L., Bakhtiar, R. and Verch, T. (2011) 'Application of miniaturized immunoassays to discovery pharmacokinetic bioanalysis'. *Journal of Pharmacological and Toxicological Methods,* 63 (3), pp. 227-235.

Roopenian, D.C. and Akilesh, S. (2007) 'FcRn: The neonatal Fc receptor comes of age'. *Nature Reviews: Immunology,* 7 (9), pp. 715-725.

Salimi-Moosavi, H., Lee, J., Desilva, B. and Doellgast, G. (2010) 'Novel approaches using alkaline or acid/guanidine treatment to eliminate therapeutic antibody interference in the measurement of total target ligand'. *Journal of Pharmaceutical and Biomedical Analysis,* 51 (5), pp. 1128-1133.

Saylor, K. and Zhang, C. (2016) 'A simple physiologically based pharmacokinetic model evaluating the effect of anti-nicotine antibodies on nicotine disposition in the brains of rats and humans'. *Toxicology and Applied Pharmacology,* 307 150-164.

Sengers, B.G., Mcginty, S., Nouri, F.Z., Argungu, M., Hawkins, E., Hadji, A., Weber, A., Taylor, A. and Sepp, A. (2016) 'Modeling bispecific monoclonal antibody interaction with two cell membrane targets indicates the importance of surface diffusion'. *mAbs,* 8 (5), pp. 905-915.

Shah, D.K. and Betts, A.M. (2012) 'Towards a platform pbpk model to characterize the plasma and tissue disposition of monoclonal antibodies in preclinical species and human'. *Journal of Pharmacokinetics and Pharmacodynamics,* 39 (1), pp. 67-86.

Shi, R., Honczarenko, M., Zhang, S., Fleener, C., Mora, J., Lee, S.K., Wang, R., Liu, X., Shevell, D.E., Yang, Z., Wang, H. and Murthy, B. (2017) 'Pharmacokinetic, pharmacodynamic, and safety profile of a novel anti-CD28 domain antibody antagonist in healthy subjects'. *The Journal of Clinical Pharmacology,* 57 (2), pp. 161-172.

Singh, A., Blank, M., Shoenfeld, Y. and Illges, H. (2008) 'Antiphospholipid syndrome patients display reduced titers of soluble CD21 in their sera irrespective of circulating anti-β2-glycoprotein-I autoantibodies'. *Rheumatology International,* 28 (7), pp. 661-665.

Slade, A., Koo, P., He, Y., Espie, P., Auger-Sarrazin, A., Rush, J. and Gergely, P. (2016) 'FRI0230 assessment of safety, pharmacokinetics and pharmacodynamics of a novel anti-CD40 monoclonal antibody, CFZ533, in healthy volunteers and in rheumatoid arthritis patients'. *Annals of the Rheumatic Diseases,* 75 (Suppl 2), pp. 516-517.

Sullivan, B.A., Tsuji, W., Kivitz, A., Peng, J., Arnold, G.E., Boedigheimer, M.J., Chiu, K., Green, C.L., Kaliyaperumal, A., Wang, C., Ferbas, J. and Chung, J.B. (2016) 'Inducible T-cell co-stimulator ligand (ICOSL) blockade leads to selective inhibition of anti-KLH IgG responses in subjects with systemic lupus erythematosus'. *Lupus Science & Medicine,* 3 (1), pp. e000146.

Sun, Y.N. and Jusko, W.J. (1998) 'Transit compartments versus gamma distribution function to model signal transduction processes in pharmacodynamics'. *Journal of Pharmaceutical Sciences,* 87 (6), pp. 732-737.

Supersaxo, A., Hein, W.R. and Steffen, H. (1990) 'Effect of molecular weight on the lymphatic absorption of water-soluble compounds following subcutaneous administration'. *Pharmaceutical Research,* 7 (2), pp. 167-169.

Swaminathan, A., Lucas, R.M., Dear, K. and Mcmichael, A.J. (2014) 'Keyhole limpet haemocyanin - a model antigen for human immunotoxicological studies'. *British Journal of Clinical Pharmacology,* 78 (5), pp. 1135-1142.

Tabrizi, M., Bornstein, G.G. and Suria, H. (2010a) 'Biodistribution mechanisms of therapeutic monoclonal antibodies in health and disease'. *The AAPS journal,* 12 (1), pp. 33-43.

Tabrizi, M., Funelas, C. and Suria, H. (2010b) 'Application of quantitative pharmacology in development of therapeutic monoclonal antibodies'. *The AAPS journal,* 12 (4), pp. 592-601.

Tanner, J., Weis, J., Fearon, D., Whang, Y. and Kieff, E. (1987) 'Epstein-barr virus gp350/220 binding to the B lymphocyte C3d receptor mediates adsorption, capping, and endocytosis'. *Cell,* 50 (2), pp. 203-213.

Tessier, J., Cuvillier, A., Glaudet, F. and Khamlichi, A.A. (2007) 'Internalization and molecular interactions of human CD21 receptor'. *Molecular Immunology,* 44 (9), pp. 2415-2425.

Thiel, J., Kimmig, L., Salzer, U., Grudzien, M., Lebrecht, D., Hagena, T., Draeger, R., Voelxen, N., Bergbreiter, A., Jennings, S., Gutenberger, S., Aichem, A., Illges, H., Hannan, J.P., Kienzler, A.K., Rizzi, M., Eibel, H., Peter, H.H., Warnatz, K., Grimbacher, B., Rump, J.A. and Schlesier, M. (2012) 'Genetic CD21 deficiency is associated with hypogammaglobulinemia'. *Journal of Allergy and Clinical Immunology,* 129 (3), pp. 801-810 e806.

Tomita, M., Kadono, T., Yazawa, N., Kawashima, T., Tamaki, Z., Ashida, R., Ohmatsu, H., Asano, Y., Sugaya, M., Kubo, M., Ihn, H., Tamaki, K. and Sato, S. (2012) 'Serum levels of soluble CD21 in patients with systemic sclerosis'. *Rheumatology International,* 32 (2), pp. 317-321.

Tooze, J.A. and Bevan, D.H. (1991) 'Decreased expression of complement receptor type 2 (CR2) on neoplastic B cells of chronic lymphocytic leukaemia'. *Clinical and Experimental Immunology,* 83 (3), pp. 423-429.

Uniprot, C. (2019) 'Uniprot: A worldwide hub of protein knowledge'. *Nucleic Acids Research,* 47 (D1), pp. D506-D515.

Vainshtein, I., Roskos, L.K., Cheng, J., Sleeman, M.A., Wang, B. and Liang, M. (2015) 'Quantitative measurement of the target-mediated internalization kinetics of biopharmaceuticals'. *Pharmaceutical Research,* 32 (1), pp. 286-299.

Van Der Graaf, P.H. and Benson, N. (2011) 'Systems pharmacology: Bridging systems biology and pharmacokinetics-pharmacodynamics (PKPD) in drug discovery and development'. *Pharmaceutical Research,* 28 (7), pp. 1460-1464.

Van Ommen, R., Vredendaal, A.E., De Gooyer, M., Van Oudenaren, A. and Savelkoul, H.F. (1994) 'The effect of IFN-gamma, alum and complete Freund adjuvant on TNP-KLH induced Ig.G(1), IgE and IgG(2a) responses in mice'. *Mediators of Inflammation,* 3 (5), pp. 387-392.

Vieira, P. and Rajewsky, K. (1988) 'The half-lives of serum immunoglobulins in adult mice'. *European Journal of Immunology,* 18 (2), pp. 313-316.

Vugmeyster, Y., Xu, X., Theil, F.P., Khawli, L.A. and Leach, M.W. (2012) 'Pharmacokinetics and toxicology of therapeutic proteins: Advances and challenges'. *World Journal of Biological Chemistry,* 3 (4), pp. 73-92.

Wang, W., Wang, E.Q. and Balthasar, J.P. (2008) 'Monoclonal antibody pharmacokinetics and pharmacodynamics'. *Clinical Pharmacology and Therapeutics,* 84 (5), pp. 548-558.

Weinstein, J.N. and Van Osdol, W. (1992) 'The macroscopic and microscopic pharmacology of monoclonal antibodies'. *International Journal of Immunopharmacology,* 14 (3), pp. 457-463.

Westermann, J. and Pabst, R. (1992) 'Distribution of lymphocyte subsets and natural killer cells in the human body'. *The clinical investigator,* 70 (7), pp. 539-544.

Whipple, E.C., Shanahan, R.S., Ditto, A.H., Taylor, R.P. and Lindorfer, M.A. (2004) 'Analyses of the in vivo trafficking of stoichiometric doses of an anti-complement receptor 1/2 monoclonal antibody infused intravenously in mice'. *The Journal of Immunology,* 173 (4), pp. 2297-2306.

Wong, H., Bohnert, T., Damian-Iordache, V., Gibson, C., Hsu, C.-P., Krishnatry, A.S., Liederer, B.M., Lin, J., Lu, Q., Mettetal, J.T., Mudra, D.R., Nijsen, M.J.M.A., Schroeder, P., Schuck, E., Suryawanshi, S., Trapa, P., Tsai, A., Wang, H. and Wu, F. (2017) 'Translational pharmacokinetic-pharmacodynamic analysis in the pharmaceutical industry: An iq consortium pk-pd discussion group perspective'. *Drug Discovery Today,* 22 (10), pp. 1447-1459.

Wu, X., Jiang, N., Fang, Y.F., Xu, C., Mao, D., Singh, J., Fu, Y.X. and Molina, H. (2000) 'Impaired affinity maturation in cr2-/- mice is rescued by adjuvants without improvement in germinal center development'. *The Journal of Immunology,* 165 (6), pp. 3119-3127.

Xu, X. and Vugmeyster, Y. (2012) 'Challenges and opportunities in absorption, distribution, metabolism, and excretion studies of therapeutic biologics'. *The AAPS journal,* 14 (4), pp. 781-791.

Yanaba, K., Bouaziz, J.D., Matsushita, T., Magro, C.M., St Clair, E.W. and Tedder, T.F. (2008) 'B-lymphocyte contributions to human autoimmune disease'. *Immunological Reviews,* 223 (1), pp. 284-299.

Yang, Z., Wang, H., Salcedo, T.W., Suchard, S.J., Xie, J.H., Schneeweis, L.A., Fleener, C.A., Calore, J.D., Shi, R., Zhang, S.X.Y., Rodrigues, A.D., Car, B.D., Marathe, P.H. and Nadler, S.G. (2015) 'Integrated pharmacokinetic/pharmacodynamic analysis for determining the minimal anticipated biological effect level of a novel anti-CD28 receptor antagonist BMS-931699'. *Journal of Pharmacology and Experimental Therapeutics,* 355 (3), pp. 506-515.

Zhang, Y., Nester, C.M., Holanda, D.G., Marsh, H.C., Hammond, R.A., Thomas, L.J., Meyer, N.C., Hunsicker, L.G., Sethi, S. and Smith, R.J. (2013) 'Soluble CR1 therapy improves complement regulation in C3 glomerulopathy'. *Journal of the American Society of Nephrology,* 24 (11), pp. 1820-1829.

Zhang, Y. and Pastan, I. (2008) 'High shed antigen levels within tumors: An additional barrier to immunoconjugate therapy'. *Clinical Cancer Research,* 14 (24), pp. 7981-7986.

Zhao, J., Cao, Y. and Jusko, W.J. (2015) 'Across-species scaling of monoclonal antibody pharmacokinetics using a minimal PBPK model'. *Pharmaceutical Research,* 32 (10), pp. 3269-3281.

Zhao, L., Ji, P., Li, Z., Roy, P. and Sahajwalla, C.G. (2013) 'The antibody drug absorption following subcutaneous or intramuscular administration and its mathematical description by coupling physiologically based absorption process with the conventional compartment pharmacokinetic model'. *Journal of Clinical Pharmacology,* 53 (3), pp. 314-325.

Zrein, M., De Marcillac, G. and Van Regenmortel, M.H. (1986) 'Quantitation of rheumatoid factors by enzyme immunoassay using biotinylated human IgG'. *Journal of Immunological Methods,* 87 (2), pp. 229-237.

Permissions

Figure 4.1 – Adapted by permission from Springer Nature: *Journal of Pharmacokinetics and Pharmacodynamics*, 40 (5), pp. 597-607. Cao, Y., Balthasar, J.P. and Jusko, W.J. 'Second-generation minimal physiologically-based pharmacokinetic model for monoclonal antibodies'. © Springer Science+Business Media New York, 2013. [License No. 4892540830699]

Figure 4.2 – Adapted by permission from John Wiley & Sons: *CPT: pharmacometrics & systems pharmacology*, 3 e96. Li, L., Gardner, I., Rose, R. and Jamei, M. 'Incorporating target shedding into a minimal PBPK-TMDD model for monoclonal antibodies'. © ASCPT, 2014. [License No. 4892541239936]

Figure 6.12 / 6.13 / 6.14 – Adapted by permission from John Wiley & Sons: *The Journal of Clinical Pharmacology*, 52 (12), pp. 1879-1890. Boulton, C., Meiser, K., David, O.J. and Schmouder, R. 'Pharmacodynamic effects of steady-state Fingolimod on antibody response in healthy volunteers: A 4-week, randomized, placebo-controlled, parallel-group, multiple-dose study'. © The Author(s), 2012. [License No. 4893001015668]

Appendix I. PK model v1 equations

SimBiology Model: PK model v1: mPBPK model

ODE's

1. **d(Plasma.mAb)/dt** = 1/Plasma*(-([L1*(1-o)]*Plasma.mAb) + (L*Lymph.mAb) - (CLp*Plasma.mAb) - ([(1-o2)*L2]*Plasma.mAb))
2. **d(TightTissue_ISF.mAb)/dt** = 1/TightTissue_ISF*(([L1*(1-o)]*Plasma.mAb) - ([L1*(1-oL)] *TightTissue_ISF.mAb))
3. **d(Lymph.mAb)/dt** = 1/Lymph*(-(L*Lymph.mAb) + ([L1*(1-oL)]*TightTissue_ISF.mAb) + ([L2*(1-oL)]*LeakyTissue_ISF.mAb))
4. **d(LeakyTissue_ISF.mAb)/dt** = 1/LeakyTissue_ISF*(-([L2*(1-oL)]*LeakyTissue_ISF.mAb) + ([L2*(1-o2)]*Plasma.mAb))

Model constituents

Name	Type	Scope	Initial Value	Unit
LeakyTissue_ISF	Compartment	Model	0.001512	Litre
mAb	Species	LeakyTissue_ISF	0	Nanomolarity
Lymph	Compartment	Model	0.002	Litre
mAb	Species	Lymph	0	Nanomolarity
Plasma	Compartment	Model	0.0010625	Litre
mAb	Species	Plasma	0	Nanomolarity
TightTissue_ISF	Compartment	Model	0.002808	Litre
mAb	Species	TightTissue_ISF	0	Nanomolarity
CLp	Parameter	Model	1.0E-5	Litre/hour
L	Parameter	Model	1.5E-4	Litre/hour
L1*(1-o)	Parameter	Model	4.554E-6	Litre/hour
L1*(1-oL)	Parameter	Model	3.96E-5	Litre/hour
L2*(1-o2)	Parameter	Model	4.231E-5	Litre/hour
L2*(1-oL)	Parameter	Model	8.04E-5	Litre/hour

Appendix II. PK model v2 equations

SimBiology Model: PK model v2: mPBPK model incorporating TMDD with shedding

ODE's

1. **d(Plasma.mAb)/dt** = 1/Plasma*(-([L1*(1-o1)]*Plasma.mAb) + (L*Lymph.mAb) - ((mAb_CLp *Plasma.mAb)*Plasma) - ((kon*Plasma.mAb*Plasma.[T,s])*Plasma-(koff*Plasma.[T,smAb]) *Plasma) - ([L2*(1-o2)]*Plasma.mAb) + (ka*Dose_Compartment.mAb))
2. **d(Plasma.[T,s])/dt** = 1/Plasma*(-((kon*Plasma.mAb*Plasma.[T,s])*Plasma-(koff*Plasma.[T,s-mAb]) *Plasma) - (([kdeg,s]*Plasma.[T,s])*Plasma) + (L*Lymph.[T,s]) - ([L2*(1o2)] *Plasma.[T,s]) - ([L1*(1-o1)]*Plasma.[T,s]))
3. **d(Plasma.[T,s-mAb])/dt** = 1/Plasma*(((kon*Plasma.mAb*Plasma.[T,s])*Plasma (koff*Plasma.[T,s-mAb])*Plasma) - ((complex_CLp*Plasma.[T,s-mAb])*Plasma) + (L*Lymph.[T,s-mAb]) - ([L2*(1-o2)] *Plasma.[T,s-mAb]) - ([L1*(1-o1)]*Plasma.[T,s-mAb]))
4. **d(TightTissue.mAb)/dt** = 1/TightTissue*(([L1*(1-o1)]*Plasma.mAb) - ([L1*(1oL)] *TightTissue.mAb) - ((kon*TightTissue.[T,s]*TightTissue.mAb)*TightTissue-(koff*TightTissue.[T,s-mAb])*TightTissue))
5. **d(TightTissue.[T,s])/dt** = 1/TightTissue*(([L1*(1-o1)]*Plasma.[T,s]) - ((kon*TightTissue.[T,s] *TightTissue.mAb)*TightTissue-(koff*TightTissue.[T,s-mAb])*TightTissue) - ([L1*(1-oL)] *TightTissue.[T,s]))
6. **d(TightTissue.[T,s-mAb])/dt** = 1/TightTissue*(((kon*TightTissue.[T,s]*TightTissue.mAb) *TightTissue-(koff*TightTissue.[T,s-mAb])*TightTissue) + ([L1*(1-o1)]*Plasma.[T,s-mAb]) - ([L1*(1-oL)] *TightTissue.[T,smAb]))
7. **d(Lymph.mAb)/dt** = 1/Lymph*(-(L*Lymph.mAb) + ([L1*(1-oL)]*TightTissue.mAb) + ([L2*(1-oL)] *LeakyTissue.mAb) - ((kon*Lymph.mAb*Lymph.[T,s])*Lymph-(koff*Lymph.[T,s-mAb])*Lymph))
8. **d(Lymph.[T,s])/dt** = 1/Lymph*(([L2*(1-oL)]*LeakyTissue.[T,s]) - (L*Lymph.[T,s]) - ((kon*Lymph.mAb *Lymph.[T,s])*Lymph-(koff*Lymph.[T,s-mAb])*Lymph) + ([L1*(1-oL)]*TightTissue.[T,s]))
9. **d(Lymph.[T,s-mAb])/dt** = 1/Lymph*(([L2*(1-oL)]*LeakyTissue.[T,s-mAb]) - (L*Lymph.[T,s-mAb]) + ((kon*Lymph.mAb*Lymph.[T,s])*Lymph-(koff*Lymph.[T,s-mAb])*Lymph) + ([L1*(1-oL)] *TightTissue.[T,s-mAb]))
10. **d(LeakyTissue.mAb)/dt** = 1/LeakyTissue*(-((kon*LeakyTissue.mAb*LeakyTissue.[T,s]) *LeakyTissue-(koff*LeakyTissue.[T,s-mAb])*LeakyTissue) - ((kon*LeakyTissue.mAb*[T,m]) *LeakyTissue-(koff*[T,m-mAb])*LeakyTissue) - ([L2*(1-oL)]*LeakyTissue.mAb) + ([L2*(1-o2)]*Plasma.mAb))

11. **d([T,m])/dt** = 1/LeakyTissue*(-(([kdeg,m]*[T,m])*LeakyTissue) - ((kon*LeakyTissue.mAb*[T,m]) *LeakyTissue-(koff*[T,m-mAb])*LeakyTissue) - (([kshed,m]*[T,m])*LeakyTissue) + (([ksyn,m]*Tm0) *LeakyTissue))
12. **d([T,m-mAb])/dt** = 1/LeakyTissue*(-(([kshed,m_mAb]*[T,m-mAb])*LeakyTissue) - (([kint,m]*[T,m-mAb])*LeakyTissue) + ((kon*LeakyTissue.mAb*[T,m])*LeakyTissue-(koff*[T,m-mAb])*LeakyTissue))
13. **d(LeakyTissue.[T,s])/dt** = 1/LeakyTissue*(-((kon*LeakyTissue.mAb*LeakyTissue.[T,s]) *LeakyTissue-(koff*LeakyTissue.[T,s-mAb])*LeakyTissue) + (([kshed,m]*[T,m])*LeakyTissue) - ([L2*(1-oL)] *LeakyTissue.[T,s]) + ([L2*(1-o2)]*Plasma.[T,s]))
14. **d(LeakyTissue.[T,s-mAb])/dt** = 1/LeakyTissue*((([kshed,m_mAb]*[T,m-mAb])*LeakyTissue) + ((kon*LeakyTissue.mAb*LeakyTissue.[T,s])*LeakyTissue-(koff*LeakyTissue.[T,s-mAb]) *LeakyTissue) - ([L2*(1-oL)]*LeakyTissue.[T,s-mAb]) + ([L2*(1-o2)]*Plasma.[T,s-mAb]))
15. **d(Dose_Compartment.mAb)/dt** = 1/Dose_Compartment*(-(ka*Dose_Compartment.mAb))

Repeated assignments

1. **LeakyTissue.Total_mTarget** = LeakyTissue.[T,m] + LeakyTissue.[T,m-mAb]
2. **Plasma.Total_Target** = Plasma.[T,s]+Plasma.[T,s-mAb]
3. **Total_mAb** = Plasma.mAb+Plasma.[T,s-mAb]

Model constituents

Name	Type	Scope	Initial Value	Unit
Dose_Compartment	Compartment	Model	0.001	Litre
mAb	Species	Dose_Compartment	0	Nanomolarity
LeakyTissue	Compartment	Model	0.001512	Litre
mAb	Species	LeakyTissue	0	Nanomolarity
T,m	Species	LeakyTissue	3.345	Nanomolarity
T,m-mAb	Species	LeakyTissue	0	Nanomolarity
T,s	Species	LeakyTissue	2.465	Nanomolarity
T,s-mAb	Species	LeakyTissue	0	Nanomolarity
Tm0	Species	LeakyTissue	3.345	Nanomolarity
Total_mTarget	Species	LeakyTissue	3.345	Nanomolarity
Lymph	Compartment	Model	0.002	Litre
mAb	Species	Lymph	0	Nanomolarity
T,s	Species	Lymph	1.39	Nanomolarity
T,s-mAb	Species	Lymph	0	Nanomolarity
Plasma	Compartment	Model	0.0010625	Litre

Name	Type	Scope	Initial Value	Unit
mAb	Species	Plasma	0	Nanomolarity
T,s	Species	Plasma	2.381	Nanomolarity
T,s-mAb	Species	Plasma	0	Nanomolarity
Total_mAb	Species	Plasma	0	Nanomolarity
Total_Target	Species	Plasma	2.381	Nanomolarity
TightTissue	Compartment	Model	0.002808	Litre
mAb	Species	TightTissue	0	Nanomolarity
T,s	Species	TightTissue	0.27	Nanomolarity
T,s-mAb	Species	TightTissue	0	Nanomolarity
complex_CLp	Parameter	Model	0.01412	1/hour
kdeg,m	Parameter	Model	0.03466	1/hour
kdeg,s	Parameter	Model	0.03851	1/hour
kint,m	Parameter	Model	0.3466	1/hour
koff	Parameter	Model	0.18	1/hour
kon	Parameter	Model	0.18	1/nanomolarity/hour
kshed,m	Parameter	Model	0.0193	1/hour
kshed,m_mAb	Parameter	Model	0.0193	1/hour
ksyn,m	Parameter	Model	0.05396	1/hour
L	Parameter	Model	1.5E-4	Litre/hour
L1*(1-o1)	Parameter	Model	4.554E-6	Litre/hour
L1*(1-oL)	Parameter	Model	3.96E-5	Litre/hour
L2*(1-o2)	Parameter	Model	4.231E-5	Litre/hour
L2*(1-oL)	Parameter	Model	8.04E-5	Litre/hour
mAb_CLp	Parameter	Model	0.01412	1/hour
ka	Parameter	Model	2.0E-4	Litre/hour

Appendix III. PK model v4 equations

SimBiology Model: PK model v4: mPBPK model incorporating TMDD with soluble synthesis route

ODE's

1. **d(Plasma.mAb)/dt** = 1/Plasma*(-([L1*(1-o1)]*Plasma.mAb) + (L*Lymph.mAb) - ((mAb_CLp*Plasma.mAb)*Plasma) - ((kon*Plasma.mAb*Plasma.[T,s])*Plasma-(koff* Plasma.[T,s-mAb])*Plasma) - ([L2*(1-o2)]*Plasma.mAb) + (ka*Dose_Compartment.mAb))
2. **d(Plasma.[T,s])/dt** = 1/Plasma*(-((kon*Plasma.mAb*Plasma.[T,s])*Plasma-(koff*Plasma.[T,s-mAb])*Plasma) - (([kdeg,s]*Plasma.[T,s])*Plasma) + (L*Lymph.[T,s]) - ([L2*(1-o2)] *Plasma.[T,s]) - ([L1*(1-o1)]*Plasma.[T,s]))
3. **d(Plasma.[T,s-mAb])/dt** = 1/Plasma*(((kon*Plasma.mAb*Plasma.[T,s])*Plasma-(koff*Plasma.[T,s-mAb])*Plasma) - ((complex_CLp*Plasma.[T,s-mAb])*Plasma) + (L*Lymph.[T,s-mAb]) - ([L2*(1-o2)]*Plasma.[T,s-mAb]) - ([L1*(1-o1)]*Plasma.[T,s-mAb]))
4. **d(TightTissue.mAb)/dt** = 1/TightTissue*(([L1*(1-o1)]*Plasma.mAb) - ([L1*(1-oL)] *TightTissue.mAb) - ((kon*TightTissue.[T,s]*TightTissue.mAb)*TightTissue-(koff*TightTissue.[T,s-mAb])*TightTissue))
5. **d(TightTissue.[T,s])/dt** = 1/TightTissue*(([L1*(1-o1)]*Plasma.[T,s]) - ((kon*TightTissue.[T,s] *TightTissue.mAb)*TightTissue-(koff*TightTissue.[T,s-mAb])*TightTissue) - ([L1*(1-oL)] *TightTissue.[T,s]))
6. **d(TightTissue.[T,s-mAb])/dt** = 1/TightTissue*(((kon*TightTissue.[T,s]*TightTissue.mAb) *TightTissue-(koff*TightTissue.[T,s-mAb])*TightTissue) + ([L1*(1-o1)]*Plasma.[T,s-mAb]) - ([L1*(1-oL)] *TightTissue.[T,s-mAb]))
7. **d(Lymph.mAb)/dt** = 1/Lymph*(-(L*Lymph.mAb) + ([L1*(1-oL)]*TightTissue.mAb) + ([L2*(1-oL)]*LeakyTissue.mAb) - ((kon*Lymph.mAb*Lymph.[T,s])*Lymph-(koff*Lymph.[T,s-mAb])*Lymph))
8. **d(Lymph.[T,s])/dt** = 1/Lymph*(([L2*(1-oL)]*LeakyTissue.[T,s]) - (L*Lymph.[T,s]) - ((kon*Lymph.mAb *Lymph.[T,s])*Lymph-(koff*Lymph.[T,s-mAb])*Lymph) + ([L1*(1-oL)]*TightTissue.[T,s]))
9. **d(Lymph.[T,s-mAb])/dt** = 1/Lymph*(([L2*(1-oL)]*LeakyTissue.[T,s-mAb]) - (L*Lymph.[T,s-mAb]) + ((kon*Lymph.mAb*Lymph.[T,s])*Lymph-(koff*Lymph.[T,s-mAb])*Lymph) + ([L1*(1-oL)] *TightTissue.[T,s-mAb]))
10. **d(LeakyTissue.mAb)/dt** = 1/LeakyTissue*(-((kon*LeakyTissue.mAb*LeakyTissue.[T,s]) *LeakyTissue-(koff*LeakyTissue.[T,s-mAb])*LeakyTissue) - ((kon*LeakyTissue.mAb*[T,m]) *LeakyTissue-(koff*[T,m-mAb])*LeakyTissue) - ([L2*(1-oL)]*LeakyTissue.mAb) + ([L2*(1-o2)]*Plasma.mAb))

11. **d([T,m])/dt** = 1/LeakyTissue*(-(([kdeg,m]*[T,m])*LeakyTissue) - ((kon*LeakyTissue.mAb *[T,m])*LeakyTissue-(koff*[T,m-mAb])*LeakyTissue) + (([ksyn,m]*Tm0)* LeakyTissue))
12. **d([T,m-mAb])/dt** = 1/LeakyTissue*(-(([kint,m]*[T,m-mAb])*LeakyTissue) + ((kon*LeakyTissue.mAb*[T,m])*LeakyTissue-(koff*[T,m-mAb])*LeakyTissue))
13. **d(LeakyTissue.[T,s])/dt** = 1/LeakyTissue*(-((kon*LeakyTissue.mAb*LeakyTissue.[T,s]) *LeakyTissue-(koff*LeakyTissue.[T,s-mAb])*LeakyTissue) - ([L2*(1-oL)]*LeakyTissue.[T,s]) + ([L2*(1-o2)] *Plasma.[T,s]) + ((kTs*Ts0)*LeakyTissue))
14. **d(LeakyTissue.[T,s-mAb])/dt** = 1/LeakyTissue*(((kon*LeakyTissue.mAb*LeakyTissue.[T,s]) *LeakyTissue-(koff*LeakyTissue.[T,s-mAb])*LeakyTissue) - ([L2*(1-oL)]*LeakyTissue.[T,s-mAb]) + ([L2*(1-o2)]*Plasma.[T,s-mAb]))
15. **d(Dose_Compartment.mAb)/dt** = 1/Dose_Compartment*(-(ka*Dose_Compartment.mAb))

Repeated assignments

4. **LeakyTissue.Total_mTarget** = LeakyTissue.[T,m] + LeakyTissue.[T,m-mAb]
5. **Plasma.Total_Target** = Plasma.[T,s]+Plasma.[T,s-mAb]
6. **Total_mAb** = Plasma.mAb+Plasma.[T,s-mAb]

Model constituents

Name	Type	Scope	Initial Value	Unit
Dose_Compartment	Compartment	Model	0.001	Litre
mAb	Species	Dose_Compartment	0	Nanomolarity
LeakyTissue	Compartment	Model	0.001512	Litre
mAb	Species	LeakyTissue	0	Nanomolarity
T,m	Species	LeakyTissue	1.3472	Nanomolarity
T,m-mAb	Species	LeakyTissue	0	Nanomolarity
T,s	Species	LeakyTissue	13.2501	Nanomolarity
T,s-mAb	Species	LeakyTissue	0	Nanomolarity
Tm0	Species	LeakyTissue	1.3472	Nanomolarity
Total_mTarget	Species	LeakyTissue	1.3472	Nanomolarity
Ts0	Species	LeakyTissue	13.2501	Nanomolarity
Lymph	Compartment	Model	0.002	Litre
mAb	Species	Lymph	0	Nanomolarity
T,s	Species	Lymph	7.49064	Nanomolarity
T,s-mAb	Species	Lymph	0	Nanomolarity
Plasma	Compartment	Model	0.0010625	Litre
mAb	Species	Plasma	0	Nanomolarity

Name	Type	Scope	Initial Value	Unit
T,s	Species	Plasma	12.8	Nanomolarity
T,s-mAb	Species	Plasma	0	Nanomolarity
Total_mAb	Species	Plasma	0	Nanomolarity
Total_Target	Species	Plasma	12.8	Nanomolarity
TightTissue	Compartment	Model	0.002808	Litre
mAb	Species	TightTissue	0	Nanomolarity
T,s	Species	TightTissue	1.472	Nanomolarity
T,s-mAb	Species	TightTissue	0	Nanomolarity
complex_CLp	Parameter	Model	0.03851	1/hour
kdeg,m	Parameter	Model	0.02888	1/hour
kdeg,s	Parameter	Model	0.03851	1/hour
kint,m	Parameter	Model	1.3863	1/hour
koff	Parameter	Model	0.18	1/hour
kon	Parameter	Model	3.6	1/nanomolarity/hour
ksyn.m	Parameter	Model	0.02888	1/hour
kTs	Parameter	Model	0.026142	1/hour
L	Parameter	Model	1.5E-4	Litre/hour
L1*(1-o1)	Parameter	Model	4.554E-6	Litre/hour
L1*(1-oL)	Parameter	Model	3.96E-5	Litre/hour
L2*(1-o2)	Parameter	Model	4.231E-5	Litre/hour
L2*(1-oL)	Parameter	Model	8.04E-5	Litre/hour
mAb_CLp	Parameter	Model	0.014118	1/hour
ka	Parameter	Model	2.0E-4	Litre/hour

Appendix IV. Characterisation of mAb 9E10

The capability of the GSK raised murine mAb 9E10 to bind to mouse CD21 was demonstrated by ELISA during antibody selection. This work was completed by Richard Priest, Discovery Antibody Selections (Stevenage, UK). In brief, appropriate wells of a 96 well plate (Nunc Maxisorp, Thermofisher Scientific) were coated with rat anti-mouse CD21 mAb 7G6 (BD Biosciences), followed by the addition of recombinant mouse CD21 (extracellular region including SCR1-16, aa 21 to 970), to result in three capture conditions; CD21, 7G6 captured CD21 and finally 7G6 alone. 9E10 or a control antibody were incubated in triplicate under each condition, with bound mAb detected via an HRP conjugated secondary anti-mouse IgG antibody (Jackson ImmunoResearch, #715-036-151) and TMB substrate (as described in chapter 2, 2.7). Illustrated in figure A1, the results demonstrated that mAb 9E10 can bind recombinant mouse CD21, but not when previously bound by mAb 7G6. An outcome that suggests mAb 9E10 binds directly to or at least nearby the 7G6 binding epitope and may act as a functional blocker.

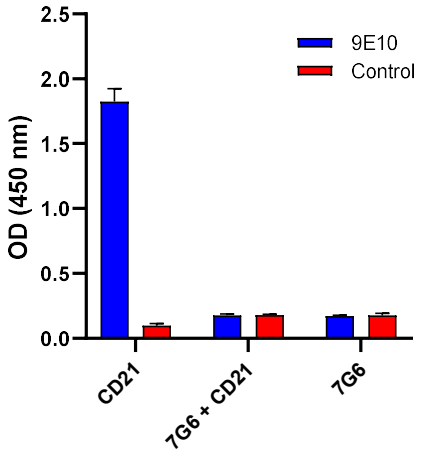

Figure A1. Confirmation that mAb 9E10 binds to recombinant mouse CD21, as demonstrated by ELISA, with binding blocked when CD21 is initially captured by mAb 7G6. Data illustrated as the mean ±SD (n=3) of the optical density (OD) measurement at a wavelength of 450 nm.

To confirm that mAb 9E10 can bind native CD21, its binding to freshly isolated mouse splenocytes was explored using flow cytometry. This work was completed by Joanne Thompson, Exploratory Biomarker Assays, (Stevenage, UK) during antibody selection, using a similar methodology to that described in chapter 2 (2.10). In brief, splenocytes were isolated from the spleens of three untreated mice, diluted to 1E6 cells per mL and a 100 µL aliquot

taken and stained with labelled anti-CD3 (BD Biosciences, APC clone 17A2, #565643), anti-CD19 (BD Biosciences, FITC clone MB19-1, #101506) and either anti-CD21 (BD Biosciences, PE clone 7G6, #552957) or PE labelled 9E10 at four dilution strengths. Lymphocytes were gated on scatter properties, with the $CD3^+$ T cell and $CD19^+$ B cell populations separated from this gate. Comparison of the resulting histograms (figure A2) suggest that mAbs 9E10 and 7G6 behave similarly, showing strong binding to CD19+ B cells and approximately 10-fold lower relative binding to CD3+ T cells. 9E10 / 7G6 binding to CD19+ B cells was shown to be concentration dependent (figure A3).

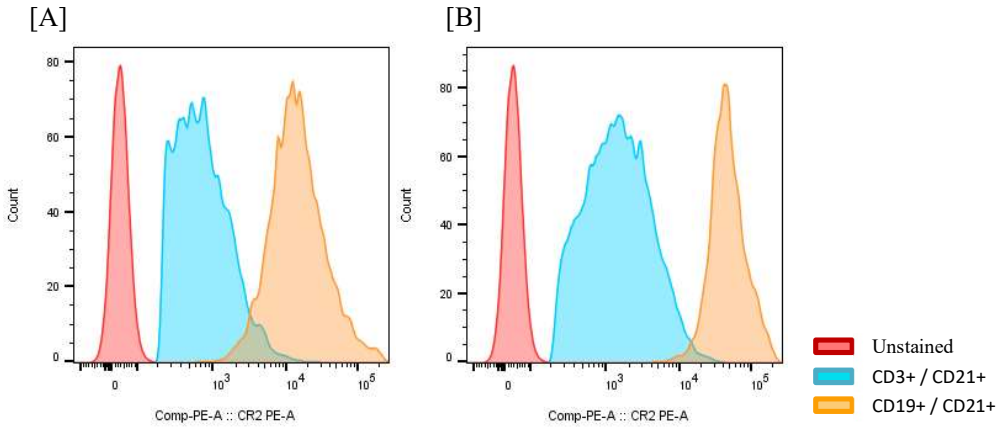

Figure A2. Anti-CD21 mAb binding to $CD19^+$ B cells (orange histogram) and $CD3^+$ T cells (blue histogram) from untreated mouse splenocytes, compared with an unstained control (red histogram), to identify the relative binding ability of **[A]** 9E10, compared with **[B]** 7G6.

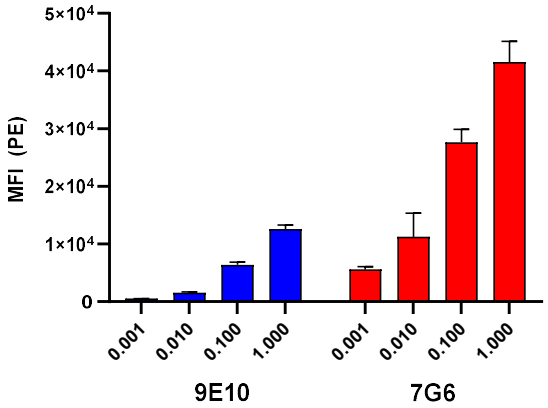

Figure A3. Anti-CD21 mAb binding to CD19+ B cells from untreated mouse splenocytes, at four dilutions (1, 1/10, 1/100 and 1/1000), as measured by flow cytometry. Binding defined by the geometric MFI of PE labelled **[A]** mAb 9E10 or **[B]** mAb 7G6. Data illustrated as the mean ±SD (n=3).

Appendix V. Estimation of mAb 7G6 and 4B2 K_d

To compare binding of the two murine CD21 mAbs (7G6 and 4B2) to native CD21 and to estimate the equilibrium dissociation constant (K_d), the mAbs were assessed through incubation with a mouse splenocyte preparation. In brief, PE conjugated 7G6 and 4B2 were titrated across a 5 log unit concentration range and incubated with mouse splenocytes (n=2), alongside relevant controls to define non-specific binding. Detection was achieved by flow cytometry, to derive the MFI of CD21 PE for the CD45R/B220+ cell population, with the binding saturation curves shown in figure A4. To calculate K_d, the total binding data was analysed using GraphPad Prism v8.1.2 (GraphPad Software, Inc), with the one site saturation model $Y = Bmax*X/(K_d+X) + NS*X + background$ (where Bmax is maximum specific binding and NS is the slope of nonspecific binding). Due to an insufficient concentration range in the initial assay to define the 7G6 K_d, the assay was repeated with altered dilution conditions, providing a K_d estimate of 0.054 nM. Both assays provided suitable data to estimate the 4B2 K_d, with a mean value of 1.65 nM adopted.

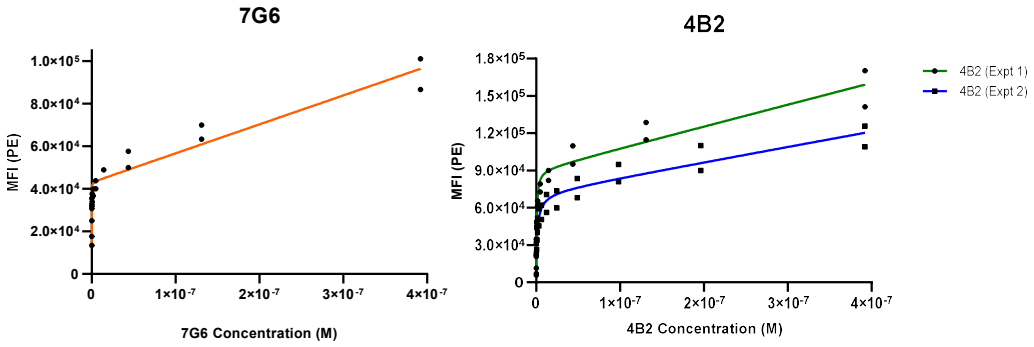

Figure A4. Comparative binding of the murine CD21 specific mAbs 7G6 and 4B2 to the CD45R+ B220+ B cell population as measured by flow cytometry following incubation with mouse splenocytes (n=2) across a 5 log unit concentration range. Data presented as the individual MFI values (symbols) and the fit curve of a one site saturation binding model (line).

Table A1. Calculated binding affinity (K_d) and coefficient of determination (R^2) of the murine CD21 specific mAbs 7G6 and 4B2 to the CD45R+ B220+ B cell population, as measured by flow cytometry following incubation with mouse splenocytes (n=2).

Experiment No.	Value	4B2	7G6
1	K_d (nM)	2.618	-
	R^2	0.929	-
2	K_d (nM)	0.680	0.054
	R^2	0.976	0.959

Appendix VI. Evaluation of the efficacy of mAb 4B2 in the IV KLH TDAR mouse experimental model

The murine CD21 specific mAb 4B2 (Kulik *et al.*, 2015) was evaluated in the IV KLH TDAR mouse experimental model, under the same conditions used to evaluate 7G6 as detailed in chapter 2 (2.3.8. PKPD study 7). The study consisted of two groups (n=10) administered either mAb 4B2 or an IgG1 isotype control IP at 20 mg/kg, one day prior to IV KLH immunisation at 1.2 mg/kg. Each group was further divided into two sub groups (n=5) sampled on alternate days between day 3 and 15. Plasma samples were isolated and analysed for antigen specific IgG / M and individual IgG isotypes as described in chapter 2 (2.7.2 / 3). On the terminal day, the spleen was excised, processed and analysed by flow cytometry for the germinal centre B cell population and for target engagement markers, as described in chapter 2 (2.10).

Results

The plasma antigen specific IgG / M concentration data collected on alternate days was combined to form composite concentration time profiles, with daily measurements, as shown in figure A5. In this study, the mean antigen specific IgG response window, defined as the difference between the baseline day 0 measurement and that taken 14 days post KLH immunisation, was 65-fold in the isotype control treatment group. In a manner similar to that observed with mAb 7G6 (chapter 5, 5.4.5), treatment with mAb 4B2 resulted in a 17-fold exacerbation of this IgG response when then compared with the isotype control response AUC. In contrast to the effect of mAb 4B2 on the specific IgG response to KLH immunisation, treatment with mAb 4B2 resulted in a 46% reduction of the mean antigen specific IgM response when compared with the isotype control response AUC.

To further investigate the observed exacerbation of the antigen specific IgG response following treatment with mAb 4B2, the individual contribution of each specific IgG isoform was explored. This was achieved by quantitative ELISA for the IgG1, IgG2b and IgG3 isotypes and by a relative antibody titre approach for IgG2c (as detailed in chapter 2, 2.7.3). The results are shown in figure A6, demonstrating that the exacerbated antigen specific IgG response is driven by a substantial increase in antigen specific antibodies of the IgG2 subclass (figure A6 C/D) that is not replicated in the antigen specific IgG1 or IgG3 isotypes (figure A6 B/E.

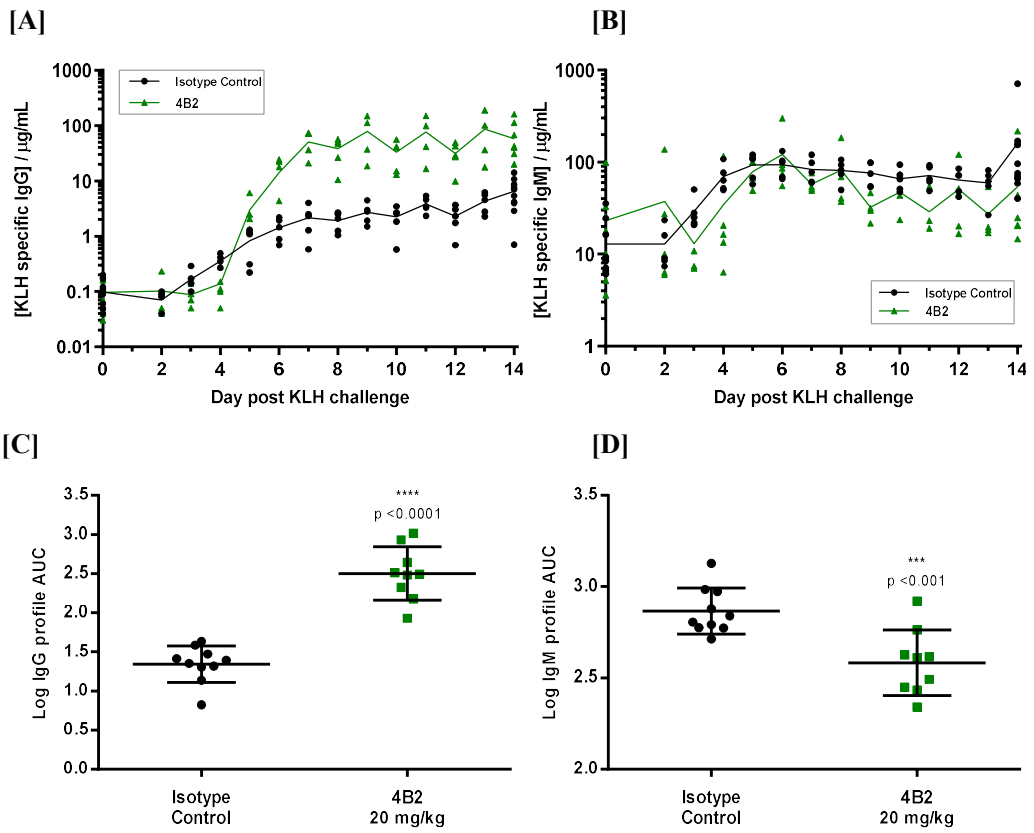

Figure A5. KLH specific **[A]** IgG and **[B]** IgM composite plasma concentration profiles in male C57BL/6 mice over 14 days following IV KLH immunisation at 1.2 mg/kg on study day 2. Mice were treated IP with either mAb 4B2 or an IgG1 isotype control on study day 1 at 20 mg/kg, 1 day prior to KLH challenge. Data illustrated as the group mean (line) and individual (symbol) values, n=10 / treatment. The KLH specific antibody data is also presented as the area under the curve (AUC) of the individual **[C]** IgG and **[D]** IgM profiles. Data illustrated as the individual (symbols) and mean +/- SD (line and bar), n=10/treatment, with statistical significance calculated using an unpaired t test, *** $p < 0.001$, **** $p < 0.0001$.

The splenic germinal centre B cell response observed in the isotype control group following IV KLH immunisation was significantly perturbed following treatment with mAb 4B2, with the results shown in figure A7. Treatment with mAb 4B2 at 20 mg/kg resulted in a 74% reduction in the number of GC B cells per spleen on day 15, when compared to the isotype control. This is an outcome in accordance with prior observations in the adjuvant driven TDAR model (PKPD study 1, chapter 5, 5.4.1).

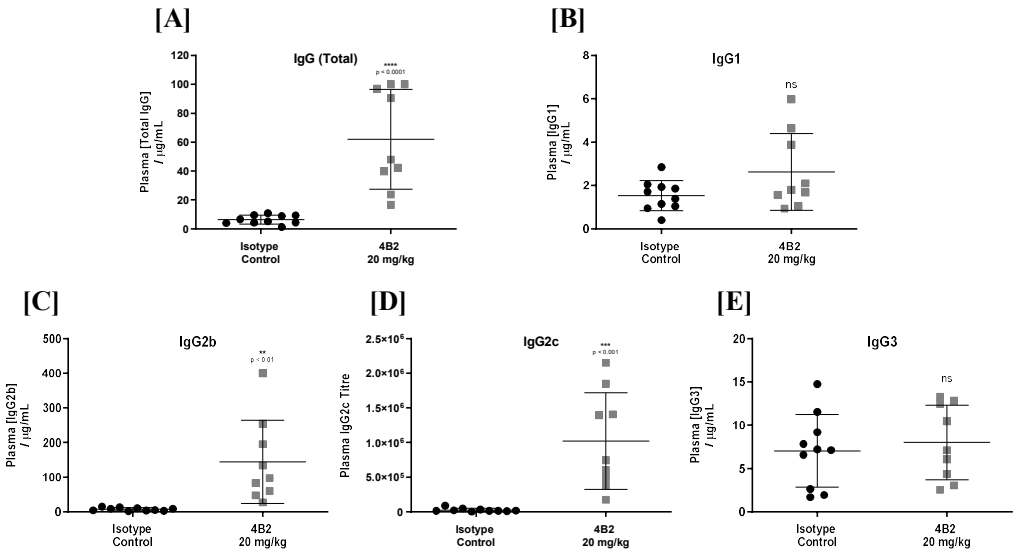

Figure A6. KLH specific IgG isotype analysis of plasma on study day 15, showing **[A]** the total IgG concentration, and the subdivision of this total response into antigen **specific [B]** IgG1, **[C]** IgG2b, **[D]** IgG2c and **[E]** IgG3, following IV KLH TD immunisation at 1.2 mg/kg to male C57BL/6 mice on study day 1. Data illustrated as the individual (symbols) and mean +/- SD (line and bar), n=10/treatment, with statistical significance calculated using an unpaired t-test, ** $p < 0.01$, *** $p < 0.001$, **** $p < 0.0001$, ns = not significant.

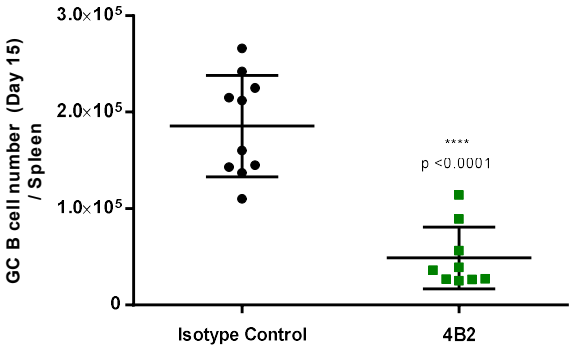

Figure A7. Splenic germinal centre B cell number per spleen (CD45+, CD19+, GL7+, FAS+) in C57BL/6 male mice on study day 15, following treatment with either mAb 4B2 or an IgG1 isotype control on study day 1 at 20 mg/kg, 1 day prior to IV KLH challenge at 1.2 mg/kg. Data illustrated as the individual (symbols) and mean ± SD (line and bar) n=10/treatment, with statistical significance calculated using an unpaired t-test, **** $p < 0.0001$.

A crude evaluation of target engagement was performed, using a trio of labelled probes to identify the presence of CD21/35 on splenic B cells by flow cytometry (figure A8), as described previously by Kulik *et al.* (2015). Treatment with mAb 4B2 significantly ($p < 0.0001$) reduced the measured MFI by >10-fold for each of the three labelled probes, when compared to the isotype control treated group. This provides direct evidence of target engagement by 4B2, as demonstrated by the reduction in signal of the competitive antibody 7G6 (figure A8A). Alongside evidence of down modulation of the receptor from the cell surface, as highlighted by a reduction in 7E9 signal (figure A8B) and at the closely related protein CD35, with the 8C12 signal also reduced (figure A8C).

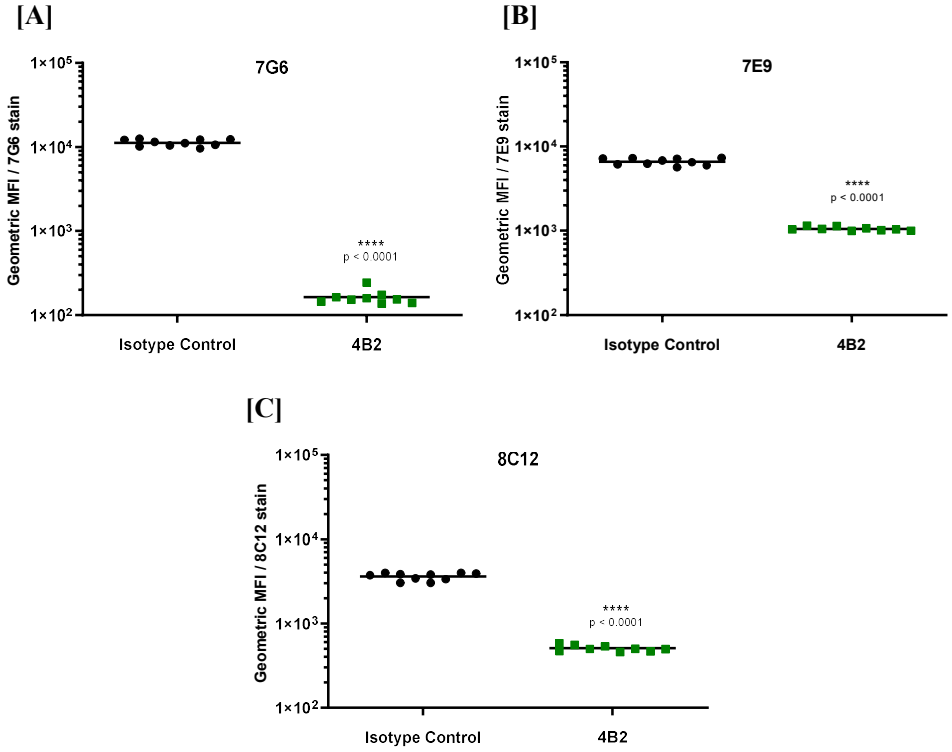

Figure A8. Splenic B cells were probed with fluorescently labelled mAbs targeting CD21/35 to investigate the extent of target engagement following termination, 15 days post IP treatment with 20 mg/kg mAb 4B2 or an IgG1 isotype control, during a mouse IV KLH TDAR study. Splenic B cells were probed with [A] PE labelled 7G6, specific for CD21/35, [B] APC labelled 7E9, specific for CD21/35, but non competitive with 4B2 [C] BV421 labelled 8C12, specific for CD35 alone. Data illustrated as the individuals (symbols) and mean ± SD (line and bar) n=10/treatment, with statistical significance calculated using an unpaired t-test, **** $p < 0.0001$.

Appendix VII. Soluble CD21/35 concentration in plasma following 20 mg/kg 7G6

Plasma samples collected during the 20 mg/kg IV arm of the 7G6 PK studies described in chapter 3 (3.3.1) were reanalysed for the concentration of soluble CD21/35 using the novel LC-MS/MS based targeted proteomics assay described in chapter 2 (2.9.3). Whilst a baseline sample was not collected in this study, the first plasma sample collected 10 minutes post dose is considered likely to represent baseline conditions for soluble target, with a mean 10.8 nM measured. The results of this analysis are displayed in figure A9, demonstrating there to be no appreciable change in soluble CD21/35 over an 8 day period following 7G6 administration.

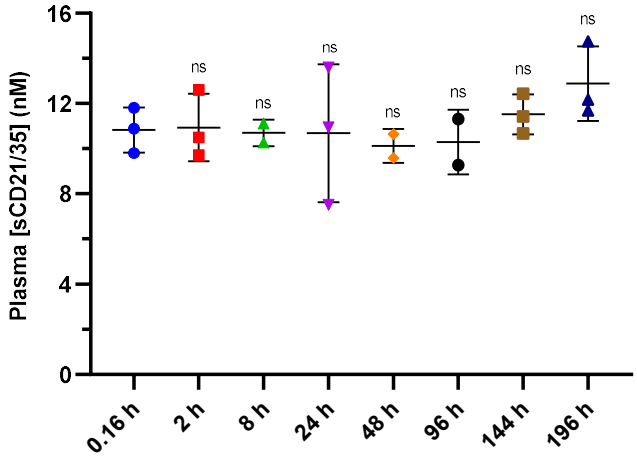

Figure A9. Soluble CD21/35 plasma concentration over 8 days following IV administration of mAb 7G6 at 20 mg/kg to the male C57BL6 mouse (n=3). Data illustrated as the individual (symbols) and mean ±SD (line and bar), n=3 per treatment (except where insufficient sample remained), with statistical significance calculated using a one way ANOVA with Dunnett's multiple comparison test, ns = not significant.

Appendix VIII. Quantification of CD21 number per cell (cynomolgus monkey)

The number of CD21 receptors per peripheral B and T cells isolated from cynomolgus monkey blood were quantified using flow cytometry within GSK by Joanne Thompson (exploratory biomarker assay group, Stevenage, UK). This was completed using a QuantiBRITE PE bead (BD Bioscience) based fluorescence quantification approach, following similar methodology to that described for mouse in chapter 2 (2.10.4). Cynomolgus whole blood, collected from untreated animals (n=9), was processed as described in chapter 2 (2.10.4) and stained with labelled anti-CD4, anti-CD8 and anti-CD20 antibodies, alongside a PE labelled anti-CD21 antibody. Lymphocytes were gated on scatter properties, before separation into CD4+ and CD8+ T cells and CD20+ B cell populations.

Table A3: Quantification of CD21 expression on the surface of lymphocyte populations isolated from the whole blood of nine individual untreated cynomolgus monkeys.

Animal	Mean receptor number per CD20+ B lymphocyte	Mean receptor number per CD4+ T lymphocyte	Mean receptor number per CD8+ T lymphocyte
A	10468	614	620
B	10652	897	663
C	9619	1217	771
D	11335	2314	929
E	13162	866	888
F	12244	714	629
G	9595	1828	924
H	7357	1316	908
I	10059	756	706
Mean	10499	1169	782
SD	1677	572	132
Range	7357-13162	614-2314	620-929

Appendix IX. Fingolimod blood binding

The Fingolimod and Fingolimod-phosphate blood binding and blood to plasma ratio in mouse (C57BL/6) were measured using standard methodology within GSK by Laura Tomlinson (Discovery DMPK, Stevenage, UK). In brief, binding to mouse blood (n=3) was determined using rapid equilibrium dialysis at nominal concentration of 1000 ng/mL, using a dialysis buffer of PBS (100 mM sodium phosphate, 150 mM sodium chloride, pH 7.4). Plates were incubated for 4 hours at 37 ºC, before sampling, matrix matching, extraction via protein precipitation and analysis using the specific LC-MS/MS assay detailed in chapter 2 (2.5). The percent unbound was determined from the measured peak area ratio of the blood and buffer wells.

The blood to plasma ratio was determined *in vitro* at a nominal concentration of 1000 ng/mL. Compound was spiked into whole blood and incubated for 60 minutes at 37 ºC, before splitting the sample into two aliquots. Plasma was extracted from one aliquot by centrifugation, prior to matrix matching, compound extraction via protein precipitation and analysis using the specific LC-MS/MS assay detailed in chapter 2 (2.5).

Table A4. *In vitro* determined fraction unbound (fu_b) and blood to plasma ratio (B:P) of Fingolimod and Fingolimod-phosphate in the C57BL/6 mouse. Data shown as the mean (n=3) and standard deviation.

Parameter	Fingolimod	Fingolimod - phosphate
Fraction unbound blood (fu_b)	<0.001	0.003 (0.000)
Blood : Plasma ratio	3.15 (0.19)	1.25 (0.17)